LATERAL BRACING OF BRIDGE GIRDERS BY METAL DECK FORMS

Approved by
Dissertation Committee:

Karl H. Frank

Joseph A. Yura

Michael D. Engelhardt

John L. Tassoulas

Stelios Kyriakides
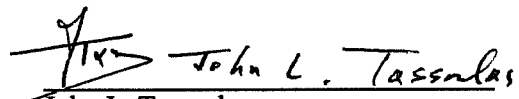
LATERAL BRACING OF BRIDGE GIRDERS BY METAL DECK FORMS

by

TODD AARON HELWIG, B.S., M.S.

DISSERTATION

Presented to the Faculty of the Graduate School of

The University of Texas at Austin

in Partial Fulfillment

of the Requirements

for the Degree of

DOCTOR OF PHILOSOPHY

THE UNIVERSITY OF TEXAS AT AUSTIN

August 1994

Dedicated to my wonderful family

ACKNOWLEDGEMENTS

After 10 plus years at the University of Texas, I could probably publish two volumes of acknowledgements if I were to thank everyone who has assisted me. I would like to thank all of the numerous students I have had the pleasure to work with. I can only hope that I have expressed my gratitude to the many individuals who have assisted me throughout the last decade.

I would like to first express my appreciation to Dr. Karl Frank for all of his guidance, advice, and friendship throughout this research study and also throughout my academic career. After studying with Professor Frank for 5 years, I feel as if I have just scratched the surface of his intellect. I am also indebted to Professor Frank and his family for providing me with a warm home to spend the last few Thanksgiving dinners.

I would also like to give a special thanks to Dr. Joseph Yura for his friendship and advice throughout my academic career. I am very grateful for the guidance that Dr. Yura has given me in coursework, research, and also in the area of non-linear particle dynamics (bowling).

To all of the Professors on my committee: Karl Frank, Joseph Yura, Michael Engelhardt, John Tassoulas, and Stelios Kyriakides, I would like to thank each of you for your advice and comments on this dissertation. In addition, I would like to thank all of you for your classroom instruction. I have thoroughly enjoyed the courses that I have taken with each of you, and will use each of you as a standard for my effectiveness as an instructor in future years.

I would also like to thank Professor John Breen for his instruction, advice, and friendship throughout my graduate education. I have especially enjoyed the time that we have spent on the golf course. Thanks are also due to Professor Ned Burns for his supervision during my M. S. degree, and his friendship throughout the rest of my career. Professor Michael Kreger has also been a great friend in graduate school. I have especially enjoyed the bowling and golf. (With all of the bowling and golf that I have mentioned, it's amazing that I'm not better than I am at either sport.)

LATERAL BRACING OF BRIDGE GIRDERS BY METAL DECK FORMS

Todd Aaron Helwig, Ph.D.
The University of Texas at Austin, 1994

Supervisor: Karl H. Frank

Steel bridge girders are prone to buckling under construction loads during the casting of the concrete for the composite deck. The buckling capacity of a girder can be significantly increased by providing bracing at either discrete locations or continuously along the girder length. One form of continuous bracing is metal deck forms that act as a shear diaphragm to restrain the top flange of a girder from lateral movement. Current AASHTO specifications do not allow bracing by metal deck forms to be considered during design, but require discrete bracing in the form of cross-frames at a maximum spacing of 25 feet.

The research described herein was undertaken to determine the bracing capacity of metal deck forms. The project consisted of an experimental and a computational study. The experimental study involved tests on the isolated deck to establish its shear strength; tests on various deck to girder connections; and a full-scale buckling test of twin girders with metal deck forms in place. The experimental portion of the study has been presented in related theses by Currah and Soderberg.

This dissertation covers the computational study, and made use of the finite element program ANSYS to study the ability of metal deck forms to provide bracing to bridge girders. A parametrical study was conducted which includes shear rigidity of the deck, shape of girder cross-section, in-plane boundary conditions, number of transverse stiffeners, type of loading, and load height. Existing closed formed solutions as well as approximate solutions were compared with the finite element results in order to develop a design approach for girders braced by deck forms.

The resulting design approach takes into consideration effects of moment gradient, load height effects, and cross-section distortion from web bend buckling and shear buckling. The approach is applicable to simply-supported girders and continuous girders.

Table of Contents

List of Tables

xii

List of Figures

CHAPTER 1

Introduction

There are several loading stages which must be considered when designing composite plate girder bridges. The critical stage for the bending capacity of the steel section usually occurs during the placement of the concrete deck. The construction load consists of the weight of the steel girder, the fresh concrete, the screed, the forms, and other equipment and personnel used to place the concrete. This entire load must be carried by the steel section alone.

The AASHTO (American Association of State Highway and Transportation Officials) [1] specification limits the girder load to the minimum of the yield load or the flexural-torsional buckling capacity of the girder. In positive bending regions, the neutral axis of the composite girder will lie very near the top flange of the steel section; therefore a small compression flange is usually employed. During the construction phase, however, this small top flange in positive bending regions makes lateral-torsional buckling critical.

The buckling capacity of a girder can be significantly increased by providing bracing at either discrete locations or continuously along the girder length. One form of continuous bracing is metal deck forms that act as a shear diaphragm to restrain the top flange of a girder from lateral movement. Previous studies, primarily in the building industry [12,16], have shown that a shear diaphragm attached to the top flange can provide a significant amount of bracing to slender beams.

Current AASHTO [1] specifications require bracing in the form of cross frames or other discrete diaphragms at a maximum spacing of 25 feet. This maximum spacing has been relaxed in the new AASHTO Load and Resistance Factor Design (LRFD) Specification, however shear diaphragms such as metal deck forms, are not presently allowed to be utilized as a bracing element to stabilize the top flange of the girder.

1.1 Forming Systems

Bridge construction techniques have greatly improved in recent years. One of the main areas where there have been several innovations has been in the area of forming systems which are used for support during the placement of the concrete deck. Traditionally, temporary forms constructed from plywood have been used. Plywood forms have many advantages some of which

1

include the availability of materials and the relative ease with which the contractor can make changes in the field. However, there are major drawbacks to the use of plywood forms. One drawback is that the forms are limited to maximum spans of approximately 8 feet. This limited span may reduce the economy of the bridge since more girders are required along the width of the bridge. Another major drawback is the difficult task of removing the temporary plywood forms after the concrete has cured. Form removal is difficult because the contractor must go under the bridge to remove the forms. Several stay-in-place systems have been developed which eliminate the need for form removal.

One of the more recent stay-in-place systems which has been utilized in the last few decades are precast concrete panels. These precast concrete forms are typically pretensioned panels that rest on the flanges of adjacent girders. While these forms are economical, there are many drawbacks to their use. Similar to the plywood forms, these precast panels have limited spans which may reduce the girder spacing and increase the number of girders required. Since the forms are very heavy, placement of the concrete panels is labor intensive and usually requires an external crane or a "truck or trolley" which rides along the girder flanges. Another major drawback to this forming system is illustrated in Figure 1.1. The camber of adjacent girders in the bridge may actually differ a significant amount. Since the concrete panels rest on the flanges of the girders, the differential camber in adjacent girders must be accounted for by pouring a larger volume of concrete over the lower girder (girder B). The problem with the differential camber is further amplified during the casting of the concrete, by the larger dead load deflection of the more heavily loaded girder.

Another type of stay-in-place system is permanent metal deck forms which will be referred to as either PMDF or metal deck forms. Figure 1.2 shows the profile of conventional metal deck forms as well as a plan view of the forming system. Adjacent sheets are usually fastened together with self-tapping screws along the seams. These self-tapping screws are also used to fasten the deck down at the ends. One attractive feature of this type of forming system is presented in Figure 1.3 which shows how the forms are attached to the girders. The metal deck forms are supported on a cold formed angle that allows the contractor to adjust the form elevation at the ends to account for differential camber between adjacent girders. A uniform deck thickness can be achieved by adjusting the form elevation and eliminating the requirement of larger volumes of concrete over any one girder.

Additional concrete
must be poured
over lower girder

Top of ConcreteDeck

precast concrete form

Differential
Camber

Girder A
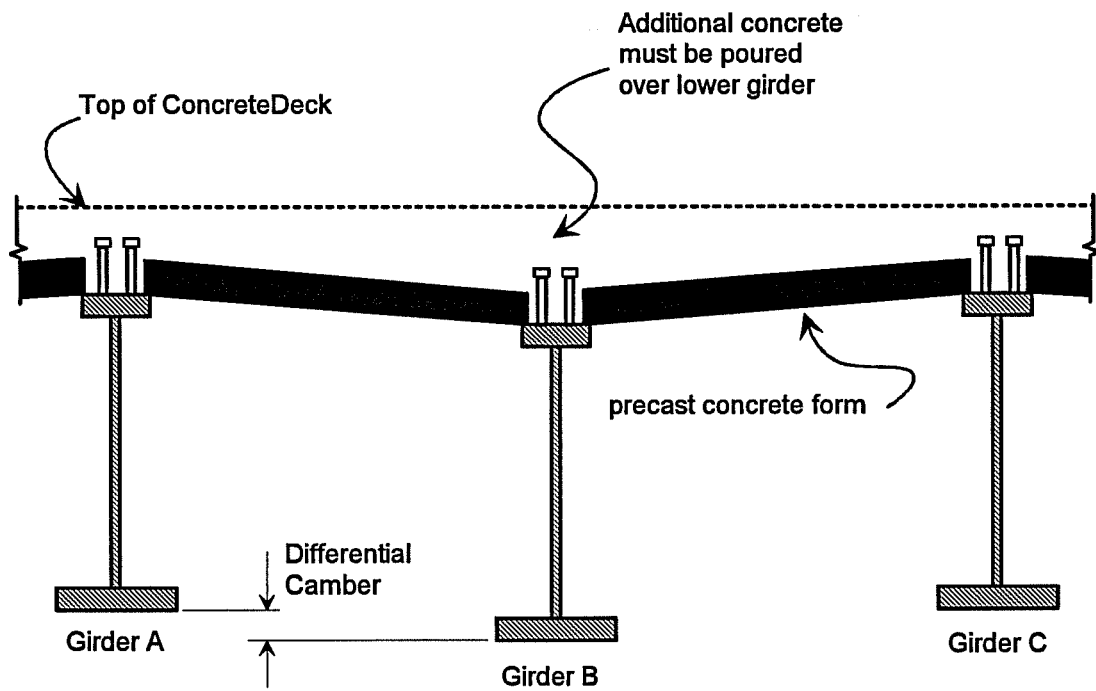
Girder B

Girder C

Figure 1.1 Differential camber of adjacent girders with precast concrete forms.

Girder 1 Top Flange

self-tapping
screws

A

A

Girder 2 Top Flange

Section A-A
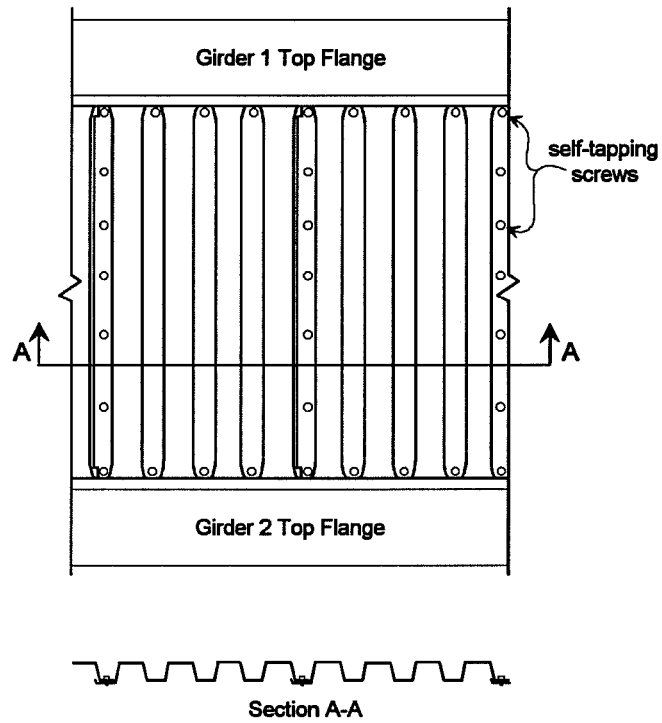
Figure 1.2 Conventional metal bridge deck forms.

Top of Concrete Deck

Metal Deck Form

Differential
Camber

Girder A
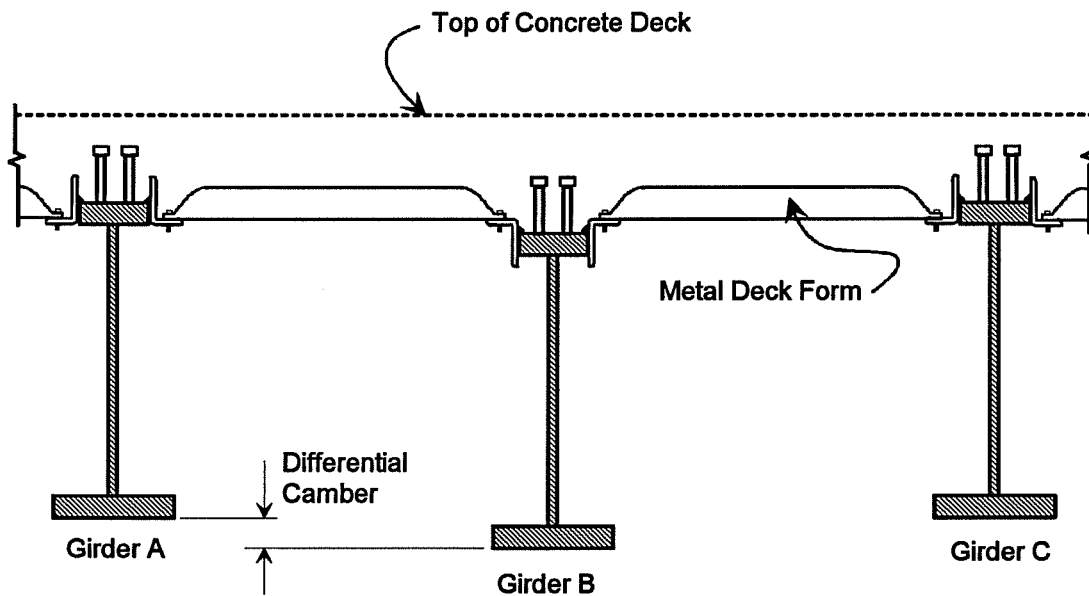
Girder B

Girder C

Figure 1.3 Differential camber of adjacent girders with metal deck forms.

One of the main advantages of PMDF over other forming systems is the much longer deck spans which make it possible to have fewer girders along the width of the bridge. Typical spans of PMDF are between 9 to 12 feet, however, some configurations of heavy gage deck can reach spans of 15 feet.

Metal deck forms consist of corrugated steel sheets which usually range from 24 to 36 in. wide. One of the downsides to conventional PMDF, is that additional concrete is required to fill the corrugations. To avoid the cost of the extra concrete, contractors often fill the corrugations with styrofoam or another cheap filler material. An alternative to using a metal deck with open corrugations is to use a cellular deck such as the one shown in Figure 1.4. In the cellular deck, individual sheets often consist of 2 "ribs" and 2 "covers". When the PMDF is installed, the "covers" of one sheet overlap the "ribs" of the adjacent sheet to create a flat form surface, thus eliminating the open corrugation.

Metal deck forms are usually more expensive than either plywood forms or precast concrete panels, however, the higher cost is often offset by the aforementioned advantages. Additional economy and better service behavior from the bridge may also be possible if the PMDF are considered as a bracing element against lateral-torsional buckling.

Lateral-torsional buckling involves a twist of the cross-section and a lateral movement of the compression flange. When the top flange is in compression, the metal deck form behaves like a shear diaphragm to brace the flange from lateral movement. This is depicted in Figure 1.5 which shows a plan view of two adjacent girders that have buckled. The lateral movement of the top flange imposes a shearing distortion on the deck panel, and the ability of the deck to resist the shear distortion is available to brace the girder.

Studies have been done in the building industry [12,16] which have shown that a shear diaphragm can provide a significant amount of bracing to beams. There are several differences, however, in the type of metal deck forms which are used in the building industry versus the type which are used in the bridge industry. Some of these differences are subtle while others are more significant. Some of the more subtle differences are the type and depth of the profile for the deck, as well as the thickness of sheet metal used to make the form. PMDF used in the bridge industry usually has a deeper profile than that used in the building industry, and the sheet metal may be considerably thicker.

covers

ribs
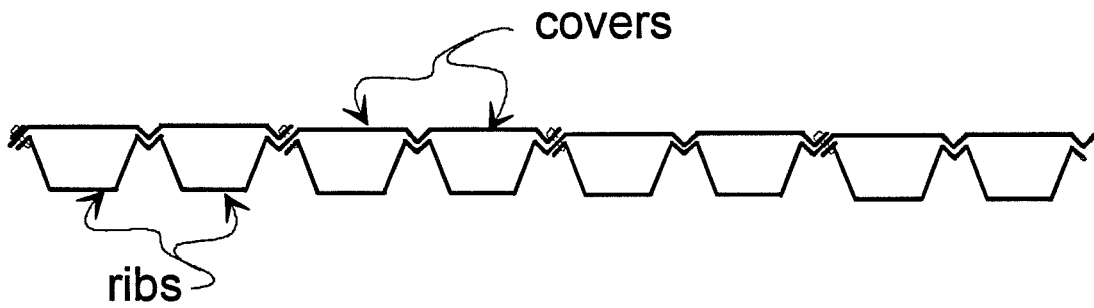
Figure 1.4 Cellular metal bridge deck forms.

A

A

γ

SECTION A-A
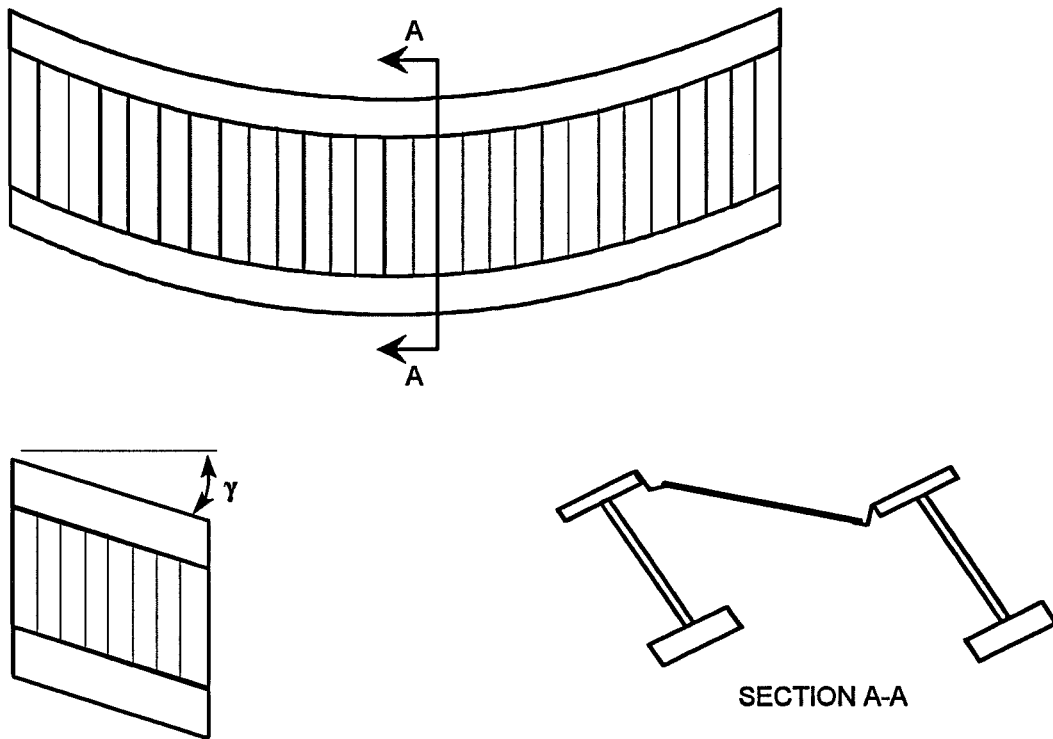
Buckling of girders causes shear
deformation in metal deck forms

Figure 1.5 Buckling girders impose shear deformation on deck forms.

Some of the more significant differences between the metal deck forms used in the building industry versus the bridge industry include the span and shape of the deck panel, as well as the method by which it is attached to the girders. The metal deck forms used in the building industry are usually fabricated in long lengths which span over a number of beams. Since the deck forms in buildings pass over the top of the beams, the forms are fastened directly to the top flange using either powder actuated fasteners or puddle welds.

Metal deck forms used in bridge applications make use of the support angle mentioned previously. Figure 1.6 shows two of the details for the angle which are used to support the deck. In detail 'A', the angle is fastened to the girder by intermittent fillet welds. This detail will be referred to as the "welded angle" detail. Due to fatigue and concern of welding problems, however, most state highway officials do not allow welding to the girder in the field, in which case detail 'B' is often employed. Detail 'B' utilizes a "strap" which spans the top flange of the girder, and the support angle is welded directly to the strap, thus eliminating any welding to the girder in the field. This detail will be referred to as the "strap" detail. There are several variations of the actual support details, some of which are outlined in greater depth in related theses by Currah [9] and Soderberg [21]. The support angle introduces an eccentricity in the connection which reduces the stiffness a significant amount.

Because the bridge deck forms only span between the girders, the ends of the deck corrugations are folded over to close and seal the deck. This is done to prevent concrete from leaking during casting of the deck. Since the ends are fully closed, warping of the deck cross-section at the ends is essentially eliminated which greatly increases the stiffness of the deck form.

If bracing of the top flange by the deck is considered, smaller flanges may result which could lead to significant economical advantages. The spacing between cross-frames could also be increased which would lead to better constructability and reduce the fatigue prone weld details.

1.2 Factors affecting Bracing Requirements

The factors affecting bracing problems can be outlined by considering the problem of a column with a lateral brace at midheight. Winter [24] used this simple problem to show that braces must satisfy both stiffness and strength requirements. Figure 1.7 shows the relationship between the buckling load, P_{cr}, and the lateral brace stiffness, β_L, for a perfectly straight column [22]. P_e in the figure is equal to $\pi^2 EI/L_b^2$, where L_b is the "unbraced length" of the column. At a stiffness $\beta_L = 2 P_e/ L_b$, "full bracing" is achieved and the column buckles between brace points.

METAL
DECK FORMS

SUPPORT
ANGLE

Detail A

STRAP (ANGLE)
12"-15" SPACING

2" CLIPS
SPACED
AT 10'-2"
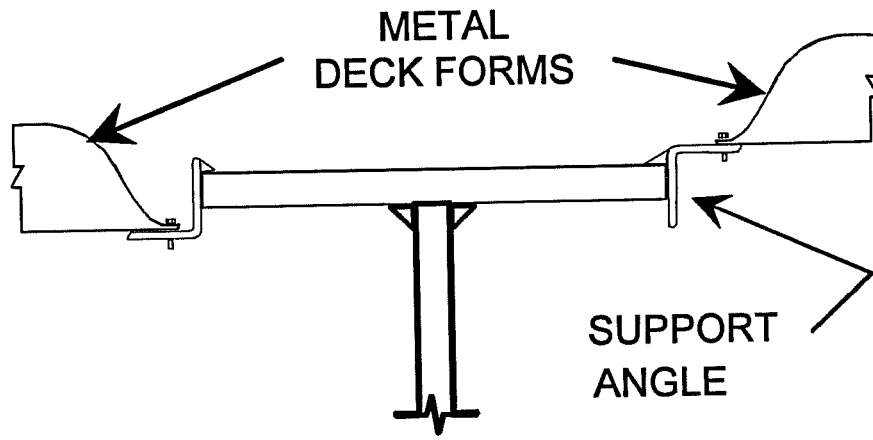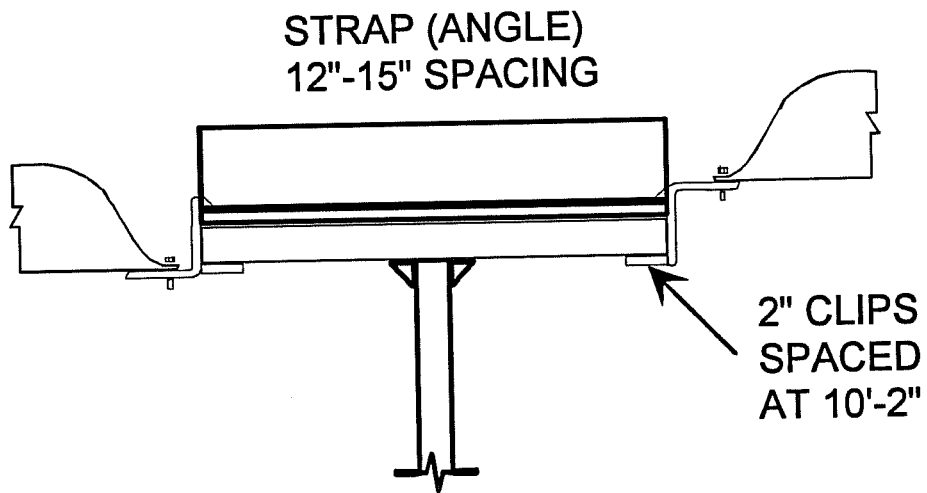
Detail B

Figure 1.6 Support details for metal deck forms.
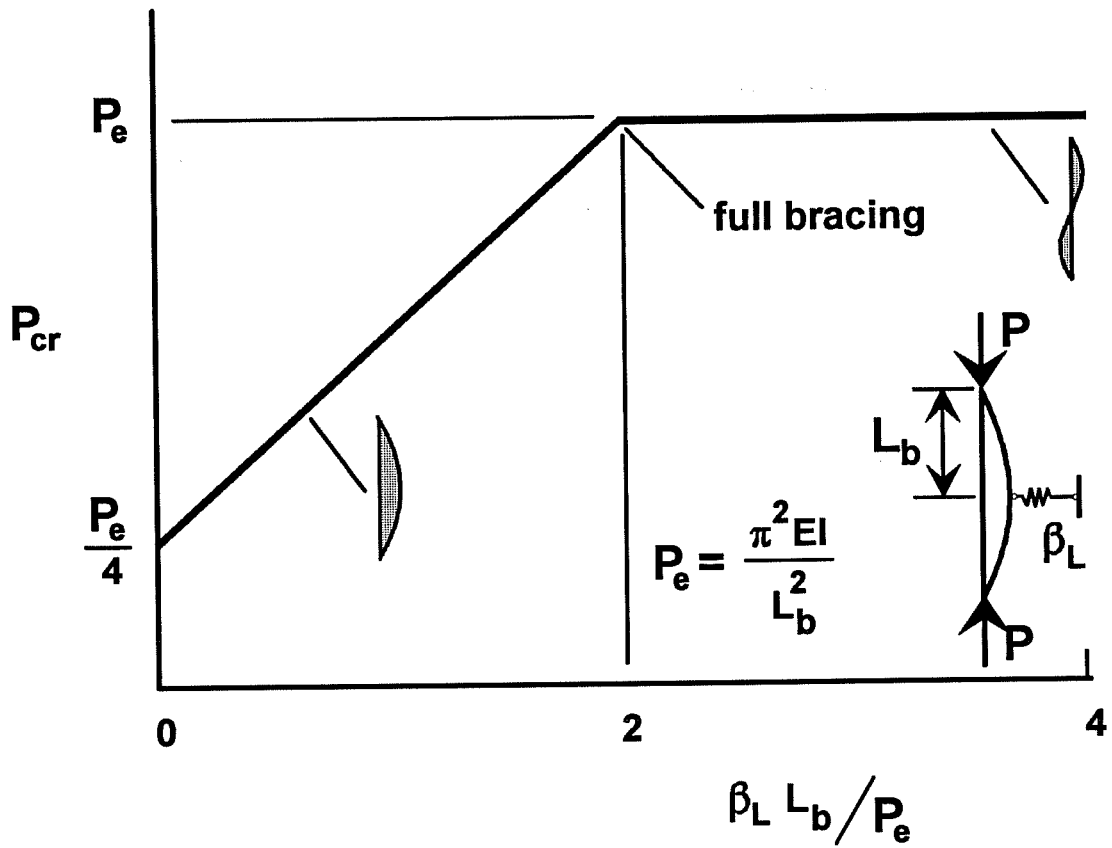
Figure 1.7 Effect of brace stiffness on buckling load.

For this column, $2 P_e / L_b$ would be referred to as the "ideal" brace stiffness for which the brace behaves similar to an immovable support (full bracing) for an initially straight member.

Winter [24] presented a simple method which could be used to establish strength and stiffness requirements for cases with "full bracing". Winter presented a "rigid-link" model in which hinges were placed in the column at brace locations. Brace stiffness requirements were found by satisfying equilibrium on the deflected structure. In addition, brace strength requirements could also be established with Winter's method for a given magnitude of imperfection at the brace location. Figure 1.8a shows a plot of load versus lateral displacement of a column using Winter's method with an initial imperfection at midheight (Δ_0) equal to $L_b/500$ (i.e. $0.002L_b$). The vertical axis has been normalized by P_e, while the total lateral displacement (Δ_T) on the horizontal axis has been normalized by the initial imperfection. With no applied load, $\Delta_T = \Delta_0$.

Figure 1.8a shows that when the ideal brace stiffness, β_i, is employed, extremely large lateral displacements result as the buckling load is approached ($P/P_e = 1$). When a brace with $\beta_L = \beta_i$ is provided, the lateral displacement of the column at a load of $0.95P_e$ is 20 times the magnitude of the initial imperfection. Figure 1.8a does indicate, however, that large displacements can be controlled by providing larger values of the brace stiffness. If twice the "ideal" brace stiffness were employed, at a load $P = P_e$, the total lateral displacement is equal to twice the initial imperfection ($\Delta_T = 2\Delta_0$). If three times the "ideal" brace stiffness were used, the total displacement at a load of $P = P_e$ is only $1.5\Delta_0$.

The brace force is denoted by F_{br}, and can be calculated with the expression $(\Delta_T - \Delta_0)\beta_L$. Figure 1.8b shows a plot of the load versus the resulting brace force for the column under consideration. When a brace with the ideal stiffness is used, the brace forces become very large as the load approaches the buckling capacity. Providing larger values of the brace stiffness reduce the brace forces considerably. If twice the "ideal" stiffness is provided, the brace force at buckling for this problem is 0.8% of P_e. The magnitude of the brace force is linearly dependent on the initial imperfection. If the initial imperfection is doubled, the brace force is also doubled.

In order to check the accuracy of Winter's method, a finite element analysis was conducted on a column with a brace at midheight and an imperfection with a magnitude of $L_b/500$. The shape of the imperfection was a half sine curve. Figures 1.9a and 1.9b show plots of the finite element results. When the Figures 1.9a and 1.9b are compared with the Figures 1.8a and 1.8b, it can be seen that Winter's method is unconservative for this case. For a brace stiffness of $2\beta_i$ and a load of $P = P_e$, Winter's model predicts that the total deflection at the brace is $2\Delta_0$
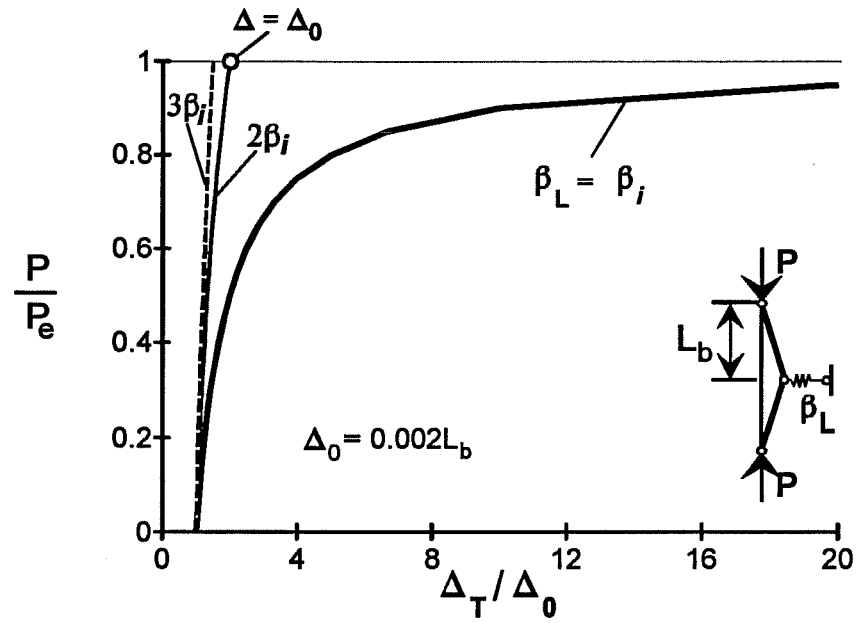
Figure 1.8a Effect of imperfection on braced column behavior.
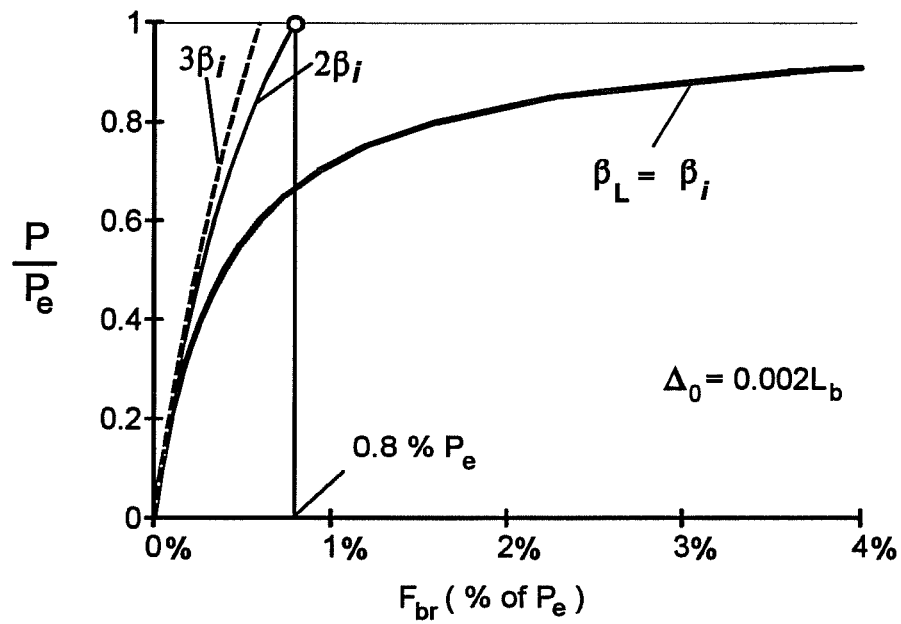
Figure 1.8b Effect of imperfection on brace force.
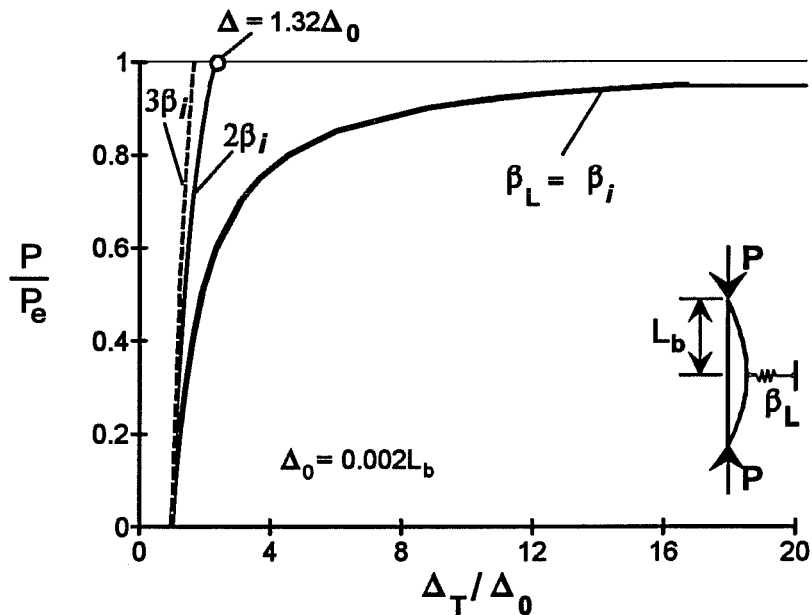
Figure 1.9a Effect of imperfection on braced column behavior.
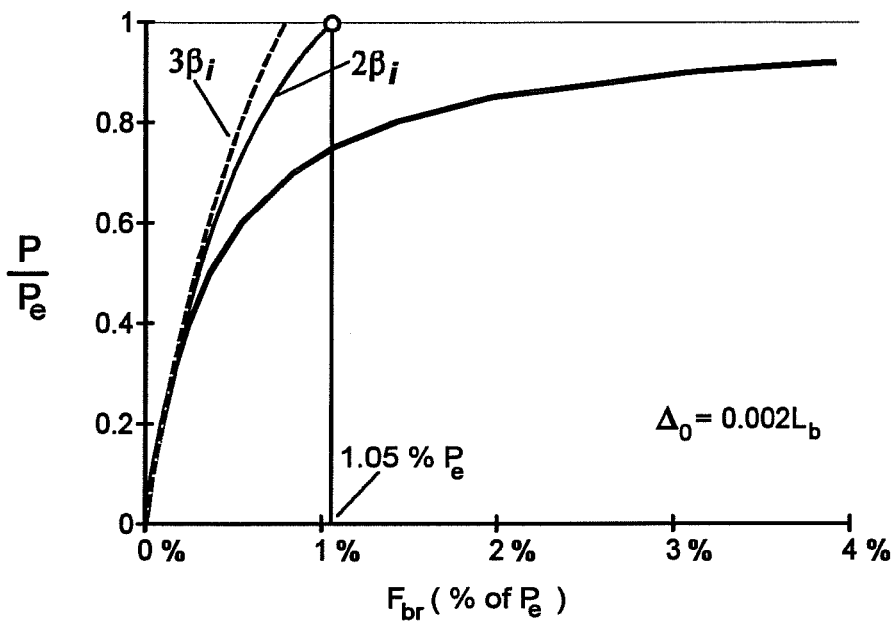
Figure 1.9b Effect of imperfection on brace force.

and a brace force of 0.8% P_e. The ANSYS results, on the other hand, predict that the total displacement would be $2.32\Delta_o$ and that the brace force would be 1.05% P_e. This matches the findings of Plaut [19] who found that the total displacement for this case was $2.33\Delta_o$.

The reason that Winter's method underestimates the displacements at the brace is because by placing a hinge at the brace location, the moment in the model must be zero at this point. In a perfect column, the moment at the brace location would be zero since it would be a point of inflection. When imperfections exist in the column, however, a moment will exist at the brace location. Depending on the shape of the initial imperfection, the displacement in the actual column may be smaller or larger than predicted by Winter's method. For the case of a half sine curve imperfection, actual displacements (and resulting brace forces) are larger than predicted by Winter's method.

While the comparison of the finite element results and the Winter model are interesting, it is more important to gain an understanding of the effect of imperfections on the ability of bracing to restrain the main member. The simple column problem has demonstrated that in order to evaluate the adequacy of a bracing system, it is necessary to consider both stiffness and strength requirements.

Although the bracing of beams is somewhat more complicated than bracing of columns, the basic concepts are the same; beam braces must satisfy both stiffness and strength requirements. The imperfections which increase brace force requirements in beams can result from a number of sources. In addition to the initial twist of the girder, the applied loading may amplify the initial twist. Figure 1.10 shows how loading a twin girder system through the metal deck forms can result in larger initial imperfections. The construction loading resulting from the wet concrete will be applied at an eccentricity to the shear center and result in a torque on the girder for this simple twin girder system.

The majority of this dissertation concentrates on the stiffness requirements for bracing of bridge girders by metal deck forms. The stiffness requirements were obtained by performing eigenvalue analyses on straight girders to obtain bifurcation loads. When transverse loading was applied to the girders in these studies, the load passed through the shear center of the section as shown in Figure 1.11. The results do not include the influence of initial imperfections upon the stiffness required to limit deformation nor the resulting brace forces. While the effects of imperfections are extremely important and must be considered for any effective bracing system,

a) Construction Load   b) Resulting Reactions on Girders
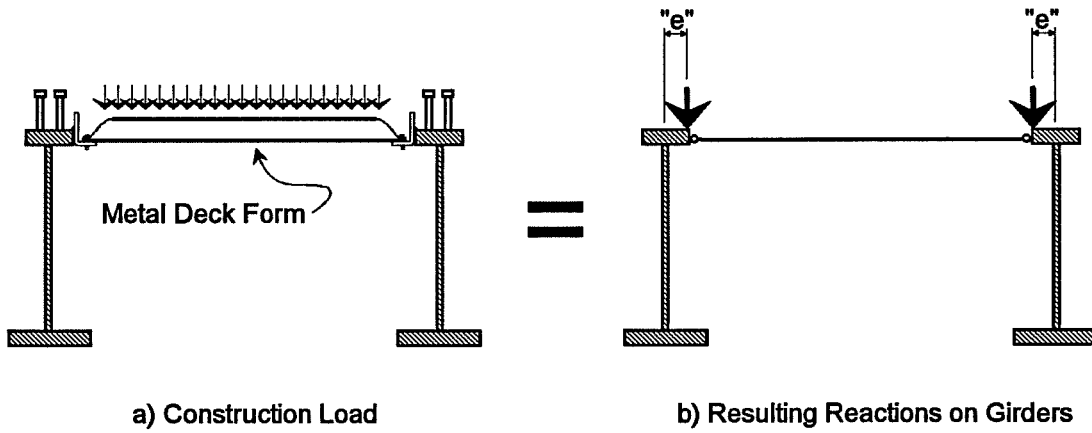
Figure 1.10 Construction load applied to deck results in an eccentric load on girders.
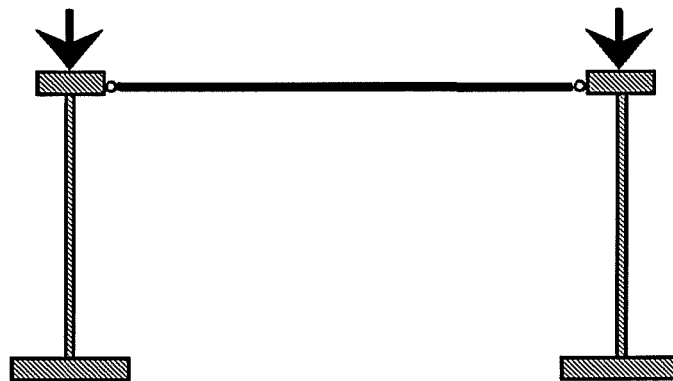
Figure 1.11 Loading for bifurcation analyses.

it was first necessary to establish stiffness requirements for diaphragm braced girders. The effects of imperfections on the lateral displacements and forces in the deck will be touched on in Chapter 9.

1.3 Shear Rigidity of Metal Deck Forms

The parameter which is of interest for bracing of girders by a shear diaphragm is the shear rigidity. The shear rigidity is typically denoted by the variable Q, and is calculated as the product of the effective shear modulus and the tributary width of deck. The effective shear modulus can be found by performing a shear test on the diaphragm as shown in Figure 1.12. The effective shear modulus, G', is defined in the expression:

$$G' = \frac{\tau'}{\gamma} = \frac{\left(\dfrac{P}{b}\right)}{\left(\dfrac{\Delta}{a}\right)} \tag{1.1}$$

G' = effective shear modulus

τ' = effective shear stress

γ = shear strain

P = load applied at the end of testing frame

a = panel width

b = width of deck panel

Δ = deflection at tip of testing frame

For design purposes, it is not practical to require testing of a particular deck to measure the effective shear modulus. The Steel Deck Institute Design Manual [17] contains a series of equations which can be used to calculate the effective shear modulus for a given metal form. Currah [9] showed that these equations produced reasonable estimates of the effective shear modulus for conventional bridge deck forms as long as the terms involving warping of the deck form were ignored.
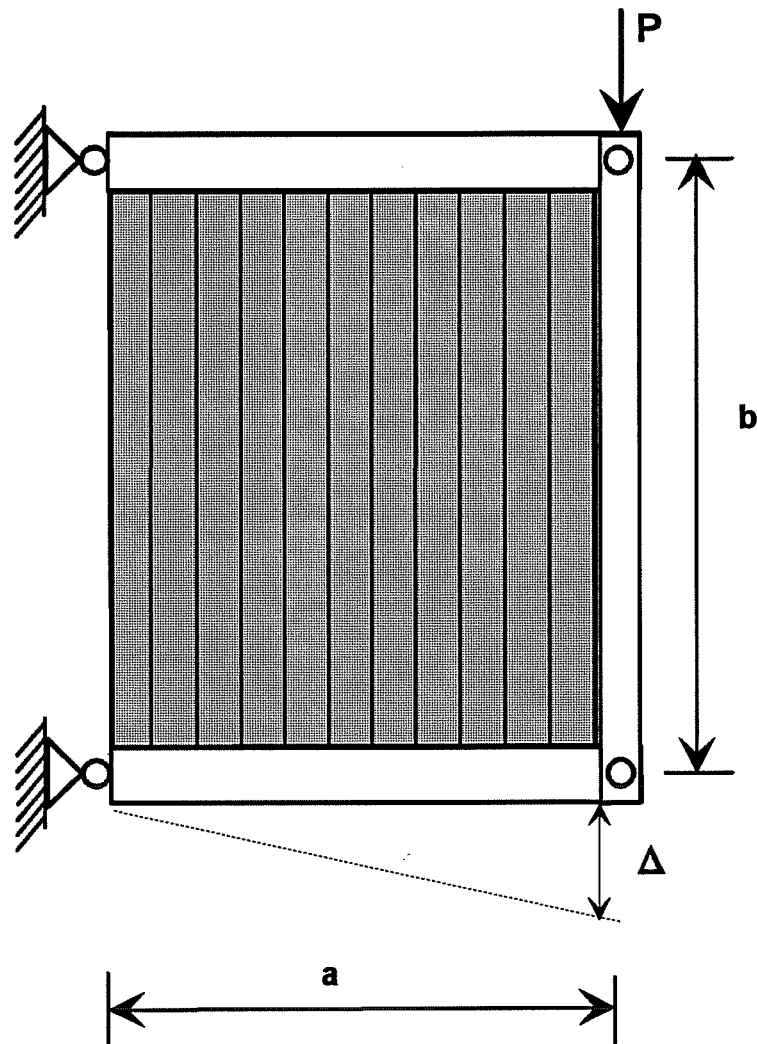
Figure 1.12 Determination of the effective shear modulus of the deck.

The tributary width of deck is assumed equal to the effective width of the deck that is bracing a single girder. In a bridge with "n" girders, "n-1" metal deck forms would typically be used. If the span of the metal decking is "s" the tributary width of the deck for a girder is given by the expression:

$$\text{tributary width} = W = \frac{(n-1)}{n} s \qquad (1.2)$$

The shear rigidity of the metal deck forms can then be calculated using:

$$Q = G' W \qquad (1.3)$$

A research study was conducted at the University of Texas at Austin to determine the ability of Permanent Metal Deck Forms to brace bridge girders during construction of the concrete deck. The research project was sponsored by the American Iron and Steel Institute, the Federal Highway Administration, and the Texas Department of Transportation. The research investigation was divided into two main areas: an experimental study and a computational study. Throughout this dissertation Permanent Steel Bridge Deck Forms will be referred to as deck forms, metal deck forms, or PMDF.

The experimental study involved four different phases of testing:

1) full size shear tests on the metal deck forms,

2) tests on the support angle,

3) full size shear tests on the entire deck assembly (support angle and deck), and

4) full size buckling test on a twin girder system with metal deck forms.

In Section 1.1 it was mentioned that deck forms are supported in the field by a cold formed angle that allows the contractor to adjust the elevation of the form to account for differential camber in adjacent girders. In the first segment of the study, however, the support angle was eliminated from the connection and the deck forms were rigidly attached to the testing frame which was used to apply a shearing distortion to the deck panel. The test results from the initial phase, therefore represented the stiffness of only the deck. Some of the values of the shear rigidity which were measured for the deck are shown in Table 1.1. The metal gage, span, and type of configuration are listed for each type of deck. The nomenclature for the different deck systems are explained in Reference 9. The cross-section of "conventional decking" was shown in Figure 1.2, while "cellular decking" was shown in Figure 1.4.

Table 1.1 Shear Rigidity for Typical Bridge Decking (no support angle)				
Deck	Span (feet - inches)	Metal Gage	Configuration	Shear Rigidity (k/rad)
LSM2224	8' - 11.5"	22	cellular	1129
LSM1716	12' - 10"	17	cellular	3234
LSM1516	12' - 10"	15	cellular	4543
BOS816	10' - 0"	16	conventional	3240
BO8.5P	7' - 8"	16	conventional	4324
BUBF14	8' - 6"	14	conventional	4488

The shear rigidities of the decks in Table 1.1 range from 1129 k/rad for the 22 gage cellular deck to 4543 k/rad for the 15 gage cellular deck. The results from this stage of the study were presented in Reference 9.

The second stage of the experimental program involved testing of the support angle for the deck forms. This phase of the investigation was conducted to measure the relative stiffness of different support conditions. Both existing field details as well as modified details were evaluated in the small scale testing of the support angle. Advice from the deck manufactures and contractors was considered along with the small scale test results in order to select the modified detail that was the most feasible, yet would provide adequate connection stiffness.

Once testing of the support angle was completed, the third stage of the experimental program was conducted. This phase of testing involved performing full size shear tests on the entire deck assembly, which consisted of the deck panel with the support angle. The full size tests to determine the shear stiffness and shear strength of the assembly were conducted on both existing details as well as the modified detail. Based on the support angle testing and the full size tests on the deck and connection systems, Soderberg [21] recommended values for the connection stiffness shown in Table 1.2. The terms "Unstiffened" and "Stiffened" have to deal with modifications that Soderberg studied for stiffening the connection. The results for the small scale

testing of the support angle as well as the full size deck tests on the entire deck assembly are reported in Reference 21.

Table 1.2 Normalized Shear Rigidity of Support Angle Connections	
Unstiffened - Q_{conn} x Deck Span/2	Stiffened - Q_{conn} x Deck Span/2
88000 kip-in/rad	242000 kip-in/rad

In order to determine the shear rigidity of the connection, the values of the normalized connection rigidities in Table 1.2 should be divided by half the span of the deck. The shear rigidity of the system, Q_{sys}, can then be calculated using:

$$\frac{1}{Q_{sys}} = \frac{1}{Q_{deck}} + \frac{1}{Q_{conn}} \qquad (1.4)$$

where:

Q_{deck} = the shear rigidity of deck,

Q_{conn} = the connection shear rigidity.

It should be noted that Q_{sys} must be less than or at best equal to the smallest of either Q_{deck} or Q_{conn}.

Tables 1.3a and 1.3b show the respective shear rigidities for the deck systems with unstiffened and stiffened support angles for the decks presented in Table 1.1. The values of the shear rigidity of the deck systems shown in Table 1.3a with the unstiffened support angle range from 668 k/rad to 1326 k/rad. The corresponding shear rigidities for the stiffened support angles shown in Table 1.3b range from 903 k/rad to 2373 k/rad. The values of the shear rigidities shown in Tables 1.3a and 1.3b are representative of the decks which were tested in the experimental phase of the test program. Based on the range of shear rigidities found in the experimental phase of testing, the range of shear rigidities for the deck system which were used in the computational studies were between 0 k/rad and 1320 k/rad.

Table 1.3a Shear Rigidity for Bridge Deck Systems - Unstiffened Support Angle				
Deck	Span (feet - inches)	Q_{deck} (k/rad)	Q_{conn} (k/rad)	Q_{sys} (k/rad)
LSM2224	8' - 11.5"	1129	1637	668
LSM1716	12' - 10"	3234	1143	844
LSM1516	12' - 10"	4543	1143	913
BOS816	10' - 0"	3240	1467	1010
BO8.5P	7' - 8"	4324	1913	1326
BUBF14	8' - 6"	4488	1725	1246

Table 1.3b Shear Rigidity for Bridge Deck Systems - Stiffened Support Angle				
Deck	Span (feet - inches)	Q_{deck} (k/rad)	Q_{conn} (k/rad)	Q_{sys} (k/rad)
LSM2224	8' - 11.5"	1129	4502	903
LSM1716	12' - 10"	3234	3143	1594
LSM1516	12' - 10"	4543	3143	1858
BOS816	10' - 0"	3240	4033	2005
BO8.5P	7' - 8"	4324	5261	2373
BUBF14	8' - 6"	4488	4745	2306

The final phase of the experimental program involved performing full size buckling tests on a twin girder system. Buckling tests were conducted with and without the metal deck forms in order to measure the bracing effect of the metal decking. Reference 21 also presents the results of the buckling tests.

1.4 Objective and Scope

This dissertation reports the results of the computational study. The computational study in this research project made use of the finite element program ANSYS to perform several eigenvalue analyses on a twin girder system with a shear diaphragm at the top flange. These finite element analyses were conducted to determine the effect of the deck shear rigidity on the buckling capacity of a twin girder system. The finite element results were compared with existing solutions for beams braced by a shear diaphragm. Existing solutions were employed along with new solutions in order to obtain a design approach for simply supported and continuous type girders braced by metal deck forms.

Eigenvalue solutions will produce the stiffness requirements for the bracing system, however, in order to be adequate, a bracing system must also satisfy strength criteria. As outlined in Section 1.2, strength requirements for a brace are significantly effected by imperfections in the main member. Chapter 9 will touch upon the effect of imperfections on the lateral displacements and forces in the deck for girders braced by a shear diaphragm.

This dissertation has been divided into 10 chapters. Chapter 2 will present the background material which is pertinent to lateral-torsional buckling and bracing by shear diaphragms. Chapter 3 will describe the development of the finite element model for the computational study and also outline the parameters which were considered. Chapter 4 presents finite element results for girders without a shear diaphragm for bracing. The finite element results presented in Chapter 4 are compared with existing solutions to account for moment gradients and load-height effects. Finite element results for simply-supported girders with fully stiffened webs and a shear diaphragm for bracing will be presented in Chapters 5 and 6. Chapter 5 presents finite element results which show the effect a shear diaphragm has on the buckling mode of fully stiffened girders, while Chapter 6 shows the effect on the buckling capacity. The finite element results for simply-supported girders with partially-stiffened and unstiffened webs and a shear diaphragm for bracing are presented in Chapter 7. Chapter 8 presents the finite element results for continuous girders with a shear diaphragm at the top flange. Design examples for girders braced by metal deck forms will be presented in Chapter 9, along with a few large-displacement analyses. The final chapter of the dissertation will present the conclusions of the research study.

CHAPTER 2

Background

This chapter presents pertinent background information on lateral torsional buckling as well as an overview of the literature on bracing by shear diaphragms. The solutions which will be presented are for elastic buckling. The material presented on lateral torsional buckling will give the reader a better understanding of the variables which affect the buckling capacity of flexural members. This material is necessary to understand the results presented in later chapters from the computational study as well as the proposed design solutions. Although facets of the behavior of discrete bracing systems will be touched upon, a more in depth study of these systems can be found in Reference 27.

2.1 Lateral Torsional Buckling

The main objective when designing steel beams and girders is to provide adequate strength and stiffness to carry in-plane loads. The type of section which usually results is an I-shaped member which has a large amount of the area located in the flanges. This type of section has a strong-axis stiffness that is often many times greater than the weak-axis stiffness, which makes the section susceptible to lateral torsional buckling. Lateral torsional buckling is a phenomenon which is shown graphically in Figure 2.1 and involves a lateral translation of the compression flange accompanied by a twist of the girder cross-section. If adequate bracing is not provided, the girder may buckle at loads well below the flexural yield strength.

The type of loading which a girder is subjected to has a significant effect on the lateral torsional buckling capacity. The next two sections of this chapter will outline the effect that different types of loading have on the buckling capacity of girders. Buckling solutions for girders subjected to constant moment will be presented in Section 2.2. Section 2.3 will explain how the buckling capacity of girders subjected to moment gradients are calculated, and also how effects of load height are handled. The behavior of discrete bracing systems compared to continuous bracing provided by a shear diaphragm at the top flange will be discussed in Section 2.4. The final section of this chapter will present some of the solutions which have resulted from past studies of bracing provided by shear diaphragms.

P

Δ

P

θ
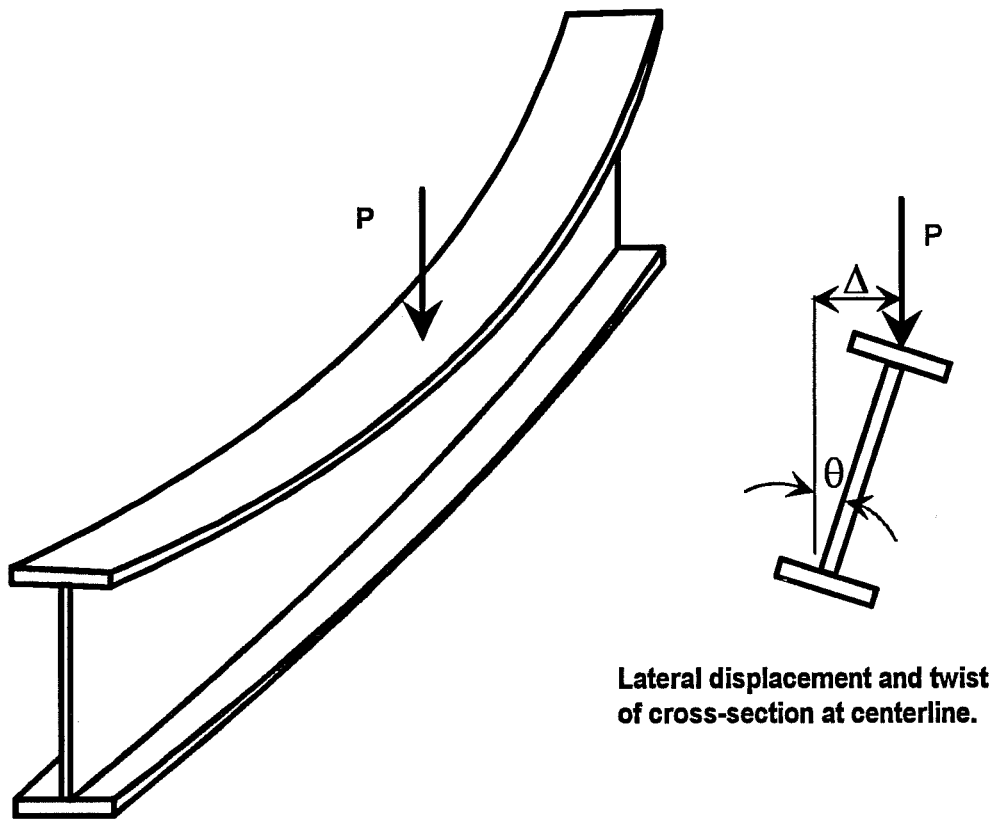
**Lateral displacement and twist
of cross-section at centerline.**

Figure 2.1 Lateral-torsional buckling of simply-supported girder.

2.2 Closed Form Solutions for Constant Moment

Most closed form solutions for lateral torsional buckling have been derived for the uniform state of bending stresses caused by constant moment. Timoshenko [23] derived the following expression for the lateral torsional buckling capacity of doubly-symmetric beams:

$$M_{cr} = \frac{\pi}{L_b} \sqrt{EI_y GJ + \frac{\pi^2 E^2 C_w I_y}{L_b^2}}$$ (2.1)

where:

M_{cr} = buckling moment

L_b = unbraced length

E = modulus of elasticity

I_y = weak-axis moment of inertia

G = shear modulus

J = St. Venant's torsional constant

$C_w = I_y d^2 \rho (1-\rho)$ = warping constant

d = distance between flange centroids

$\rho = I_{yc} / I_y$

I_{yc} = moment of inertia of compression flange about axis through web.

The unbraced length in the equation is the distance between points of full bracing on the girder. For beams, a full brace is a restraint that allows no twist at a point. For a doubly-symmetric section, I_{yc} is equal to $I_y/2$, so the resulting warping constant $C_w = I_y d^2/4$. The above equation can be derived from either the differential equations of bending or by energy methods assuming the twist of the cross-section along the girder length is a sine curve. Timoshenko's equation gives very good estimates of the buckling load for doubly-symmetric sections.

Bridge girders, however, are typically composite sections in which the steel girder and the concrete slab combine to carry in-plane loads. Because of the large compression element present in the deck of the completed bridge, the steel girder for a composite section will usually have a smaller top flange than the bottom flange. Lateral torsional buckling during construction is critical since the steel girder supports the entire construction load. The smaller top flange of the steel

girder gives the section a single plane of symmetry, for which solutions other than Equation 2.1 must be employed.

Equation 2.2a was recommended by Kitipornchai and Trahair [15] for singly-symmetric sections. In order to simplify the equation, the solution has been expressed as a function of a number of variables given by Equations 2.2b, 2.2c, and 2.2d. Since the flanges are different sizes for a singly-symmetric section, the C_w no longer simplifies to $I_y d^2/4$ which was observed for doubly-symmetric sections. When calculating the value of "a" in Equation 2.2b, the expression for the warping constant, C_w, must be taken as $I_y d^2 \rho (1-\rho)$. The value of ρ is given by the ratio I_{yc} /I_y, where I_{yc} is the weak axis moment of inertia of the compression flange. The term B_1 is a variable that accounts for the degree of mono-symmetry and is given by Equation 2.2c. The solution from Kitipornchai and Trahair makes use of another term, β_x, which also deals with the mono-symmetry of the section. Equation 2.2d is used to calculate β_x, where I_x is the strong axis moment of inertia, and y_0 is the distance from the shear center to the centroid and is positive if the shear center is between the centroid and the tension flange.

$$M_{cr} = \frac{\pi}{L} \sqrt{EI_y GJ} \left(B_1 + \sqrt{1 + \frac{\pi^2 a^2}{L^2} + B_1} \right) \qquad (2.2a)$$

$$a = \sqrt{\frac{EC_w}{GJ}} = \sqrt{\left(\frac{E}{GJ}\right)\left(I_y d^2 (\rho(1-\rho))\right)} \qquad (2.2b)$$

$$B_1 = \frac{\pi}{2} \frac{\beta_x}{L} \sqrt{\frac{EI_y}{GJ}} \qquad (2.2c)$$

$$\beta_x = \frac{1}{I_x} \int_{dA} y(x^2 + y^2)\, dA - 2y_0 \qquad (2.2d)$$

Equations 2.2a-2.2d are a complicated series of expressions to predict the buckling capacity of singly-symmetric sections and, therefore, several approximate equations have been derived which are easier to use.

Equation 2.3a shows the approximate solution recommended for singly-symmetric sections in the American Institute of Steel Construction (AISC) specification [3]. This equation is actually just a simplified version of Equation 2.2a-2.2d. Equations 2.3b and 2.3c define the variables B_1 and B_2 which are used in Equation 2.3a.

$$M_{cr} = \frac{\pi}{L_b} \sqrt{EI_y GJ} \left(B_1 + \sqrt{(1 + B_2 + B_1^2)} \right) \qquad (2.3a)$$

$$B_1 = 2.25(2\rho - 1)\left(\frac{d}{L_b}\right)\sqrt{\frac{I_y}{J}} \qquad (2.3b)$$

$$B_2 = 25 (1 - \rho)\left(\frac{I_{yc}}{J}\right)\left(\frac{d}{L_b}\right)^2 \qquad (2.3c)$$

The variables which are used in the AISC equations have the same definition as previously defined for Equation 2.2.

The equation in the AASHTO Specification [1] for lateral torsional buckling is just a modified version of Timoshenko's solution to handle singly-symmetric sections and is given in the following expression:

$$M_{cr} = \pi E \left(\frac{I_{yc}}{L_b}\right)\sqrt{\frac{2G}{E}\left(\frac{J}{I_{yc}}\right) + \pi^2 \left(\frac{d}{L_b}\right)^2} \qquad (2.4)$$

The variables which appear in Equation 2.4 have the same definition as defined for Equations 2.1-2.3 with the exception of the variable "d". The variable "d" in the AASHTO Specification is defined as the overall girder depth, while in Equations 2.1-2.3 "d" is taken as the distance between flange centroids. Throughout this dissertation, the value of "d" which will be used in the AASHTO equation for lateral-torsional buckling will be taken as the distance between flange centroids. The

actual definition of "d" in the AASHTO Specification will produce results which are slightly more unconservative, however, the difference should be relatively small for most cases. It should be noted that Equation 2.3a and 2.4 appear slightly different in the specifications because numerical values for π, E = 29000000 psi., and G = 11800000 psi. have been substituted.

A comparison of the equations has been made for the sections shown in Figure 2.2. Sections #1 and #2 are doubly-symmetric sections, while section #3 is a singly-symmetric section with flange sizes equal to the extreme values of the two doubly-symmetric sections. The ratio of I_{yc}/I_y (ρ) for section #3 is 0.167. This is close to the minimum value of 0.1 which is permitted for bridge girders by the AASHTO Specification [1]. The sections in Figure 2.2 were used extensively in the finite element analyses performed in this study. Although the majority of the results from the finite element studies will be presented in Chapters 4 through 9, some of the finite element results will be presented in this chapter to compare with the predictions from the published solutions.

Tables 2.1 and 2.2 show comparisons of results using Equations 2.1 through 2.4 for the respective sections #1 and #2 which are the doubly-symmetric sections. In addition to the buckling moment predictions using the published solutions, finite element results have also been tabulated for each of the cases. The finite element program ANSYS [5] was used to perform the analyses. Below each of the estimates from Equations 2.1, 2.2a, 2.3a, and 2.4, the percent difference with respect to the ANSYS solution is shown in parenthesis. A positive percentage indicates that the equation is conservative with respect to the finite element results, while a negative percentage indicates that the equation predicts a larger buckling load than the finite element solution. For doubly-symmetric sections, Equation 2.2 from Kitipornchai and Trahair [15] gives the exact same answer as Timoshenko's solution. For the doubly-symmetric sections, all of the equations give very good estimates of the buckling load with respect to the finite element results.

It should be noted that if the definition for "d" in the AASHTO equation for lateral-torsional buckling was taken as it is defined in the specification (over-all girder depth), the percent difference between the equation and the ANSYS results would be 2.2%, 1.6% and 1.8% for lengths of 25, 50, and 75 feet, respectively. Similar differences were observed for sections #2 and #3 when the actual definition of the "d" from the AASHTO Specification were used.
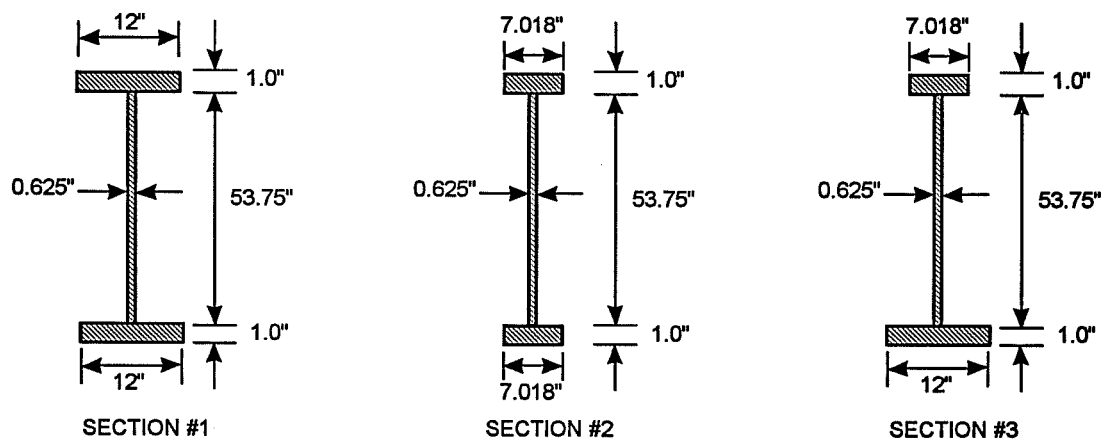
Figure 2.2 Cross-sections for comparison of closed form solutions.

Table 2.1 Section #1					
Unbraced Length (feet)	Timoshenko Equation 2.1	Kit. & Trahair Equation 2.2a	AISC LRFD Equation 2.3a	AASHTO Equation 2.4	ANSYS Results for Constant Moment
25	27478 k-in. (-0.8%)	27478 k-in. (-0.8%)	27422 k-in. (-0.6%)	27455 k-in. (-0.7%)	27266 k-in.
50	8420 k-in. (-0.6%)	8420 k-in. (-0.6%)	8433 k-in. (-0.8%)	8417 k-in. (-0.6%)	8368 k-in.
75	4670 k-in. (-1.1%)	4670 k-in. (-1.1%)	4689 k-in. (-1.5%)	4670 k-in. (-1.1%)	4618 k-in.

Table 2.2 Section #2					
Unbraced Length (feet)	Timoshenko Equation 2.1	Kit. & Trahair Equation 2.2a	AISC LRFD Equation 2.3a	AASHTO Equation 2.4	ANSYS Results for Constant Moment
25	6606 k-in. (1.8%)	6606 k-in. (1.8%)	6615 k-in. (1.6%)	6603 k-in. (1.8%)	6726 k-in.
50	2489 k-in. (2.2%)	2489 k-in. (2.2%)	2503 k-in. (1.6%)	2490 k-in. (2.1%)	2544 k-in.
75	1538 k-in. (0%)	1538 k-in. (0%)	1549 k-in. (-0.7%)	1539 k-in. (-0.1%)	1538 k-in.

Tables 2.3 and 2.4 show comparisons of results using Equations 2.1-2.4 for the singly-symmetric section #3. In Table 2.3 the small flange is in compression, while in Table 2.4 the

larger flange is in compression. Although Timoshenko's solution is not applicable for singly-symmetric sections, estimates for the buckling load of section #3 have been tabulated. Timoshenko's solution produces unconservative estimates of the buckling load when the small flange is in compression, and conservative estimates when the larger flange is in compression. The large percent difference between Timoshenko's solution and the finite element results clearly demonstrates why a different solution is required for singly-symmetric sections.

The solution by Kitipornchai and Trahair's produced estimates of the buckling load which agreed very well with the finite element results. The AISC equation was slightly unconservative with respect to the finite element results when the small flange is in compression and conservative when the larger flange is in compression, however the equation produced very good estimates of the buckling load.

The AASHTO expression was conservative with respect to the ANSYS results when the small flange was in compression and unconservative when the larger flange was in compression. The AASHTO expression was quite conservative when the small flange was in compression, particularly for the longer span lengths. When the larger flange was in compression, the AASHTO equation prediction was closer to the finite element studies. Although the predictions with the AASHTO expression did not agree as well as the other expressions with the singly-symmetric sections, the equation is significantly easier to use.

Table 2.3 Section #3 - Small Compression Flange					
Unbraced Length (feet)	Timoshenko Equation 2.1	Kit. & Trahair Equation 2.2a	AISC LRFD Equation 2.3a	AASHTO Equation 2.4	ANSYS Results for Constant Moment
25	16104 k-in. (-120.8%)	7288 k-in. (0.1%)	7513 k-in. (-3.0%)	6856 k-in. (6.0%)	7293 k-in.
50	5341 k-in. (-70.4%)	3096 k-in. (1.2%)	3189 k-in. (-1.7%)	2655 k-in. (15.3%)	3135 k-in.
75	3112 k-in. (-47.6%)	2102 k-in. (0.3%)	2158 k-in. (-2.3%)	1657 k-in. (21.4%)	2109 k-in.

Table 2.4 Section #3 - Big Compression Flange					
Unbraced Length (feet)	Timoshenko Equation 2.1	Kit. & Trahair Equation 2.2a	AISC LRFD Equation 2.3a	AASHTO Equation 2.4	ANSYS Results for Constant Moment
25	16104 k-in. (38.9%)	26261 (0.3%)	25488 (3.1%)	27144 (-3.36%)	26339 k-in.
50	5341 k-in. (32.0%)	7840 (0.2%)	7683 (2.2%)	8161 (-3.9%)	7854 k-in.
75	3112 k-in. (26.3%)	4210 (0.3%)	4155 (1.6%)	4463 (-5.7%)	4221 k-in.

2.3 Effects of Moment Gradient and Load Height

The solutions presented in Section 2.2 are for beams subjected to constant moment. When beams are subjected to loadings which cause a moment gradient, the buckling capacity may be substantially larger than predicted by those equations. Variable moment along the girder length is accounted for with a C_b factor. The moment gradient is usually caused by transverse loads. The fourth edition of the Structural Stability Research Council (SSRC) guide [13] defines the C_b value as the moment magnifier for transverse loading applied at the shear center. For doubly symmetric beams, the shear center lies at midheight of the section, whereas on singly-symmetric sections the shear center lies above or below midheight depending on the relative flange sizes.

The equations presented in Section 2.2 are often presented with a C_b factor. In the AASHTO specification for the value for C_b is given by the following expression:

$$C_b = 1.75 + 1.05 \left(\frac{M_1}{M_2}\right) + 0.3 \left(\frac{M_1}{M_2}\right)^2 \leq 2.3 \qquad (2.5)$$

M_1 and M_2 are the respective smaller and larger end moments in the unbraced beam segment under consideration. The ratio of M_1 to M_2 is taken as positive when double curvature results and

negative for single curvature. This equation is somewhat restricted, however, since it is only valid for cases in which there is no applied loading between brace points. When the moment between the supports is greater than one of the end moments, AASHTO suggests using C_b = 1.0 but allows larger values to be used by consulting the SSRC guide.

The AISC Specification [3] uses the following expression for C_b for a girder buckling between points of full bracing (cross-frames):

$$C_b = \frac{12.5 M_{max}}{2.5 M_{max} + 3M_2 + 4M_{cl} + 3M_4}$$ (2.6)

where:

M_{max} is the maximum moment between full braces,

M_2 is the moment at the quarter point between full braces,

M_{cl} is the moment at midway between full braces, and

M_4 is the moment at the three quarters point between full braces.

The absolute value is used for all of the moments in Equation 2.6 and the expression is valid for any shape moment diagram. An expression similar to Equation 2.6 was first presented by Kirby and Nethercot, however, the expression was modified by Yura to produce better estimates. In future chapters, Equation 2.6 will be referred to as the "modified Kirby-Nethercot" equation.

For a girder subjected to a moment gradient, the buckling capacity is calculated as the product of the corresponding C_b value and the buckling moment predicted by one of the lateral-torsional buckling formulas for constant moment. Some of the C_b values are tabulated in Figure 2.3 for a few common load cases. Equation 2.5 is not valid for the load cases shown in Figure 2.3 since loading is applied between the brace points. Equation 2.6 agrees well with the corresponding values of C_b recommended in the SSRC guide. Referring to Figure 2.3, if a girder is subjected to a point load at midspan, Equation 2.6 would predict a C_b value of 1.32 which indicates a buckling moment 32 percent higher than the buckling moment for the same girder subjected to a constant moment. If the girder were subjected to a distributed load, the equation would lead to an estimate of the buckling moment 14 percent higher than for the same girder subjected to a constant moment.

Lateral-torsional buckling involves a lateral movement of the girder and a simultaneous twist about the shear center. Under transverse loading, the height of the application of the load

Case	Moment Diagram	SSRC Guide	Eqn. 2.6
Constant Moment		1.00	1.00
Point Load @ Midspan		1.35	1.32
Uniform Distributed Load		1.12	1.14

Figure 2.3 Typical C_b values.

has a significant effect on the buckling capacity. For example, compared to loading applied at midheight, transverse loads applied at the top flange cause an overturning torque that "drives" the girder laterally, while loads applied at the bottom flange provide a stabilizing effect. The effects of load height on the buckling capacity are shown in Figure 2.4 which presents finite element results for section #1 with a transverse point load applied at midspan. The graph is a plot of the buckling moment at midspan versus the girder span for a transverse load applied at the bottom flange, midheight and the top flange. The curves show that the height of transverse loading has a significant effect on the buckling moment. As the span of the girders increases, the effect of load height becomes less significant.

The fourth edition of the SSRC guide [13] has tabulated factors that can be used to account for load height effects in doubly-symmetric beams by modifying the C_b factor. The modified C_b value for load height will be referred to as C_b^*. The method in the SSRC guide uses different combinations of two variables, A and B, to account for load height effects. The variable "A" is defined as the traditional C_b value: the SSRC guide recommends values of 1.35 for a point load at midspan and 1.13 for a uniform distributed load. The variable "B" is dependent on the type of loading and the warping stiffness of the cross-section. For the two basic load cases of a point load at midspan, and a uniform distributed load, the SSRC Guide uses the following two expressions for the variable "B":

Point Load at Midspan: $\quad B = 1 - 0.180W^2 + 0.649W$

Uniform Distributed Load: $\quad B = 1 - 0.154W^2 + 0.535W$

The coefficient W is sometimes referred to as the beam parameter and is given by:

$$W = \frac{\pi}{L} \sqrt{\frac{E\, C_w}{G\, J}} \qquad (2.7)$$

where:

L is the distance between discrete braces,

E is the modulus of elasticity,

C_w is the warping coefficient,

G is the shear modulus, and

J is the St. Venant torsional constant.
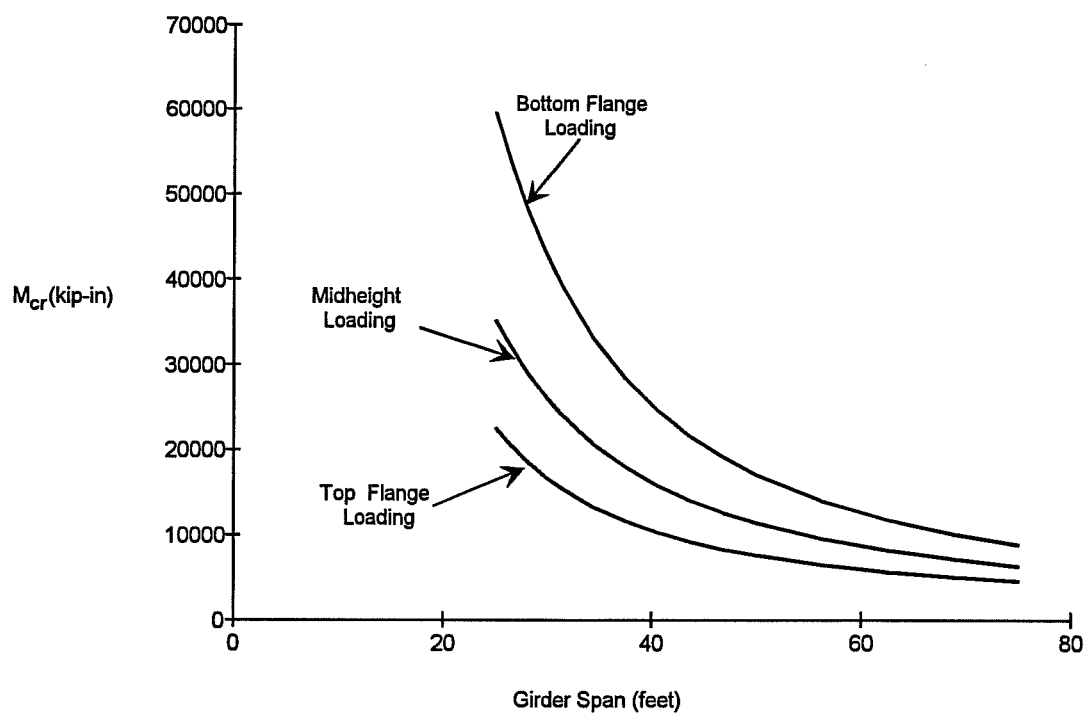
Figure 2.4 M_{cr} vs. girder span for section #1 with a point load applied at variable load heights.

Depending on load height, the SSRC guide uses the following definitions for C_b^* :

Top flange loading:	C_b^*	$=$	A/B	$=$	C_b/B
Load at shear center:	C_b^*	$=$	A	$=$	C_b
Bottom flange loading:	C_b^*	$=$	AB	$=$	$C_b B$.

In order to get a better understanding of the equations in the SSRC Guide it is worthwhile to consider how B and C_b^* vary with the beam parameter, W. Figure 2.5 shows a plot of how B varies with the beam parameter, W. By considering the equations for B, the abscissa of the maximum on the curve can be found by differentiating with respect to W and setting the expression equal to zero, as follows:

$$dB/dW = -0.360W + 0.649 = 0 \quad : \quad W = 1.803 \quad \text{point load at midspan}$$

$$dB/dW = -0.308W + 0.535 = 0 \quad : \quad W = 1.737 \quad \text{distributed loading}$$

The effect on C_b^* for top flange loading and bottom flange loading can be seen in Figures 2.6a and 2.6b, respectively.

Unless the equation is altered errors will be encountered; however, very large errors could be avoided by putting a limit on the equation such as the following:

$$\text{If } W \geq 1.75 : \qquad B = 1.585 \qquad \text{point load @ midspan}$$

$$B = 1.464 \qquad \text{distributed load}$$

These values for B were arrived at by putting in the limiting values of W for which the B - W plot has zero slope, back into the equations for B. The resulting limiting values for C_b^* for top and bottom loading are given in the Table 2.5. These are the minimum value of C_b^* for top flange loading, and the maximum value for bottom flange loading.

Table 2.5 Limiting values of C_b^* from SSRC Guide (4th Edition) Equations [13]		
	C_b^* Top Flange Loading	C_b^* Bottom Flange Loading
Point Load @ Midspan	0.85	2.14
Distributed Load	0.76	1.64

Tables 2.6a and 2.6b show the values for W and B for the two doubly-symmetric sections 1 and 2 (shown previously in Figure 2.2) for the respective cases of a point load at midspan and a uniform distributed load. As the variable 'B' approaches 1, the effects of load height become
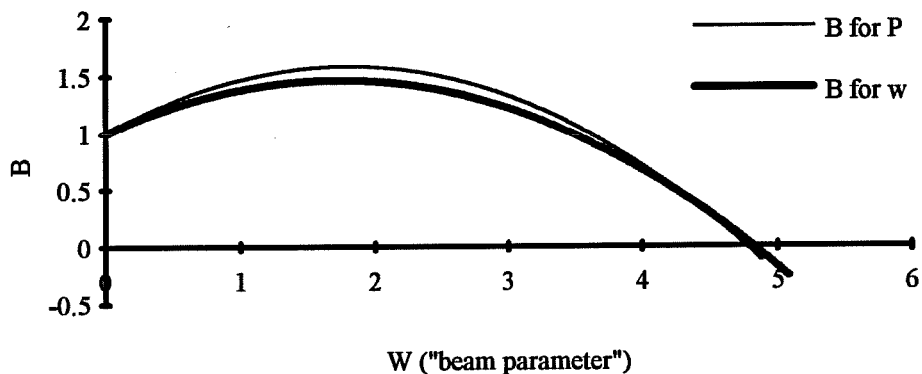
Figure 2.5 Variation of B for SSRC Method with W, the "beam parameter".
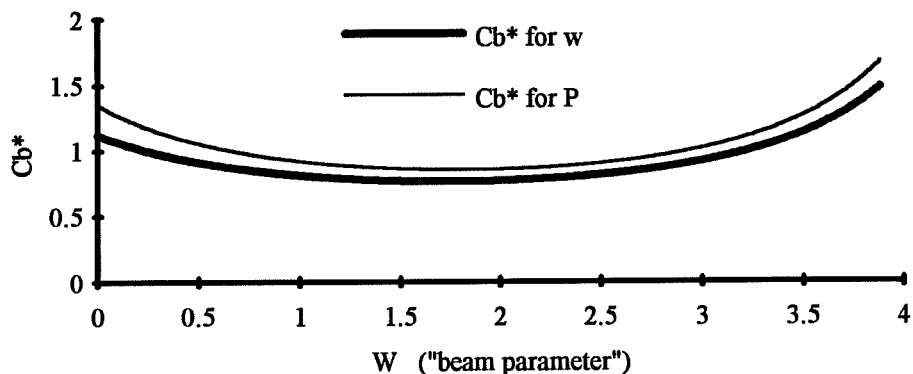
Figure 2.6a Variation of Cb*top with W, for distributed and point loads.
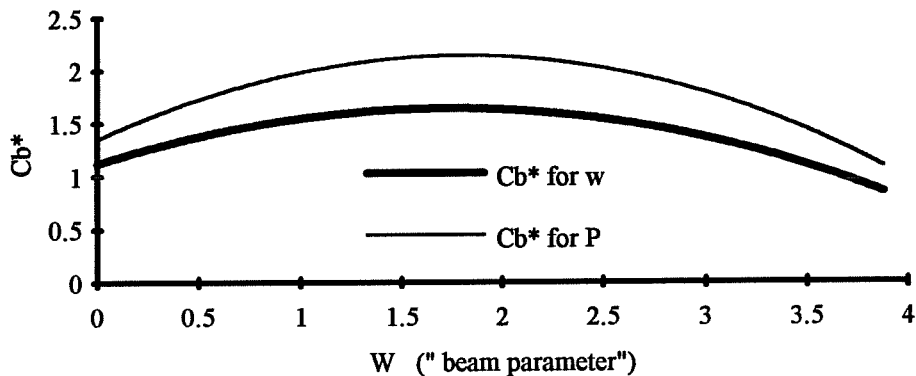
Figure 2.6b Variation of Cb*bottom with W, for distributed and point loads.

less significant. The two tables show that for a given length and girder cross-section, the equations predict that load height effects will be more significant for a point load at midspan than for a distributed load.

Table 2.6a Point Load at Midspan				
	Section #1		Section #2	
Length	W	B	W	B
25 feet	2.23 (>1.75)	1.55 (1.585)	1.17	1.51
50 feet	1.12	1.50	0.58	1.32
75 feet	0.74	1.38	0.39	1.22

Table 2.6b Uniform Distributed Load				
	Section #1		Section #2	
Length	W	B	W	B
25 feet	2.23 (>1.75)	1.43 (1.464)	1.17	1.42
50 feet	1.12	1.41	0.58	1.26
75 feet	0.74	1.31	0.39	1.18

For section #1 with a 25 foot span, it should be noted that the beam parameter, W, exceeds the value of 1.75 so that the limiting values of B would be employed. These values have been shown in parentheses in Tables 2.6a and 2.6b.

Tables 2.7a and 2.7b show values of C_b^* for top and bottom flange loading for the respective load cases of a point load at midspan and a uniform distributed load. As the girders get longer the effects of load height become less significant. This is shown as an increase in C_b^* for top flange loading and a reduction for bottom flange loading. Recalling that the beam

parameter value W had exceeded 1.75 for section #1 with a 25 foot span, the limiting values of C_b^* have been shown in parentheses in Table 2.7a and 2.7b.

Table 2.7a C_b^* for a Point Load at Midspan				
	Section #1		Section #2	
Length	C_b^* TOP	C_b^* BOT	C_b^* TOP	C_b^* BOT
25 feet	0.87 (0.85)	2.09 (2.14)	0.89	2.04
50 feet	0.90	2.02	1.02	1.78
75 feet	0.98	1.86	1.11	1.65

Table 2.7b C_b^* for a Distributed Load				
	Section #1		Section #2	
Length	C_b^* TOP	C_b^* BOT	C_b^* TOP	C_b^* BOT
25 feet	0.78 (0.76)	1.60 (1.64)	0.79	1.58
50 feet	0.79	1.58	0.89	1.41
75 feet	0.85	1.47	0.95	1.32

The method for accounting for load height effects in the third edition of the SSRC Guide [14] is different than in the fourth edition which was outlined above. In order to account for load height effects, the following equation is employed in the third edition of the SSRC Guide:

$$M_{cr} = \frac{C_1 \pi^2 EI_y d}{2(KL)^2} \left[\sqrt{1 + C_2^2 + \frac{(KL)^2 GJ}{\pi^2 EC_w}} \pm C_2 \right] \qquad (2.8)$$

where:

C_1 = the factor for moment gradient (C_b),

E = modulus of elasticity of beam material,

I_y = weak-axis moment of inertia,

d = depth of cross-section (taken as distance between flange centriods),

K = effective length factor for weak-axis bending,

L = girder span,

G = shear modulus of beam material,

J = torsional constant,

C_w = warping constant, and

C_2 = coefficient to account for load height.

The C_2 value which accounts for load height effects is taken as 0.45 for a distributed load and 0.55 for a point load at midspan. The plus or minus sign in front of the C_2 within the brackets is dependent on the load height. If the load is applied at the bottom flange, the C_2 is added to the term in brackets, while the C_2 is subtracted if the load is applied at the top flange.

Yura [27] has suggested that load height effects from top flange loading can be estimated if the warping term is neglected in the closed formed equations. The warping term in Timoshenko's solution in Equation 2.1 is the term with the C_w. In order to estimate the buckling capacity for top flange loading, the warping term would be neglected and the equation would be multiplied by the appropriate C_b value. The resulting expression is shown as follows:

$$M_{cr \; TopFlangeLoading} = C_b \; \frac{\pi}{L_b} \sqrt{EI_y GJ} \qquad (2.9)$$

Equation 2.9 will be compared with finite element results in Chapter 4, along with the SSRC equations for load height.

For singly-symmetric sections, the SSRC guide does not directly address the effects of load height, but refers to approximate solutions in the literature from Clark and Hill [8] as well as Anderson and Trahair [4]. Clark and Hill have presented a very complicated nomograph that is valid for both doubly-symmetric and singly-symmetric sections. In order to check the accuracy of the nomograph, the doubly-symmetric section #2 was considered with a 25 foot length. For constant moment, the nomograph gave an estimate of 6440 kip-in which is close to the ANSYS buckling moment of 6726 kip-in which was previously shown in Table 2.2. When top flange loading was considered on section #2 with an unbraced length of 25 feet, the nomograph predicted a buckling moment of 8425 kip-in. This is significantly higher than the value from the finite

element analysis which was 6045 k-in. A value of C_b^* can be calculated by dividing by the buckling moment from ANSYS for constant moment (6726 k-in from Table 2.2):

$$C_b^* = 8425 \, / \, 6726 = 1.25$$

This is significantly larger than the C_b^* predicted by the SSRC method in Table 2.7a which was 0.89. There is a large possibility for human error using the nomograph. In addition, the nomograph is limited to unbraced lengths less than 500 inches, and the values of Kl/r are limited to values less than 190. The value of Kl/r for the top flange loading for the example considered above had to be estimated at 210 since it actually was off the scale of the chart.

The paper by Anderson and Trahair presented a table which makes use of 3 different parameters: δ, K, and ϵ which are used to determine either γ_P or γ_W. The parameters γ_P or γ_W are used to find the respective buckling loads P or w depending on whether the load consisted of a point load at midspan or a distributed load. The variables are given in Equations 2.10a-2.10e.

$$\delta = \frac{\beta_x}{L} \sqrt{\frac{EI_y}{GJ}} \tag{2.10a}$$

$$K = \sqrt{\frac{\pi^2 EC_w}{GJL^2}} \tag{2.10b}$$

$$\epsilon = \frac{a^*}{L} \sqrt{\frac{EI_y}{GJ}} \tag{2.10c}$$

$$\gamma_P = \frac{PL^2}{\sqrt{EI_y GJ}} \tag{2.10d}$$

$$\gamma_W = \frac{WL^3}{\sqrt{EI_y GJ}} \qquad (2.10e)$$

The variable δ is the mono-symmetry parameter, which is a measure of the difference in flange sizes. The torsional stiffness of the section is indicated by the variable K. The variable ϵ is a measure of the load height with the variable a^* equal to the distance above the shear center that the load is applied. The variables γ_P or γ_W are related to the type of loading: a point load (P) at midspan, or a distributed load (w). By using the three variables δ, K, and ϵ, and using linear interpolation, the tables generate γ_P or γ_W so that the buckling load (P or w) can be found. In order to find γ_P or γ_W, the designer must perform 6 different stages of linear interpolation with the 3 parameters δ, K, and ϵ.

Considering section #2 with a 25 foot length and a midspan point load at the midheight, the tables estimate the buckling load at 9141 kip-in. This is only 0.7 percent different from the value of 9080 kip-in which was found using the finite element program ANSYS. Using the buckling capacity for constant moment from the ANSYS solution as a base (6726 k-in) the resulting C_b can be calculated as follows:

$$C_b = 9141 / 6726 = 1.36$$

This is close to the recommended value of 1.35 in the SSRC guide (1.32 resulted from the modified Kirby-Nethercot formula).

Considering top flange loading on the same girder, the bucking moment was estimated at 5292 kip-in using the tables in Anderson and Trahair's paper. The ANSYS buckling moment for top flange loading was 6045 kip-in which yields a 12 percent difference. The resulting value of C_b^* is calculated as follows:

$$C_b^* = 5292 / 6726 = 0.79$$

This is smaller than the value of 0.89 (Table 2.7a) which was predicted using the method in the SSRC guide.

The tables in the Anderson and Trahair paper were used to predict the buckling load for top flange loading on the singly-symmetric section #3 which was shown in Figure 2.2. Girder lengths of 50 and 75 feet were used. An attempt was made to use a length of 25 feet, however the values of δ and ϵ were out of the range of the table. The resulting values of P and w which were estimated are shown in Table 2.8. In addition, the corresponding values from ANSYS are

also tabulated. The tables from the Anderson and Trahair paper do a relatively good job of accounting of load height effects, however, the tables are not very practical for design.

Table 2.8 Anderson and Trahair Estimates for Top Flange Loading on Section #3				
LENGTH	Anderson and Trahair P_{cr} Top Flange Loading	ANSYS P_{cr} Top Flange Loading	Anderson and Trahair w_{cr} Top Flange Loading	ANSYS w_{cr} Top Flange Loading
50 feet	17.8 kips (10.1%)	19.8 kips	51.1 lb/in (12.9%)	58.7 lb/in
75 feet	9.7 kips (3.1%)	9.4 kips	19.3 lb/in (-3.8%)	18.6 lb/in

The methods of accounting for load height which have been presented are for simply-supported girders with no bracing between the supports. Figure 2.7 shows the moment diagram which would result if braces were placed at the third points of a girder subjected to a point load at midspan. In this case, effects of load height should not be too severe since 66% of the moment which causes buckling is present at the ends of the unbraced length. In addition, the exterior thirds of the girder would provide some warping restraint to the middle third of the girder which should increase the buckling capacity of the girder.

Dux and Kitipornchai [10] presented results for beams with two intermediate braces and a distributed load applied at variable load height. The beams which were used in the studies presented by Dux and Kitipornchai had a beam parameter, W (Equation 2.7), equal to 1.0. Dux and Kitipornchai found that beams with top flange loading experienced a larger relative increase in the buckling load when intermediate bracing was introduced compared to beams with loading at the shear center or at the bottom flange when intermediate bracing was introduced.

The accuracy of the SSRC method for considering load height effects on unbraced girders will be checked with respect to the ANSYS [5] results for doubly-symmetric and singly-symmetric sections in Chapter 4. Finite element results which demonstrate the effect of load height on girders with intermediate braces will also be presented in Chapter 4.
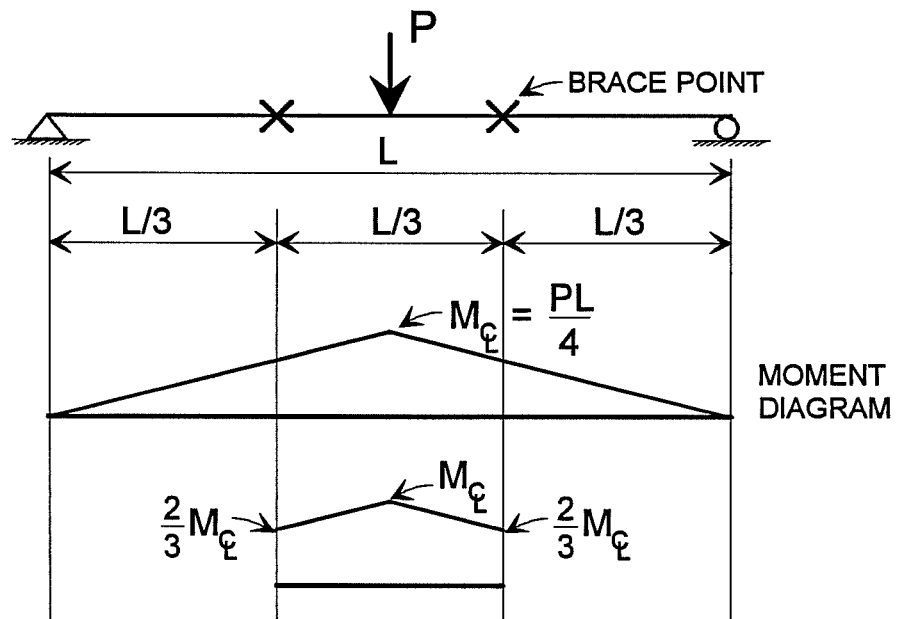
Figure 2.7 Moment diagram for a simple span subjected to a centerline point load.
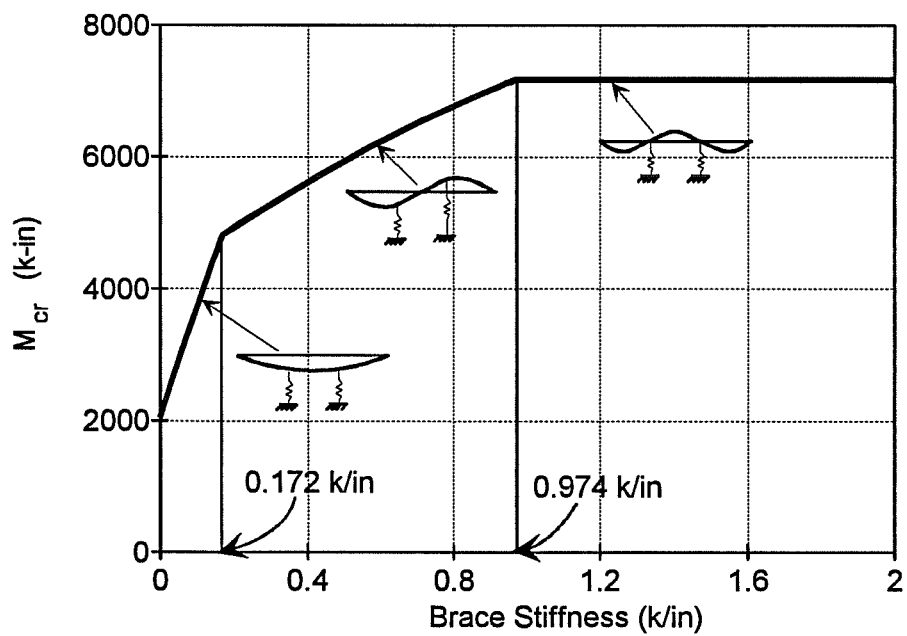
Figure 2.8 Effect of discrete brace stiffness on buckling moment.

2.4 Discrete and Continuous Bracing Systems

The buckling capacity of slender beams can be significantly increased by providing bracing. Bracing can be provided from many sources, however, it will generally fit into one of the two following categories:

1) discrete bracing, or

2) continuous bracing.

Yura has conducted an in depth study of "discrete" bracing, i.e. braces that restrain a member at a single point [26]. The purpose of this section is to distinguish the behavior of continuous bracing by metal deck forms compared to discrete bracing systems.

When discrete braces are used, the mode shape of the buckled girder is dependent upon the brace stiffness. Figure 2.8 shows a plot of the buckling moment versus the brace stiffness for the doubly-symmetric section #2 which was shown in Figure 2.2. The girder is 75 feet long and is restrained by discrete braces at the third points. The discrete braces consist of lateral springs at the top flange. The girder is subjected to constant moment.

For relatively low values of the brace stiffness, the buckled shape of the girder resembles a half sine curve. The mode changes into that of a full sine curve at a brace stiffness of 0.172 k/in. With the change in mode shape, the braces become less effective which results in a reduction in the slope of the curve. There is another change in mode shapes at a stiffness of 0.974 k/in. This would be referred to as the "ideal" brace stiffness, because the brace behaves like an immoveable support, and buckling occurs between the braces. The analysis which was performed on the discrete bracing system, however, does not reflect the detrimental effects of imperfections in the girder. In a real girder, a larger stiffness than the "ideal" stiffness would have to be provided in order to achieve full bracing without excessive brace forces. Winter [24] as well as Yura [26] have shown that providing twice the "ideal" brace stiffness will reduce the magnitude of the brace forces and allow the bracing system to provide full bracing.

In general, increasing the brace stiffness produces a succession of changes in the mode shape until the girder buckles between the braces. With each change in mode shape, the bracing system becomes less effective which results in a reduction in the increase in the buckling load for a given increase in brace stiffness. The girder will generally buckle in a mode shape for which the bracing system is the least effective.

Results will be presented in Chapter 5 which show that girders braced by a shear diaphragm do not exhibit a succession of changes in mode shape with increasing deck shear

rigidity. Girders braced by a shear diaphragm always buckle between the cross-frames or other discrete braces. There are no changes in the mode shape with increasing deck shear rigidity, so the plot of M_{cr} versus the shear rigidity does not have any sudden changes in slope. This is shown in Figure 2.9 for section #1 which is subjected to a constant moment. The graph is a plot of M_{cr} versus the deck shear rigidity.

2.5 Bracing by Shear Diaphragms at the Top Flange

Although current AASHTO provisions do not allow bracing by metal deck forms to be considered during the design process, previous studies in the building industry have demonstrated that metal cladding can significantly increase the buckling capacity of beams. The most significant work on diaphragm bracing was performed at Cornell during the 1960's and early 1970's. A closed form solution for beams braced by a shear diaphragm resulted from these studies and was presented by Errera et al. [12]. Errera presented the following expression which is an energy based solution which assumes that the lateral displacement and twist of the cross-section were a sine curve:

$$M_{cr} = \sqrt{\left(\frac{\pi^2 EI_y}{L^2} + Q\right)\left(\frac{\pi^2 EC_w}{L^2} + GJ + Qe^2\right)} + Qe \qquad (2.11)$$

The variables in Equation 2.11 which have not been previously defined are as follows:

M_{cr} = buckling moment of girder braced by a shear diaphragm

Q = effective shear modulus multiplied by tributary width of deck for girder

e = distance from center of gravity of the girder to plane of shear diaphragm.

Lawson and Nethercot [16] presented the Errera solution and defined "e" as the distance between the plane of the decking and the beam shear center. For doubly-symmetric sections, the shear center and center of gravity are both located at midheight of the cross-section. It is not clear what to use for "e" for singly-symmetric sections for which the geometric centroid and the shear center do not coincide.
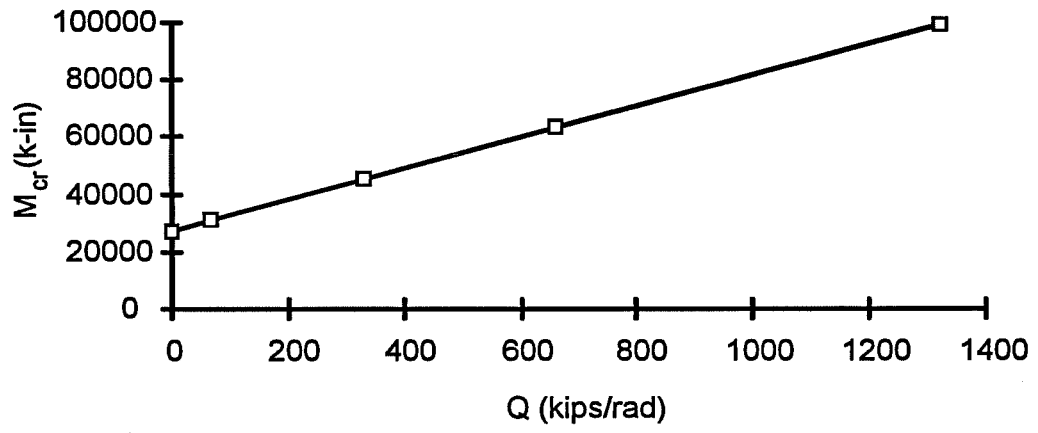
Figure 2.9 M_{cr} vs. Q for section #1 for constant moment for L=25'.

Errera [12] as well as Nethercot and Trahair [18] have suggested that a simple approximation for the buckling capacity for a girder braced by a shear diaphragm on the top flange can be obtained with the expression $M_{cr} = M_g + 2Qe$, in which M_g is the buckling capacity of the girder with no deck for bracing.

As with most closed form solutions, Equation 2.8 is valid for girders subjected to a constant moment. Very little has been published for cases when a beam braced by a shear diaphragm is subjected to a moment gradient and transverse loads applied at different load heights. In a paper by Lawson and Nethercot [16], the Errera energy solution was displayed with a moment gradient factor applied to the entire expression. Lawson and Nethercot have also recommended using the following expression which is an energy based expression for beams subjected to transverse loading applied at the top flange:

$$M_{cr} = C_b d \left[\frac{-P_e g}{2} + \frac{Q(1-g)}{2} + \sqrt{\left(\frac{-P_e g}{2} + \frac{Q(1-g)}{2} \right)^2 - \frac{Q^2}{4} + \left(\frac{P_e}{2} + \frac{Q}{2} \right) \left(\frac{P_e}{2} + 2P_T + \frac{Q}{2} \right)} \right] \quad (2.12)$$

where:

d = the depth of the girders,

P_e = the weak axis Euler load = $(\pi^2 E I_y / L^2)$,

C_b = the factor for moment gradient, and

g = the factor to take into account load height.

Lawson and Nethercot have recommended using traditional C_b and "g" values. For a point load at the midspan top flange the value of "g" is 0.55, while the value of "g" for a distributed load is 0.45.

The majority of the recommendations in the literature concerning bracing by shear diaphragms have dealt with simply supported girders; no solutions have been published to handle continuous girders braced by a shear diaphragm at the top flange. When girders are continuous, both the top and bottom flange have regions subjected to compression so the buckling mode is more complex and can involve large lateral translations of both flanges. The shear diaphragm can brace the top flange, however, the diaphragm has no effect on the bottom flange. The only work previously presented which has dealt with continuous type girders with top flange bracing was conducted by Yura. The following expression was presented by Yura for girders which have the top flange continuously braced and transverse loading applied at the top flange [25]:

$$C_b = 3.0 - \frac{2}{3}\left(\frac{M_1}{M_0}\right) + \frac{8}{3}\frac{M_{cl}}{\left(M_0 + M_1^{\ *}\right)} \qquad M_1^{\ *} \ \text{is explained below} \qquad (2.13)$$

This C_b equation is for a girder segment with full bracing at the ends and subjected to a moment causing compression in the bottom flange at one or both ends. M_0 and M_1 are the two end moments, while M_{cl} is the moment at the centerline of the beam segment. In the equation, M_0 will always cause compression in the bottom flange, while M_1 may or may not cause bottom flange compression. If both end moments cause compression in the bottom flange, the value of M_1 in the denominator of the last term is taken as zero. The M_1 which would be taken as zero if both end moments cause compression in the bottom flange has been marked with an asterisk. The C_b resulting from Equation 2.13 is to be applied to the buckling moment of the girder treating the bottom flange as the compression flange (i.e. apply the C_b to M_{AASHTO} treating the bottom flange as the compression flange). The results for continuous girders will be presented in Chapter 7.

2.6 Summary

This chapter outlined lateral-torsional buckling of beams. Solutions were presented which predicted the lateral-torsional buckling capacity of beams subjected to constant moment. For doubly-symmetric sections, all of the solutions which were presented agreed very well with the results from the finite element program ANSYS. The solutions which were valid for singly-symmetric sections also had good agreement with the finite element results. Many of the solutions for singly-symmetric sections, however, were cumbersome and required extensive calculations. The AASHTO formula for lateral torsional buckling was valid for both singly-symmetric and doubly-symmetric sections, and was relatively simple to use. The AASHTO buckling equation was conservative with respect to the finite element results when the small flange of a singly-symmetric section was in compression. When the larger flange was in compression the AASHTO equation was slightly unconservative, however, the equation produced reasonable estimates of the capacity when compared to the ANSYS results.

The effect of moment gradients is handled with the use of a C_b factor. The expression for the C_b which appears in the AASHTO specification is not very practical for design since it is only valid for straight-line moment diagrams. The modified Kirby-Nethercot formula is a relatively simple expression to use, and is valid for any shape moment diagram. The modified Kirby-

Nethercot formula agreed well with the recommended C_b values in the SSRC Guide for a point load at midspan and a distributed load.

The method in the SSRC Guide which accounts for load height effects modifies the C_b factor. The SSRC Guide method is valid for doubly-symmetric sections, however the Guide recommends solutions in the literature for singly-symmetric sections. One of the solutions from the literature was presented by Clark and Hill [8] and consisted of a nomograph which would estimate the buckling capacity for cases with constant moment, moment gradients, and load height effects. The nomograph was used to predict the buckling capacity of a doubly-symmetric beam subjected to constant moment. The buckling moment from the nomograph agreed relatively well with the results from a finite element analysis. When the same beam was subjected to a transverse load applied at the top flange, on the other hand, the estimate generated with the nomograph was quite unconservative with respect to the finite element results. The nomograph was difficult to use and had a high potential for human error. In addition, the nomograph was limited to a maximum span of 500 inches, and a maximum beam slenderness (KL/r) of 190.

Another solution from the literature which was considered was the solution presented by Anderson and Trahair [4] which consisted of a series of tables to account for moment gradients and effects of load height. The tables produced reasonable estimates of the buckling load when compared to the ANSYS results for doubly-symmetric and singly-symmetric sections, however, up to six stages of linear interpolation were required to obtain a solution. In addition, the tables have limits to the geometry of the girder and loading conditions which can be considered. In general, neither of the solutions for singly-symmetric girders which were considered from the literature were practical for design.

The accuracy of the equations in the SSRC Guide which account for load height effects will be compared with the finite element results for doubly-symmetric sections in Chapter 4. In addition, the validity of the method in the SSRC Guide will also be checked for singly-symmetric sections. The behavior of girders with intermediate braces and loading applied at the top flange will be considered in Chapter 4.

Beams continuously braced by a shear diaphragm at the top flange behave quite differently than beams braced by discrete bracing. Increases in the stiffness of discrete braces cause changes in the buckling mode shape up until the beam buckles between the discrete braces. Simply-supported beams continuously braced by a shear diaphragm, on the other hand, do not change mode shapes with increasing diaphragm shear rigidity. The beams will buckle between the

points of discrete bracing, regardless of the shear rigidity provided for the diaphragm. Finite element results which show this will be presented in Chapters 5 and 6.

Several research studies were conducted at Cornell University during the 1960's and 1970's. This work resulted in an energy solution which was presented by Errera [12] for simply-supported beams braced by a shear diaphragm which are subjected to constant moment. The equation contains a parameter "e" which is defined in Errera as the distance from the center of gravity to the plane of decking, while Lawson and Nethercot [16] define "e" as the distance from the shear center to the plane of decking. In doubly-symmetric girders, the shear center and center of gravity coincide at midheight, however, there is some question as to what to use for "e" in singly-symmetric girders for which the shear center and center of gravity lie at two different locations.

There is also some uncertainty in the use of the equation for cases with moment gradient. Lawson and Nethercot [16] recommended using the C_b factor on the entire Errera energy expression. Lawson and Nethercot also recommended an energy expression for top flange loading on beams braced by a shear diaphragm at the top flange. Both of these recommendations will be compared with the finite element results in Chapter 6.

Continuous girders braced by a shear diaphragm have not been significantly covered in the literature. Yura [25] has presented a C_b expression for continuous beams with the top flange continuously braced and transverse loading applied at the top flange. This expression may provide a design solution for continuous girders braced by a shear diaphragm at the top flange. Bracing of continuous girders braced by a shear diaphragm at the top flange will be considered in Chapter 8.

Chapter 3

Finite Element Model

3.1 Introduction

The three-dimensional finite element program ANSYS [5] was used to perform the finite element modeling on an IBM RISC workstation series 560. The computational study primarily concentrated on eigenvalue analyses to determine bifurcation loads. An eigenvalue buckling analysis is a linear-elastic solution which can demonstrate the influence of brace stiffness upon the buckling capacity of a straight pair of girders. Since the effect of imperfections are not reflected in a bifurcation solution, it is not possible to determine brace strength requirements in an eigenvalue analysis. Some large displacement results will be presented in Chapter 9 which demonstrate the effect of imperfections on forces in the diaphragm, however the majority of the computational results in this dissertation will concentrate on stiffness requirements of the shear diaphragm.

The results from the ANSYS studies were compared with closed formed solutions in order to confirm the accuracy of the model. Some of these comparisons were made in Chapter 2. Additional comparisons will be made in Chapter 4.

3.2 Finite Element Model

The purpose of the computational phase of the study was to determine the ability of metal deck forms to increase the buckling capacity of bridge girders. The system to be modeled is shown in Figure 3.1, which shows a twin girder system with corrugated metal deck forms spanning between the girders.

The first stage of the finite element modeling was to determine the different characteristics of the deck which were to be modeled. Figure 3.2 shows how the actual deck is connected and the various stiffness characteristics available. A top view of the deformation that is imposed on the deck as the top flanges of the girders deflect laterally is shown in Figure 3.2a. The deflecting girders impose in-plane bending on the metal deck forms. In addition, Figure 3.2b shows that the deck is also subjected to "out-of-plane" bending due to the twisting of the girders. The deck is also subjected to shear deformation which is depicted in Figure 3.2c. It was necessary to determine which of these different stiffness were to be modeled in the computational study.
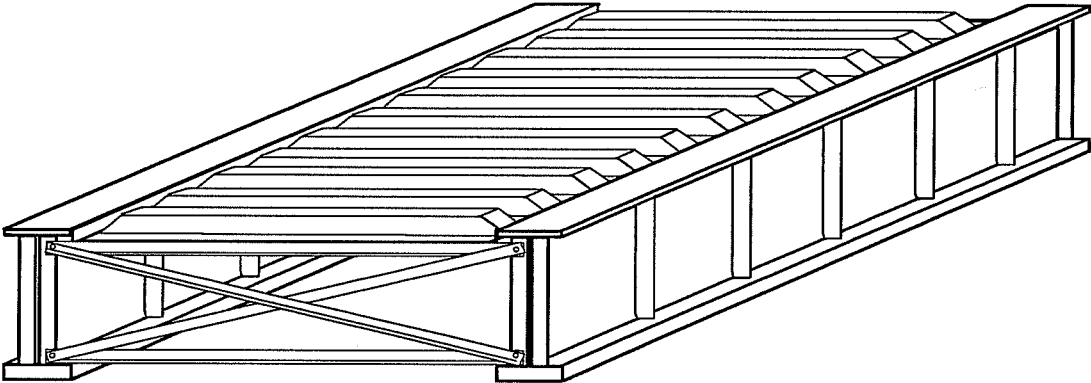
Figure 3.1 Twin girder and metal deck system.
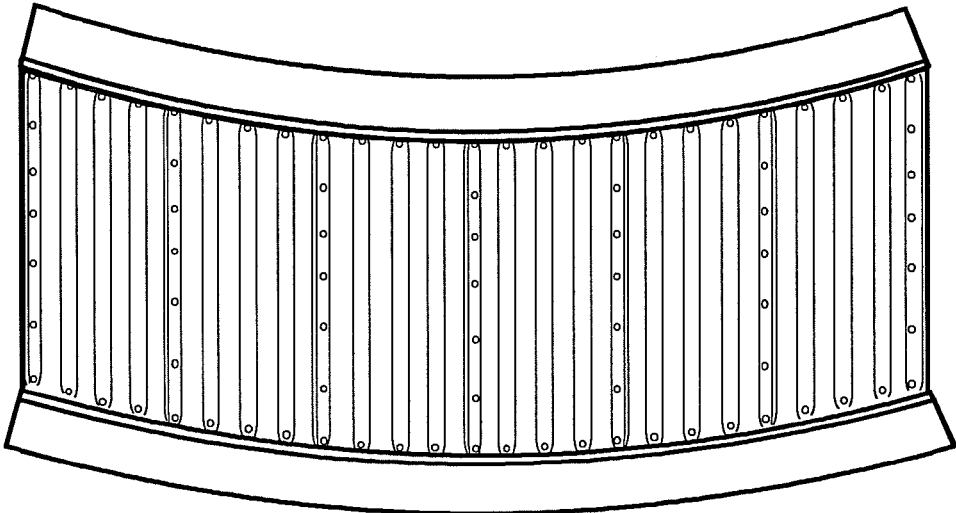
(a) "In-Plane" Bending Stiffness of Metal Deck
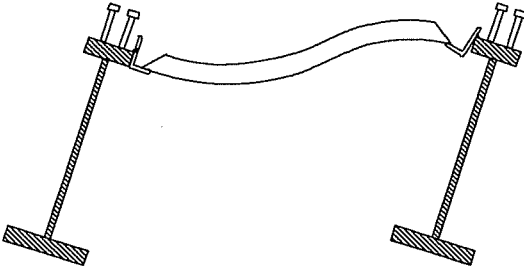
(b) "Out-of -Plane" Bending
Stiffness of Metal Deck
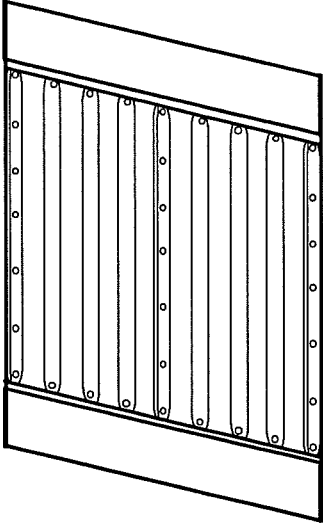
(c) Shear Stiffness of Metal Deck

Figure 3.2 Stiffness characteristics of metal deck forms.

If the deck is to possess any significant in-plane flexural stiffness, it must be able to develop bending stresses transverse to the corrugations. The profile of the deck is shown in Figure 3.3. It is assumed that the deep profile of the deck corrugations would significantly limit the bending stiffness due to distortions of the corrugations.

Figure 3.2b demonstrated that the twisting of the girders may also impose out-of-plane bending in the deck forms. The twisting girders would bend the deck in double curvature. The rotational restraint, however, would be minimal due to thin thickness of the sheeting coupled with flexible support angle.

Buckling of the girders also imposes a shear distortion on the deck. The corrugations in the deck would reduce the shear stiffness; however, the reduction was not believed to be as significant as in the case of the bending stiffness. It was necessary, therefore, to develop a model for the deck which possessed only shear stiffness.

The finite element model which was used in the studies is shown in Figure 3.4. The girders were modeled using eight-node shell elements. Each flange was built up with two shell elements; one element on either side of the web. The aspect ratio of the flange elements ranged from approximately three to five depending on the flange width. Eight-node shell elements were also used to model the web and the transverse web stiffeners. The number of elements in the web depth were varied between three and six. The aspect ratio of the web elements was very close to one for the majority of the cases analyzed. The sensitivity of the finite element model to the fineness of the mesh was checked for the different problems considered so as to avoid problems with excessive element distortions.

Several different finite element schemes were used in the development of the model for the deck. Initially, the deck was modeled as flat panels with the modulus of elasticity of steel (E = 29000 ksi). Four-node shell elements were used to model the deck. The thickness of the deck elements was varied to change the in-plane shear rigidity. Local buckling problems in the deck were encountered, however, since a very small thickness of the deck was required to achieve stiffness magnitudes of the order of those measured experimentally. To avoid this problem, a deck with a unit thickness was used and its modulus of elasticity was altered to vary the shear rigidity. This change was made since plate buckling is a linear function of the modulus of elasticity and a function of the cube of the thickness. Since a unit thickness was used, the cube of the thickness did not have the detrimental effect that was encountered with thicknesses much less than one.

Low Stiffness Transverse
to Corrugations
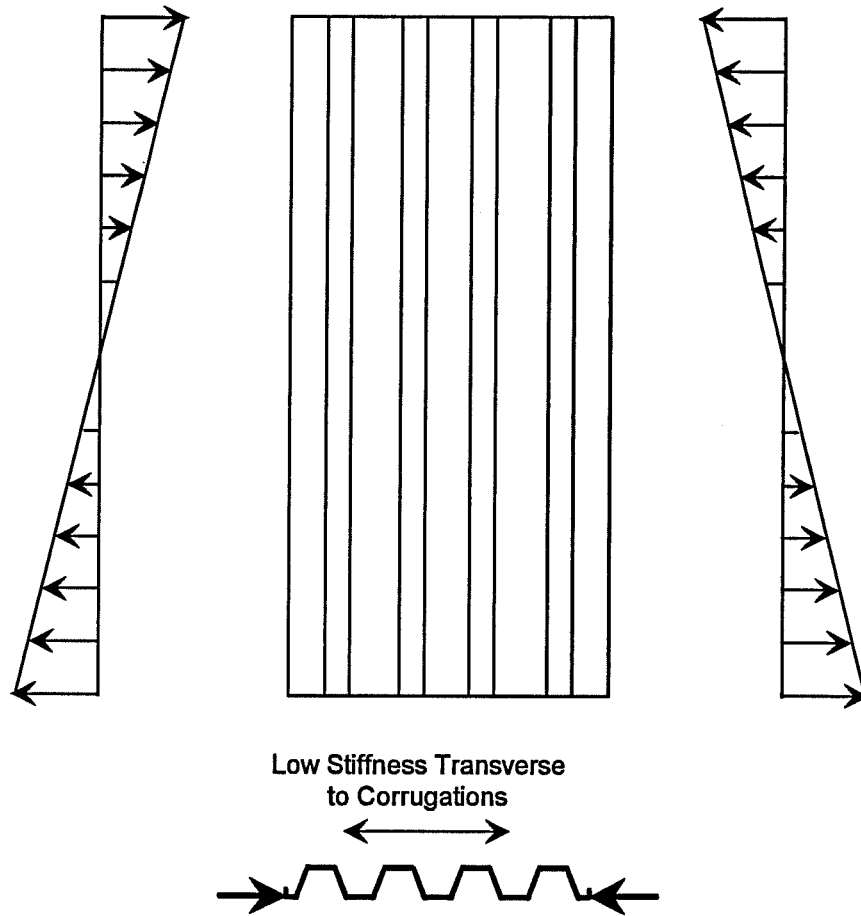
Figure 3.3 Low in-plane flexural stiffness due to corrugations.
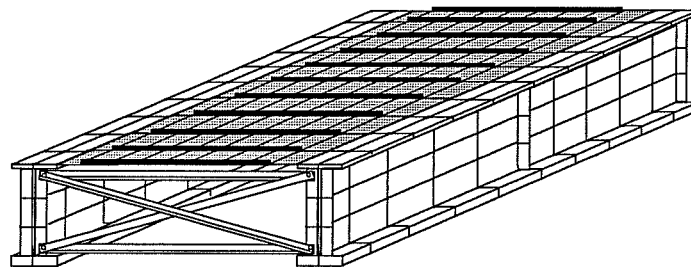
▨ SHELL ELEMENT SIMULATING DECK,
UNIT THICKNESS, VARIABLE "E"

■ DECK STIFFENING BEAMS (I = 10 in^4)

Figure 3.4 Twin girder finite element model.

Although using a unit thickness and a variable modulus of elasticity did work well for most analyses, some local buckling problems were still encountered. To combat this problem, deck stiffening beams were introduced which ran transverse to the longitudinal axis of the girders. The stiffening beams had no in-plane stiffness and had an out-of-plane stiffness of the same order as the corrugations of the metal deck forms.

The aspect ratio of the shell elements for the deck was maintained as close to one as possible. The deck was divided into discrete panels 1 element wide and 10-14 elements long. The corners of the panels were coupled to the centerline of the top flange of the girders in the x, y, and z directions. Figure 3.5 depicts how the deck was modeled by showing adjacent deck panels which span between two girders that have buckled. Since only the corners of the panels are fastened to the girders, the deck only experiences shearing deformation when the girders displace. In addition, because only the translational degrees of freedom are coupled between the girder and deck, the girder flange receives no rotational restraint from the deck.

The experimental phase of this study made use of a rigid frame to perform shear tests on the deck forms. The use of this frame has been outlined in References 9 and 21 and also described briefly in Chapter 1. A finite element model similar to the rigid testing frame was used to determine the magnitude of the modulus of elasticity of the deck material which should be provided for a given shear stiffness. The deck was modeled exactly the same in both the shear frame analyses and the eigenvalue analyses with the girders. Figure 3.6 shows a sketch of the finite element model for the shear frame. The beams of the testing frame were modeled using two-dimensional beam elements. A truss element was used to model the tension tie at the end of the frame.

The effective shear modulus of the shear diaphragm is defined by Equation 3.1. The term "shear stiffness" is often used interchangeably with the term "effective shear modulus" for G'. In Equation 3.1, G' is the effective shear modulus (shear stiffness) of the deck panel, P is the applied

$$G' = \frac{P\,a}{\Delta_{shear}\,b} \qquad (3.1)$$

load, "a" is the panel width, "b" is the span of the deck, and Δ_{shear} is the resulting shearing displacement in the panel. G' has the units of k/in/rad. As shown in Figure 3.6, the equation was rearranged to solve for the displacement, Δ_{shear}, for a corresponding shear modulus. For a given

The translational degrees-of-freedom in the x, y, and z-directions are coupled between the corner nodes of the deck panels and the centerline nodes of the top flange. Buckling of the girders can therefore only impose shearing deformations on the deck forms.

Four-node shell elements of deck panel

Deck stiffening beams. The beams only have out-of-plane stiffness.

Denotes coupling of translational degrees-of-freedom in x, y, and z-direction between deck and girder nodes

Eight-node shell elements of top flange of girder

Figure 3.5 Finite element model of metal deck forms as a shear diaphragm.
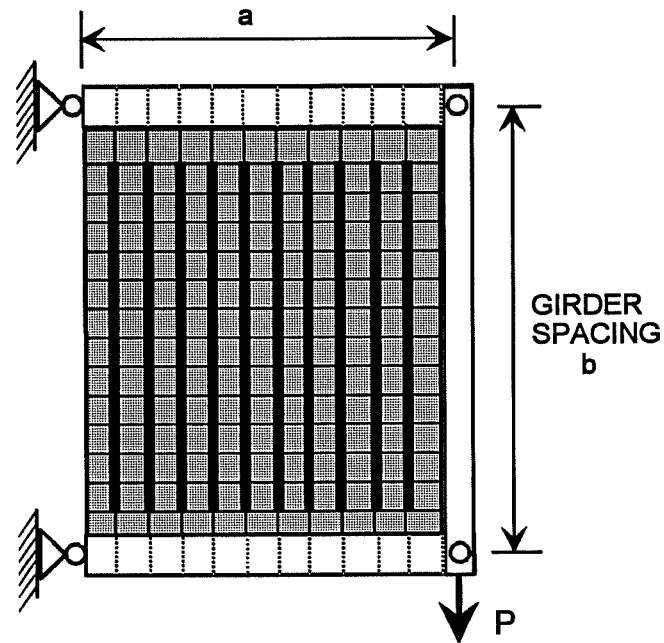
Figure 3.6 Finite element model for determining shear stiffness of deck.

applied load and panel geometry, the modulus of elasticity of the deck material was altered until the right deflection was achieved for the desired shear modulus. The same deck geometry and material modulus of elasticity was then used in a buckling analysis to determine the ability of the deck to brace the girders.

The girder spacing for each of the different cross-sections which were considered in the computational study was maintained to give a deck span of 132 inches for each case. The shear rigidity, Q, is calculated as the product of the effective shear modulus, G', and the tributary width of the deck, "w". For the case of a twin girder system with a single deck spanning between them, the tributary width, "w", is equal to half the deck span. The values of the modulus of elasticity for the deck which were used in the study are tabulated in Table 3.1. Since the shear analysis on the deck panels was a linear elastic problem, the modulus of elasticity required for a given shear rigidity should have been a linear variation. Therefore, the modulus of elasticity for a Q=660 k/rad should have been ten times the value for a Q=66 k/rad. The values which are shown in Table 3.1, however, deviate slightly from a linear variation. The reason for this is because a separate analysis was conducted for each different shear rigidity, and the deflections were rounded to the nearest thousandth of an inch. The deviation from a linear variation, however is very slight and will not have a significant effect the accuracy of the analyses.

Table 3.1 Modulus of Elasticity of Deck for Various Shear Stiffness Values		
G' (k/in/rad)	Q (k/rad)	E (psi)
1	66	199700
5	330	999100
10	660	1999800
20	1320	3996500

3.3 Computational Scope

Several different variables were considered in the computational study. Extensive parametric studies were conducted using the girder cross-sections previously shown in Figure 2.1 of Chapter 2. These cross-sections are shown again in Figure 3.7. Section #1 and #2 are doubly-symmetric sections, while section #3 is a singly-symmetric section. The top flange of section #3 is the same size as the section #2 flanges, while the larger bottom flange is the same size as the section #1 flanges. It should be noted that the reason a flange width of 7.018" was used on section #2 and #3 is to locate the shear center of the singly-symmetric section along a line of nodes in the finite element model for loading purposes. By making the top flange 7.018", the shear center on section #3 was located at one sixth of the web depth above the centroid of the bottom flange.

The parameters varied in the study are the following:

1) shear rigidity of deck,

2) in-plane boundary conditions of girders,

3) distance between discrete braces (points of full bracing),

4) load type (constant moment, concentrated point load, or distributed load)

5) load height

6) number of transverse stiffeners, and

7) girder cross-section.

Recalling from Table 3.1, the shear rigidities of the deck which were considered consisted of Q = 0, 66, 330, 660, 1320. This range of values was used since it represented the range of the rigidities which were measured for the deck system from the experimental phase of the project.

It was mentioned in Chapter 2 that buckling of continuous girders is complex because at different locations along the girder the top and bottom flanges are in compression. The buckling mode can involve large lateral displacements of both flanges. The exterior span of a continuous girder will typically have zero moment at the exterior support, and moment at the interior support causing compression in the bottom flange. In order to simulate an exterior span of a continuous girder, the in-plane boundary conditions of the girders were modeled as propped cantilevers. Likewise, in order to model a typical interior span of a continuous girder, the girders were modeled with both ends fixed from in-plane rotation.

In addition to the propped cantilever and fixed ended boundary conditions, the girders were also modeled as simply supported. For all of the girders considered in the study, points of
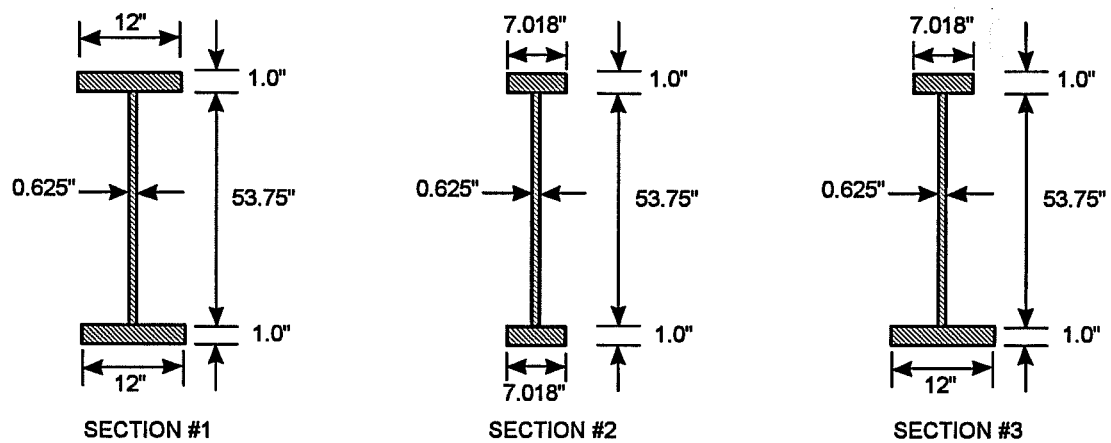
Figure 3.7 Cross-sections considered in computational study.

discrete bracing (i.e. cross-frames) were modeled by rigidly supporting the girders laterally at the top and bottom of the web. All of the girders were free to warp at the end supports.

The girders which were simply supported were subjected to the most load variations: constant moment, a concentrated load applied at midspan, and a uniformly distributed load. The transverse loading was applied at the bottom flange, midheight, and the top flange. In addition, the singly-symmetric section was loaded at the shear center, which was located below midheight. Discrete bracing was provided at the ends of the girders. Three different girder lengths were used: 25 feet, 50 feet, and 75 feet. The 25 foot length matches the current AASHTO limit on the maximum spacing between cross frames.

The simply supported girders had two different transverse stiffener spacings. In the first case, which is referred to as "fully stiffened", 0.5 in. x 4 in. transverse stiffeners were located at every element division which was equal to 18.75 in. This was done to increase the web shear and bend buckling capacity so that the effectiveness of the deck to resist lateral-torsional buckling could be established. The second case of stiffener spacing had transverse stiffeners spaced at 1.37 times the web depth and is referred to as "partially stiffened". The final stiffener spacing which was considered had stiffeners located at the two supports and at the midspan of the girders. This stiffener spacing was referred to as "unstiffened". The partially stiffened and unstiffened web cases were used to determine the influence of web distortions on the effectiveness of the deck. The partially stiffened and unstiffened girders were subjected to a concentrated load applied at midheight and the top flange, and also to constant moment.

For the models which were simulating continuous type girders, the type of loading consisted of a uniform distributed load applied at the top flange. The girders in this part of the study had a length of 75 feet. Three different spacings of cross-frames were considered: 25 feet, 37.5 feet, and 75 feet. The girders were modeled with fully stiffened webs in which stiffeners were spaced at 18.75 inches, and also with stiffeners only in regions where a cross frame was located which included the ends of the girders. These two stiffener spacings will again be referred to as "fully-stiffened" and "unstiffened".

To extend the range of girder geometry which was considered, a number of analyses were conducted on cross-sections in addition to sections #1, #2, and #3. Since the additional sections were used for limited cases, the cross-sectional geometry will be introduced in the appropriate chapters.

Chapter 4 will present the finite element results for girders without a deck for bracing. The Chapter 4 results will cover load cases with constant moment, moment gradients, and effects of load height on simply-supported girders with fully-stiffened webs. Chapters 5 and 6 will also present finite element results for simply-supported girders with fully-stiffened webs. The girders in these chapters, however, will have a shear diaphragm at the top flange for bracing. Chapter 7 will present the results for simply-supported girders with partially-stiffened and unstiffened webs and a shear diaphragm for bracing. Chapter 8 will present finite element results for the continuous girders with fully-stiffened and partially-stiffened webs and bracing by a shear diaphragm.

CHAPTER 4

Effects of Moment Gradient and Load Height on Unbraced Simply-Supported Girders

4.1 Introduction

The effects of moment gradient and load height were discussed in Chapter 2. This chapter presents the finite element results for girders subjected to a moment gradient caused by transverse loads applied at various load heights. The girders which are considered in this chapter do not have a deck for bracing. The finite element results will be compared with the solutions for moment gradients and load height effects outlined in Chapter 2. Results for both singly-symmetric and doubly-symmetric cross-sections will be presented.

Section 4.2 will present results for girders subjected to a moment gradient. The results for girders subjected to transverse loading applied at various load heights will be presented in Section 4.3. Section 4.4 will outline the results for girders with intermediate bracing. Finally, the results will be summarized in Section 4.5.

4.2 Comparison of C_b Factors with ANSYS Results

The closed formed solutions which were presented in Chapter 2 were derived for cases with a constant moment. Chapter 2 also outlined the method used to handle moment gradients with a C_b factor which is a multiplier applied to the solution for constant moment. The fourth edition of the SSRC guide [13] defines the C_b factor as the moment multiplier to find the buckling loads for transverse loads applied at the shear center.

The buckling moment of an unbraced girder with a moment gradient is calculated with the following expression:

$$M_{cr} = C_b \, M_{constant\,moment} \tag{4.1}$$

The value of $M_{constant\,moment}$ in Equation 4.1 is calculated using one of the closed formed solutions presented in Chapter 2 such as Timoshenko's solution or the AASHTO expression. It is possible to check the accuracy of the C_b equations presented in Chapter 2 with the ANSYS results by rearranging Equation 4.1. The C_b from ANSYS is calculated by dividing the buckling

65

moment for the case with a moment gradient by the buckling moment for the constant moment case which is shown in the following expression:

$$C_{b\,ANSYS} = \frac{M_{cr\,moment\,gradient}}{M_{cr\,uniform\,moment}} \qquad (4.2)$$

Comparisons will only be made with the AISC C_b formula (modified Kirby-Nethercot formula) because the AASHTO formula is not valid for the cases considered in this study since the moment diagram is not linear.

A number of different girder cross-sections will be considered in this chapter. The first cross-sections which will be considered are sections #1, #2, and #3 which were shown in Chapters 2 and 3. These sections are shown again for convenience in Figure 4.1.

Table 4.1 shows the yield moments of sections #1, #2, and #3 assuming a yield stress of 50 ksi. These moments are presented in order to give the reader a relative indicator to the magnitude of the buckling moments which will be presented in this chapter.

Table 4.1 : Yield Moments for Sections #1, #2, and #3 (F_y = 50 ksi)	
Cross-Section	Yield Moment, M_y (kip-in)
#1	47626
#2	36686
#3	33985

Tables 4.2 and 4.3 show the comparison of the C_b values for the doubly-symmetric sections #1 and #2, respectively. The ANSYS results show that the C_b values do vary slightly for different girder cross-sections and the length does have a small effect, however the modified Kirby-Nethercot formula does a good job of estimating the C_b value.
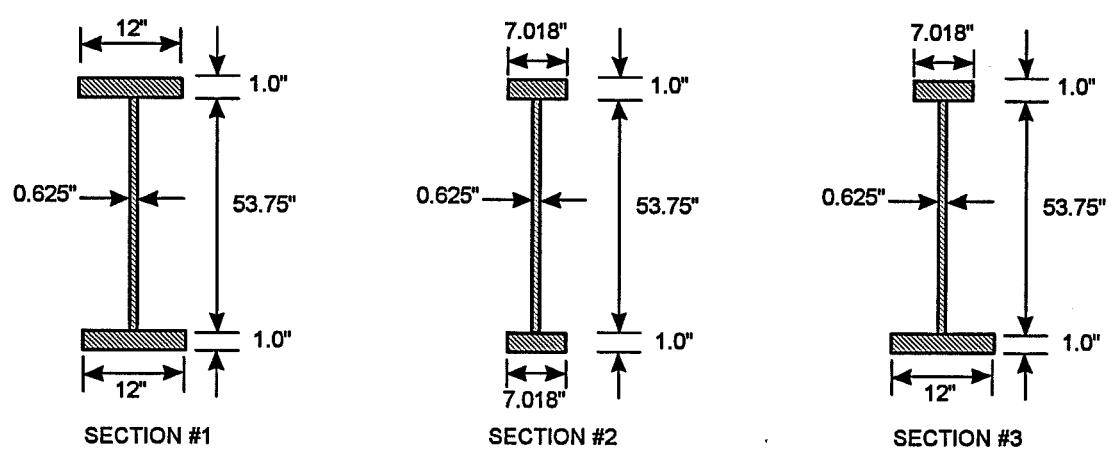
Figure 4.1 Cross-sections considered in computational study.

Table 4.2 Section #1 - C_b Comparison		
Situation	P @ CL Midheight	w @ Midheight
Modified Kirby-Nethercot Formula (AISC)	1.32	1.14
L = 25 feet	1.29	1.12
L = 50 feet	1.35	1.13
L = 75 feet	1.36	1.13

Table 4.3 Section #2 - C_b Comparison		
Situation	P @ CL Midheight	w @ Midheight
Modified Kirby-Nethercot Formula (AISC)	1.32	1.14
L = 25 feet	1.35	1.13
L = 50 feet	1.36	1.13
L = 75 feet	1.36	1.13

Moment gradients applied to doubly-symmetric girders are relatively well understood. It is accepted that the moment gradient caused by transverse loading applied at midheight can be handled by just a C_b factor, while transverse loads applied above or below midheight cause additional effects due to load height. The midheight location of a doubly-symmetric girder corresponds to the location of both the shear center and the geometric centroid. When transverse loads are applied to singly-symmetric girders, on the other hand, it is not clear where the load should be applied so that effects of load height do not exist. Therefore, the load was applied to the singly-symmetric section #3 at midheight and the shear center to study this problem. In addition, the load was also applied at the geometric centroid for lengths of 25 and 50 feet. The distance from the top flange centroid to the load locations for section #3 are as follows:

1) midheight of the girders: 27.38"

2) center of gravity of the girders: 29.97"

3) shear center of girders: 45.62".

The C_b values for section #3 are shown in Tables 4.4a, 4.4b, and 4.4c for the three different loading positions. The tables show that when the load is applied at the midheight location, the ratio of the moment gradient to the constant moment is closest to the C_b values from the modified Kirby-Nethercot formula. When the load was applied at the geometric centroid and the shear center, larger values of the $C_{b\ ANSYS}$ resulted which are indicative of load height effects for loading applied lower on the girder cross-section. The lower position of the load increases the buckling moment, as well as the corresponding value of $C_{b\ ANSYS}$.

Table 4.4a Section #3 - C_b Comparison - Midheight Loading		
Situation	P @ CL Midheight	w @ Midheight
Modified Kirby-Nethercot Formula (AISC)	1.32	1.14
L = 25 feet	1.34	1.13
L = 50 feet	1.34	1.12
L = 75 feet	1.33	1.12

Table 4.4b Section #3 - C_b Comparison - Centroid Loading		
Situation	P @ CL Midheight	w @ Midheight
Modified Kirby-Nethercot Formula (AISC)	1.32	1.14
L = 25 feet	1.40	1.17
L = 50 feet	1.39	1.15

Table 4.4c Section #3 - C_b Comparison - Shear Center Loading		
Situation	P @ CL Midheight	w @ Midheight
Modified Kirby-Nethercot Formula (AISC)	1.32	1.14
L = 25 feet	1.94	1.50
L = 50 feet	1.76	1.39
L = 75 feet	1.64	1.31

In order to gain better understanding of C_b values for singly-symmetric sections, additional cross-sections were considered. Figure 4.2 shows the cross-sections which were used to further these studies. A bottom flange 12 in. wide and 1 in. thick was used on all sections, while the distance between flange centroids was maintained at 60 in. Seven different top flanges were used to vary the section properties. The location of the shear center and the geometric centroid are given relative to the bottom flange centroid.

Section 'A' had a top flange which was only 2 in. wide and 0.25 in. thick. This section was essentially a T-section which is demonstrated by the location of the shear center, 0.07 in. from the bottom flange centroid. The shear center for a T-section lies at the intersection of the web and the flange. The thickness of the web was set equal to 0.7349 inches so that the geometric centroid would correspond with a line of nodes. Loading on section A was applied at midheight, the geometric centroid, and the bottom flange which was only 0.07 in. below the shear center.

Tables 4.5a and 4.5 show the C_b values from the ANSYS results for three different load heights for a point load at midspan and a uniform distributed load, respectively. Girder spans of 25, 50, and 75 feet were considered. The SSRC guide recommends C_b values of 1.35 for a point load at midspan, and 1.12 for a uniform distributed load.

Section	B_{top}	T_{top}	$\dfrac{I_{yc}}{I_y}$	y_{shear} center bottom	$y_{centroid}$ bottom
Section A	2"	0.25"	0.001	0.07"	24.00"
Section B	2"	1"	0.005	0.28"	24.77"
Section C	4"	1"	0.036	2.14"	25.96"
Section D	6"	1"	0.111	6.67"	27.06"
Section E	8"	1"	0.229	13.71"	28.11"
Section F	10"	1"	0.366	21.99"	29.08"
Section G	12"	1"	0.500	30.00"	30.00"

Figure 4.2 Additional sections considered for study of C_b factors for singly-symmetric sections.

Table 4.5a Point Loading at Midspan of Section A			
LENGTH	P @ Midheight	P @ Centroid	P @ Shear Center
25	1.18	1.30	2.08
50	1.15	1.24	1.75
75	1.17	1.24	1.64

Table 4.5b Uniform Distributed Loading on Section A			
LENGTH	w @ Midheight	w @ Centroid	w @ Shear Center
25	1.07	1.15	1.57
50	1.06	1.12	1.39
75	1.06	1.11	1.31

For the T-section, loading at the geometric centroid produced C_b values closest to the traditional values. Loading at the shear center caused C_b values which were too high, while loading at midheight produced values which were too low. This differs from what was found for section #3 in Table 4.4a and 4.4b which showed that midheight loading produced C_b values closer to the traditional values. The size of the top flange of the "T-section" was increased as shown by sections B through G in Figure 4.2 to determine when loading at midheight could be predicted using the traditional C_b values.

Table 4.6a and 4.6b show the C_b values which resulted from midheight loading on sections B-G. Three different lengths were considered for the girders. The webs of the girders had 5 in. wide stiffeners which were 0.5 in. thick. The spacing of the stiffeners was 60 in. for the 50 and 75 foot spans and 30 in. for the 25 foot span.

Table 4.6a P @ Midheight of Singly-Symmetric Sections (Eqn. 4.2 - 1.32)			
Section	25 Foot Span	50 Foot Span	75 Foot Span
Section B	1.23	1.18	1.20
Section C	1.31	1.27	1.26
Section D	1.33	1.32	1.31
Section E	1.33	1.34	1.33
Section F	1.33	1.34	1.34
Section G	1.31	1.32	1.34

Table 4.6b w @ Midheight of Singly-Symmetric Sections (Eqn. 4.2 - 1.12)			
Section	25 Foot Span	50 Foot Span	75 Foot Span
Section B	1.09	1.07	1.07
Section C	1.11	1.10	1.10
Section D	1.12	1.11	1.11
Section E	1.12	1.12	1.12
Section F	1.12	1.12	1.13
Section G	1.12	1.12	1.13

Tables 4.6a and 4.6b show that loading at midheight of section D produces C_b values which are essentially the same as the values given by the modified Kirby-Nethercot formula. Referring back to Figure 4.2, section D had a top flange width of 6 in. and a thickness of 1 inch. The ratio of I_{yc} / I_y was 0.111. This is very close to 0.1 which is the minimum value the AASHTO specification will allow for bridge girders. This demonstrates that for most practical cross-sections used in bridges, traditional C_b values can be used for loading applied at midheight.

To summarize, the modified Kirby-Nethercot formula had very good agreement with the ANSYS results for doubly-symmetric sections with transverse loads applied at midheight. The modified Kirby-Nethercot equation also had good agreement with the ANSYS results when transverse loads were applied at midheight of singly-symmetric sections with ratios of I_{yc}/ I_y greater than 0.1. For singly-symmetric girders with I_{yc}/ I_y greater than 0.1, loading applied below midheight (closer to tension flange) produced buckling loads which were larger than predicted by the modified Kirby-Nethercot formula.

4.3 Effects of Load Height on Buckling Capacity

It was mentioned in Chapter 2 that the relative height that transverse loads are applied on the cross-section has a significant effect on the resulting buckling load. This section will present the finite element results for transverse loads applied at variable load height on simply-supported girders with no bracing between supports. The transverse loading consisted of either a point load applied at midspan or a uniform distributed load. The loads were applied at the top flange and the bottom flange.

Yura [27] has suggested that an estimate of the buckling capacity for girders with transverse loads applied at the top flange can be obtained by neglecting the warping term in the closed formed solutions. The resulting expression is shown as follows:

$$M_{cr\ TopFlangeLoading} = C_b\ \frac{\pi}{L_b}\ \sqrt{EI_yGJ}$$ (4.3)

Equation 4.3 will be compared with finite element results for the three sections which were shown in Figure 4.1. C_b values from the modified Kirby-Nethercot formula will be used in Equation 4.3 for these comparisons. For the singly-symmetric section #3, the AASHTO equation will be used with the warping term neglected.

Tables 4.7a, 4.7b, and 4.7c show comparisons of the ANSYS results and Equation 4.3 for sections #1, #2, and #3. The moments which are shown in the tables are the maximum moment which would occur at midspan. "P" in the tables denotes a top flange point load applied at midspan while a "w" denotes a distributed load applied at the top flange. The percentage difference between Equation 4.3 and the ANSYS results has been shown in parentheses below the estimate of Equation 4.3. The percent difference is based on the ANSYS results and a negative

percentage indicates that Equation 4.3 is unconservative with respect to the ANSYS results while a positive percentage indicates that the equation is conservative.

Table 4.7a Section #1 - Comparison of Equation 4.3 and ANSYS Results Top Flange Loading				
L (feet)	Eqn. 4.3b - P	ANSYS - P	Eqn. 4.3b - w	ANSYS - w
25	14841 kip-in (34.3%)	22583 kip-in	12817 kip-in (37.2 %)	20401 kip-in
50	7421kip-in (1.9%)	7566 kip-in	6409 kip-in (5.2%)	6762 kip-in
75	4947 kip-in (-9.6%)	4514 kip-in	4273 kip-in (-7.1%)	13989 kip-in

Table 4.7b Section #2 - Comparison of Equation 4.3b and ANSYS Results Top Flange Loading				
L (feet)	Eqn. 4.5b - P	ANSYS - P	Eqn. 4.5b - w	ANSYS - w
25	5677 kip-in (6.1%)	6045 kip-in	4903 kip-in (9.4 %)	5412 kip-in
50	2838 kip-in (-8.5%)	2616 kip-in	2451 kip-in (-6.7%)	2297 kip-in
75	1892 kip-in (-10.6%)	1710 kip-in	1634 kip-in (-10.2%)	1483 kip-in

Table 4.7c Section #3 - Comparison of Equation 4.3b and ANSYS Results Top Flange Loading				
L (feet)	Eqn. 4.5b - P	ANSYS - P	Eqn. 4.5b - w	ANSYS - w
25	6180 kip-in (3.6%)	6413 kip-in	5337 kip-in (6.9 %)	5734 kip-in
50	3090 kip-in (-4.5%)	2956 kip-in	2669 kip-in (-1.1%)	2641 kip-in
75	2061 kip-in (2.8%)	2120 kip-in	1780 kip-in (5.7%)	1888 kip-in

For the respective load cases of a point load and a distributed load applied at the top flange of section #1 with a 25 foot span, the estimates from Equation 4.3 were 34.3% and 37.2% smaller than the ANSYS. The equation is quite conservative in these cases, however, the span to depth ratio of this case is approximately 5.5 which is not very practical. Equation 4.3 was slightly unconservative for a few cases, however, for many of the cases considered conservative estimates of the buckling capacity were obtained. Although the accuracy of Equation 4.3 did fluctuate slightly, neglecting the warping term is a very simple method to account for top flange loading.

The method for accounting for load height effects in the fourth edition of the SSRC Guide [13] is considerably different than the method presented in the third edition of the SSRC Guide [14]. These two methods were outlined in Chapter 2. The fourth edition of the SSRC guide accounts for load height effects by modifying the C_b value. The variable C_b^* will be used to denote the C_b value modified for load height effects. The buckling capacity is calculated by multiplying the buckling moment from one of the closed form equations for constant moment by the value for C_b^* for the corresponding load case.

Estimates using the C_b^* from the fourth edition of the SSRC Guide [13] for the doubly-symmetric section #1 and #2 were presented in Chapter 2. These estimates of C_b^* will be denoted as $C_b^*{}_{SSRC}$ and will be compared with the ANSYS results. The equation which is presented in the third edition of the SSRC Guide [14] will be divided by the equation for bucking of the corresponding girder with constant moment loading in order to calculate a $C_b^*{}_{SSRC}$. The two different values of $C_b^*{}_{SSRC}$ will be denoted by either the 3rd edition or the fourth edition of the appropriate SSRC Guide. A C_b^* from the ANSYS results is calculated by dividing the

buckling moment which results from top flange loading, by the buckling capacity of the same girder subjected to constant moment. This will be denoted as $C_b^*{}_{ANSYS}$.

Table 4.8a shows a comparison of the $C_b^*{}_{SSRC}$ and the $C_b^*{}_{ANSYS}$ for a point load at the midspan top flange on the two doubly-symmetric sections, while Table 4.8b shows the corresponding values for a uniform distributed load at the top flange. Next to the values of $C_b^*{}_{SSRC}$ in the tables, there is a percentage in parentheses which indicates the percent difference in the C_b^* between the ANSYS and the SSRC value. The percent difference is based on the ANSYS results, and a positive percentage indicates the method in the corresponding SSRC Guide is conservative with respect to the finite element results while a negative percentage indicates the prediction is unconservative.

Table 4.8a Point Load at Midspan Top Flange					
	Section #1			Section #2		
Length	$C_b^*{}_{ANSYS}$	3rd Ed. $C_b^*{}_{SSRC}$	4th Ed. $C_b^*{}_{SSRC}$	$C_b^*{}_{ANSYS}$	3rd Ed. $C_b^*{}_{SSRC}$	4th Ed. $C_b^*{}_{SSRC}$
25 feet	0.83	0.83 (0.0%)	0.85[a] (-4.8%)	0.90	0.90 (0.0%)	0.89 (+1.1%)
50 feet	0.90	0.91 (-1.1%)	0.90 (0.0%)	1.03	1.03 (0.0%)	1.02 (+1.0%)
75 feet	0.98	0.98 (0.0%)	0.98 (0.0%)	1.11	1.11 (0.0%)	1.11 (0.0%)

[a]The "minimum" value of C_b^* was used for the fourth edition method since W > 1.75.

Table 4.8b Distributed Load at Top Flange					
	Section #1			Section #2		
Length	C_b^* ANSYS	3rd Ed. C_b^* SSRC	4th Ed. C_b^* SSRC	C_b^* ANSYS	3rd Ed. C_b^* SSRC	4th Ed. C_b^* SSRC
25 feet	0.75	0.76 (-1.3%)	0.76[a] (-1.3%)	0.80	0.81 (-1.2%)	0.79 (+1.2%)
50 feet	0.81	0.81 (0.0%)	0.79 (-2.5%)	0.90	0.90 (0.0%)	0.89 (+1.0%)
75 feet	0.86	0.87 (0.0%)	0.85 (+1.2%)	0.96	0.96 (0.0%)	0.95 (+1.0%)

[a]The "minimum" value of C_b^* was used for the fourth edition method since W > 1.75.

Referring to the ANSYS results in Table 4.8a, for a midspan point load applied at the top flange, the C_b^* ANSYS values range from 0.83 to 1.11 depending on the girder span and the section. Comparing this range to the value of C_b = 1.32 from the modified Kirby-Nethercot equation for midspan loading at midheight shows that there is a substantial reduction in the buckling load due to top flange loading. This reduction also shows up when the results for a distributed load are compared. The C_b^* ANSYS values in Table 4.8b range from 0.75 to 0.96 compared to the value of C_b = 1.14 which resulted from the modified Kirby-Nethercot equation for loading at midheight.

The tables also demonstrate that effects of load height are more dominant in members with a larger warping stiffness. Section #1 has a significantly higher warping stiffness than section #2, and the value of C_b^* for a given length is smaller for section #1 than for section #2. This dependency on the warping stiffness also shows up when comparing the values of C_b^* for various lengths of a given section. There is a reduction in the warping stiffness as the length is increased and the corresponding C_b^* ANSYS values increase.

The methods for accounting for load height in the third and the fourth edition of the SSRC Guide each provide good estimates of the effects for load height when compared to the ANSYS results. The "minimum" C_b^* had to be used for the fourth edition SSRC Guide values for section #1 with a 25 foot span.

Tables 4.9a and 4.9b show a comparison between the ANSYS and the SSRC values of C_b^* for bottom flange loading on the doubly-symmetric sections. The trends in these tables are similar to those observed for top flange loading except that the load height effect with bottom flange loading is a benefit instead of a detriment. In this case, members with a higher warping stiffness receive more of a benefit than less stiff members.

Table 4.9a Point Load at Midspan Bottom Flange					
	Section #1			Section #2		
Length	C_b^* ANSYS	3rd Ed. C_b^* SSRC	4th Ed. C_b^* SSRC	C_b^* ANSYS	3rd Ed. C_b^* SSRC	4th Ed. C_b^* SSRC
25 feet	2.19	2.18 (0.0%)	2.14[a] (-4.8%)	2.05	2.03 (0.0%)	2.04 (+1.1%)
50 feet	2.04	2.01 (-1.1%)	2.02 (0.0%)	1.79	1.77 (0.0%)	1.78 (+1.0%)
75 feet	1.89	1.86 (0.0%)	1.86 (0.0%)	1.66	1.64 (0.0%)	1.65 (0.0%)

[a]The "minimum" value of C_b^* was used for the fourth edition method since $W > 1.75$.

Table 4.9b Distributed Load at Bottom Flange						
	Section #1			Section #2		
Length	C_b^* ANSYS	3rd Ed. C_b^* SSRC	4th Ed. C_b^* SSRC	C_b^* ANSYS	3rd Ed. C_b^* SSRC	4th Ed. C_b^* SSRC
25 feet	1.67	1.68 (-1.3%)	1.64[a] (-1.3%)	1.59	1.58 (-1.2%)	1.58 (+1.2%)
50 feet	1.58	1.57 (0.0%)	1.58 (-2.5%)	1.42	1.41 (0.0%)	1.41 (+1.0%)
75 feet	1.48	1.47 (0.0%)	1.47 (+1.2%)	1.33	1.33 (0.0%)	1.32 (+1.0%)

[a]The "minimum" value of C_b^* was used for the fourth edition method since W > 1.75.

The SSRC guide provisions for load height provide a relatively accurate method for calculating the buckling load when transverse loading is applied at the top or bottom flange of doubly-symmetric sections.

The SSRC guide does not directly address the problem of load height effects on singly-symmetric sections other than to recommend approximate solutions in the literature. Solutions by Clark and Hill and also Anderson and Trahair were considered in Chapter 2. The published solutions were compared with the finite element results from ANSYS for the singly-symmetric section #3. In some cases the published solutions produced reasonable estimates of the buckling load. The nomograph presented by Clark and Hill was limited to a maximum span of 500 inches and a maximum beam slenderness (KL/r) of 190. The nomograph had a large potential for human error with its use. The tables presented by Anderson and Trahair also had geometric limits to the sections which could be solved, and required 6 stages of linear interpolation to obtain an answer. In general, the solutions were found to be cumbersome and impractical for design.

A desirable solution for approximating load height effects in singly-symmetric girders would be a method similar to the SSRC Guide equations for doubly-symmetric sections. It is possible to check the accuracy of the SSRC equations on the singly-symmetric section. For singly-

symmetric sections, only the method of accounting for load height effects in the fourth edition of the SSRC Guide will be compared with ANSYS results.

The method from the fourth edition of the SSRC Guide was outlined in Chapter 2. The method makes use of the following expression to calculate the beam parameter, W:

$$W = \frac{\pi}{L} \sqrt{\frac{E\,C_w}{G\,J}} \qquad (4.4)$$

For singly-symmetric sections the warping term C_w is defined by the following expression:

$$C_w = I_y\, d^2\, \rho\, (1-\rho) \qquad (4.5)$$

The variable ρ is equal to $I_{yc}\,/\,I_y$, where I_{yc} is the moment of inertia of the compression flange about an axis through the web, and I_y is the weak axis moment of inertia. For a doubly-symmetric section $\rho = 0.5$ which results in a simpler expression for $C_w = I_y d^2/4$.

A comparison was made between the ANSYS results for the singly-symmetric section #3 and the SSRC Guide predictions for $C_b{}^*$. Different values of $C_b{}^*{}_{SSRC}$ were calculated using the following two values of C_w for the calculation of the beam parameter,"W":

1) calculating "W" using $C_{w\ Unsym} = I_y d^2 \rho\, (1-\rho\ )$

2) calculating "W" using $C_{w\ Sym} = I_y d^2/4$

Case 1 makes use of the actual definition of C_w, while case 2 makes use of the C_w equation for doubly-symmetric sections. The different definitions lead to the following two results for section #3, $C_{w\ Unsym} = 71943\ \text{in}^4$, and $C_{w\ Sym} = 129495\ \text{in}^4$.

The expressions for the term "B" were given in Chapter 2. The values for W and B are shown in Tables 4.10a and 4.10b for the respective cases of a point load at midspan, and a distributed load on section #3.

Table 4.10a Point Load at Midspan of Singly-Symmetric Section				
	Section #3 - $C_{w\ Unsym}$		Section #3 - $C_{w\ Sym}$	
Length	W	B	W	B
25 feet	1.38	1.55	1.86 (>1.75)	1.58
50 feet	0.69	1.36	0.93	1.45
75 feet	0.46	1.26	0.62	1.33

Table 4.10b Distributed Load on Singly-Symmetric Section				
	Section #3 - $C_{w\ Unsym}$		Section #3 - $C_{w\ Sym}$	
Length	W	B	W	B
25 feet	1.38	1.44	1.86 (>1.75)	1.46
50 feet	0.69	1.30	0.93	1.36
75 feet	0.46	1.21	0.62	1.27

Recalling from chapter 2, the solution in the fourth edition of the SSRC Guide is a curve fit which does not make sense for values of W greater than 1.75. It is necessary to limit the value of B to 1.46 in these cases. This was necessary for the 25 foot span girders using the symmetrical C_w in Tables 4.10a and 4.10b.

Table 4.11a shows a comparison of the $C_b{}^*{}_{SSRC}$ and the $C_b{}^*{}_{ANSYS}$ for a point load at the midspan top flange on the singly-symmetric section, while Table 4.11b shows the corresponding values for a uniform distributed load at top flange. Using the actual warping stiffness in the SSRC equations gives results which are slightly unconservative. The results using an artificial warping stiffness tend to be more conservative, and also are closer to the ANSYS results.

Table 4.11a Point Load at Midspan Top Flange				
	Section #3 - $C_{w\ Unsym}$		Section #3 - $C_{w\ Sym}$	
Length	C_b^* ANSYS	4th Ed. C_b^* SSRC	C_b^* ANSYS	4th Ed. C_b^* SSRC
25 feet	0.88	0.87 (+1.1%)	0.88	0.85 (+3.4%)
50 feet	0.94	0.99 (-5.3%)	0.94	0.93 (+1.1%)
75 feet	1.01	1.07 (-5.9%)	1.01	1.02 (-1.0%)

Table 4.11b Distributed Load at Top Flange				
	Section #3 - $C_{w\ Unsym}$		Section #3 - $C_{w\ Sym}$	
Length	C_b^* ANSYS	C_b^* SSRC	C_b^* ANSYS	C_b^* SSRC
25 feet	0.79	0.78 (+1.3%)	0.79	0.77 (+2.5%)
50 feet	0.84	0.86 (-2.4%)	0.84	0.82 (+2.4%)
75 feet	0.90	0.93 (-3.3%)	0.90	0.88 (+2.2%)

The comparison between the ANSYS and the SSRC values of C_b^*, for bottom flange loading on the singly-symmetric section are shown in Tables 4.12a and 4.12b.

Table 4.12a Point Load at Midspan Bottom Flange				
	Section #3 - $C_{w \, actual}$		Section #3 - $C_{w \, artificial}$	
Length	$C_b^* \, ANSYS$	$C_b^* \, SSRC$	$C_b^* \, ANSYS$	$C_b^* \, SSRC$
25 feet	2.38	2.09 (+12.2%)	2.38	2.13 (+10.5%)
50 feet	2.03	1.84 (+9.4%)	2.03	1.96 (+3.4%)
75 feet	1.82	1.70 (+6.6%)	1.82	1.80 (+1.1%)

Table 4.12b Distributed Load at Bottom Flange				
	Section #3 - $C_{w \, actual}$		Section #3 - $C_{w \, artificial}$	
Length	$C_b^* \, ANSYS$	$C_b^* \, SSRC$	$C_b^* \, ANSYS$	$C_b^* \, SSRC$
25 feet	1.75	1.61 (+8.0%)	1.75	1.64 (+6.3%)
50 feet	1.55	1.46 (+9.0%)	1.55	1.52 (+1.9%)
75 feet	1.42	1.36 (+4.2%)	1.42	1.42 (0.0%)

In order to increase the range of cross-sections considered, the SSRC equations were also compared with the ANSYS results for the sections labeled shallow #1, #2, and #3 and deep #1, #2, and #3, which are shown in Figures 4.3a and 4.3b. The shallow sections had depths which were half the depth of the normal sections (i.e. sections #1, #2, and #3), while the deep sections were twice the depth of the normal sections. The girders had the same flange sizes as the normal depth girders of the same section number (i.e. shallow #1 has the same flange sizes as section #1). The girders were subjected to a distributed load at the top flange. Tables 4.13a, 4.13b, and 4.13c show the values of W and B for the girders for the different lengths. The warping term, C_w, for a doubly-symmetric section was used for the singly-symmetric section shallow #3 and deep #3. In the cases in which W was greater than 1.75, B had to be limited to 1.46.
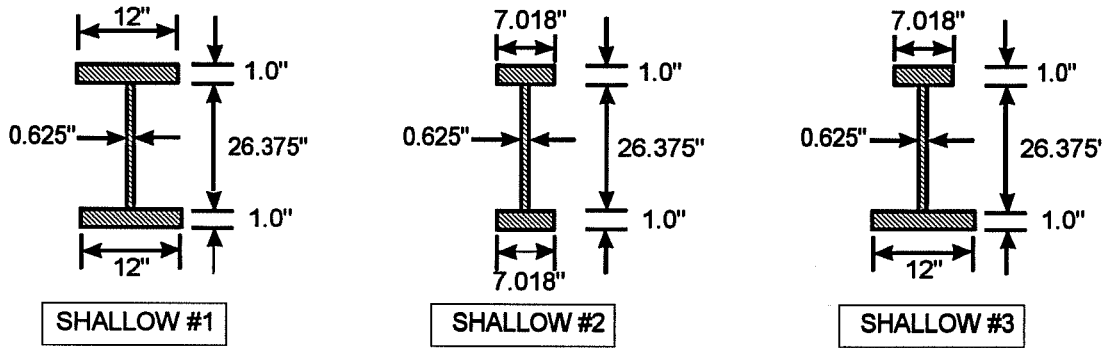
Figure 4.3a Shallow cross-sections considered.
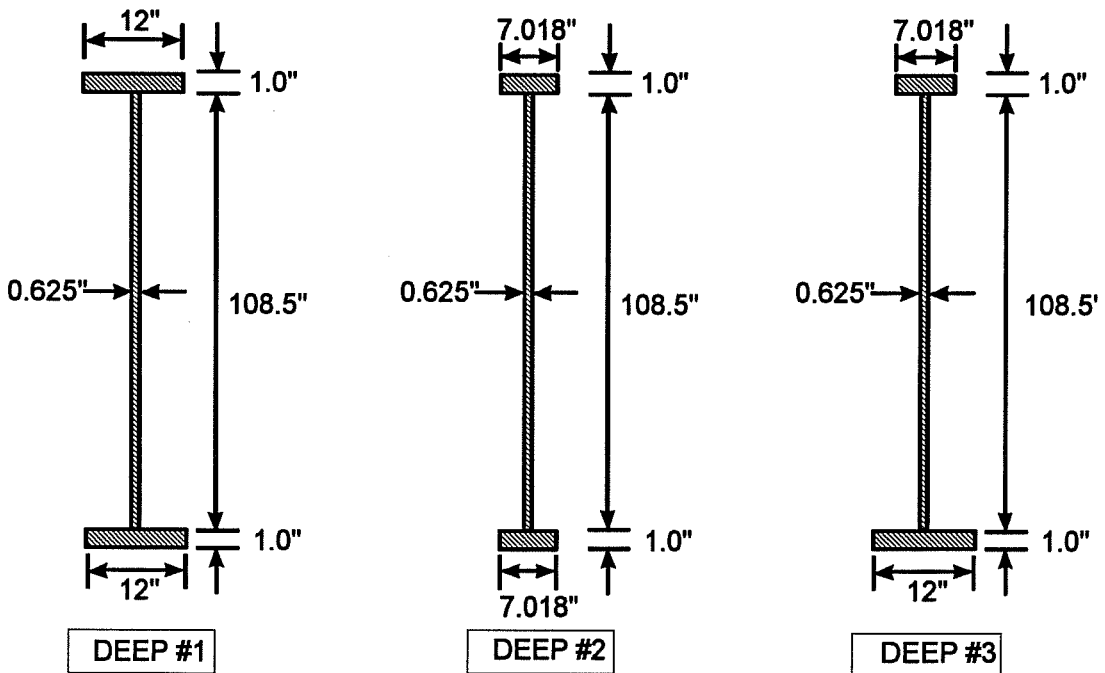
Figure 4.3b Deep cross-sections considered.

Table 4.13a Distributed Load on Shallow #1 and Deep #1				
	Shallow #1		Deep #1	
Length	W	B	W	B
25 feet	1.23	1.42	3.82 (>1.75)	0.79 (1.46)
50 feet	0.62	1.27	1.91(>1.75)	1.46 (1.46)
75 feet	0.41	1.19	1.28	1.43

Table 4.13b Distributed Load on Shallow #2 and Deep #2				
	Shallow #2		Deep #2	
Length	W	B	W	B
25 feet	0.67	1.29	1.91(>1.75)	1.46 (1.46)
50 feet	0.34	1.16	0.96	1.37
75 feet	0.22	1.11	0.64	1.28

Table 4.13c Distributed Load on Shallow #3 and Deep #3				
	Shallow #3		Deep #3	
Length	W	B	W	B
25 feet	1.04	1.39	3.12 (>1.75)	1.17 (1.46)
50 feet	0.52	1.24	1.56	1.46
75 feet	0.35	1.17	1.04	1.39

Tables 4.14a, 4.14b, and 4.14c show the values of $C_b^*{}_{ANSYS}$ and $C_b^*{}_{SSRC}$ for the shallow and deep girders. As with previous tables, the number in parenthesis indicates the percent error of the SSRC equation with respect to the ANSYS results.

Table 4.14a Distributed Load at Top Flange on Shallow #1 and Deep #1					
	Shallow #1			Deep #1		
Length	$C_b^*{}_{ANSYS}$	3rd Ed. $C_b^*{}_{SSRC}$	4th Ed. $C_b^*{}_{SSRC}$	$C_b^*{}_{ANSYS}$	3rd Ed. $C_b^*{}_{SSRC}$	4th Ed. $C_b^*{}_{SSRC}$
25 feet	0.80	0.80 (0%)	0.79 (+1.2%)	0.71	0.74 (-4.2%)	0.77[a] (-8.4%)
50 feet	0.89	0.89 (0%)	0.88 (+1.1%)	0.76	0.77 (-1.3%)	0.77[a] (-1.3%)
75 feet	0.95	0.95 (0%)	0.94 (+1.0%)	0.80	0.80 (0%)	0.78 (+2.5%)

[a]The "minimum" value of C_b^* was used for the fourth edition method since W > 1.75.

Table 4.14b Distributed Load at Top Flange on Shallow #2 and Deep #2					
	Shallow #2			Deep #2		
Length	$C_b^*{}_{ANSYS}$	3rd Ed. $C_b^*{}_{SSRC}$	4th Ed. $C_b^*{}_{SSRC}$	$C_b^*{}_{ANSYS}$	3rd Ed. $C_b^*{}_{SSRC}$	4th Ed. $C_b^*{}_{SSRC}$
25 feet	0.88	0.88 (0%)	0.87 (+1.1%)	0.76	0.77 (-1.3%)	0.77[a] (-1.3%)
50 feet	0.98	0.98 (0%)	0.96 (+2.0%)	0.83	0.83 (0%)	0.82 (+1.2%)
75 feet	1.02	1.02 (0%)	1.01 (+1.0%)	0.90	0.89 (1.1%)	0.88 (+2.2%)

[a]The "minimum" value of C_b^* was used for the fourth edition method since W > 1.75.

Table 4.14c Distributed Load at Top Flange on Shallow #3 and Deep #3				
	Shallow #3		Deep #3	
Length	C_b^* ANSYS	4th Ed. C_b^* SSRC	C_b^* ANSYS	4th Ed. C_b^* SSRC
25 feet	0.83	0.80 (+3.6%)	0.77	0.77[a] (0.0%)
50 feet	0.91	0.90 (+1.1%)	0.80	0.77 (+3.8%)
75 feet	0.97	0.96 (+1.0%)	0.84	0.81 (+3.6%)

[a]The "minimum" value of C_b^* was used for the fourth edition method since W > 1.75.

For the doubly-symmetric sections, the methods from 3rd and the 4th editions of the SSRC Guide each provided good estimates of the effects of top flange loading when compared to the finite element results. Since the "curve fit" from the 4th edition of the SSRC Guide does not provide good estimates for the sections with beam parameters, W, greater than 1.75, minimum limits were imposed. The percent error for the section deep #1 was 8.4% unconservative with respect to the finite element results. The reason for this large percent error is because the equation in the 4th edition of the SSRC guide The SSRC equations do a very good job of predicting the effects of load height, with the exception of the 25 foot long girders for Deep #1 and Deep #3. The percent error for some of these cases were therefore relatively high with respect to the finite element results, however, if the minimum limits were not imposed these errors would have been significantly larger. The method in the 4th edition of the SSRC Guide did a good job of estimating the load height effects on the singly-symmetric sections, particularly when the warping coefficient was approximated with the expression for doubly-symmetric sections, $C_w = I_y d^2 / 4$.

As a final check on the accuracy of the SSRC guide equations for load height on singly-symmetric sections, the sections previously shown in Figure 4.2 were considered. These sections are repeated in Figure 4.4 for convenience.

Tables 4.15a and 4.15b show the C_b^* values for top flange loading on sections A-G for loading consisting of a point load at midspan and a distributed load, respectively. The girders had a 25 foot span. The percent difference between the values from the SSRC Guide and the ANSYS

B_{top}

T_{top}

60"

0.73493"

1"

12"

Section	B_{top}	T_{top}	$\dfrac{I_{yc}}{I_y}$	$y_{shear\ center\ bottom}$	$y_{centroid\ bottom}$
Section A	2"	0.25"	0.001	0.07"	24.00"
Section B	2"	1"	0.005	0.28"	24.77"
Section C	4"	1"	0.036	2.14"	25.96"
Section D	6"	1"	0.111	6.67"	27.06"
Section E	8"	1"	0.229	13.71"	28.11"
Section F	10"	1"	0.366	21.99"	29.08"
Section G	12"	1"	0.500	30.00"	30.00"

Figure 4.4 Additional sections considered for study of C_b factors for singly-symmetric sections.

results are shown in parentheses. The percent difference is given with respect to the ANSYS results, and a negative percentage indicates that the SSRC Guide equations are unconservative with respect to the ANSYS results. The corresponding results for top flange loading on sections A-G with lengths of 50 feet and 75 feet are shown in Tables 4.16a, 4.16b, 4.17a, and 4.17c.

Table 4.15a P @ Top Flange of Sections A-G with 25 Foot Span			
Section	ANSYS C_b^*	SSRC C_b^* - $C_{w\ Unsym}$	SSRC C_b^* - $C_{w\ Sym}$
A	0.77	1.26 (-63.6 %)	0.85 (-10.4%)
B	0.82	1.29 (-57.3%)	0.85 (-3.6%)
C	0.87	1.01(-16.1%)	0.85 (2.3%)
D	0.88	0.90 (-2.3%)	0.85 (3.4%)
E	0.87	0.86 (1.1%)	0.85 (2.3%)
F	0.86	0.85 (1.1%)	0.85 (1.1%)
G	0.83	0.86 (-3.6%)	0.86 (-3.6%)

Table 4.15b w @ Top Flange of Sections A-G with 25 Foot Span			
Section	ANSYS $C_b{}^*$	SSRC $C_b{}^*- C_{w\ Unsym}$	SSRC $C_b{}^*- C_{w\ Sym}$
A	0.76	1.27 (-67.1%)	0.76 (0%)
B	0.78	1.00 (-28.2%)	0.76 (2.6%)
C	0.79	0.88 (-11.4%)	0.76 (3.8%)
D	0.79	0.8 (-1.3%)	0.76 (3.8%)
E	0.78	0.77 (1.3%)	0.76 (2.6%)
F	0.77	0.77 (0%)	0.77 (0%)
G	0.75	0.78 (-4.0%)	0.78 (-4.0%)

Table 4.16a P @ Top Flange of Sections A-G with 50 Foot Span			
Section	ANSYS $C_b{}^*$	SSRC $C_b{}^*- C_{w\ Unsym}$	SSRC $C_b{}^*- C_{w\ Sym}$
A	0.82	1.30 (-58.5%)	0.94 (-14.6%)
B	0.84	1.26 (-50.0%)	0.95 (-13.1%)
C	0.90	1.14 (-26.7%)	0.95 (-5.6%)
D	0.94	1.04 (-10.6%)	0.95 (-1.1%)
E	0.94	0.97 (-3.2%)	0.94 (0%)
F	0.93	0.93 (0%)	0.92 (1.1%)
G	0.90	0.90 (0%)	0.90 (0%)

Table 4.16b w @ Top Flange of Sections A-G with 50 Foot Span			
Section	ANSYS C_b^*	SSRC C_b^* - $C_{w\ Sym}$	SSRC C_b^* - $C_{w\ Sym}$
A	0.82	1.31 (-59.8%)	0.83 (-1.2%)
B	0.82	1.06 (-29.3%)	0.83 (-1.2%)
C	0.84	0.97 (-15.5%)	0.83 (1.2%)
D	0.84	0.90 (-7.1%)	0.83 (1.2%)
E	0.84	0.85 (-1.2%)	0.82 (2.4%)
F	0.82	0.82 (0%)	0.81 (1.2%)
G	0.81	0.80 (1.2%)	0.80 (1.2%)

Table 4.17a P @ Top Flange of Sections A-G with 75 Foot Span			
Section	ANSYS C_b^*	SSRC C_b^* - $C_{w\ Unsym}$	SSRC C_b^* - $C_{w\ Sym}$
A	0.87	1.32 (-51.7%)	1.02 (-17.2%)
B	0.90	1.29 (-43.3%)	1.03 (-14.4%)
C	0.96	1.20 (-25.0%)	1.03 (-7.3%)
D	0.99	1.11 (-12.1%)	1.03 (-4.1%)
E	1.01	1.05 (-4.0%)	1.02 (-1.0%)
F	1.00	1.01 (-1.0%)	1.00 (0%)
G	0.98	0.98 (0%)	0.98 (0%)

Table 4.17b w @ Top Flange of Sections A-G with 75 Foot Span			
Section	ANSYS C_b^*	SSRC C_b^*- $C_{w\ Unsym}$	SSRC C_b^*- $C_{w\ Sym}$
A	0.86	1.32 (-53.5%)	0.89 (-3.5%)
B	0.88	1.08 (-22.7%)	0.89 (-1.14%)
C	0.89	1.01 (-13.5%)	0.89 (0%)
D	0.89	0.95 (-6.7%)	0.89 (0%)
E	0.89	0.91 (-2.2%)	0.88 (1.1%)
F	0.88	0.88 (0%)	0.87 (1.14%)
G	0.86	0.86 (0%)	0.86 (0%)

Results from the Tables 4.15-4.17 have also been plotted in Figures 4.5-4.7. The values of C_b^* have been plotted on the vertical axis versus the values of $I_{yc}/$ I_y on the horizontal axis. If an artificial warping term is used, the equations from the SSRC guide do a very good job of estimating the effects of top flange loading for values of $I_{yc}/$ I_y greater than approximately 0.1. This is similar to what was observed in Section 4.2 for the C_b values for midheight loading on these sections.

Figure 4.5a Effect of I_{yc} / I_y on C_b^* for P at midspan top flange.
(25 foot span)

Figure 4.5b Effect of I_{yc} / I_y on C_b^* for w at top flange.
(25 foot span)

Figure 4.6a Effect of I_{yc} / I_y on C_b^* for P at midspan top flange.
(50 foot span)

Figure 4.6b Effect of I_{yc} / I_y on C_b^* for w at top flange.
(50 foot span)

Figure 4.7a Effect of I_{yc} / I_y on C_b* for P at midspan top flange.
(75 foot span)

Figure 4.7b Effect of I_{yc} / I_y on C_b* for w at top flange.
(75 foot span)

The singly-symmetric sections A-G were also subjected to loading at the bottom flange. The results from these load cases are shown in Tables 4.18-4.20.

Table 4.18a P @ Bottom Flange of Sections A-G with 25 Foot Span			
Section	ANSYS $C_b{}^*$	SSRC $C_b{}^*$ - C_w Unsym	SSRC $C_b{}^*$ - C_w Sym
A	2.08	1.45 (30.3%)	2.14 (-2.9%)
B	2.21	1.54 (30.3%)	2.14 (3.2%)
C	2.41	1.81(24.9%)	2.14 (11.2%)
D	2.39	2.02 (15.5%)	2.14 (10.5%)
E	2.31	2.12 (8.2%)	2.14 (7.4%)
F	2.24	2.14 (4.5%)	2.13 (4.9%)
G	2.18	2.11 (3.2%)	2.11 (3.2%)

Table 4.18b w @ Bottom Flange of Sections A-G with 25 Foot Span			
Section	ANSYS $C_b{}^*$	SSRC $C_b{}^*$ - C_w Unsym	SSRC $C_b{}^*$ - C_w Sym
A	1.58	1.43 (9.5%)	1.64 (-3.8%)
B	1.64	1.25 (23.8%)	1.64 (0%)
C	1.75	1.43 (18.3%)	1.64 (6.3%)
D	1.75	1.57 (10.3%)	1.64 (6.3%)
E	1.71	1.63 (4.7%)	1.64 (4.1%)
F	1.69	1.63 (3.6%)	1.63 (3.6%)
G	1.66	1.61 (3.0%)	1.61 (3.0%)

Table 4.19a P @ Bottom Flange of Sections A-G with 50 Foot Span			
Section	ANSYS C_b^*	SSRC $C_b^* - C_{w\ Unsym}$	SSRC $C_b^* - C_{w\ Sym}$
A	1.75	1.40 (20.0%)	1.93 (-10.3%)
B	1.79	1.45 (19.0%)	1.92 (-7.3%)
C	1.94	1.60 (17.5%)	1.92 (1.0%)
D	2.00	1.76 (12.0%)	1.93 (3.5%)
E	2.02	1.88 (6.9%)	1.95 (3.5%)
F	2.02	1.96 (3.0%)	1.98 (2.0%)
G	2.01	2.01 (0%)	2.01 (0%)

Table 4.19b w @ Bottom Flange of Sections A-G with 50 Foot Span			
Section	ANSYS C_b^*	SSRC $C_b^* - C_{w\ Unsym}$	SSRC $C_b^* - C_{w\ Sym}$
A	1.39	1.39 (0%)	1.51 (-8.6%)
B	1.40	1.19 (15%)	1.51 (-7.9%)
C	1.49	1.29 (13.4%)	1.51 (-1.3%)
D	1.52	1.39 (8.6%)	1.51 (0.7%)
E	1.54	1.48 (3.9%)	01.52(1.3%)
F	1.55	1.53 (1.3%)	1.54 (0.6%)
G	1.56	1.57 (-0.6%)	1.57 (-0.6%)

Table 4.20a P @ Bottom Flange of Sections A-G with 75 Foot Span			
Section	ANSYS C_b^*	SSRC C_b^*- $C_{w\ Unsym}$	SSRC C_b^*- $C_{w\ Sym}$
A	1.64	1.39 (15.2%)	1.78 (-8.5%)
B	1.66	1.42 (14.4%)	1.77 (-6.6%)
C	1.73	1.52 (12.1%)	1.77 (-2.3%)
D	1.79	1.64 (8.4%)	1.78 (0.6%)
E	1.83	1.73 (5.5%)	1.79 (2.2%)
F	1.86	1.81 (2.7%)	1.82 (2.20%)
G	1.88	1.86 (1.1%)	1.86 (1.1%)

Table 4.20b w @ Bottom Flange of Sections A-G with 75 Foot Span			
Section	ANSYS C_b^*	SSRC C_b^*- $C_{w\ Unsym}$	SSRC C_b^*- $C_{w\ Sym}$
A	1.32	1.38 (-4.5%)	1.41 (-6.8%)
B	1.33	1.17 (12.0%)	1.41 (-6.0%)
C	1.37	1.24 (9.5%)	1.40 (-2.2%)
D	1.40	1.32 (5.7%)	1.41 (-0.7%)
E	1.43	1.38 (3.5%)	1.42 (0.7%)
F	1.45	1.43 (1.4%)	1.44 (0.7%)
G	1.47	1.46 (0.7%)	1.46 (0.7%)

Results from the Tables 4.18-4.20 have also been plotted in Figures 4.8-4.10. The values of C_b^* have been plotted on the vertical axis versus the values of I_{yc}/I_y on the horizontal axis.
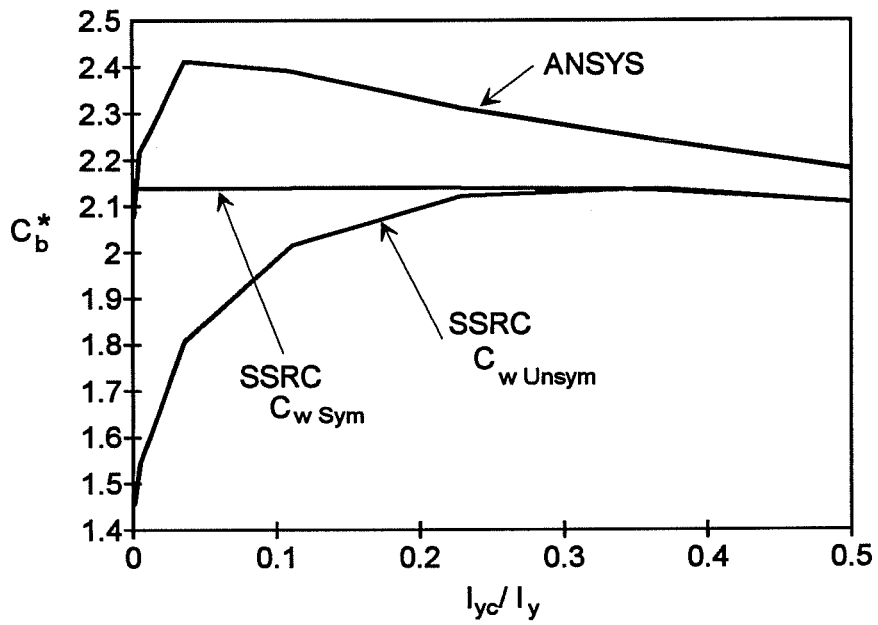
Figure 4.8a Effect of I_{yc} / I_y on C_b^* for P at midspan bottom flange.
(25 foot span)
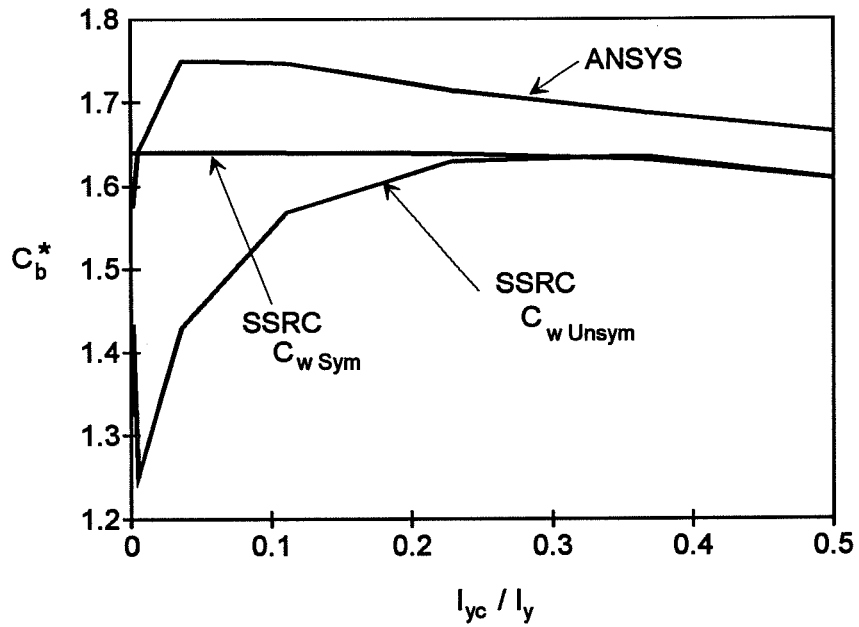
Figure 4.8b Effect of I_{yc} / I_y on C_b^* for w at bottom flange.
(25 foot span)
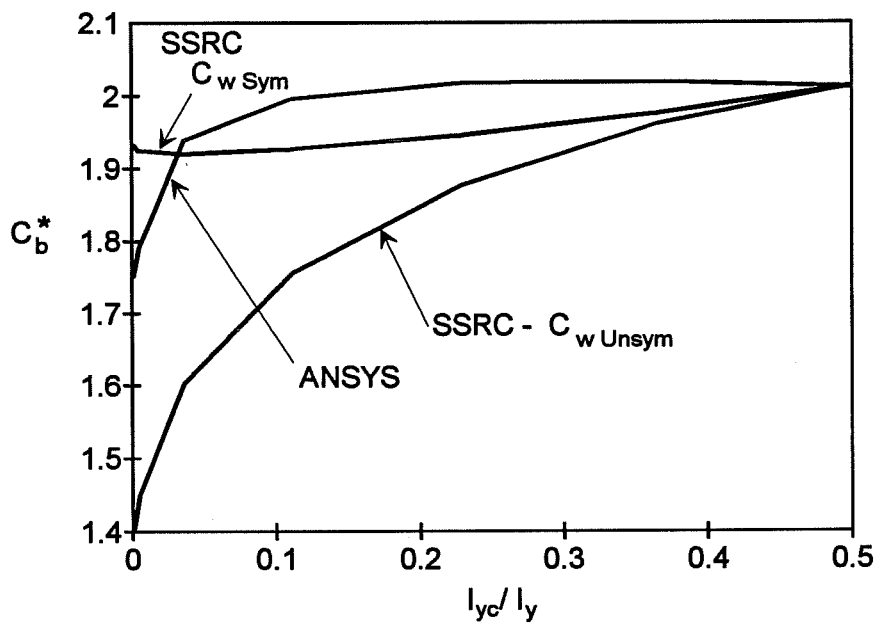
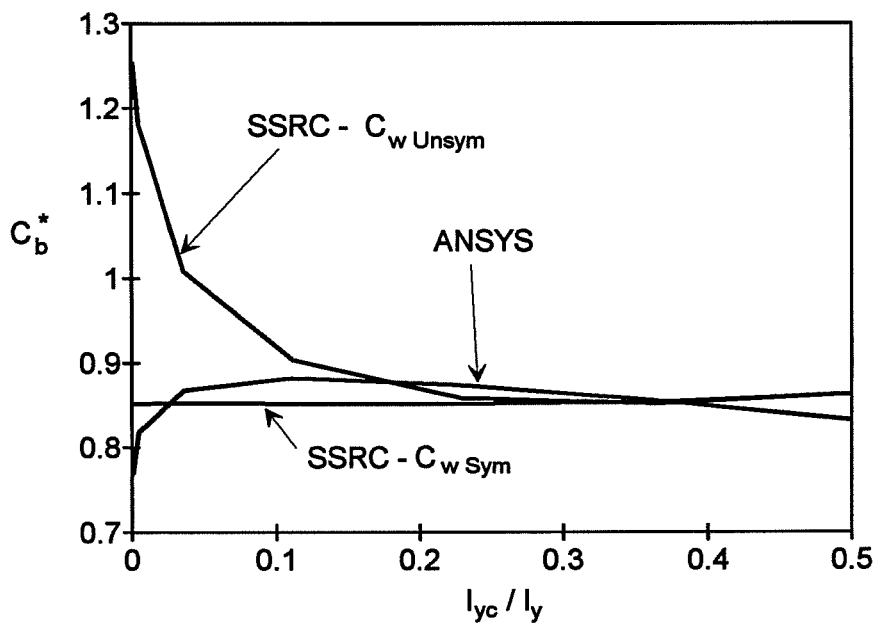**Figure 4.9a Effect of I_{yc} / I_y on C_b^* for P at midspan bottom flange.**
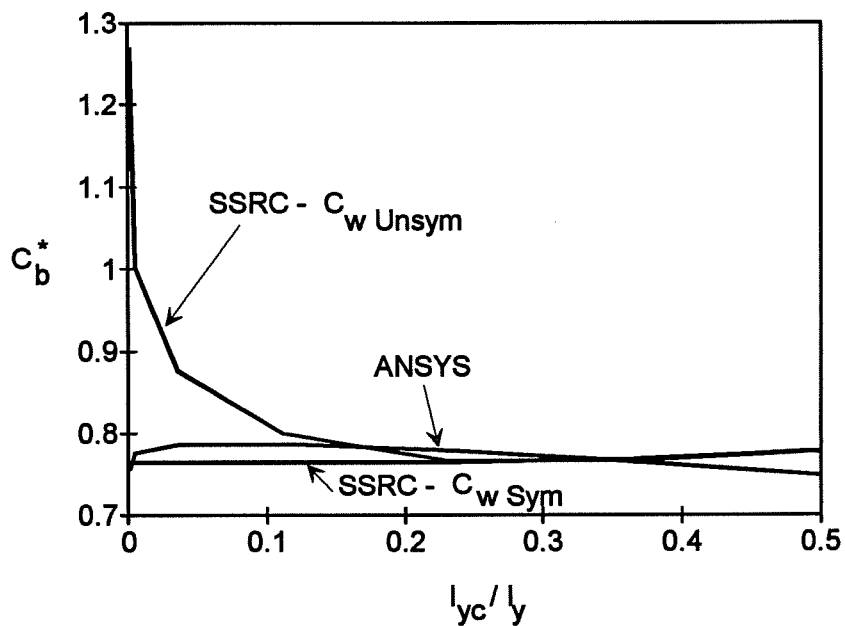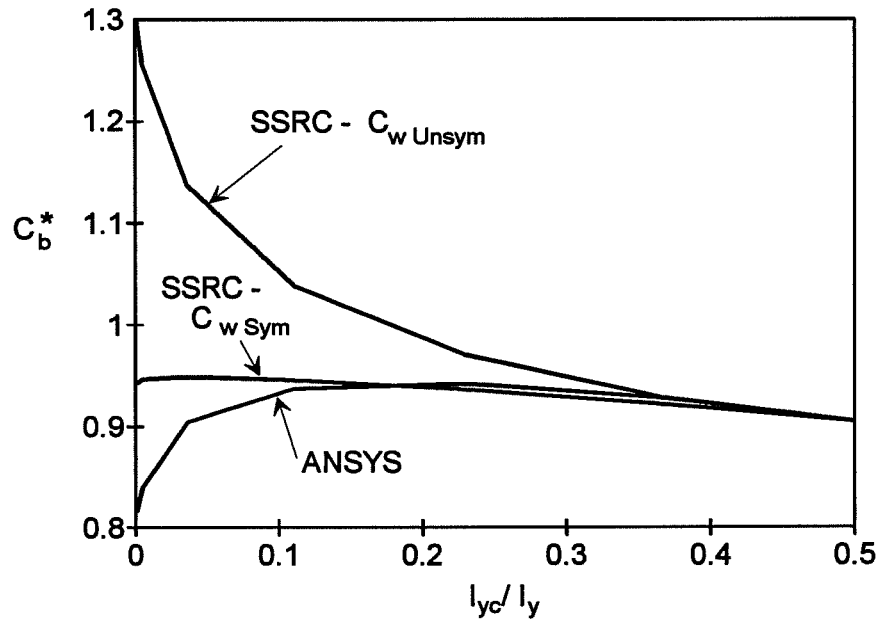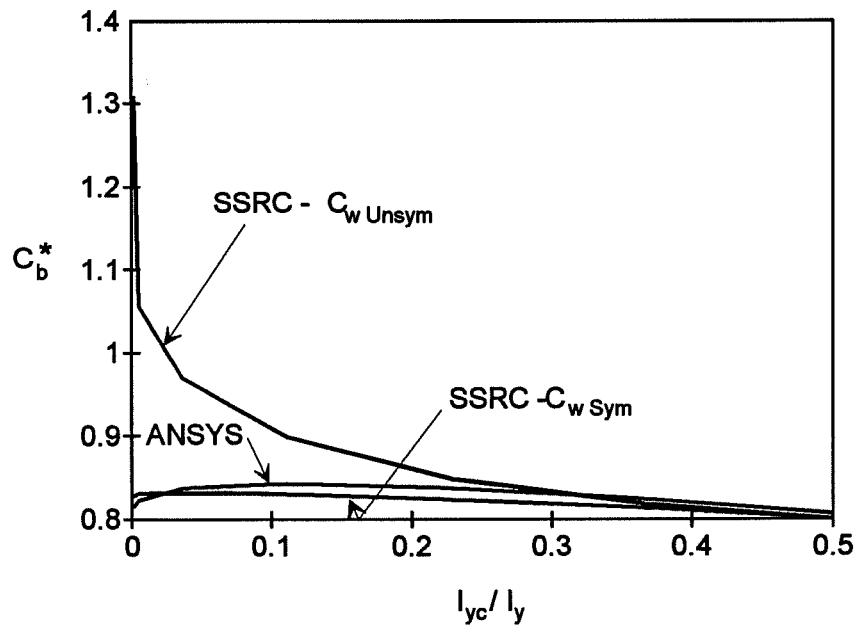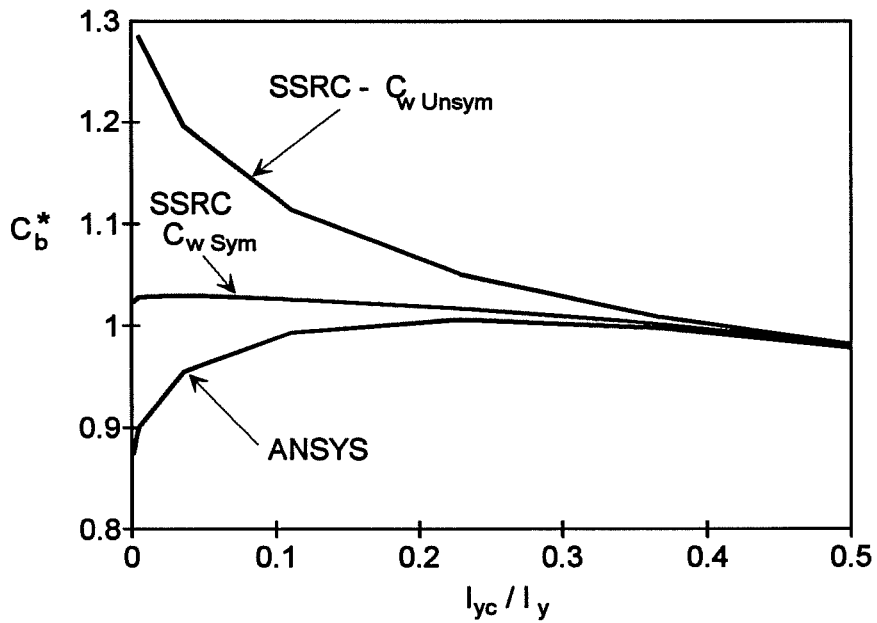(50 foot span)
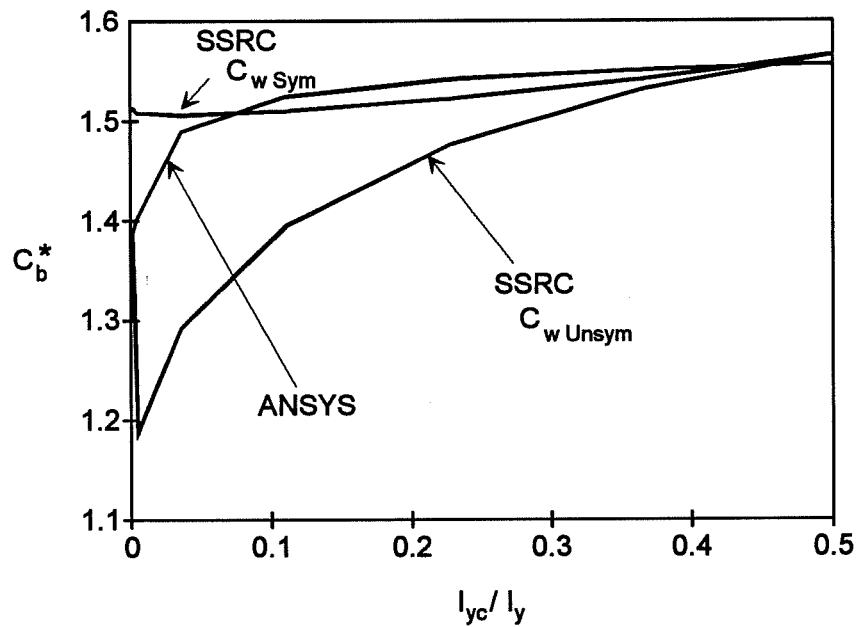
Figure 4.9b Effect of I_{yc} / I_y on C_b^* for w at bottom flange.
(50 foot span)
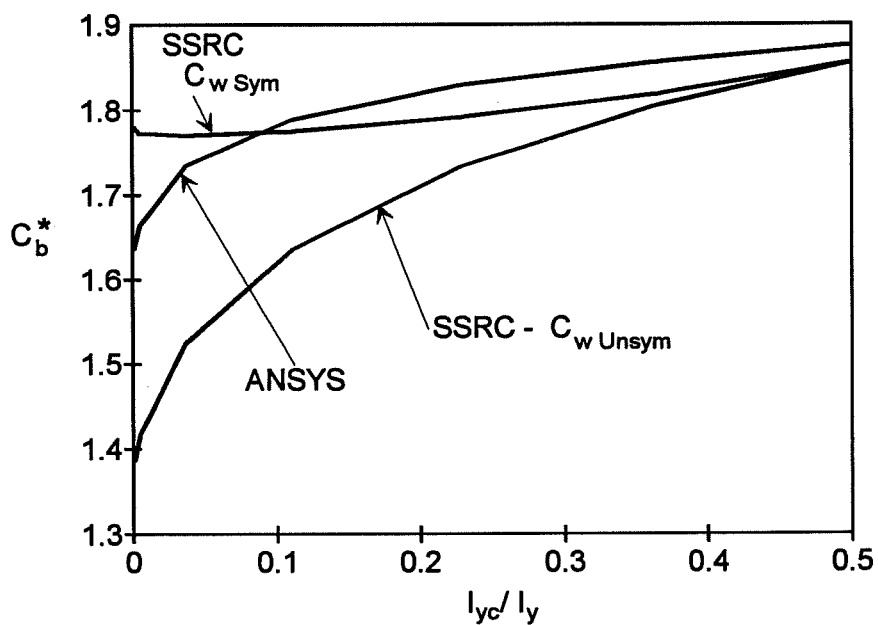
Figure 4.10a Effect of I_{yc} / I_y on C_b* for P at midspan bottom flange.
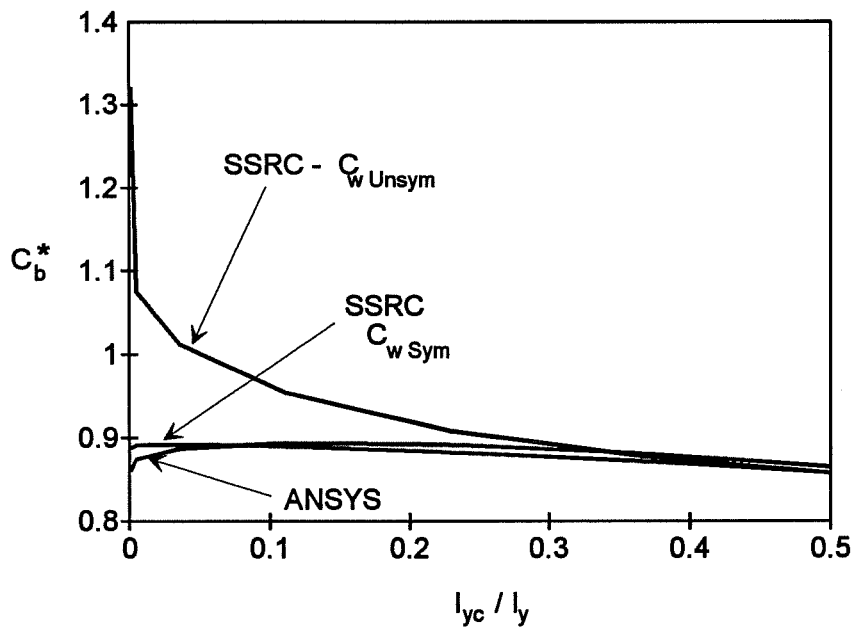**(75 foot span)**
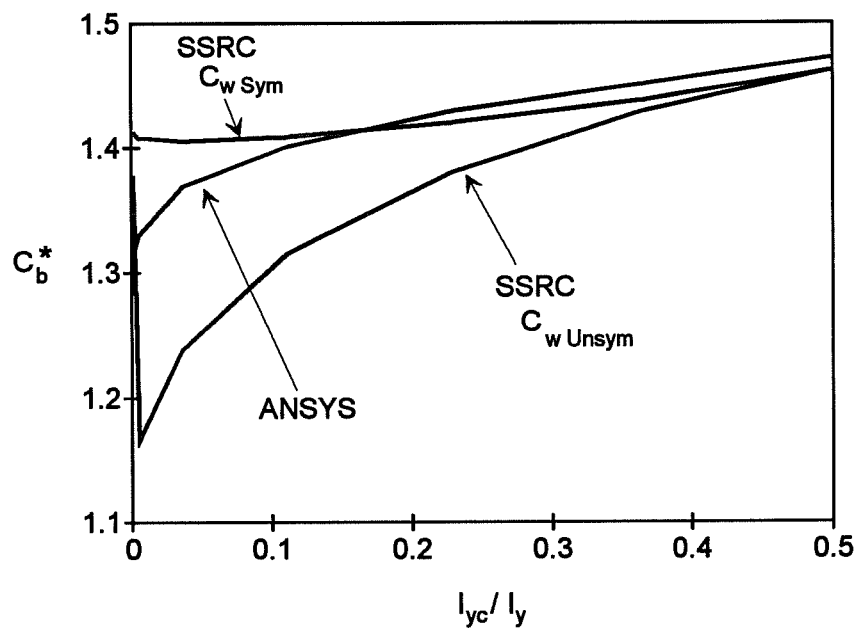
Figure 4.10b Effect of I_{yc} / I_y on C_b* for w at bottom flange.
(75 foot span)

In general, the equations in the 3rd and 4th editions of the SSRC Guide provide a good estimate of the load height effects for doubly-symmetric sections. Although they are not intended for singly-symmetric sections, the equations in the 4th edition of the SSRC Guide do a good job of estimating the buckling load for these girders as well. The equations are more accurate and in some cases conservative if the singly-symmetric section is treated like a doubly-symmetric section for calculating the warping term ($C_w = I_y d^2 / 4$).

4.4 Load Height Effects in Girders with Intermediate Bracing

The methods of accounting for load height which have been presented in the previous section are for simply supported girders with no bracing between the supports. Most beams, however, have intermediate braces (cross-frames) to reduce the unbraced length. No solutions were found in the literature for load height effects on girders with intermediate braces. Figure 4.11 shows the moment diagram which would result if braces were placed at the third points of a girder subjected to a point load at midspan. Effects of load height on this problem are significantly different than the cases studied in Section 4.3. If the beam is prismatic, the middle third of the beam would be critical for lateral-torsional buckling. The moment diagram of the critical beam segment is quite different than for simply-supported beams with no intermediate braces. The moment at the ends of the middle third are 66.7% of the moment at the centerline of the beam segment. The moments at the brace points generally do not impose any load height effects. Therefore, only 33.3% of the midspan moment generates load height effects. In addition, the exterior thirds of the girder would provide some warping restraint to the middle third which would increase the buckling capacity of the girder.

This section presents the finite element results for simply supported beams with intermediate braces at the third points. Two load cases were considered: a point load applied at the midspan top flange and a distributed load applied at the top flange. Figures 4.12a and 4.12b show the respective moment diagrams for beams with a point load at midspan and a distributed load. The beams have discrete braces at the third points. The boundary conditions which were used to model the middle third of the beam are shown below each of the figures for the entire beam segment. The middle third of the beam was modeled as a simply supported beam with a moment at the support and the corresponding transverse loading applied at the top flange. The beams had cross-frames at the "supports", but the warping restraint that would normally be offered by the exterior thirds of the beam was neglected and the flanges were free to warp. The length
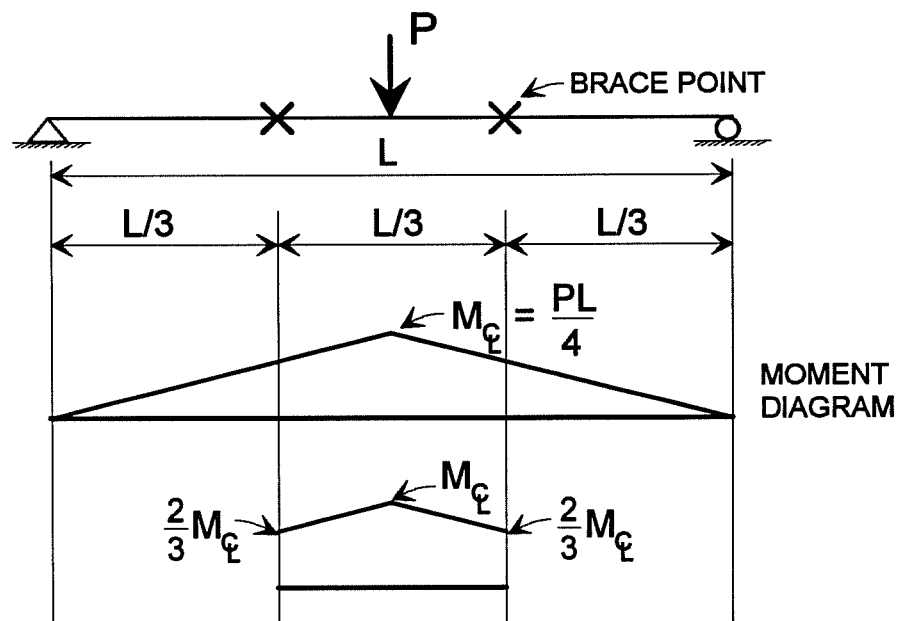
Figure 4.11 Moment diagram for point load applied at the centerline of a simple span.

$$M_{C\!\!\!\!L} = \frac{PL_g}{4}$$

MOMENT DIAGRAM

$$L_g$$

$$L_b$$

$$P_b = \frac{4}{3L_b}$$

$$\frac{2}{3}k"$$ $$\frac{2}{3}k"$$

brace point

MODEL BEAM

$$M_{C\!\!\!\!L} = \frac{\frac{2}{3}k" + \frac{(\frac{4}{3L_b})L_b}{4}}{} = 1k"$$
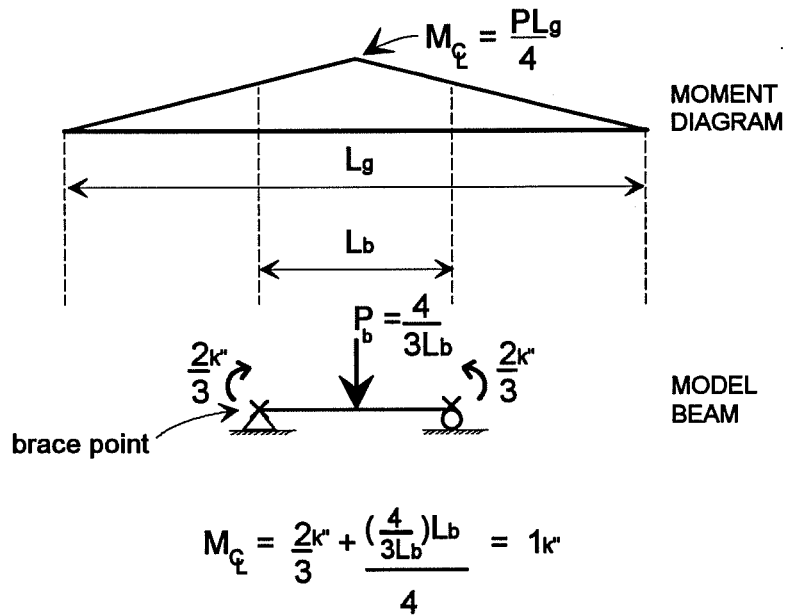
Figure 4.12a Model of beam with cross-frames @ third points and point load @ midspan.

$$M_{C\!\!\!\!L} = \frac{wL_g^2}{8}$$

MOMENT DIAGRAM

$$L_g$$

$$L_b$$

$$w_b = \frac{0.111*8}{L_b^2}$$

$$0.889 k"$$ $$0.889 k"$$

brace point

MODEL BEAM

$$M_{C\!\!\!\!L} = 0.889 k" + \left(\frac{0.111*8}{L_b^2} \right) \frac{L_b^2}{8} = 1k"$$
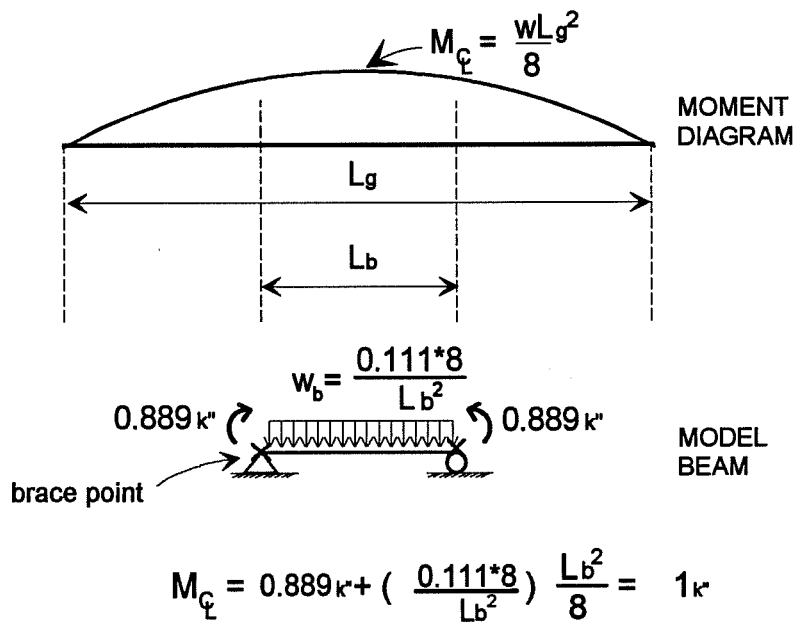
Figure 4.12b Model of beam with cross-frames @ third points and distributed load.

of the "middle third" of the beam is shown as a length L_b, so that the length of the hypothetical beam which was being modeled was equal to $L_g = 3 \times L_b$.

For the load case consisting of a point load at midspan, the moment which was applied at the support or "brace" was 0.667 k-in. The transverse load applied at midspan was equal to $4 \times (0.333 \text{ k-in}) / L_b$, which produced a midspan moment of 1 k-in. The eigenvalue which resulted from a bifurcation analysis therefore represented the midspan moment which would occur at buckling.

Similar loading was applied in the case consisting of a uniform distributed load. The moment which was applied at the support or "brace" was 0.889 k-in. The distributed load applied at the top flange was $8 \times (0.111 \text{ k-in})/L^2$ which resulted in a midspan moment of 1 k-in.

A value of the C_b^* factor to account for load height effects could then be calculated for the finite element results using the following expression:

$$C_{b\ ANSYS}^* = \frac{M_{CL\ Top\ Flange}}{M_{Uniform\ Moment}} \qquad (4.6)$$

In Equation 4.6, $M_{CL\,Top\,Flange}$ is the midspan moment which results when the girder buckles from top flange loading, while $M_{Constant\ moment}$ is the buckling capacity for constant moment. Three different lengths were used for the beams considered: 25 feet, 37.5 feet, and 50 feet. The full lengths of the respective beams which were being simulated would therefore be equal to 75 feet, 112.5, and 150 feet. The first set of cross-sections which were considered in this study were the three sections shown previously in Figure 4.1.

In addition to subjecting the girders to loading at the top flange, the girders were also loaded at midheight. A $C_{b\ ANSYS}$ value was calculated using the same expression in Equation 4.8 except $M_{CL\ Top\ Flange}$ was replaced with the midspan moment caused by loading applied at midheight ($M_{CL\ Midheight}$). These $C_{b\ ANSYS}$ values were compared to values predicted using the modified Kirby-Nethercot formula. Tables 4.21a and 4.21b show the comparison for the respective load cases of a midheight point load applied at midspan and a distributed load applied at midheight. The values in Tables 4.21a and 4.21b are representative of the results found for all of the cross-sections considered in this section. For all of the cross-sections which were considered, the $C_{b\ ANSYS}$ values for midheight loading ranged from 1.08-1.11 for a point load at midspan, and

from 1.01-1.02 for a uniform distributed load. These values compared very well with the modified Kirby-Nethercot formula.

Table 4.21a Section #1 C_b values for P @ Midheight Braces at 3rd Points - Middle Third Segment		
L (feet)	C_b ANSYS	C_b Kirby Nethercot
25	1.10	1.09
37.5	1.10	1.09
50	1.11	1.09

Table 4.21b Section #1 C_b values for w @ Midheight Braces at 3rd Points - Middle Third Segment		
L (feet)	C_b ANSYS	C_b Kirby Nethercot
25	1.02	1.01
37.5	1.02	1.01
50	1.02	1.01

The results in Section 4.3 showed that loads applied at the top flange caused a significant reduction in the buckling load when compared to loading applied at midheight. The reduction in buckling load is not quite as significant when intermediate braces are present. Tables 4.22a, 4.22b, and 4.23c show the values of the C_b^* which resulted from the finite element studies for the respective sections #1, #2, and #3 with top flange loading. For the three different lengths and different cross-sections, all of the C_b^* are very close to 1.00. The values range from 0.96 to 1.02.

Additional cross-sections were considered to increase the range of geometry which were considered. The shallow and deep sections which were previously shown in Figures 4.3a and 4.3b were considered.

Table 4.22a Section #1 C_b^* values for P @ Top Flange and w @ Top Flange Braces at 3rd Points - Middle Third Segment		
L (feet)	P @ Top Flange C_b^*ANSYS	w @ Top Flange C_b^*ANSYS
25	0.96	0.97
37.5	0.98	0.98
50	0.99	0.98

Table 4.22b Section #2 C_b^* values for P @ Top Flange and w @ Top Flange Braces at 3rd Points - Middle Third Segment		
L (feet)	P @ Top Flange C_b^*ANSYS	w @ Top Flange C_b^*ANSYS
25	0.99	0.98
37.5	1.01	0.99
50	1.02	0.99

Table 4.22c Section #3 C_b^* values for P @ Top Flange and w @ Top Flange Braces at 3rd Points - Middle Third Segment		
L (feet)	P @ Top Flange C_b^*ANSYS	w @ Top Flange C_b^*ANSYS
25	0.97	0.97
37.5	0.98	0.98
50	1.00	0.98

Tables 4.23a, 4.23b, and 4.23c show the values of the C_b^* which resulted from the finite element studies for the respective sections shallow #1, #2, and #3. For the three different lengths and different cross-sections, all of the C_b^* are close to 1.00. The values range from 0.98 to 1.05.

Table 4.23a	Shallow #1 C_b^* values for P @ Top Flange and w @ Top Flange Braces at 3rd Points - Middle Third Segment	
L (feet)	P @ Top Flange $C_b^*{}_{ANSYS}$	w @ Top Flange $C_b^*{}_{ANSYS}$
25	0.98	0.98
37.5	1.00	0.98
50	1.02	0.99

Table 4.23b	Shallow #2 C_b^* values for P @ Top Flange and w @ Top Flange Braces at 3rd Points - Middle Third Segment	
L (feet)	P @ Top Flange $C_b^*{}_{ANSYS}$	w @ Top Flange $C_b^*{}_{ANSYS}$
25	1.02	0.99
37.5	1.04	1.00
50	1.05	1.00

Table 4.23c	Shallow #3 C_b^* values for P @ Top Flange and w @ Top Flange Braces at 3rd Points - Middle Third Segment	
L (feet)	P @ Top Flange $C_b^*{}_{ANSYS}$	w @ Top Flange $C_b^*{}_{ANSYS}$
25	0.99	0.98
37.5	1.01	0.99
50	1.03	0.99

Tables 4.24a, 4.24b, and 4.24c show the values of the C_b^* which resulted from the finite element studies for the respective sections deep #1, #2, and #3. For the three different lengths and different cross-sections, all of the C_b^* are close to 1.00. The values range from 0.96 to 1.00.

Table 4.24a Deep #1 C_b^* values for P @ Top Flange and w @ Top Flange Braces at 3rd Points - Middle Third Segment		
L (feet)	P @ Top Flange C_b^* ANSYS	w @ Top Flange C_b^* ANSYS
25	0.96	0.97
37.5	0.96	0.97
50	0.97	0.97

Table 4.24b Deep #2 C_b^* values for P @ Top Flange and w @ Top Flange Braces at 3rd Points - Middle Third Segment		
L (feet)	P @ Top Flange C_b^* ANSYS	w @ Top Flange C_b^* ANSYS
25	0.97	0.97
37.5	0.98	0.98
50	1.00	0.98

Table 4.24c Deep #3 C_b^* values for P @ Top Flange and w @ Top Flange Braces at 3rd Points - Middle Third Segment		
L (feet)	P @ Top Flange C_b^* ANSYS	w @ Top Flange C_b^* ANSYS
25	0.96	0.97
37.5	0.97	0.97
50	0.98	0.98

For each of the different cross-sections considered, there was a slight increase in C_b^* with an increase in length. This is because there is a reduction in the warping stiffness of the section with increasing length. The effects of load height become less significant with a reduction in the warping stiffness. Although the C_b^* values did vary a small amount with increasing length, the

values were relatively uniform. For the nine different cross-sections, and three different lengths which were considered for each, the range of C_b^* values was between 0.96 and 1.05. In general, the values of C_b^* were relatively close to 1.00.

For beams with intermediate bracing and top flange loading, the C_b^* value could be taken as 1.00. Some of the $C_{b\ ANSYS}^*$ values did fall slightly below 1.00, however this analysis was somewhat conservative since there would be some warping restraint available from the girder segments on the exterior thirds of the beam.

4.5 Summary

This chapter has presented finite element results for several different sections which have been subjected to a variety of loading conditions. These results have demonstrated the behavior of singly-symmetric and doubly-symmetric girders subjected to moment gradients and load height effects. These girders did not have a shear diaphragm for bracing, however, cases with and without intermediate bracing were studied.

Reasonable estimates of the buckling load for top flange loading were obtained by neglecting the warping term in the closed formed solutions. Although the accuracy of this approach did fluctuate slightly with respect to the finite element studies, it is the simplest approach to account for top flange loading.

The modified Kirby-Nethercot formula had very good agreement with the ANSYS results for doubly-symmetric sections with transverse loads applied at midheight. The modified Kirby-Nethercot equation also had good agreement with the ANSYS results when transverse loads were applied at midheight of singly-symmetric sections with ratios of I_{yc}/I_y greater than 0.1. For singly-symmetric girders with I_{yc}/I_y greater than 0.1, loading applied below midheight (closer to tension flange) produced buckling loads which were larger than predicted by the modified Kirby-Nethercot formula.

For girders subjected to transverse loads applied at the top and bottom flange, the equations in the 3rd and 4th editions of the SSRC Guide provided good estimates of the load height effects for doubly-symmetric sections. For the equations in the 4th edition of the SSRC Guide, it was necessary for some of the girders to limit the value of C_b^* when the beam parameter, W, was greater than 1.75. Although the equations in the 4th edition of the SSRC Guide are not intended for singly-symmetric sections, good estimates of load height were obtained for singly-symmetric girders with I_{yc}/I_y greater than approximately 0.1. The equations were more

accurate and in some cases conservative if the singly-symmetric section was treated like a doubly-symmetric section for calculating the warping coefficient.

For beams with intermediate bracing and top flange loading, the C_b^* value can be taken as 1.00. Some of the $C_{b\ ANSYS}^*$ values did fall slightly below 1.00, however this analysis was somewhat conservative since there would be some warping restraint available from the girder segments on the exterior thirds of the beam.

CHAPTER 5

Buckled Shapes of Fully-Stiffened Simply Supported Girders
Braced by a Shear Diaphragm

5.1 Introduction

The purpose of the computational portion of the study was to investigate the ability of metal deck forms to provide bracing to bridge girders. Chapter 3 outlined the parameters which were considered in the computational phase of this investigation. This chapter as well as the next, will present the finite element results for the fully-stiffened girders which were simply supported. The girders have no intermediate cross-frames. The influence of the shape of the cross-section, girder length, deck shear rigidity, type of loading, and load height on the buckled shape will be presented in this chapter. Chapter 6 will present the influence of these variables on the buckling capacity.

It is very important to gain an understanding of the effect of bracing systems on the buckled shape of girders. Changes in the buckled shape give a direct indication of changes in the effectiveness of a bracing system. Section 5.2 will outline the parameters which will be analyzed in this chapter. The buckled shapes of girders subjected to constant moment will be presented in Section 5.3. This will be followed by the effect of moment gradients and load height on the buckled shapes in Sections 5.4 and 5.5. The final section in this chapter will summarize the influence of the various parameters on the buckled shapes. Throughout this chapter, references will be made to the "lateral displacements" of the flanges. The "lateral displacements" are actually the eigenvector for the first mode of the buckled shape.

Although a number of different values of the deck shear rigidity were used in the study, the majority of the plots in this chapter will present comparisons of displaced shapes for girders with no deck versus girders braced by the stiffest deck considered (Q=1320). The two extremes will be compared to accentuate any differences in the buckled shape that the deck causes. Likewise, the effects of girder span on the buckled shape will also be made by comparing results for the shortest girder spans of 25 feet with the longest spans of 75 feet.

113

5.2 Buckled Shapes for Fully-Stiffened Girders

When energy methods are used to derive closed formed solutions, it is necessary to assume a shape for the buckled girders. In the derivation of Timoshenko's [23] closed formed solution for doubly-symmetric girders, the cross-sectional twist along the length was taken as a sine curve which is the classical solution for a differential equation. A sine curve was also assumed for the lateral displacement of the top flange and the cross-sectional twist for Errera's energy solution [12] when bracing of the girders is provided by a shear diaphragm at the top flange. It is of interest to compare the displacements from the finite element results for constant moment loading with the displacements assumed in the derivations. Additionally, it is worthwhile to study the behavior of girders subjected to other loading conditions to provide a better understanding of how loading conditions affect the behavior of girders braced by a shear diaphragm at the top flange.

In order to make comparisons of the buckled shapes, three different types of plots will be shown for the various girder systems discussed:

> a) lateral displacement of the top and bottom flange along the girder length,
>
> b) twist of the cross-section along the girder length,
>
> c) and location of the center of twist of the cross-section relative to the girder depth along the girder length.

The vertical axis of the plots of the lateral displacement of the top and bottom flange has been normalized by the value of the lateral displacement of the top flange at midspan of the girder. Likewise, the vertical axis of the plot of cross-sectional twist was normalized by the magnitude of the twist at midspan of the girders. The axes were normalized so that a sine curve could also be plotted on the graphs as a reference shape. The twist of the cross-section was calculated by subtracting the lateral displacement of the bottom flange from that of the top flange and dividing by the distance between the flange centroids.

The location of the center of twist has been normalized by the girder depth and the is presented relative to the top flange. Figure 5.1 depicts changes in the center of twist and how these shifts affect the ratio C.T./d in which C.T. is the distance to the center of twist from the top flange, and d is the girder depth. When the ratio of the center of twist distance to girder depth is less than one, the center of twist lies within the depth of the girder which indicates that the top and bottom flanges are moving in opposite directions. When the ratio is exactly equal to 1 the center of twist lies at the centroid of the bottom flange, and when the ratio is greater than one, the center of twist lies below the bottom flange.

Buckled
Girder

Vertical
Axis of
Unbuckled
Girder

C.T./d > 1

Center
of Twist

d

C.T.

Center
of Twist

d

C.T.
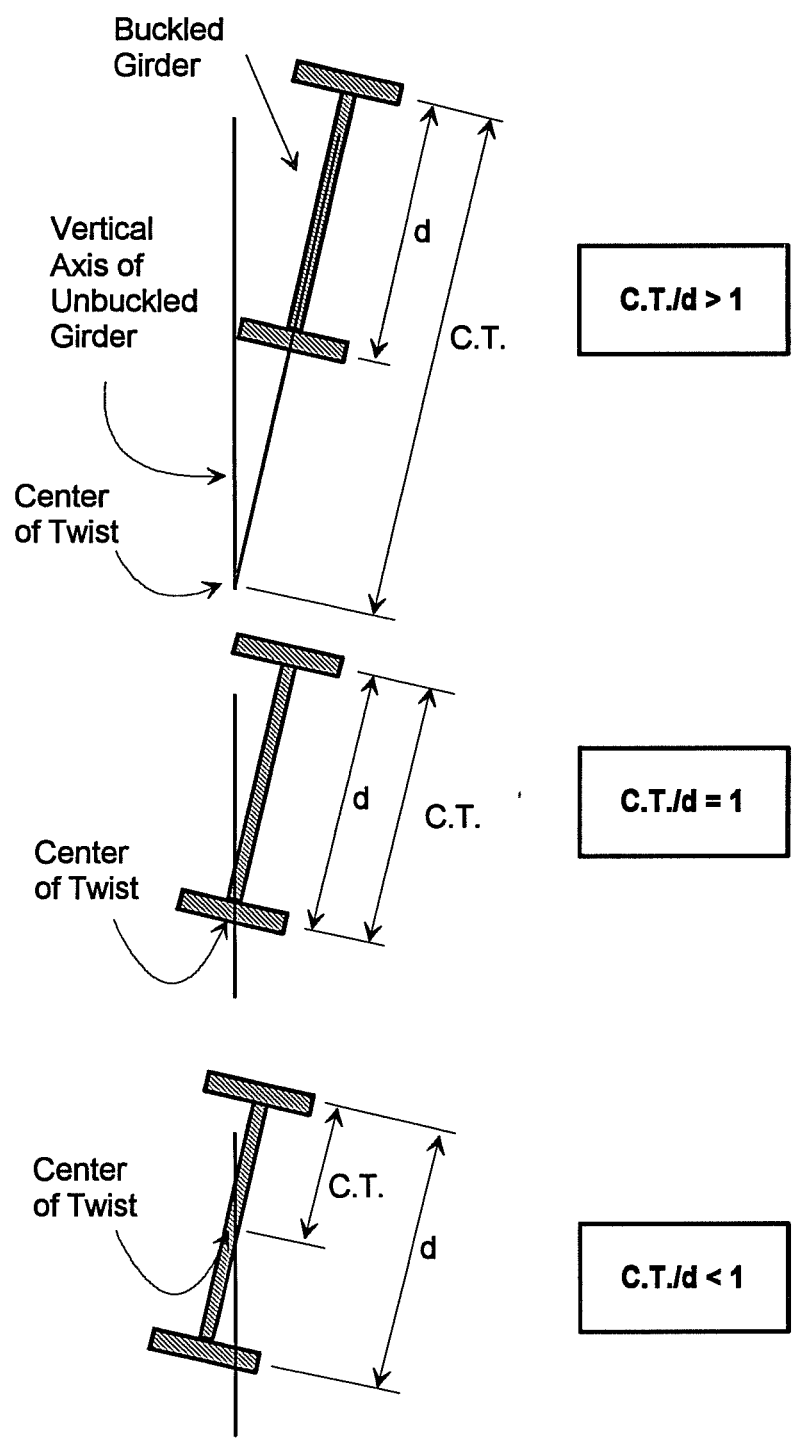
C.T./d = 1

Center
of Twist

C.T.

d

C.T./d < 1

Figure 5.1 Location of center of twist (C.T.).

Changes in the location of the center of twist give an indication of changes in the effectiveness of a bracing system. As the center of twist moves up on the girder cross-section, the effectiveness of the deck as a bracing element decreases. A better understanding of this can be gained by considering the extreme case if the center of twist were to lie at the top flange along the entire girder length. If this were the case, the top flange would have zero lateral displacement. Increasing the deck shear rigidity would therefore have no effect on the buckling capacity since the deck is not engaged as a bracing element.
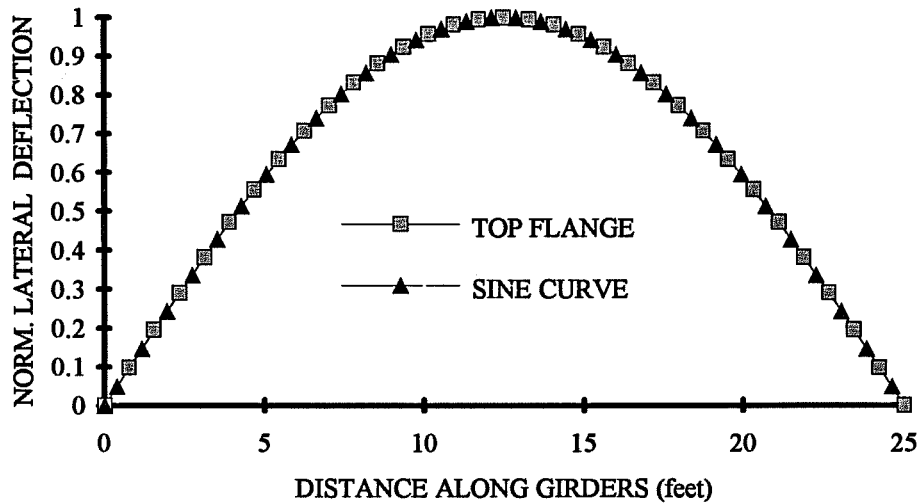
5.3 Constant Moment

The first portion of this study utilized three girder cross-sections. Lengths of 25, 50, and 75 feet were considered for each girder cross-section. A figure showing the three cross-sections was presented in Chapters 2 and 3, however for convenience it is repeated in Figure 5.2. These cross-sections will be used extensively in the finite element study.

Figure 5.3a shows a plot of the lateral displacement of the top flange along the length of section #1 which was subjected to constant bending moment. The girder was unbraced along the 25 feet length. A sine curve has also been plotted in this figure. The two curves are coincident. Figure 5.3b shows a plot of the cross-sectional twist along the length for the same girder. This curve is also coincident with a sine curve. When the length of the girders was increased to 75 feet, the lateral displacement and twist remained a sine curve. This is shown in Figure 5.4a and 5.4b for section #3 which is the singly-symmetric girder. These curves are representative of the lateral displacement of the top flange and cross-sectional twist for the all of the cross-sections considered when no bracing was provided with constant moment loading. Regardless of the span or cross-section, when there is no deck bracing the girders, the lateral displacement and twist are a sine curve.

When the deck was introduced as a bracing element, the lateral displacement of the top flange and the cross-sectional twist was unchanged for the doubly-symmetric sections #1 and #2. This is shown in Figures 5.5a and 5.5b, which show the lateral displacement and twist of section #2 for a 75 foot length and a deck shear rigidity of 1320. The displacements are once again coincident with a sine curve. This supports the assumption for the displaced shape which was made in the derivation of Errera's solution. The singly-symmetric section showed a slight change when the deck was introduced, however the change was minute. This is shown in Figures 5.6a and 5.6b for a 25 foot length, and in Figures 5.7a and 5.7b for a 75 foot length. The displacement
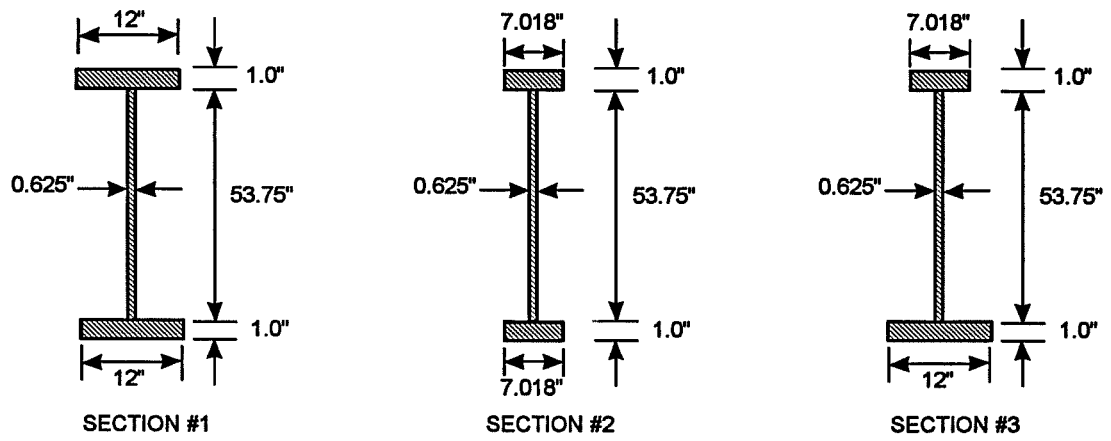
Figure 5.2 Cross-sections considered in computational study.

Figure 5.3a Lateral displacement of top flange vs. sine curve for section #1, L=25', No Deck, Constant Moment.
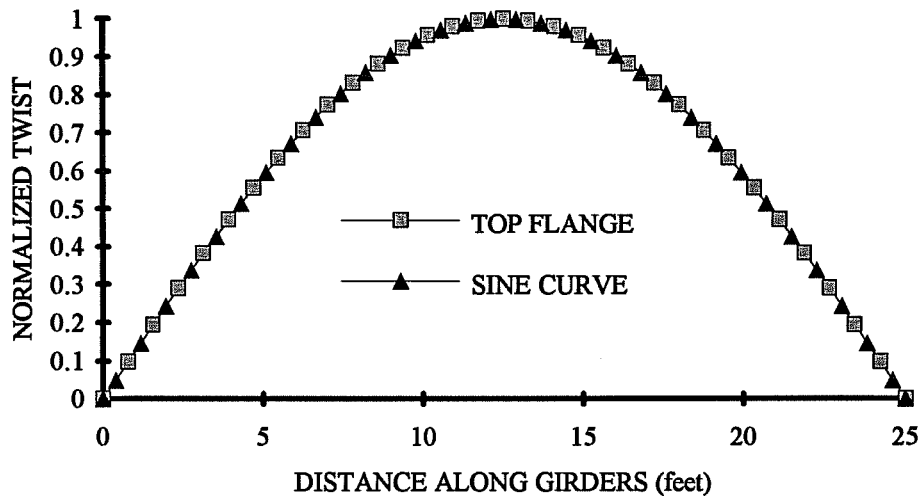
Figure 5.3b Cross-sectional twist vs. sine curve for section #1, L=25', No Deck, Constant Moment.
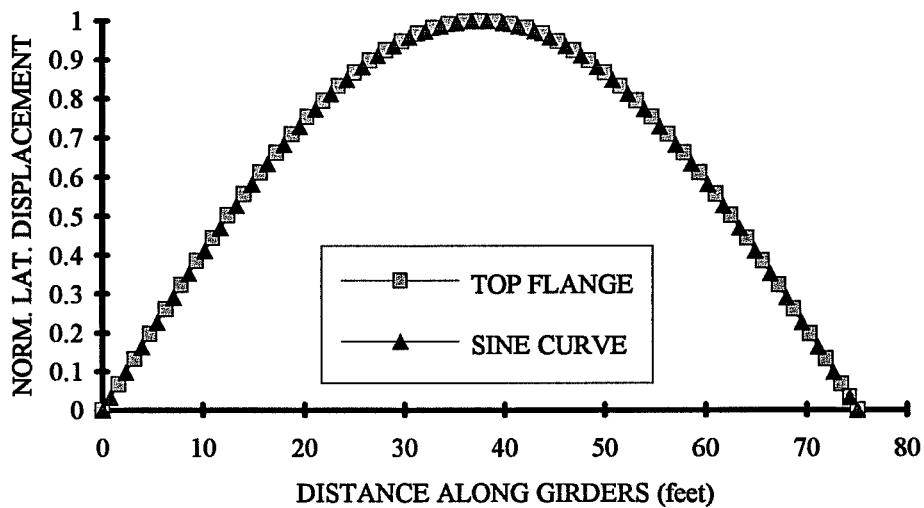
Figure 5.4a Lateral displacement of top flange vs. sine curve for section #3,
L=75', No Deck, Constant Moment.
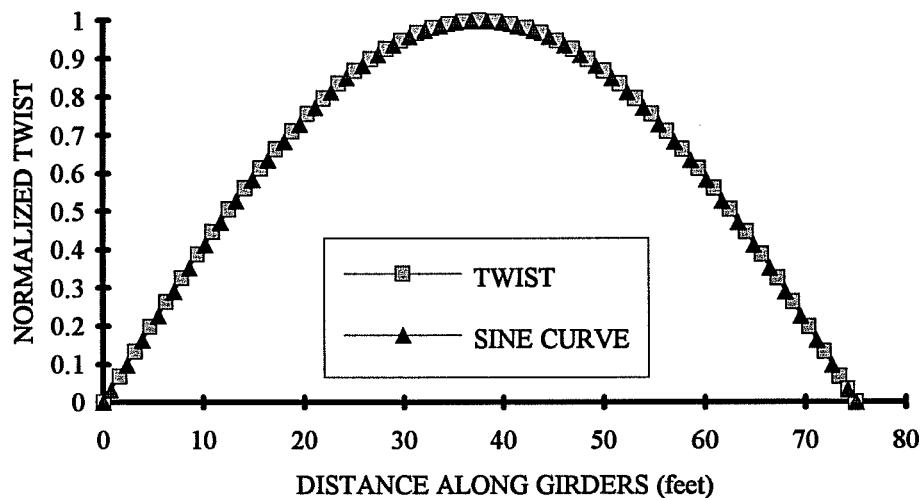
Figure 5.4b Cross-sectional twist vs. sine curve for section #3,
L=75', No Deck, Constant Moment.
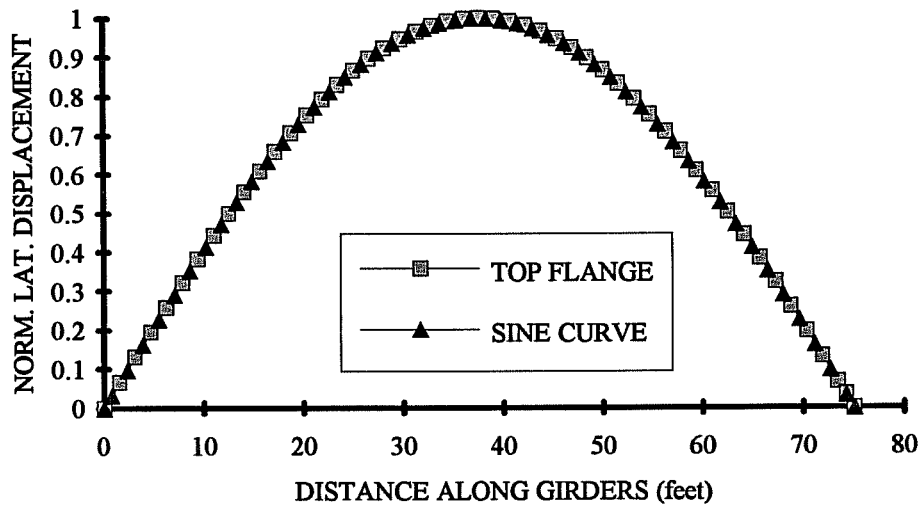
Figure 5.5a Lateral displacement of top flange vs sine curve for section #2, L=75', Q=1320, Constant Moment.
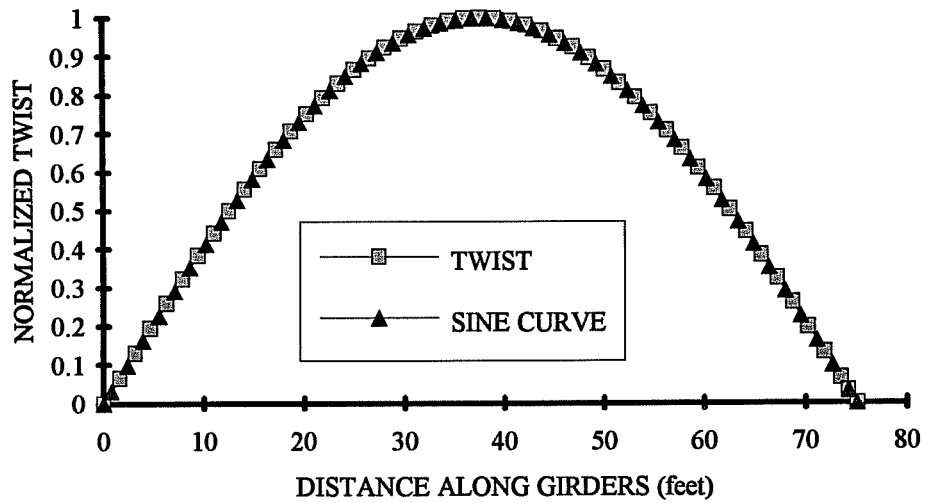
Figure 5.5b Cross-sectional twist vs sine curve for section #2, L=75', Q=1320, Constant Moment.

Figure 5.6a Lateral displacement of top flange vs. sine curve for section #3,
L=25', Q=1320, Constant Moment.

Figure 5.6b Cross-sectional twist vs. sine curve for section #3,
L=25', Q=1320, Constant Moment.

Figure 5.7a Lateral displacement of top flange vs. sine curve for section #3,
L=75', Q=1320, Constant Moment.

Figure 5.7b Cross-sectional twist vs. sine curve for section #3,
L=75', Q=1320, Constant Moment.

curves show a very slight deviation from the sine curve, however for all practical purposes the displaced shapes can be taken as a sine curve.

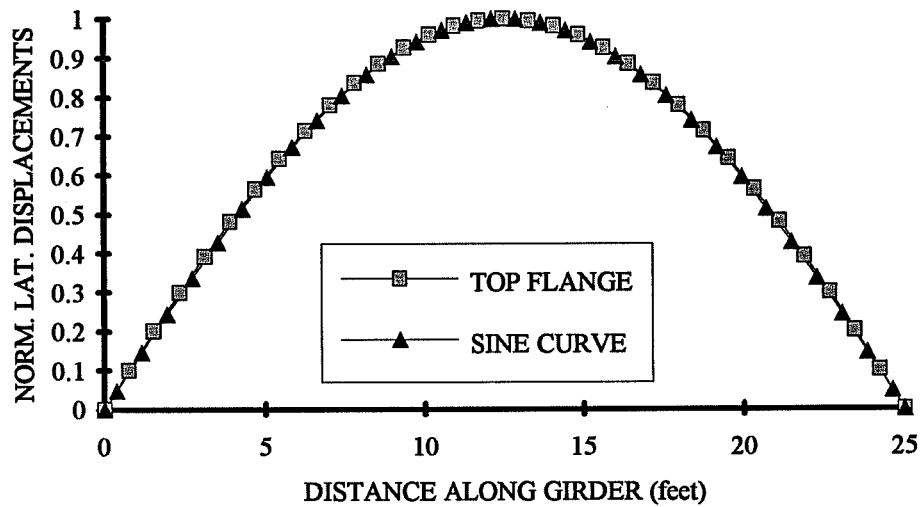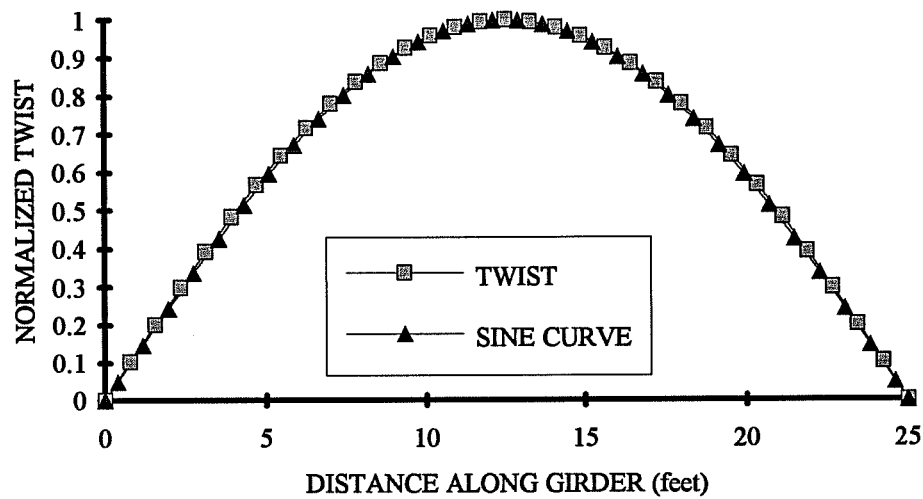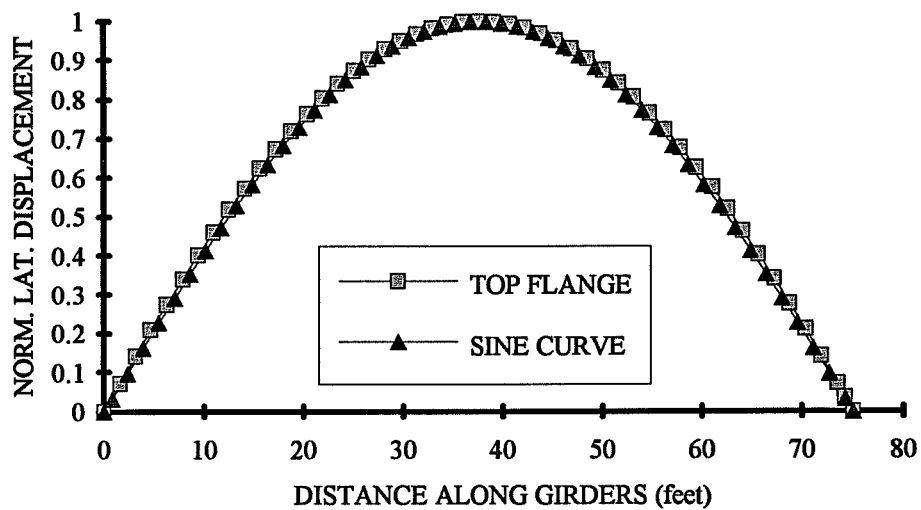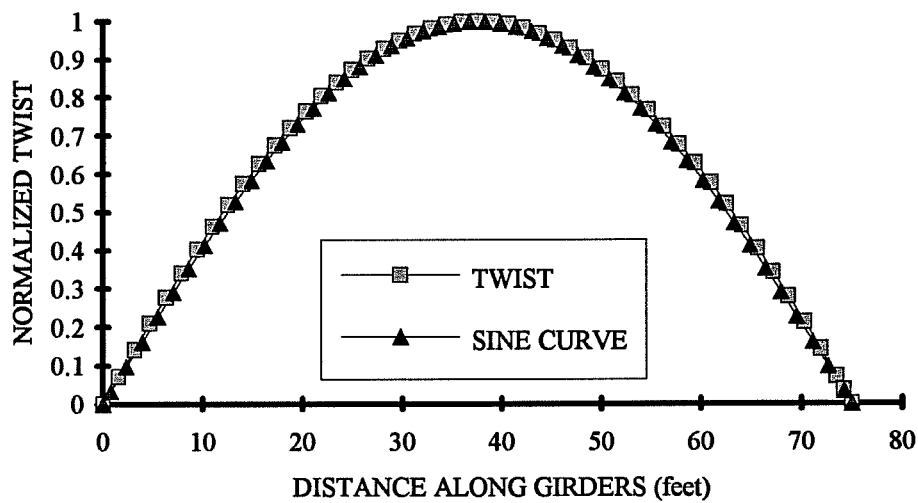Since the graphs which have been presented have shown that the lateral displacement of the top flange and the cross-sectional twist are essentially a sine curve, there is the implication that the lateral displacement of the bottom flange is also a sine curve. Figures 5.8a and 5.8b show the lateral displacement of the bottom flange with respect to a sine curve. The figures show that the lateral displacement of the bottom flange is essentially coincident with the sine curve.

Figure 5.9a shows the location of the center of twist along the 25 foot span of section #1 which is subjected to constant moment. For a given value of the shear rigidity, the location of the center of twist is essentially fixed along the length of the girder. As the shear rigidity of the deck is increased, the location of the center of twist moves up slightly, approaching the bottom flange (center of twist/D = 1). Figure 5.9b shows the location of the center of twist of section #1 with a 75 foot girder length. For a given deck rigidity, the location of the center of twist on the longer girder was further below the bottom flange than for the shorter girder of the same cross-section. The plot with a longer girder length also shows that the location of the center of twist is much more sensitive at smaller values of the shear rigidity, Q, than at higher values. For example, there is a much larger change in the location of the center of twist when Q was changed from 0 to 66 than when it was changed from 660 to 1320. For the larger values of the shear rigidity, the center of twist was approaching the bottom flange. The location of the center of twist was essentially uniform along the girder length for all of the cross-sections subjected to constant moment. In the remainder of this section, graphs of the center of twist location will be plotted for the value at midspan versus increasing shear rigidity.

Figure 5.10 shows the location of the midspan center of twist with increasing deck shear rigidity for section #2 with girder lengths of 25 feet and 75 feet. The lower lateral stiffness of section #2 causes the center of twist of the unbraced girders to drop considerably below the locations recorded for section #1. It is worthwhile to mention again that a larger value of the C.T./D indicates that the center of twist is located farther below the girder. As the shear rigidity was increased, the center of twist approached the bottom flange (C.T./D =1).

The locations of the midspan center of twist with increasing deck shear rigidity of section #3 are shown for girder lengths of 25 feet and 75 feet in Figure 5.11. The singly-symmetric section behaved similar to the two doubly-symmetric sections. The location of the center of twist
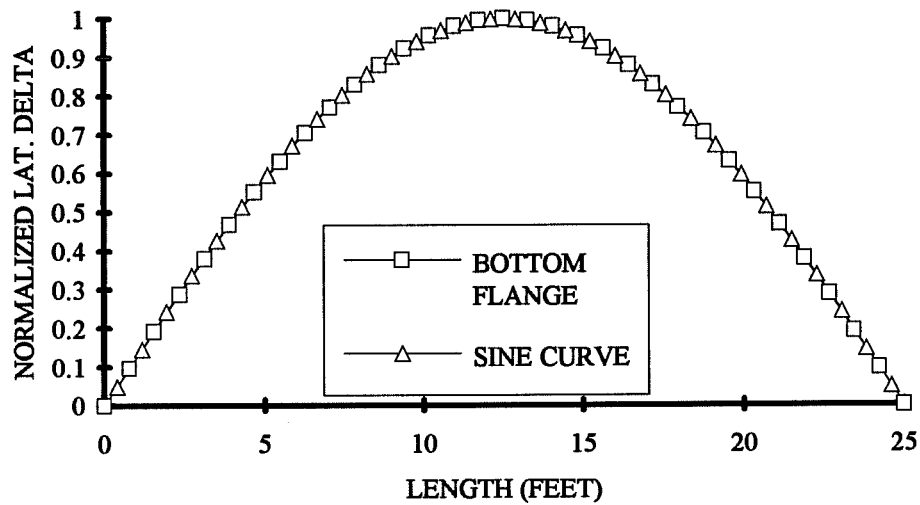
Figure 5.8a Lateral displacement of bottom flange vs. sine curve for section #2
L=25', No Deck, Constant Moment
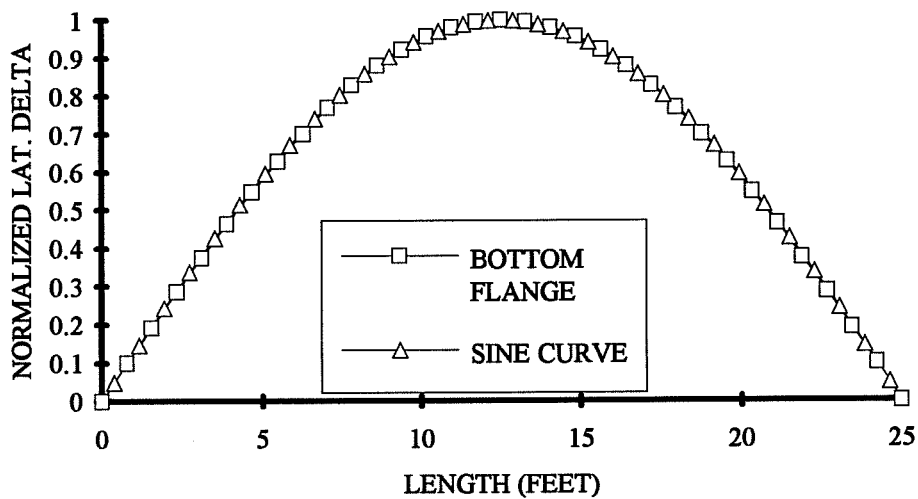
Figure 5.8b Lateral displacement of bottom flange vs. sine curve for section #2
L=25', Q=1320, Constant Moment
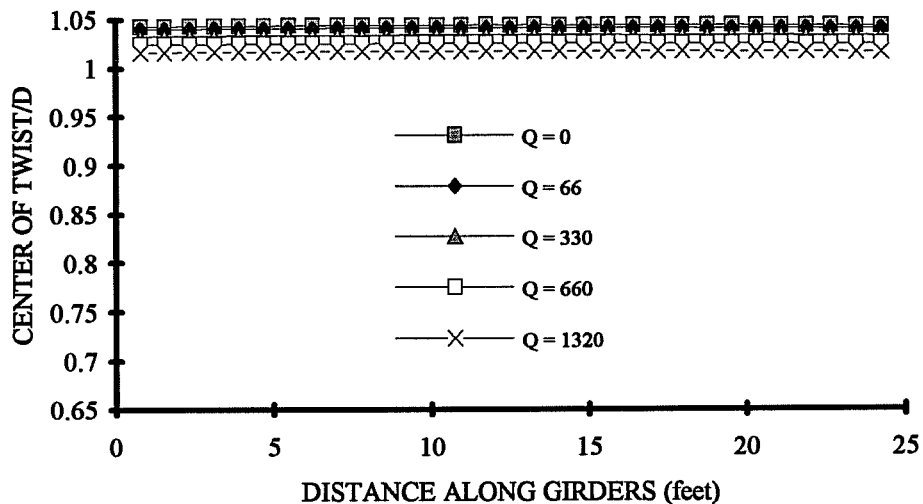
**Figure 5.9a Center of twist from top flange for section #1,
L=25', Constant Moment.**
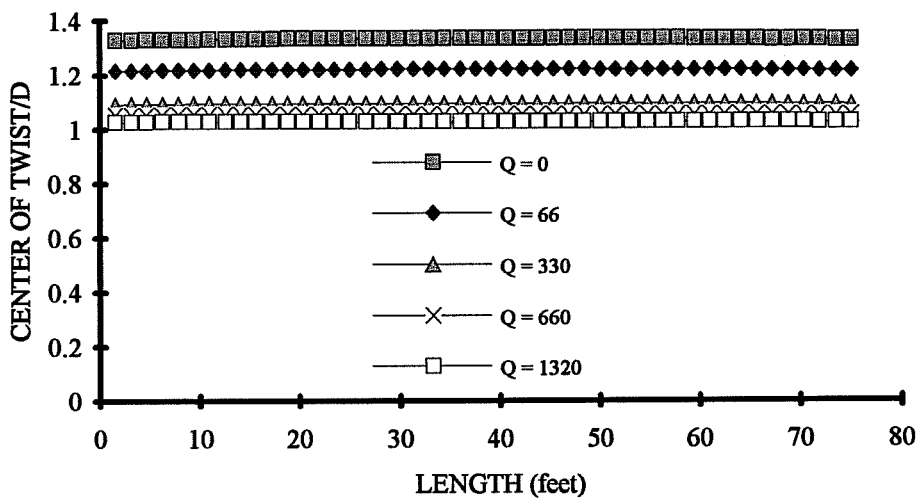
**Figure 5.9b Center of twist from top flange for section #1,
L=75', Constant Moment.**
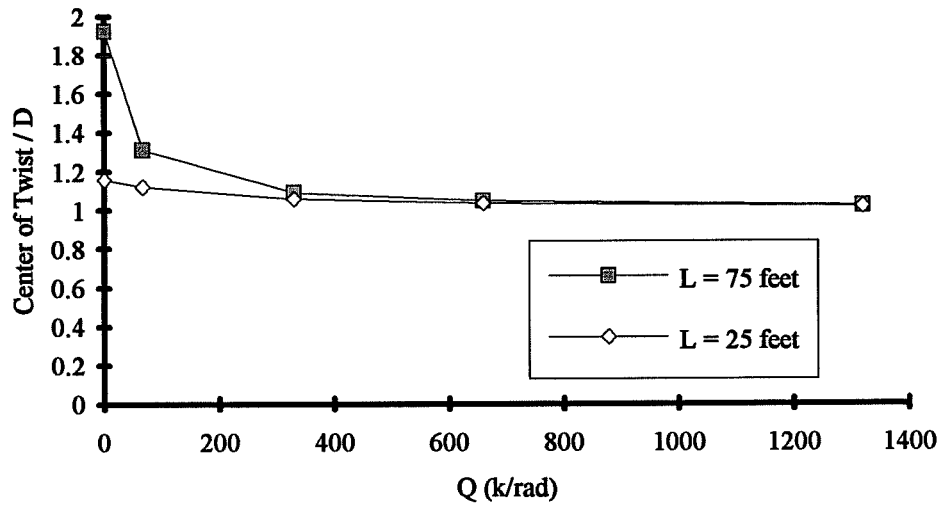
Figure 5.10 Location of midspan center of twist with deck shear rigidity for for section #2
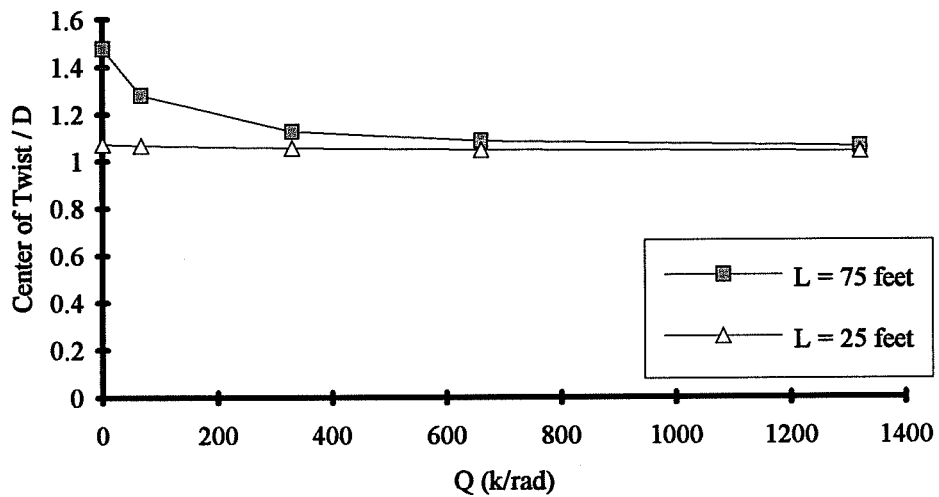
Figure 5.11 Location of midspan center of twist with deck shear rigidity for for section #3.

along the girder length was essentially fixed for a given value of the shear rigidity. As the shear rigidity was increased the center of twist approached the bottom flange.

The results presented for the constant moment cases have shown that the center of twist moves up as the shear rigidity is increased, however the top and bottom flange have lateral displacements which remain very close to a sine curve for all the cases considered. This indicates that the relative magnitudes of the lateral deflection of the top and bottom flanges change as the shear stiffness of the deck is altered. Figures 5.12a, 5.12b, and 5.12c show the lateral displacements for the top and bottom flanges for the respective sections #1, #2, and #3. All of the girders have a 75 foot length. The curves are shown for cases with no deck and also for a deck with a shear rigidity of 1320. These plots show that when a deck is used to brace the top flange of a girder, the shape of the top flange does not change, however the relative movement of the bottom flange is substantially reduced.

5.4 Moment Gradient

The closed formed equations from Timoshenko and from Errera are for cases in which the girders are subjected to a constant moment. The previous section has shown that the assumption of a sine curve for the lateral displacement of the top flange and cross-sectional twist match the finite element results for nearly all cases. Since, however, most girders are not subjected to constant moment, it is of interest to get an indication for how the buckled shape is affected with a moment gradient. The cases which were studied with a moment gradient consisted of a point load at the midspan centerline and also a uniform distributed load. In both of the load cases which are being reported in this section, the transverse load was applied at midheight.

Figures 5.13a and 5.13b show the respective lateral displacement of the top flange and twist of the cross-section along the 75 foot length of section #2 with no deck present. The girders have been subjected to a point load at midspan. A sine curve has also been plotted on these curves to give a reference for the displaced shape. There is a small deviation from the sine curve along the length of the girder for both the lateral displacement and twist, however, both curves are very similar to the sine curve. This was observed for all three sections when no deck was present to brace the girders.

When the deck is introduced as a bracing element, the buckled shape changes a great deal. Figures 5.14a and 5.14b show the buckled shape for section #2 with a 25 foot length and a deck shear rigidity of 1320. The girders were subjected to a point load at midspan. The lateral
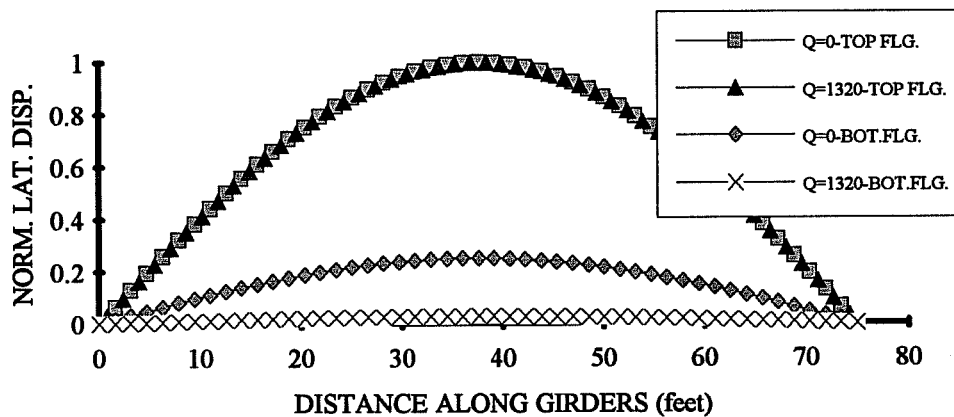
Figure 5.12a Lat. disp. of top and bot. flange for section #1, L = 75', Constant moment

Figure 5.12b Lat. disp. of top and bot. flange for section #2, L = 75', Constant moment
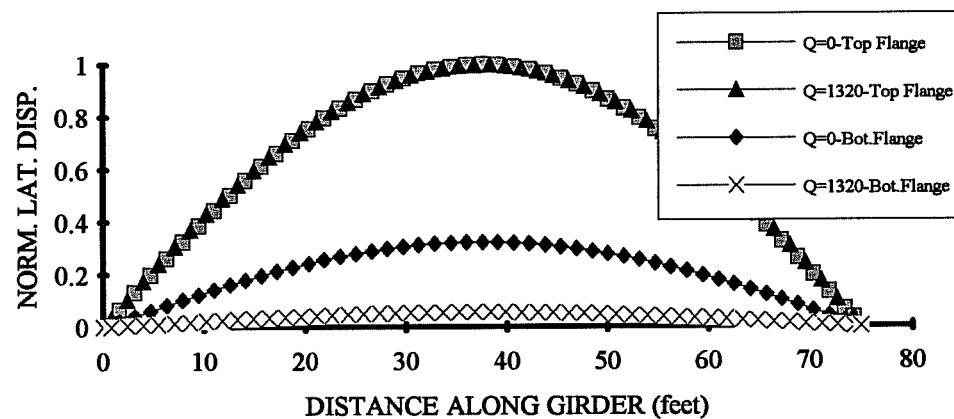
Figure 5.12c Lat. disp. of top and bot. flange for section #3, L = 75', Constant moment
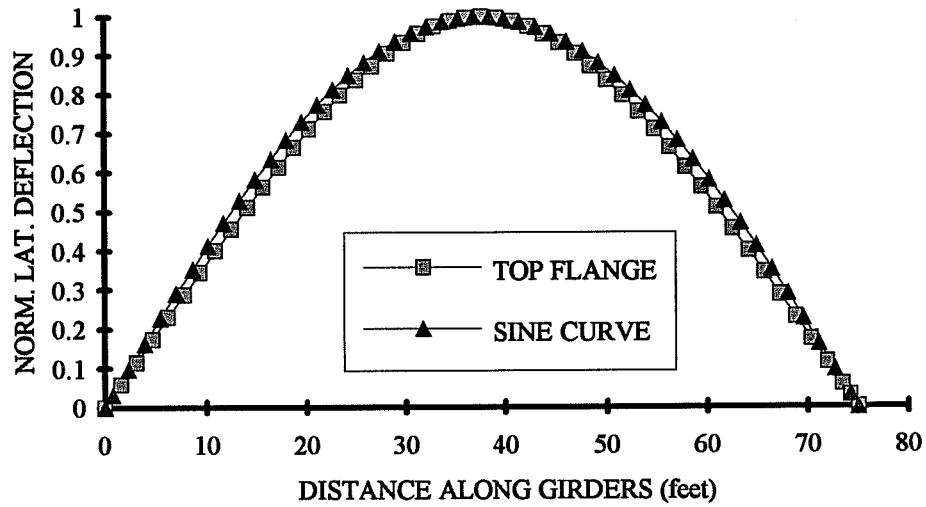
**Figure 5.13a Lateral displacement of top flange vs sine curve for section #2, L=75', No Deck, P @ midheight.**
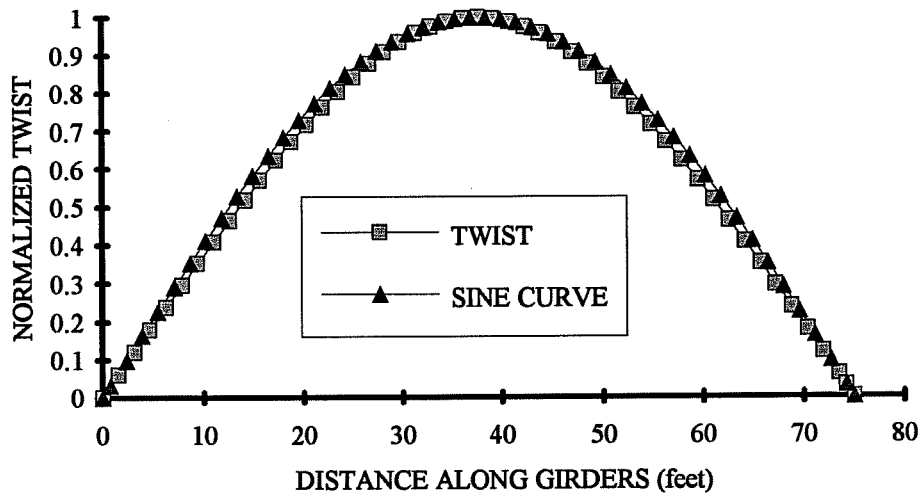
Figure 5.13b Cross-sectional twist vs sine curve for section #2, L=75', No Deck, P @ midheight.
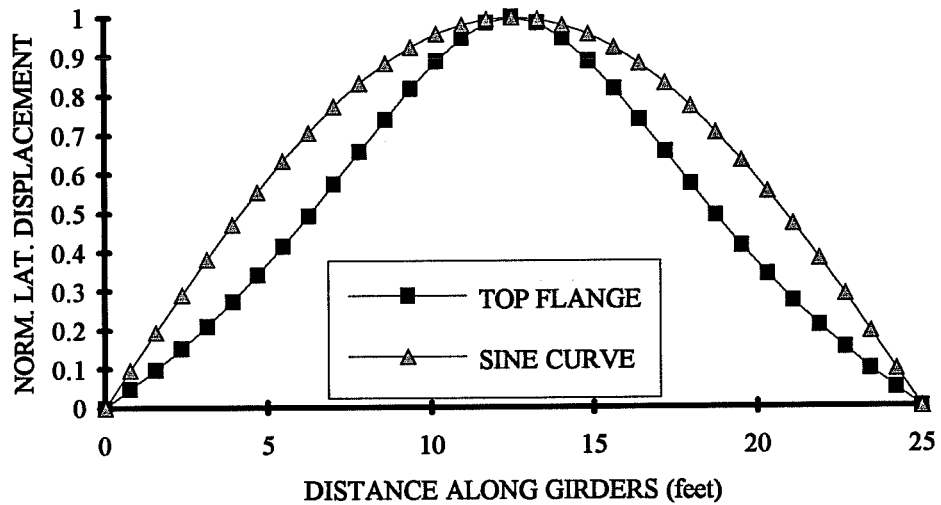
Figure 5.14a Lateral displacement of top flange vs. sine curve for section #2, L = 25', P @ CL midheight, Q=1320.

Figure 5.14b Cross-sectional twist vs. sine curve for section #2, L = 25', P @ CL midheight, Q=1320.

displacement deviates a great deal from the sine curve. When the deck is used for bracing, the top flange does not deflect as much near the supports where the moment is low. The twist of the girder along the length takes a slightly different shape than the lateral displacement of the top flange. This difference was amplified as the length of the girders was increased. Figures 5.15a and 5.15b show the corresponding displacements for section #2 with a 75 foot length and a deck shear rigidity of 1320. The lateral displacement has the same basic shape, however the twisted shape has changed when compared to the shorter girders.

When the type of loading consisted of uniformly distributed load at midheight, the deviation from the sine curve was slightly smaller than the case with a point load at midheight, however the deviation was still substantial. Figures 5.16a and 5.16b show the respective lateral displacement of the top flange and the cross-sectional twist for section #2 with a 75 foot length and a deck shear rigidity of 1320 for a loading consisting of a uniform distributed load.

For girders subjected to constant moment, there was a uniform shift in the location of the center of twist with increases in the deck shear rigidity. A different behavior was observed in girders subjected to moment gradient. Figure 5.17a shows the location of the center of twist for three different loading conditions on section #1 with no deck present. The girders were 75 feet long and the load cases shown consist of constant moment, a distributed load at midheight, and a point load at the centerline midheight. The center of twists for all three load cases are relatively close together. Although the location of the center of twist is relatively constant along the girder length for the constant moment case, the center of twist location for the cases with moment gradient show a small amount of variance. Figure 5.17b shows the effect on the three loading cases when the deck is introduced as a bracing element. Unlike the case with constant moment which experienced a uniform shift of the center of twist all along the girder length, the center of twist moved up more at the support than at the centerline for the two cases with moment gradient. The center of twist was the highest up on the section for the case of a point load at midspan. The center of twist for the case with a distributed load was lower on the section.

Figure 5.18a shows the location of the center of twist along the 25 foot length of section #1 when the girder is subjected to a point load at the centerline midheight. With no deck, the curve is relatively flat and the center of twist lies slightly above the bottom flange (i.e. center of twist/D < 1). As the shear rigidity was increased, the center of twist moved up further within the depth of the girder. When the length of section #1 was increased to 75 feet, the center of twist for the girder with no deck moved down relative to the same section with a 25 foot length. This

**Figure 5.15a Lateral displacement of top flange vs sine curve for section #2,
L=75', P @ midheight, Q=1320.**
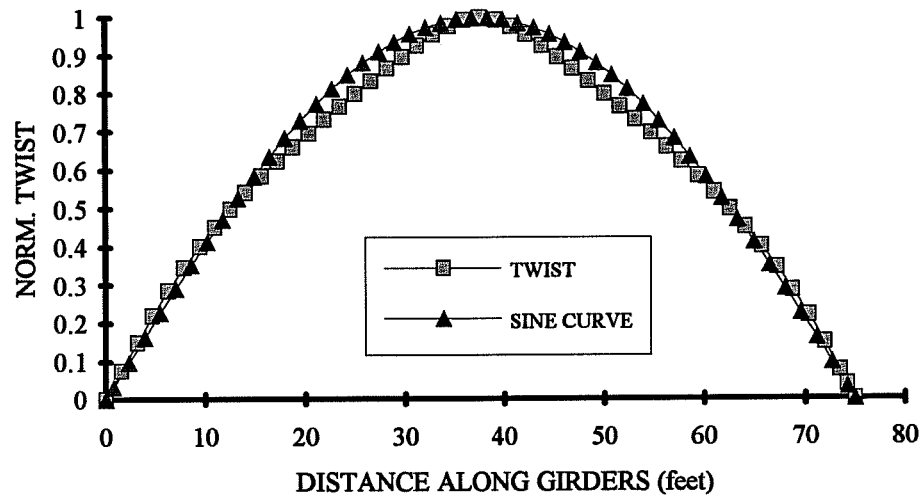
**Figure 5.15b Cross-sectional twist vs sine curve for section #2,
L=75', P @ midheight, Q=1320.**

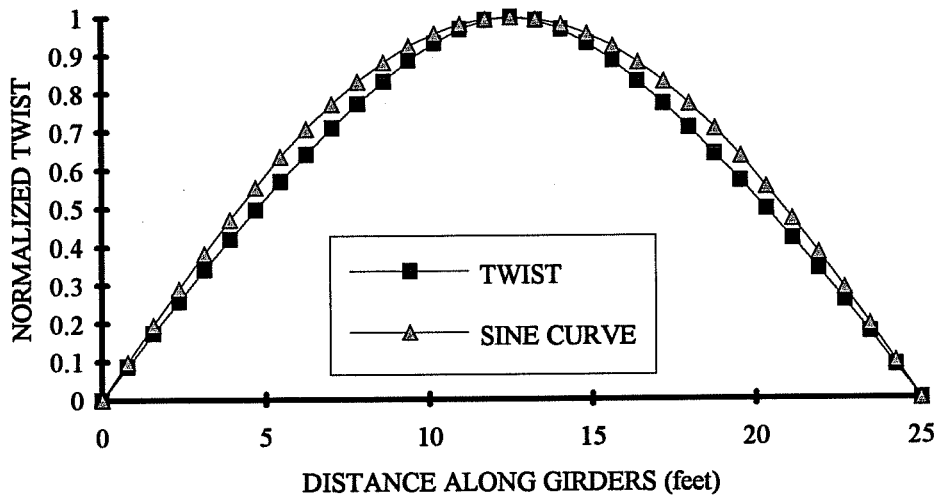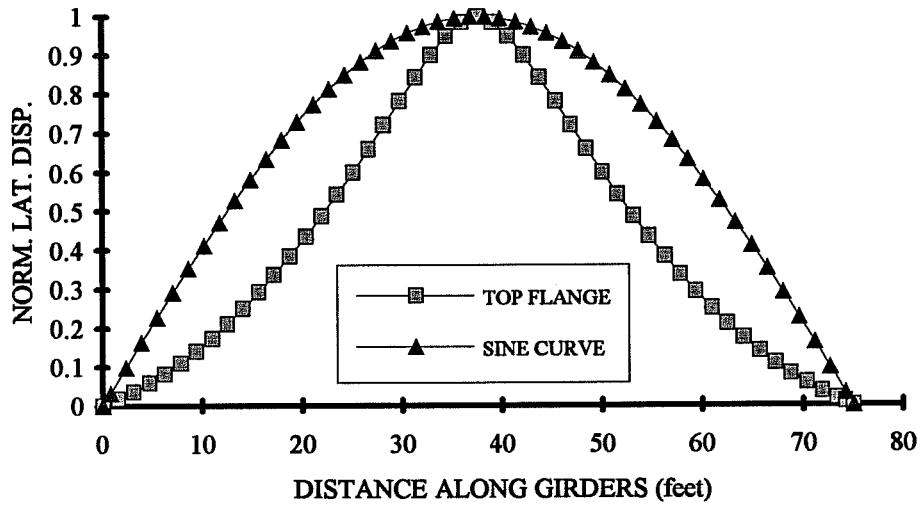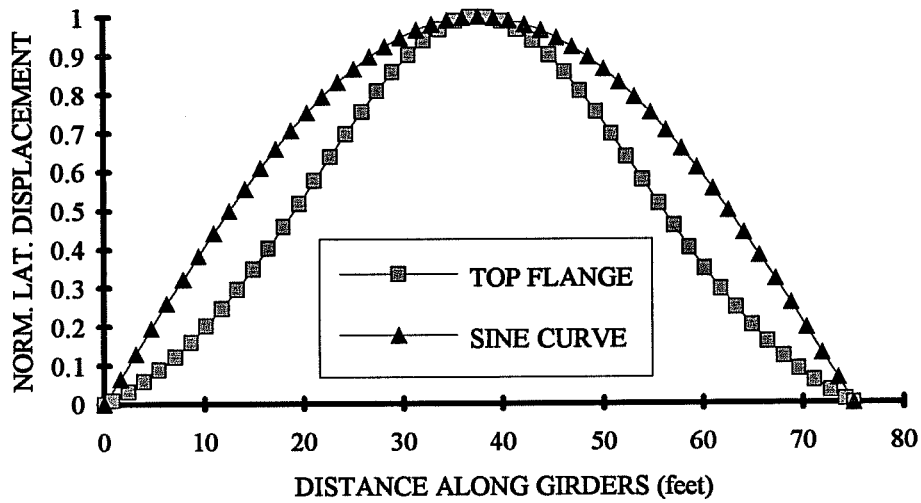**Figure 5.16a Lateral displacement of top flange vs. sine curve for section #2, L=75', w @ midheight, Q=1320.**
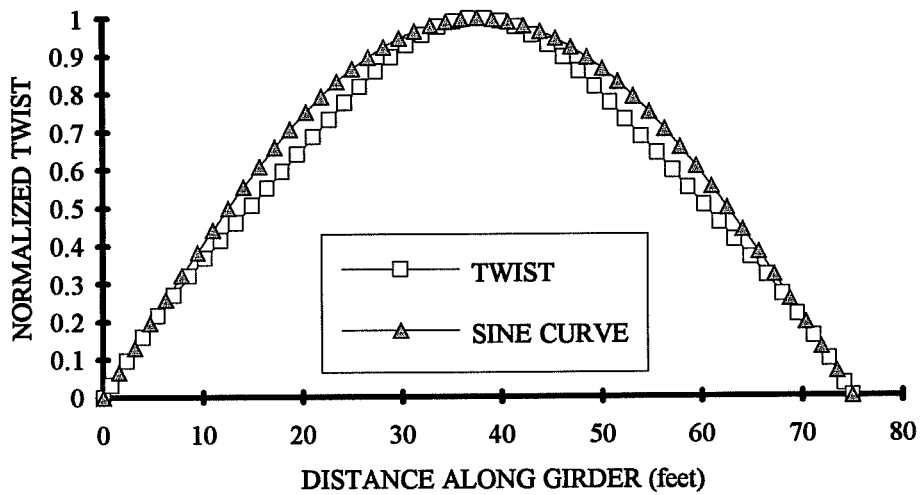
Figure 5.16b Cross-sectional twist vs. sine curve for section #2, L=75', w @ midheight, Q=1320.
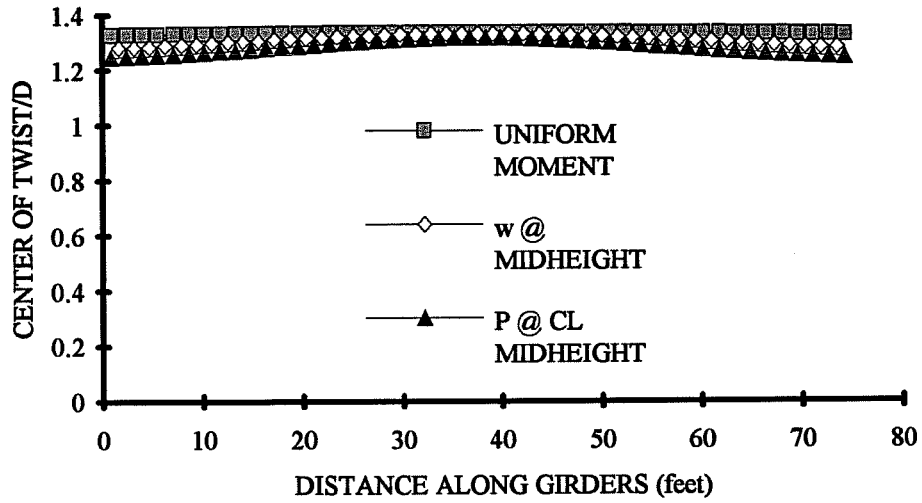
Figure 5.17a Center of twist from top flange for section #1, L=75', Q=0.
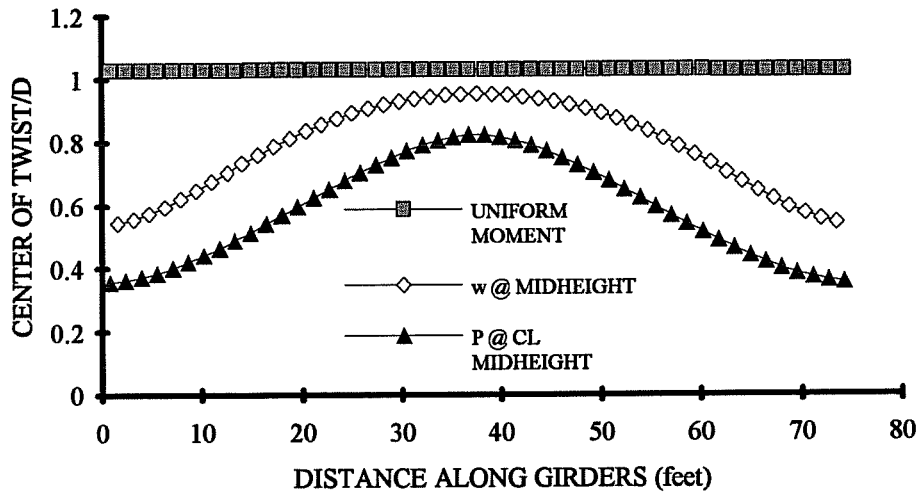
Figure 5.17b Center of twist from top flange for section #1, L=75', Q=1320.
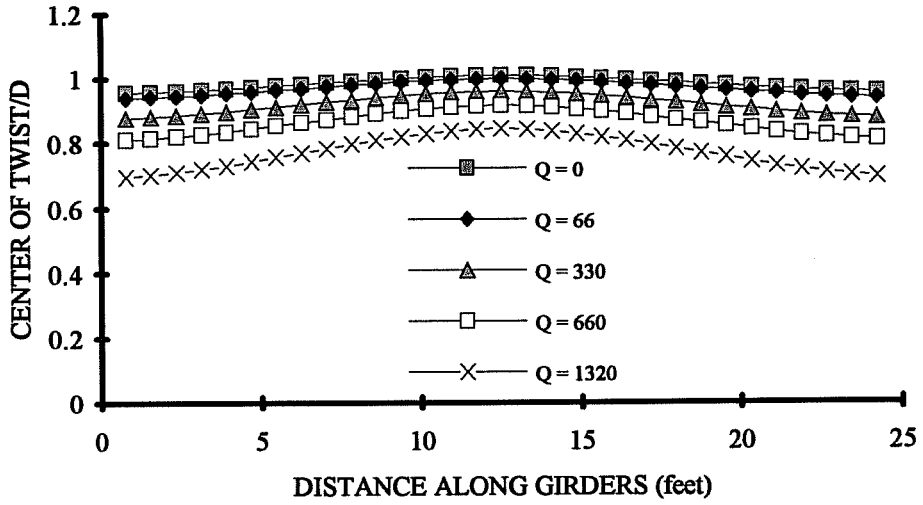
Figure 5.18a Center of twist from top flange for section #1,
L=25', P @ CL midheight.
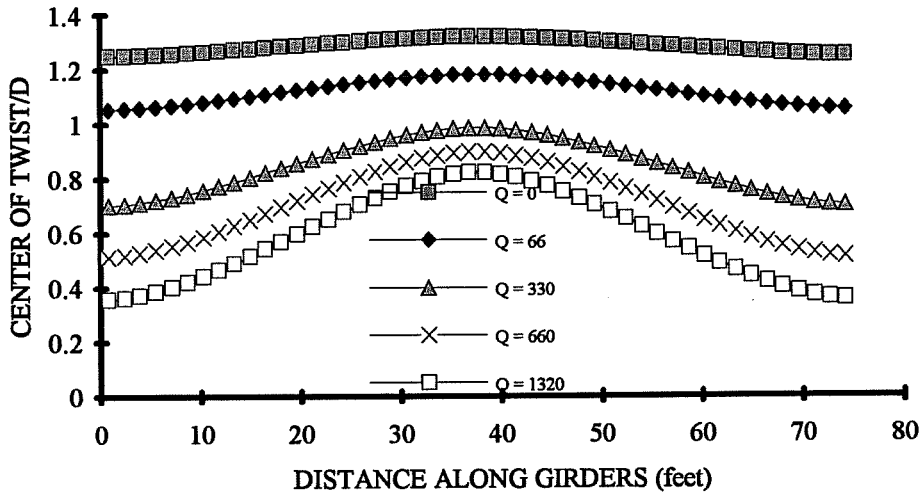
Figure 5.18b Center of twist from top flange for section #1,

L=75', P @ CL midheight.

is shown in Figure 5.18b. As the shear rigidity was increased, the migration of the center of twist followed the same basic trends as the 25 foot length, except the center of twist moved even further up on the section. For a Q = 1320, the center of twist was above midheight near the support section.

When section #2 which has a smaller lateral stiffness than the other sections was analyzed with no deck, the center of twist was considerably further below (larger C.T./d) the locations observed for the other cross-sections considered. This can be observed for the line Q=0 shown in Figures 5.19a and 5.19b which show plots of C.T./d along the girder length for respective girder spans of 25 feet and 75 feet. The location of the center of twist of section #2 is very sensitive to changes in the deck shear rigidity, particularly the 75 foot span girder. In Figure 5.19b, with no deck, the location of the center of twist on the 75 foot long is relatively uniform along the girder length, however, a small increase in deck rigidity caused a very large shift in the location of the center of twist. In this case, the center of twist near the supports gets very close to the top flange for larger values of the shear rigidity.

Figures 5.20a and 5.20b show the location of the center of twist for the singly-symmetric section #3 subjected to a point load at midspan. The effect of the deck on the center of twist is basically the same as the effect observed on the two doubly-symmetric sections.

It was observed in the section dealing with girders subjected to constant moment that as the shear stiffness of the deck was increased, the center of twist of the cross-section moved up on the section while the top flange maintained the same basic shape. This migration of the center of twist was due to a reduction in the relative magnitude of the lateral deflection of the bottom flange with respect to the top flange. The plots of lateral displacement of the top flange for girders subjected to moment gradients have shown that the deck causes a significant change in the buckled shape of the top flange. Figures 5.21a, 5.21b, and 5.21c show the lateral displacements for the top and bottom flanges for the respective sections #1, #2, and #3. All of the girders have a 75 foot length and are subjected to a distributed load at midheight. The curves are shown for cases with no deck and cases for a deck with a shear rigidity of 1320. The curves show that when the deck is introduced as a bracing element, both the top and bottom flange undergo significant changes in the buckled shape as the center of twist moves up within the depth of the girder.
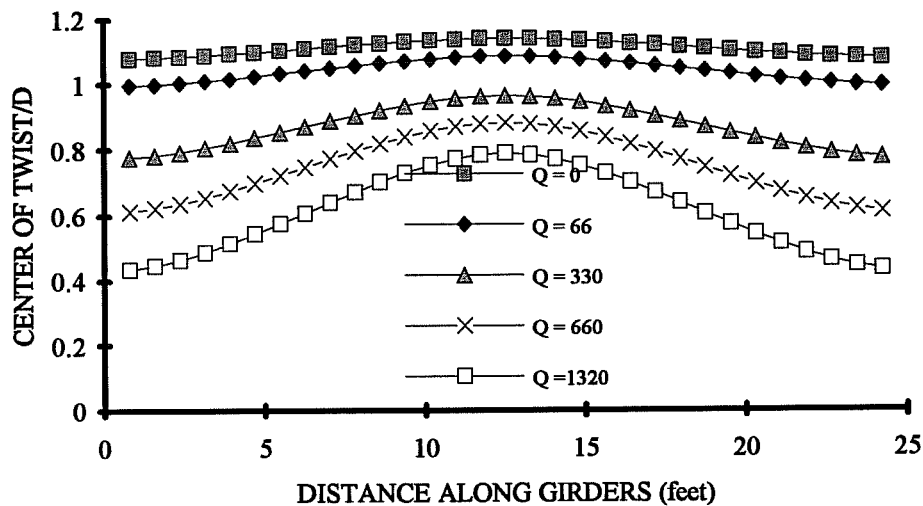
**Figure 5.19a Center of twist from top flange for section #2,
L=25', Variable Q, P @ CL midheight.**
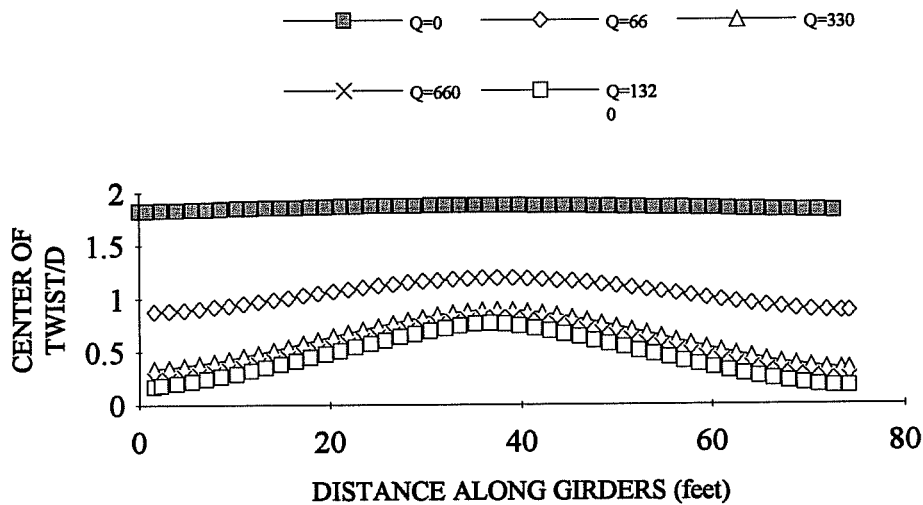
**Figure 5.19b Center of twist from top flange for section #2,
L=75', Variable Q, P @ CL midheight.**
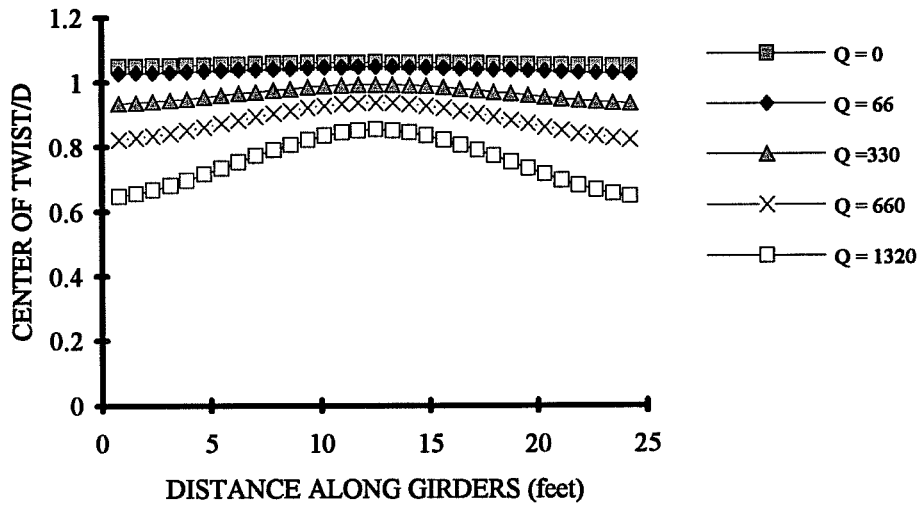
Figure 5.20a Center of twist from top flange for section #3,
L=25', P @ CL midheight, variable Q.
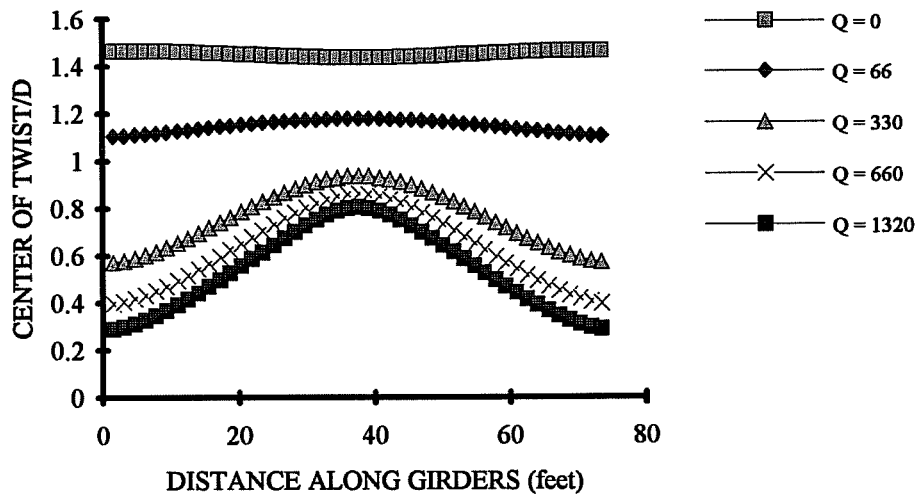
Figure 5.20b Center of twist from top flange for section #3,

L=75', P @ CL midheight, variable Q.
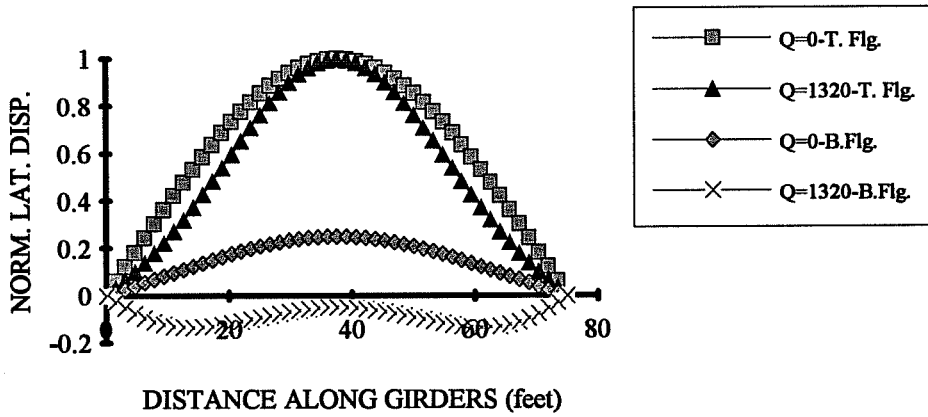
Figure 5.21a Lateral displacement of top and bottom flange for section #1
          L=75 ft. , w @ midheight
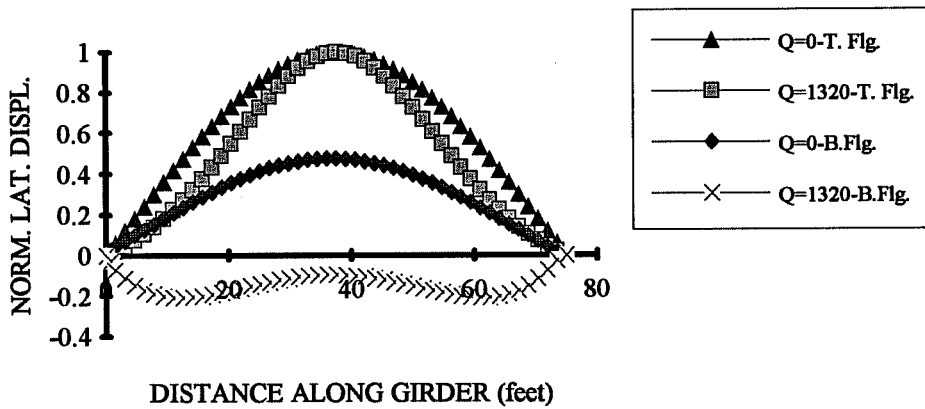
Figure 5.21b Lateral displacement of top and bottom flange for section #2
          L=75 ft. , w @ midheight
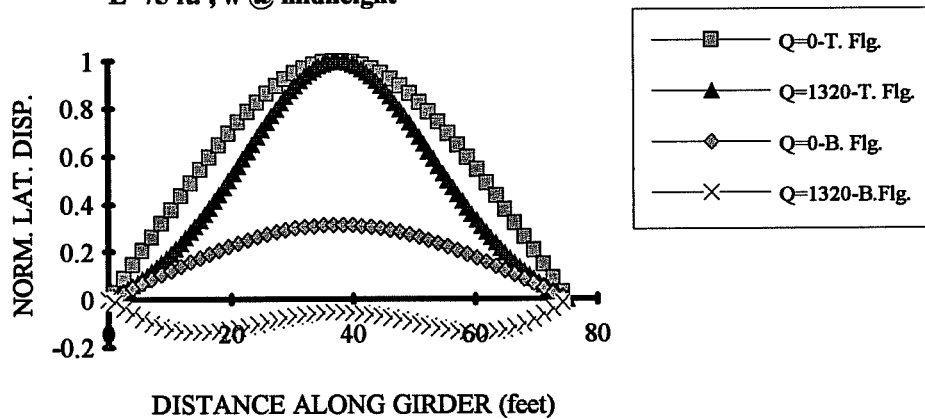
Figure 5.21c Lateral displacement of top and bottom flange for section #3

5.4 Load Height

In addition to applying the transverse loads at midheight, the load was also applied at the bottom and top flange. The effect load height has on the buckling load was outlined in chapters 2 and 4. Loads that are applied higher up on the section tend to reduce the buckling load due to the tendency of these loads to cause an overturning torque on the girder. This section will present results which demonstrate the effect of load height on the buckled shape of the girders. The previous section showed that when no deck is used as a bracing element and a girder is subjected to a moment gradient, there was a slight change in the buckled shape of the top flange when compared to the constant moment case. When the deck was introduced as a bracing element, both the top and bottom flanges experienced significant changes in the buckled shape. In order to get a feel for the effect of load height on the buckled shape, lateral displacements of the girders at the top and bottom flange will be compared to results with the load at midheight.

Figure 5.22a shows the lateral displacement of the top and bottom flange for section #2 subjected to a point load at the midspan of the girders. The girders are 25 feet long and there is no deck as a bracing element. The transverse load was applied at three load heights. For all three load positions, the top flange takes the same shape. The bottom flange, however, does experience a change relative to the top flange as the load height is changed. This indicates that the center of twist migrates upward as the height of the load is increased. Figure 5.22b shows the corresponding curves if a deck with a shear rigidity of 1320 is used to brace the girders. Regardless of the load height, the top flange takes the same shape. The bottom flange, on the other hand, experiences a large change in shape as the load height is changed. When the load is applied at the top flange, the bottom flange has a larger lateral displacement than the top flange. The same type of behavior was observed when the length of the girders was increased to 75 feet. Figures 5.23a and 5.23b are the corresponding curves for section #2 when a length of 75 feet was used.

When the girders were loaded with a uniform distributed load at different load heights, similar behavior was observed when no deck was present. Figure 5.24a shows the lateral displacement of the top and bottom flanges along the 75 foot length of section #2 subjected to a distributed load at the three different load heights. For all three load heights, the top flange experiences the same shape lateral displacement, while the bottom flange does change slightly. When the deck is used as a bracing element as shown in Figure 5.24b, on the other hand, both the
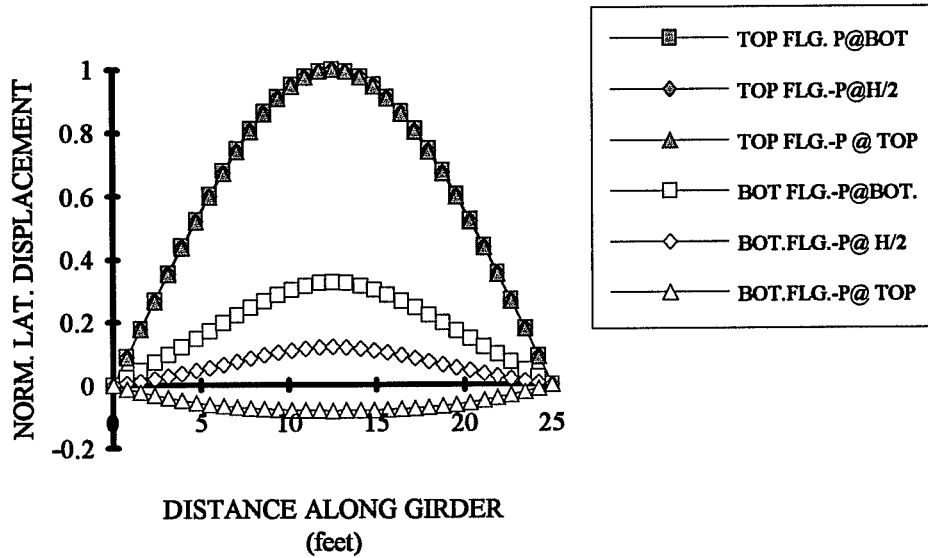
**Figure 5.22a Lateral displacement of top and bottom flange for section #2,
L=25', P @ Variable load height, Q=0.**
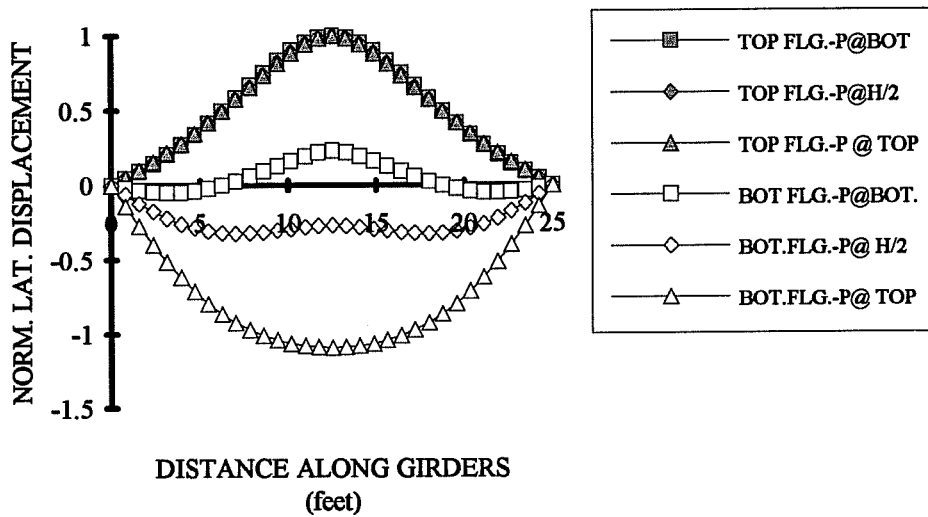
**Figure 5.22b Lateral displacement of top and bottom flange for section #2,
L=25', P @ Variable load height, Q=1320.**
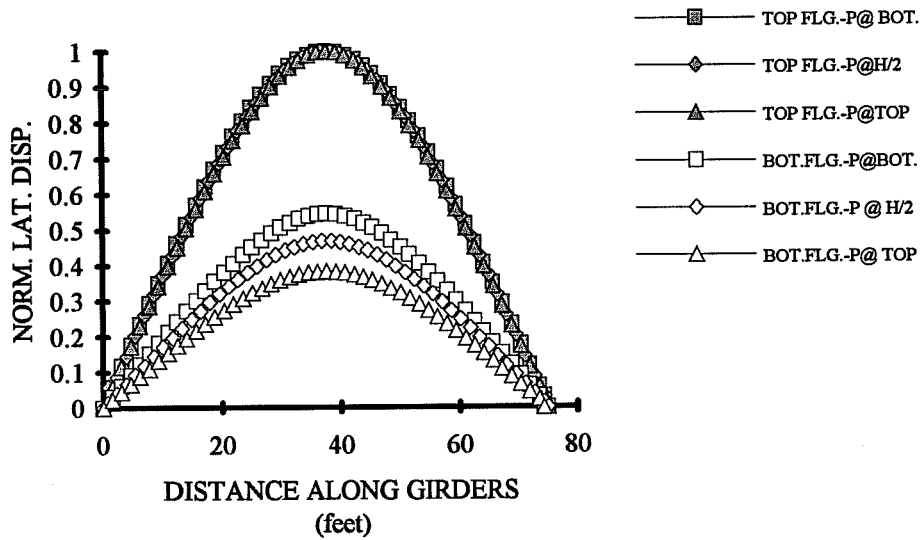
**Figure 5.23a Lateral displacement of top and bottom flange for section #2,
L=75', P @ variable height, Q=0.**
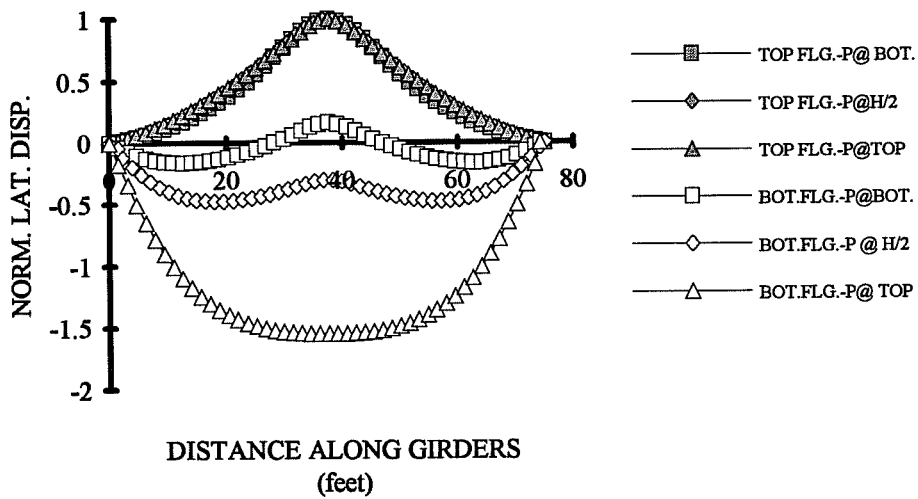
**Figure 5.23b Lateral displacement of top and bottom flange for section #2,
L=75', P @ variable height, Q=1320.**
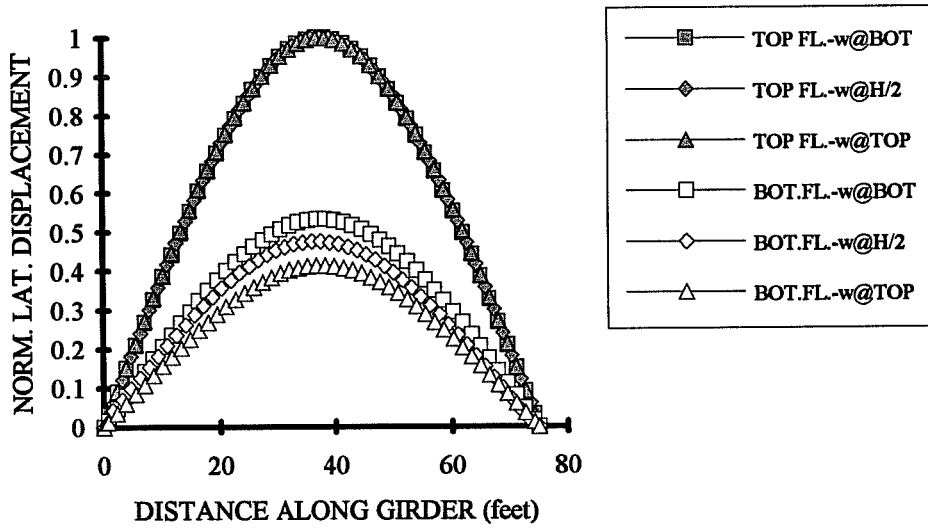
Figure 5.24a Lateral displacement of top and bottom flange for section #2, L=75', w @ variable height, Q=0.
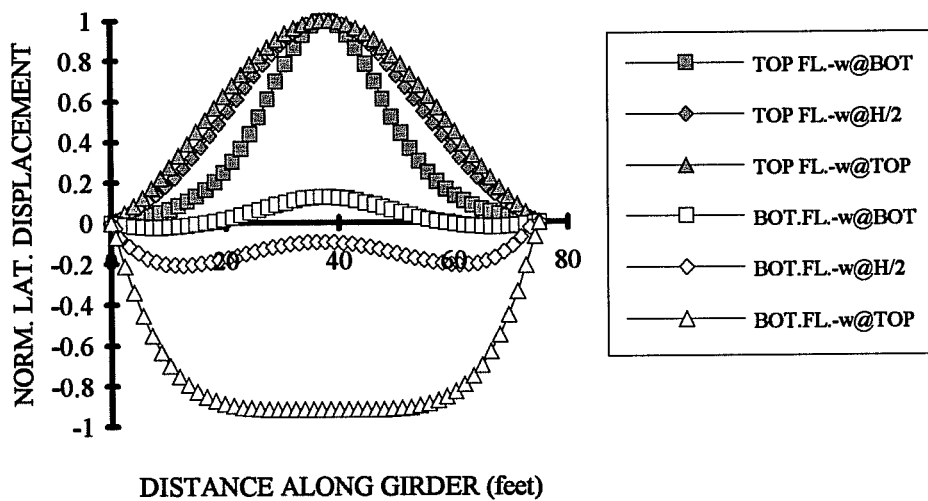
Figure 5.24b Lateral displacement of top and bottom flange for section #2, L=75', w @ variable height, Q=1320.

top and the bottom flanges experience very different lateral displacements depending on the load height.

The reason the height of a point load at midspan does not have a very noticeable effect on the buckled shape of the top flange is probably due to the fact that the deck is not very effective at midspan where the shear distortion that the deck undergoes is relatively small. When the load is spread out along the length, on the other hand, the height of the load affects every single point along the girder length.

5.5 Summary of Effect of Deck on Buckled Shapes

The lateral displacement and cross-sectional twist are a sine curve for girders subjected to constant moment with no deck as a bracing element. When the deck was provided for bracing, the lateral displacement and twist of doubly-symmetric girders remained a sine curve. There was a small amount of deviation for singly-symmetric girders, however, for all practical purposes, the shape can be taken as a sine curve. The center of twist of girders subjected to constant moment with diaphragm bracing was nearly uniform along the girder length and approached the bottom flange with increasing shear rigidity of the diaphragm.

The lateral displacement of the top and bottom flange of unbraced girders with a moment gradient deviated slightly from a sine curve, however, a good approximation of the buckled shape could still be attained with a sine curve. When the deck was introduced as a bracing element, the buckled shape of the girders changed a great deal from a sine curve. Near the support, where the bending moment was low, the deck provided a large amount of restraint to lateral movement of the top flange. The center of twist varied along the length of the girder, and was the highest on the section at the supports. Moment gradients caused by a point load at midspan had a higher center of twist than the same girder subjected to a uniform distributed load. Increases in the girder length also caused higher locations of the center of twist.

The height of a point load at midspan, did not change the buckled shape of the top flange a significant amount, however, the center of twist was much higher on the section for top flange loading. Variable load height for uniform distributed loads changed the buckled shapes of both flanges. The center of twist for uniform distributed loads was highest on the section with top flange loading.

CHAPTER 6

Buckling Capacity of Fully-Stiffened Simply Supported Girders
Braced by a Shear Diaphragm

6.1 Introduction

The previous chapter presented some of the finite element results which showed how the buckling mode was affected when bracing was provided by a shear diaphragm. These results were presented in an effort to gain some insight into the behavior of a twin girder system braced by a shear diaphragm at the top flange. This chapter will present results which demonstrate how the buckling capacity of a simply supported girder is enhanced when bracing is provided by a shear diaphragm at the top flange. The results presented in this chapter are for girders with transverse stiffeners spaced at 18.75 inches. These girders will be referred to as "fully-stiffened".

Similar to the previous chapter which dealt with displaced shapes, the results will be broken down into different sections based on the type of loading. The results for girders subjected to a constant moment will be presented in Section 6.2. Section 6.3 will present the results for girders loaded by transverse loads (moment gradient) applied at midheight of the section. The results for transverse loads applied at variable load heights will be presented in Section 6.4. Finally, the results will be summarized in Section 6.5. For brevity, as the results are presented, comparisons will be made with existing closed formed solutions and other approximate solutions.

6.2 Buckling Capacity of Girders Subjected to Constant Moment

This section presents the results for girders braced by a shear diaphragm which are subjected to constant moment. The section has been divided into two sub-sections. The first sub-section will present the ANSYS results for girders braced by a shear diaphragm at the top flange. The second sub-section will compare the ANSYS results with closed-formed solutions and also approximate solutions.

6.2.1 Finite Element Results for Girders Braced by a Shear Diaphragm

This section presents finite element results for the girders with a shear diaphragm at the top flange which are subjected to constant moment. Results for sections #1, #2, and #3 will be presented first. These sections have been shown in the previous chapters; however they are shown

again in Figure 6.1. Figure 6.2a, 6.2b, and 6.2c show the plots of buckling moment versus the shear rigidity of the deck for sections #1, #2, and #3, respectively. The plot for each section has the results for girder lengths of 25, 50, and 75 feet.

For the results of each girder length, the y-intercept corresponds to the buckling capacity of the individual girder with no deck as a bracing element. The capacity of the girders with no deck (Q=0) will be referred to as M_g. For sections with a relatively large warping stiffness (shorter spans), M_g is essentially an inverse function of the length squared $(1/L^2)$. For longer spans, the stiffness is dominated by St. Venant's torsional stiffness, and M_g is essentially a function of the inverse of the length $(1/L)$. Because of the relationship between the girder length and the buckling capacity, for the girders shown in Figure 6.2a, 6.2b, and 6.2c, there is a much larger difference in M_g between girders with the 25 and 50 foot lengths when compared to the difference in M_g for the 50 and 75 foot long girders. It should be pointed out that M_g for the 25 foot long girder represents the capacity of the 75 foot long girder with cross-frames at the third points (25 feet). There is a substantial increase in the buckling capacity when the deck is used as a bracing element. Referring to the curve for the 75 foot long section #1 in Figure 6.2a, providing a deck with a shear rigidity of 660 k/rad increases the buckling capacity enough to exceed M_g (Q=0) for the 25 long girder. This indicates that for section #1, a deck with a shear rigidity of 660 k/rad can provide more bracing to the girder than cross-frames spaced at 25 feet. Figures 6.2b and 6.2c show that for the respective sections #2 and #3, a smaller deck shear rigidity is required to exceed the bracing capacity of cross-frames at the third points of the 75 foot long girders.

Although the curves in Figures 6.2a, 6.2b, and 6.2c appear to be linear, there is a slight reduction in slope as the shear rigidity is increased. For a given deck rigidity, adjacent curves appear to be offset by the difference between M_g for the individual girder lengths. This can be confirmed by subtracting M_g from the buckling capacity of the system (M_{cr}) to obtain the increase in the buckling moment that the deck provides. This will be denoted as M_{deck} and is given by the following expression:

$$M_{deck} = M_{cr} - M_g \qquad (6.1)$$

The value of M_{deck} versus Q for the sections #1, #2, and #3 is shown in Figures 6.3a, 6.3b, and 6.3c, respectively. Each of the plots has the results for lengths of 25, 50, and 75 feet. The curves are essentially coincident up until a shear rigidity of approximately 660 kips/rad. The curves do
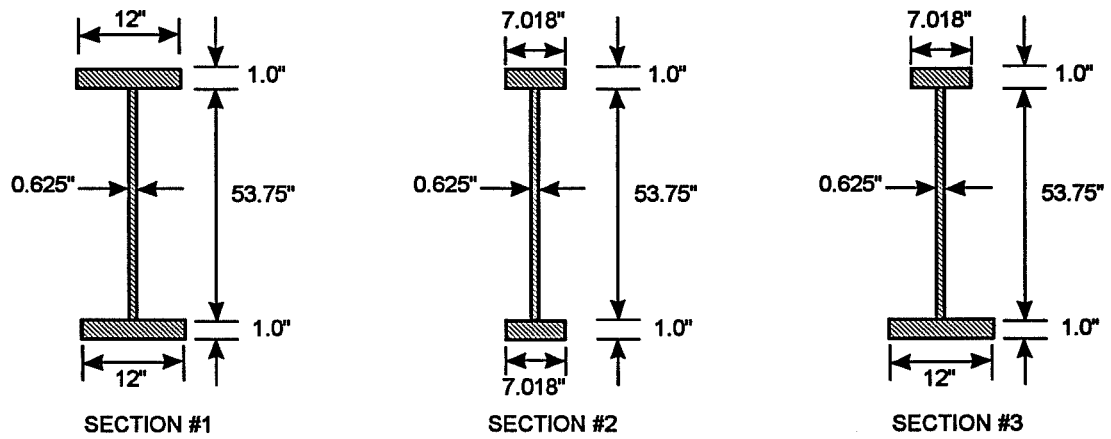
Figure 6.1 Cross-sections considered in computational study.
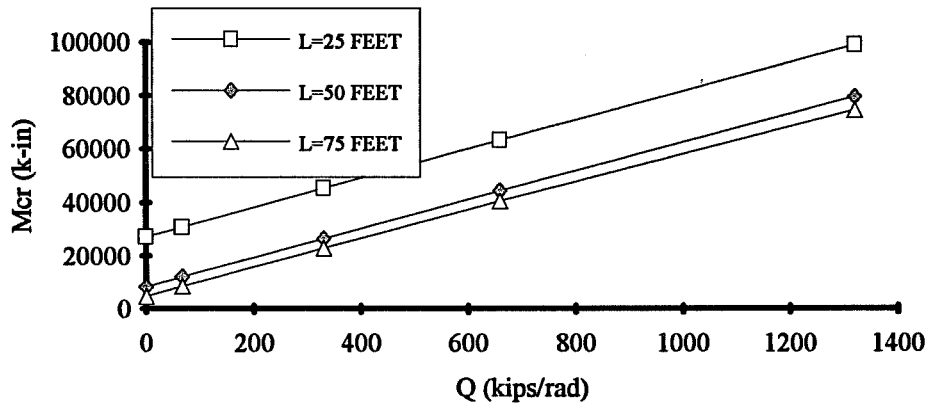
Figure 6.2a Mcr vs. Q for section #1 with uniform moment.
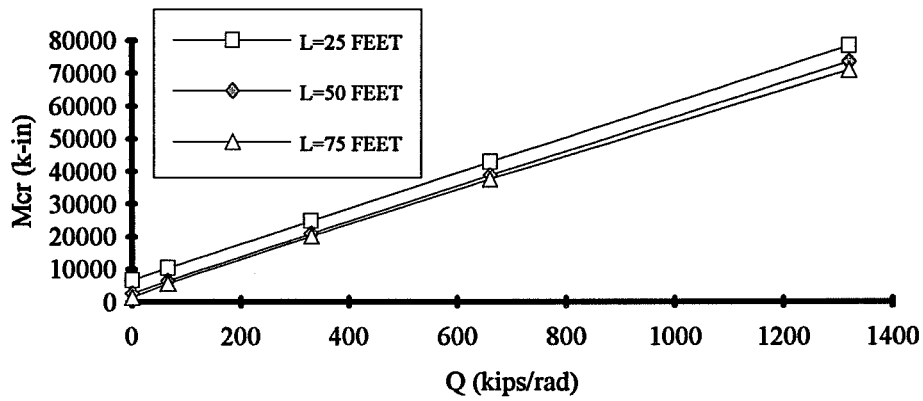
Figure 6.2b Mcr versus Q for section #2 with uniform moment.
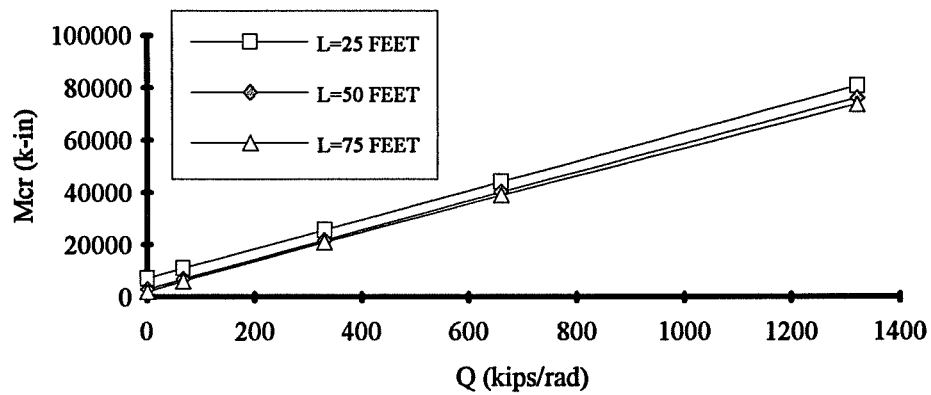
Figure 6.2c Mcr versus Q for section #3 with uniform moment.
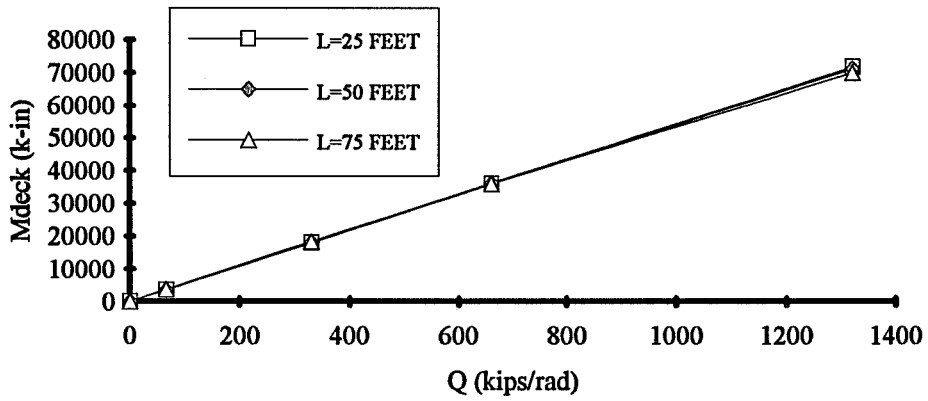
Figure 6.3a Mdeck versus Q for section #1 with constant moment.
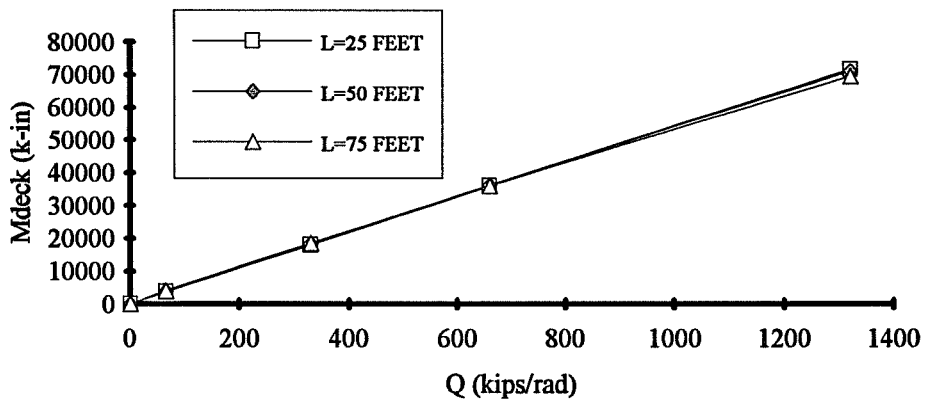
Figure 6.3b Mdeck versus Q for section #2 with constant moment.
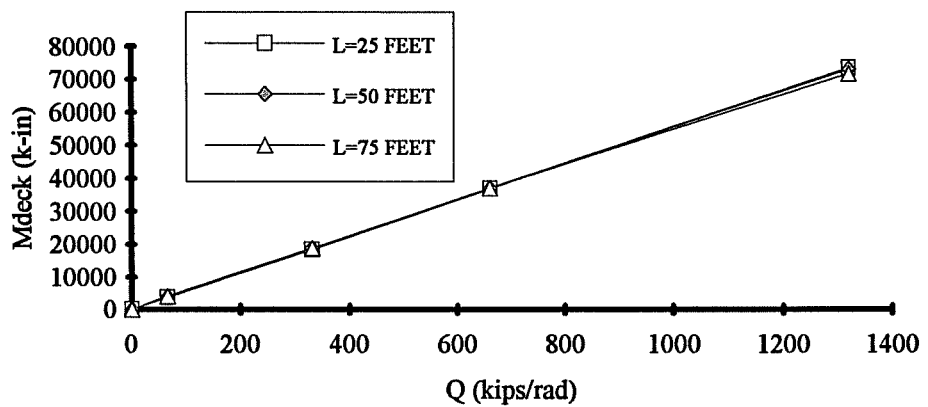
Figure 6.3c Mdeck versus Q for section #3 with constant moment.

deviate slightly from one another at the highest shear rigidity of 1320, however, the value of M_{deck} for constant moment loading is essentially independent of the span.

The curves for the three different cross-sections can be plotted on the same figure for a given length to determine the influence of the cross-section upon M_{deck}. This is shown in Figures 6.4a, 6.4b, and 6.4c which show plots of M_{deck} versus Q for the three cross-sections for respective lengths of 25, 50 and 75 feet. The curves for sections #1 and #2 are nearly coincident for all three lengths. The curve for the singly-symmetric section (#3) deviates slightly from the other two curves at higher values of the shear rigidity, however, it is extremely close to the other curves.

It is of interest to study the behavior of sections with a different girder depth to determine if the effectiveness of the deck is altered. In Chapter 4, girders with different depths were introduced to expand the range of geometry in the study. These sections are shown again in Figures 6.5a and 6.5b. The depth of the girders in Figure 6.5a are half of the depth of sections #1, #2, and #3 which have been considered so far in this chapter. The depth of the girders in Figure 6.5b are twice the depth of sections #1, #2, and #3. The flange sizes for the new sections are identical to the flanges used in sections #1, #2, and #3. The respective cross-sections shown in Figures 6.5a and 6.5b are designated "shallow" #1, #2, and #3, and also "deep" #1, #2, and #3. It was observed in the behavior of sections #1, #2, and #3 that the deck was slightly less effective on longer girders than on shorter girders. So as to consider only the worst case, only 75 foot girder lengths were considered in with the shallow and deep girder cross-sections.

Figure 6.6 shows a plot of M_{cr} versus Q for the three shallow sections. For a given shear rigidity the two doubly symmetric sections appear to be offset by the capacity of the unbraced girder M_g. The singly-symmetric section, shallow #3, has a slightly steeper slope than the other two sections. This was also observed for the deeper sections, which are shown in Figure 6.7. The singly-symmetric section, deep #3, has nearly the same initial capacity (Q=0) of deep #2 and approaches the plot of deep #1 for larger values of the shear rigidity.

Figures 6.8a, and 6.8b show plots of M_{deck} versus Q for the shallow sections and deep sections, respectively. In both graphs, the lines plot very close together up to a shear rigidity of 660 kips/rad, and then diverge slightly for higher values of the shear rigidity. This is similar to what was observed for the normal depth sections. Figure 6.9 shows a plot of M_{deck} versus Q for girders with variable depth. The girders have the flanges of section #1 (12 in. x 1 in.). The deck is the least effective for the shallow section. For a given value of the shear rigidity, M_{deck} for the normal depth section (section #2) appears to be roughly twice that of the shallow section, while
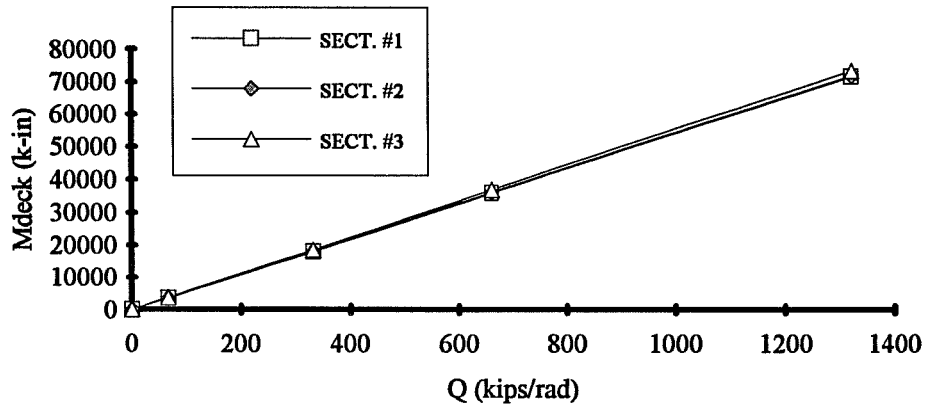
Figure 6.4a : Mdeck versus Q for 25 foot span with uniform moment.
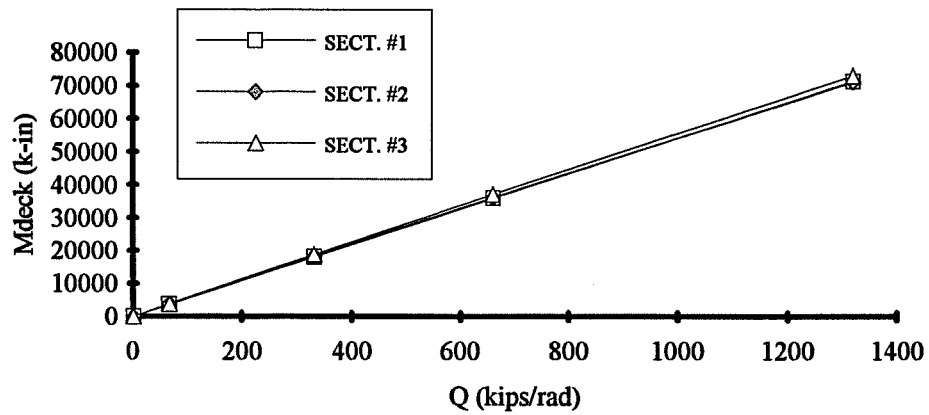
Figure 6.4b: Mdeck versus Q for 50 foot span with uniform moment.
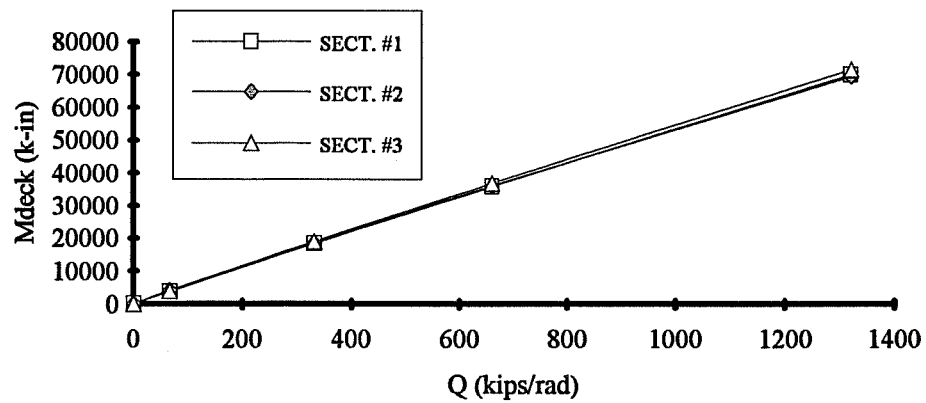
Figure 6.4c: Mdeck versus Q for 75 foot span with uniform moment.
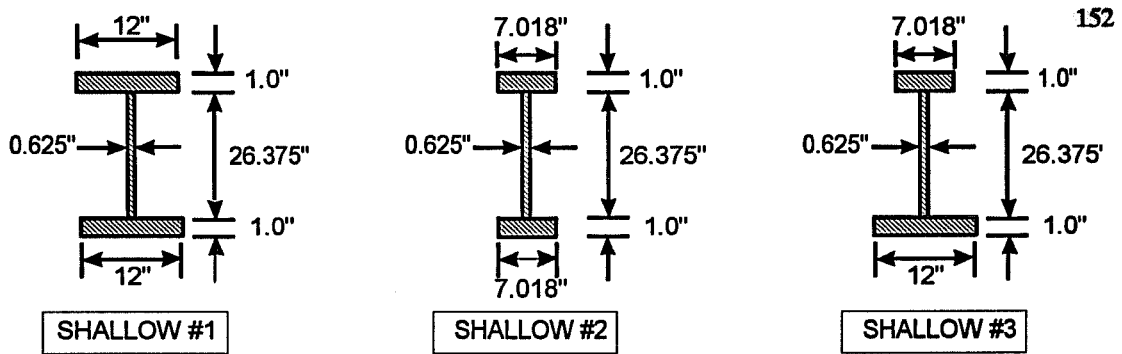
Figure 6.5a Shallow cross-sections considered.
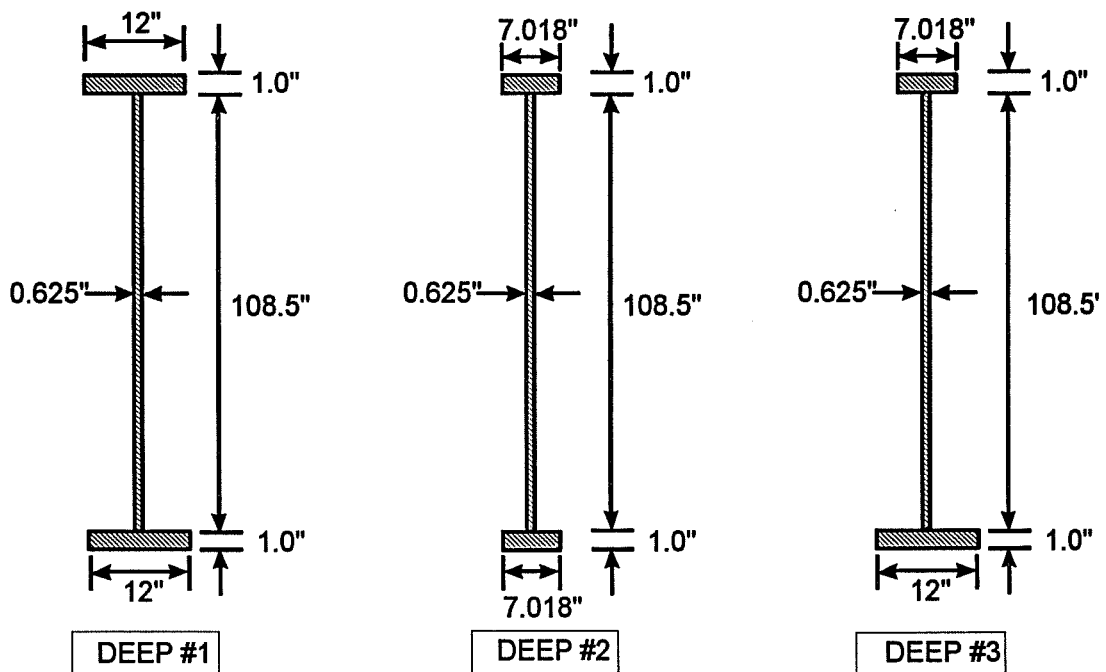
Figure 6.5b Deep cross-sections considered.
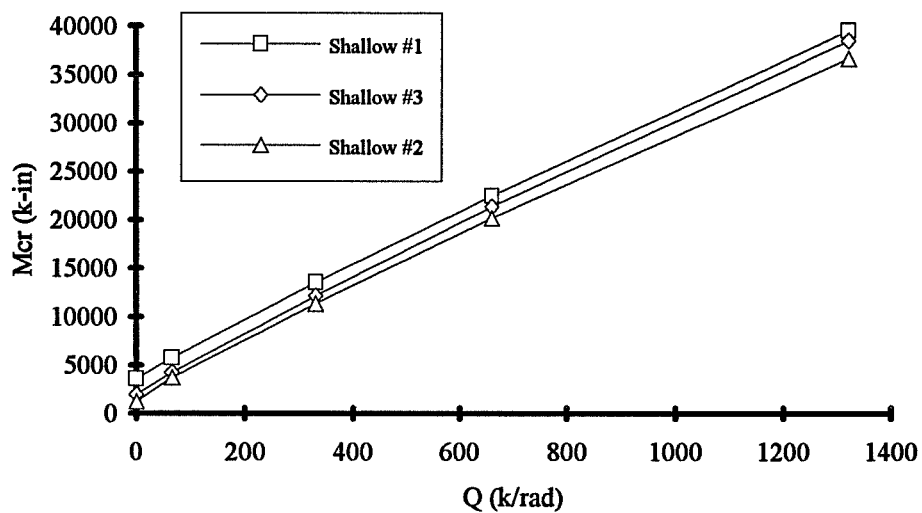
Figure 6.6 : Mcr versus Q for shallow girders with constant moment.
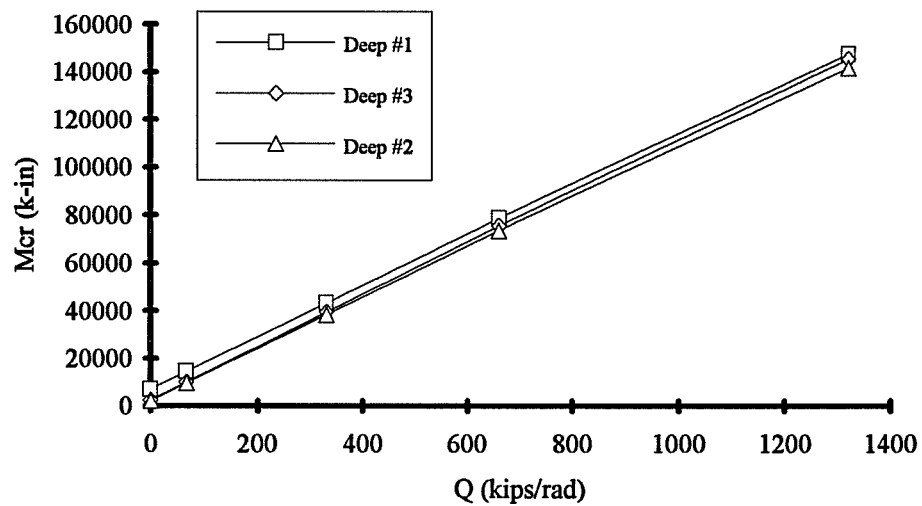
Figure 6.7 : Mcr versus Q for deep girders with constant moment.
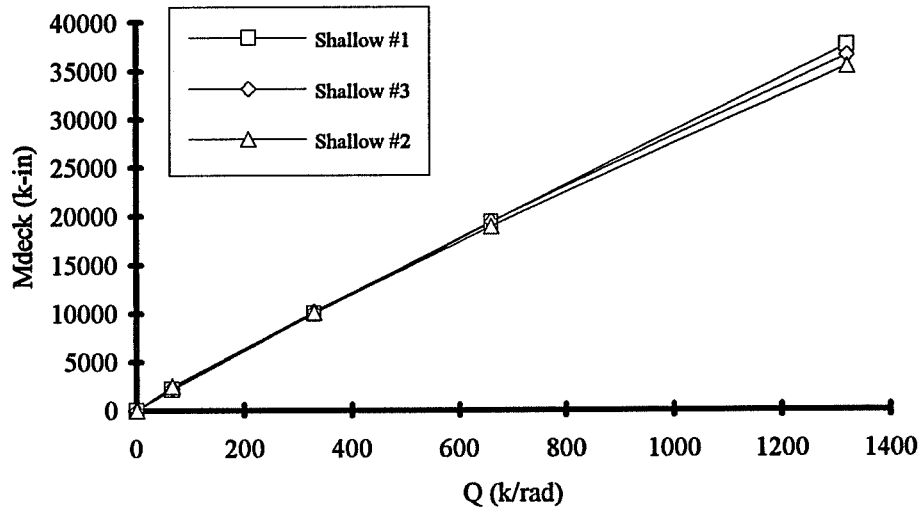
Figure 6.8a : Mdeck versus Q for shallow girders with constant moment.
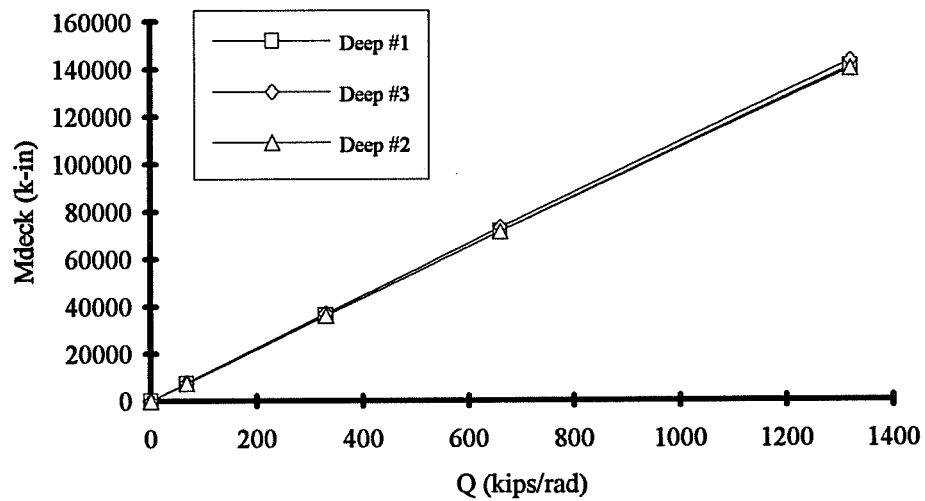
Figure 6.8b : Mdeck versus Q for deep girders with constant moment.
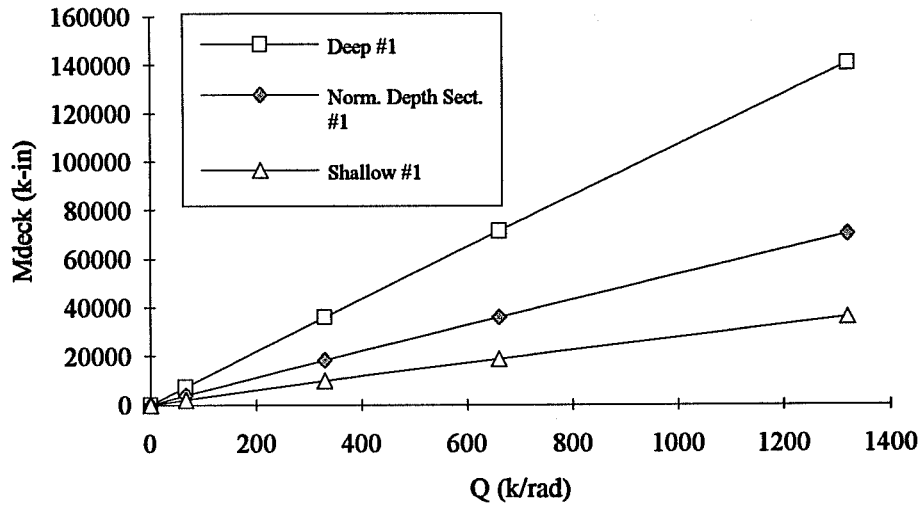
Figure 6.9 : Mdeck versus Q for variable depth girders with section #1 flanges and 75 foot span.
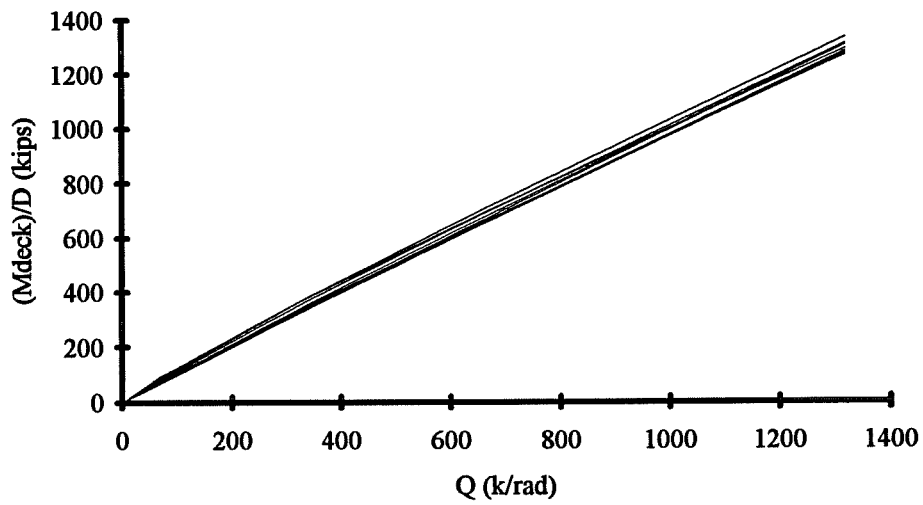
Figure 6.10 : Mdeck/D versus Q for variable depth girders with all flange sizes and a 75 foot span.

M_{deck} for the deep section appears to be roughly four times that of the shallow section. An interesting comparison can be made if M_{deck} for each of the different sections is normalized by the corresponding depth. Table 6.1 shows the values of M_{deck}/d for a shear rigidity of 660 kips/rad for each of the different sections considered. The values range from 653 kips to 707.6 kips which is a 7.7% difference based on the maximum value of 707.6. This is a relatively small difference for the variety of cross-sections considered.

Table 6.1 Values of M_{deck}/d for Q = 660 kips/rad			
Flanges	Shallow Section	Normal Section	Deep Section
Section #1 Flanges	690.3	657.3	653.0
Section #2 Flanges	691.8	659.5	653.0
Section #3 Flanges	707.6	675.9	667.7

Figure 6.10 shows a plot of M_{deck}/d versus Q for all nine of the 75 foot long sections which have been considered. This plot shows that even though many of the sections have drastically different depths, M_{deck}/d plots very close together which indicates that the effectiveness of the deck is nearly linearly dependent on the girder depth for loading consisting of constant moment.

The plots of M_{deck} versus Q with constant moment loading have indicated the following:

    1. the increase in M_{deck} with Q is approximately linear,

    2. the increase in M_{deck} is independent of girder span or unbraced length,

    3. the increase in M_{deck} is essentially a linear function of the girder depth.

The previous discussion has outlined the effect of a deck as a bracing element to increase the buckling capacity of a girder. It is necessary, however, to address the effect of the mode shape on the buckling capacity. In Chapter 2, the behavior of discrete bracing systems was described. The figure which was used in Chapter 2 to explain the behavior is shown again in Figure 6.11. As the discrete brace stiffness was increased, the girders exhibited a succession of changes in mode shape until buckling of the girder occurred between the braces. With each change in mode shape the effectiveness of the bracing system was decreased.
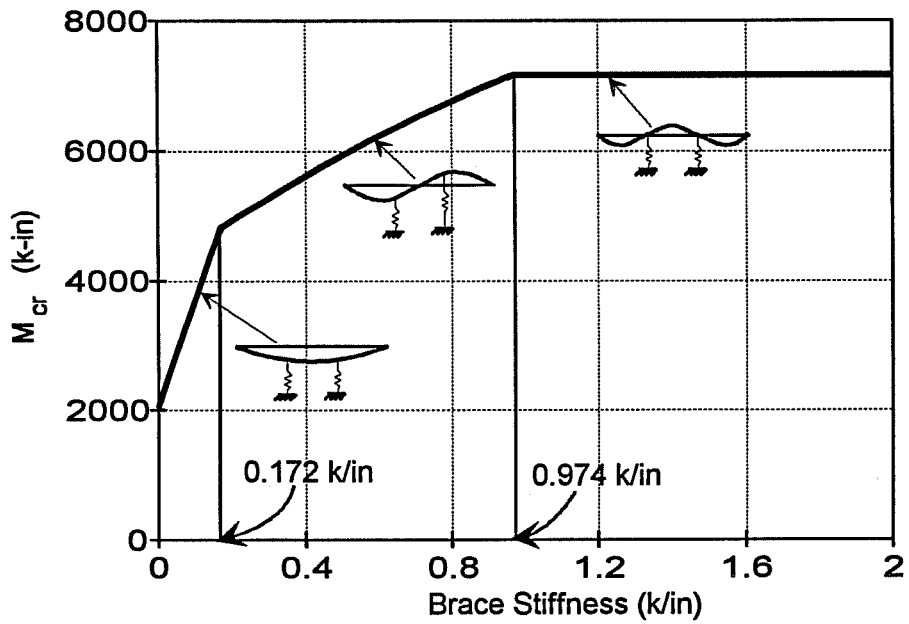
Figure 6.11 Effect of discrete brace stiffness on buckling moment.
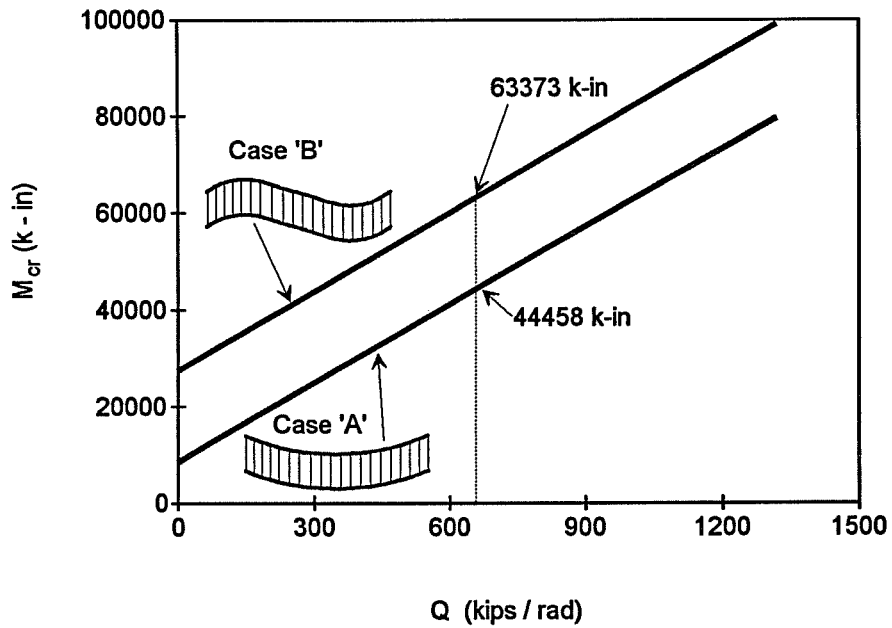
Figure 6.12 Hypothetical situation of girder changing buckling modes from "half-sine" curve to "full sine" curve.

It was stated in Chapter 2, and also shown in Chapter 5, that girders braced by a shear diaphragm will always have the same basic mode shape. Changing the shear rigidity of the deck may cause subtle changes in the buckled shape, however the girder will always buckle between points of full bracing provided by discrete braces. A girder with a cross frame at midspan will always buckle in two "half sine" curves, regardless of the rigidity provided for the shear diaphragm.

The reason there is not a change in the number of "half-sine" curves is because the increase in the buckling capacity due to the deck is not heavily dependent on the span of the girder, i.e. M_{deck} is not significantly affected by the span of the "half-sine" curve. On the other hand, the buckling capacity of the unbraced girder, M_g, is dependent on the number of "half-sine" curves. If the girder were to buckle in more "half-sine" curves, M_g would increase, which would actually increase the buckling capacity of the girder ($M_{cr} = M_{deck} + M_g$). This is shown graphically in Figure 6.12 which shows a plot of M_{cr} versus Q for section #2 with a 50 foot span. Two different cases of discrete bracing are shown: discrete bracing at the supports only (50 feet between cross-frames) which is denoted as case 'A', and discrete bracing at the supports and midspan (25 feet between cross-frames) which is denoted as case 'B'. Case 'B' with a 25 foot spacing between cross-frames actually represents the hypothetical situation if case 'A' were to change buckled shapes to a "full sine" curve instead of a "half-sine" curve. For example, if the 50 foot long girder were to change from a "half-sine" curve to a "full-sine" curve at a shear rigidity of 660 kips/rad, the buckling moment would change from 44458 k-in to 63278 k-in. This will not take place, since the buckled shape of the girder will always be a mode which makes the bracing system the least effective. Buckling will only occur between points of full bracing provided by discrete braces.

6.2.2 Comparison of Constant Moment Results with Closed Formed Solutions

The finite element studies presented in Section 6.2.1 have demonstrated that the contribution of the deck is relatively constant from section to section as long as the girder depth is maintained. In addition to gaining a better understanding of the behavior of girders braced by a shear diaphragm, the purpose of the finite element studies was to compare the results with existing closed formed solutions so as to develop a simple method to predict the buckling capacity of these girder systems. Chapter 2 outlined some of the existing closed formed solutions which can be used to predict the buckling capacity of girders. The most readily available solution for

girders braced by a shear diaphragm located at the top flange is an energy based solution which was first derived by Errera [12] and is shown in Equation 6.2.

$$M_{cr} = \sqrt{\left(\frac{\pi^2 E I_y}{L_b^2} + Q\right)\left(\frac{\pi^2 E C_w}{L_b^2} + GJ + Qe^2\right)} + Qe \qquad (6.2)$$

M_{cr} = buckling moment of diaphragm braced girder,

L_b = unbraced length,

E = modulus of elasticity,

I_y = weak-axis moment of inertia,

G = shear modulus,

J = St. Venant's torsional constant,

$C_w = I_y \, d^2 \, \rho \, (\, 1\text{-}\rho \,)$ = warping constant,

d = distance between flange centroids,

$\rho = I_{yc} / I_y$,

I_{yc} = moment of inertia of compression flange about axis through web,

Q = shear rigidity of deck = G' x tributary width of deck,

G' = effective shear modulus of deck,

e = there are multiple definitions in the literature:

        1) distance from geometric centroid to plane of decking,

        2) distance from shear center to plane of decking.

For doubly-symmetric sections the geometric centroid and shear center coincide at midheight so e is equal to d/2.

Equation 6.2 was developed for doubly-symmetric girders subjected to constant moment. Since sections #1 and #2 were doubly-symmetric, the finite element results for these sections can be compared directly with this solution.

Figure 6.13 shows a comparison of the ANSYS results and the Errera solution for section #1. The ANSYS results for lengths of 25, 50, and 75 feet are shown with a filled in marker. The predictions from the Errera solution are shown with the corresponding marker unfilled. Many of the ANSYS data points are not visible because the Errera solution plots directly on top of the

ANSYS results. It should be noted that at first glance, Equation 6.2 appears to be relatively complex, however, Figure 6.13 shows the equation is approximately linear. The equation does a very good job of predicting the buckling capacity. There is a slight deviation between the Errera prediction and the finite element results for larger values of the shear rigidity, however, the difference is quite small. Table 6.2 shows the values of the moment from ANSYS and the Errera solution for variable shear rigidity. The percent difference of the closed-formed solution with respect to the finite element results is shown in parentheses beneath the moment predicted by the Errera solution. A negative percent means the Errera solution gives unconservative estimates with respect to the finite element results. The percent difference is much less than 2% in nearly all the cases except for the 75 foot girder length with Q=1320 which is 3.7%.

Table 6.2 Section #1 Constant Moment Results					
	Q = 0	Q = 66	Q = 330	Q = 660	Q = 1320
ANSYS -25'	27266	30880	45293	63278	98994
Errera -25'	27454 (-0.7%)	31077 (-0.6%)	45557 (-0.6%)	63644 (-0.6%)	99804 (-0.8%)
ANSYS -50'	8368	12058	26454	44458	79594
Errera -50'	8417 (-0.6%)	12096 (-0.3%)	26675 (-0.8%)	44805 (-0.8%)	80988 (-1.8%)
ANSYS -75'	4618	8440	22954	40603	74734
Errera -75'	4670 (-1.1%)	8459 (-0.2%)	23151 (-0.9%)	41305 (-1.7%)	77500 (-3.7%)

The results for section #2 are shown in Figure 6.14. There is very good correlation between the ANSYS results and the Errera solution for the 25 foot length. The results for the 50 and 75 foot length also compare relatively well, however the results plot so close together it is very difficult to distinguish between the different curves. The results for section #2 are shown in Table 6.3. The Errera solution is well within 2% of the ANSYS results in the majority of the cases
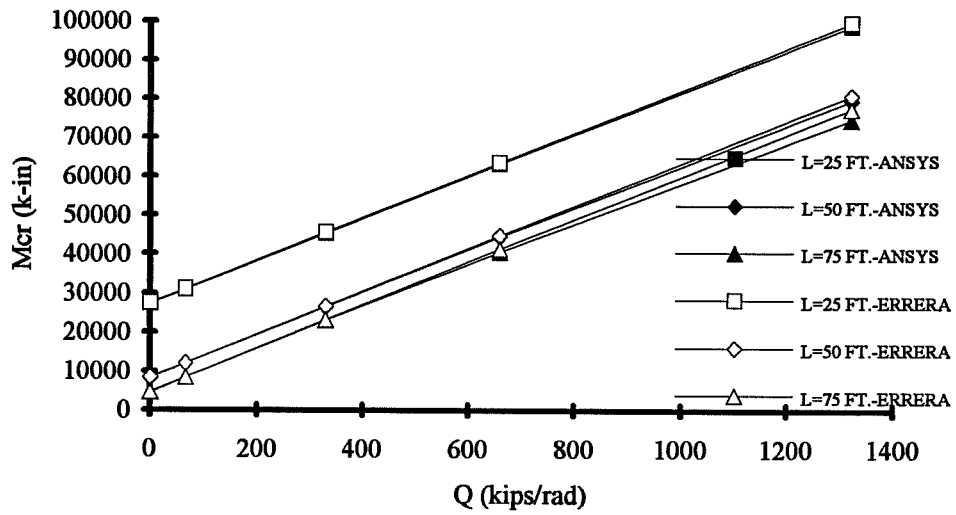
Figure 6.13 : Mcr versus Q for section #1 - comparison between ANSYS results and Errera solution for constant moment.
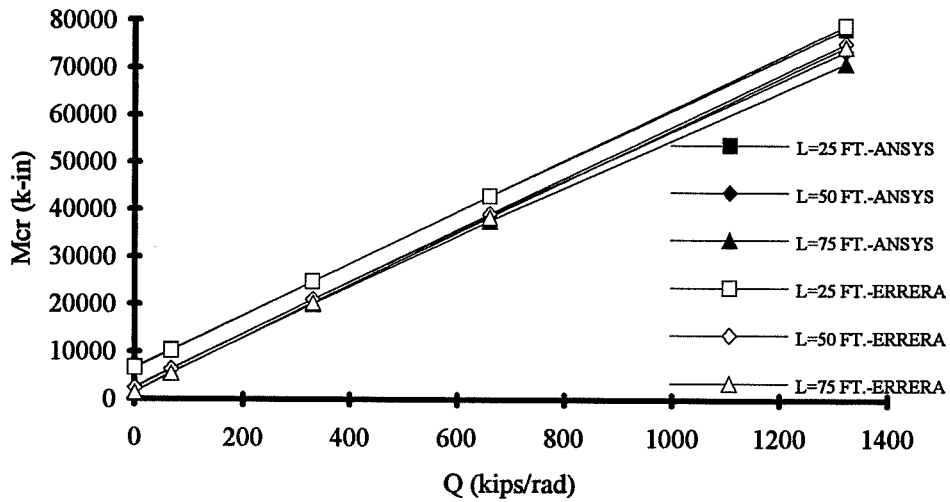
Figure 6.14 : Mcr versus Q for section #2 - comparison between ANSYS results and Errera solution for constant moment.

considered with the exception of the 75 foot long girder with the deck shear rigidity of 1320 which has a 4.9% difference.

Table 6.3 Section #2 Constant Moment Results					
	Q = 0	Q = 66	Q = 330	Q = 660	Q = 1320
ANSYS -25'	6726	10392	24881	42872	78492
Errera -25'	6604 (1.8%)	10272 (1.2%)	24818 (0.3%)	42925 (-0.1%)	79089 (-0.8%)
ANSYS -50'	2544	6431	21005	38822	73647
Errera -50'	2490 (2.1%)	6352 (1.2%)	21025 (-0.1%)	39152 (-0.8%)	75325 (-2.3%)
ANSYS -75'	1538	5654	20175	37644	71134
Errera -75'	1539 (0.1%)	5590 (1.1%)	20319 (-0.7%)	38453 (-2.1%)	74627 (-4.9%)

The results for sections #1 and #2 have shown that the Errera solution does a very good job of predicting the capacity of doubly-symmetric girders. Most bridge girders, however, have a different size top and bottom flange which make the sections singly-symmetric. The Errera solution should be modified slightly in order to approximate the capacity of singly-symmetric girders. Timoshenko's [23] classic solution for lateral torsional buckling of doubly symmetric girders is shown in the following expression:

$$M_g = \frac{\pi}{L_b}\sqrt{EI_yGJ + \frac{\pi^2 E^2 I_y^2 d^2}{4L_b^2}} \qquad (6.3)$$

Referring back to Errera's energy solution, if $C_w = I_y d^2/4$ and $e = d/2$ are substituted into the Errera expression and the term under the radical is expanded, the expression can be reorganized to produce the expression shown in the following expression:

$$M_{cr} = \sqrt{\left[\frac{\pi^2}{L_b^2}\left(EI_yGJ + \frac{\pi^2E^2I_y^2d^2}{4L_b^2}\right)\right] + \left[\frac{Qd^2}{2}\frac{\pi^2EI_y}{L_b^2} + QGJ + \frac{Q^2d^2}{4}\right]} + \frac{Qd}{2} \qquad (6.4a)$$

The first expression within the radical which is enclosed in square brackets is equal to Timoshenko's formula squared. The solution can therefore be rewritten as shown in Equation 6.4b in which M_g is equal to the capacity of the girder with no deck for bracing. When there is no deck ($Q=0$), the Errera solution reduces to Timoshenko's solution.

$$M_{cr} = \sqrt{M_g^2 + \left[\frac{Qd^2}{2}\frac{\pi^2EI_y}{L_b^2} + QGJ + \frac{Q^2d^2}{4}\right]} + \frac{Qd}{2} \qquad (6.4b)$$

The AASHTO formula is shown in Equation 6.5. As outlined in Chapter 2 the AASHTO formula for lateral torsional buckling essentially matches Timoshenko's equation for doubly-symmetric sections, but also gives approximations for singly-symmetric girders.

$$M_{AASHTO} = \pi E\left(\frac{I_{yc}}{L_b}\right)\sqrt{\frac{2G}{E}\left(\frac{J}{I_{yc}}\right) + \pi^2\left(\frac{d}{L_b}\right)^2} \qquad (6.5)$$

Therefore, the term M_g in square brackets in the Equation 6.4b could be replaced with the AASHTO expression squared. If the weak axis moment of inertia is also replaced with twice the moment of inertia of the compression flange ($I_y = 2I_{yc}$), the following expression results:

$$M_{cr} = \sqrt{(M_{AASHTO})^2 + \left[\frac{Qd^2}{2}\frac{\pi^2E(2I_{yc})}{L_b^2} + QGJ + \frac{Q^2d^2}{4}\right]} + \frac{Qd}{2} \qquad (6.6)$$

When a doubly-symmetric section is considered, Equation 6.6 will produce results which are essentially identical to the original Errera solution, however, this modified Errera solution also permits singly-symmetric sections to be considered.

In order to separate the contribution of the deck from the capacity of the unbraced girder in the original Errera solution, the variable "e" was set equal to d/2. It was stated in Chapter 2 as well as earlier in this section that it was unclear what to use for "e" in singly-symmetric sections. Therefore comparisons will be made using the Equation 6.7.

$$M_{cr} = \sqrt{(M_{AASHTO})^2 + \left[2Qe^2 \, \frac{\pi^2 E(2I_{yc})}{L_b^2} + QGJ + Q^2 \, e^2 \right]} + Qe \qquad (6.7)$$

Three different distances will be considered for the variable "e":

     1) the distance from the plane of the decking to midheight of the girders,

     2) the distance from the plane of the decking to the center of gravity of the girders,

     3) and, the distance from the plane of the decking to the shear center of the girders.

Figure 6.15a shows a plot of M_{cr} versus Q for section #3 with the case of 25 foot long girders. The variable "e" has the following values depending on the distance which is used in the equation:

     1) midheight of the girders: 27.38"

     2) center of gravity of the girders: 29.97"

     3) shear center of girders: 45.62"

The plot clearly shows that when "e" is taken as the distance from the plane of the deck to the midheight of the girders, the best correlation between ANSYS and the equation is obtained. This is also demonstrated in Figures 6.15b and 6.15c which show M_{cr} versus Q for section #3 with respective lengths of 50 and 75 feet. The actual magnitudes of the buckling moment for ANSYS and the Errera solution using e = d/2 are presented in Table 6.4, which shows that the modified Errera solution does a very good job of predicting the buckling load when compared to the finite element results. The Errera solution is well within 2% of the ANSYS results in the majority of the cases considered with the exception of the 75 foot long girder with the deck shear rigidity of 1320 which has a 4.9% difference.
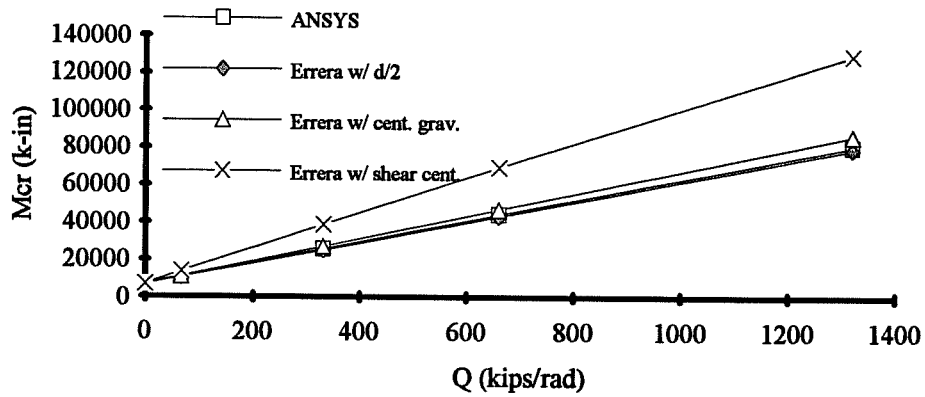
Figure 6.15a : Mcr versus Q for section #3 with a 25 foot span and constant moment - Errera solution with variable definition of "e".
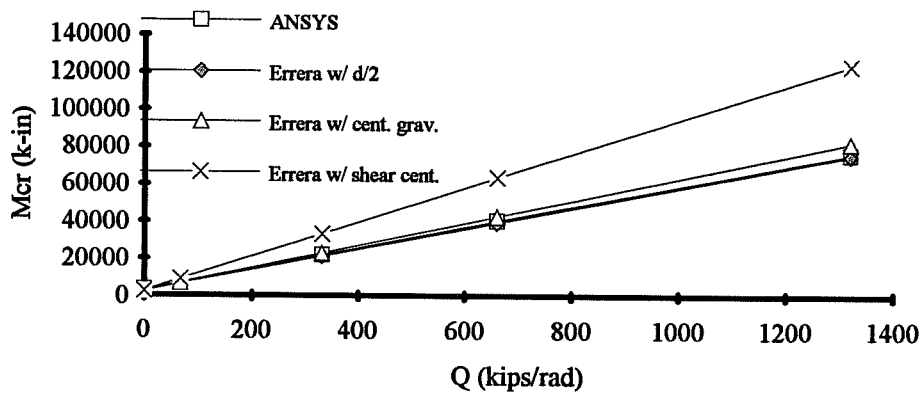
Figure 6.15b : Mcr versus Q for section #3 with a 50 foot span and constant moment - Errera solution with variable definition of "e".
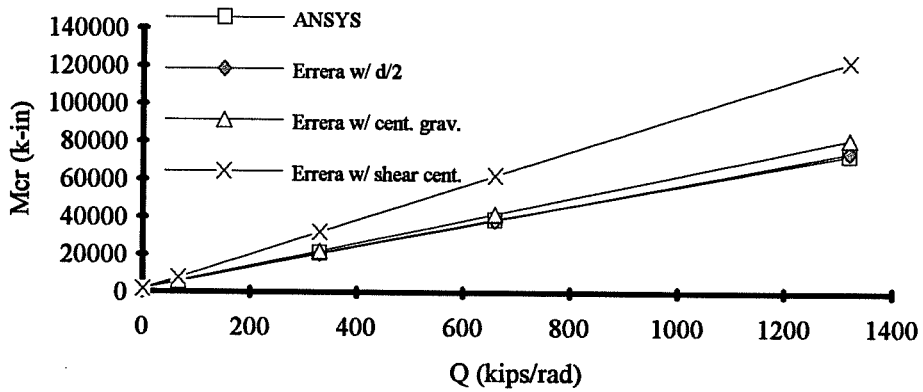
Figure 6.15c : Mcr versus Q for section #3 with a 75 foot span and constant moment - Errera solution with variable definition of "e".

Table 6.4 Section #3 Constant Moment Results					
	Q=0	Q= 66	Q = 330	Q = 660	Q = 1320
ANSYS -25'	7293	11006	25800	44237	80778
Errera -25'	6856 (6.0%)	10540 (4.2%)	25116 (2.6%)	43237 (2.3%)	79412 (1.7%)
ANSYS -50'	3135	6964	21890	40262	76205
Errera -50'	2655 (15.3%)	6574 (5.6%)	21311 (2.6%)	39460 (2.0%)	75646 (0.7%)
ANSYS -75'	2109	6107	21048	39114	73788
Errera -75'	1657 (26.2%)	5795 (5.1%)	20603 (2.1%)	38760 (0.9%)	74948 (-1.6%)

It was mentioned in Chapter 2 that Errera [11] as well as Nethercot and Trahair [18] have recommended that a conservative estimate of the buckling capacity of girders braced a shear diaphragm at the top flange can be made by using the following expression:

$$M_{cr} = M_{AASHTO} + Q\, d \qquad\qquad (6.8)$$

In the above expression, the capacity of the girder with no deck, M_g, has been replaced with M_{AASHTO}. This approximation has been plotted in Figures 6.16a, 6.16b, and 6.16c along with the results for the three different sections with respective lengths of 25, 50, and 75 feet. The ANSYS results have a filled in marker, while the approximate solution has the corresponding marker unfilled. For most of the cases plotted, the line and markers for the ANSYS results can not be distinguished from the approximate solution because the lines plot directly on top of one another. These plots show that the approximation provides very good estimates of the buckling capacity in all the cases with the exception of section #2 with a 75 foot length and a shear rigidity of 1320, however, even in this case the approximation is very close to the ANSYS results.
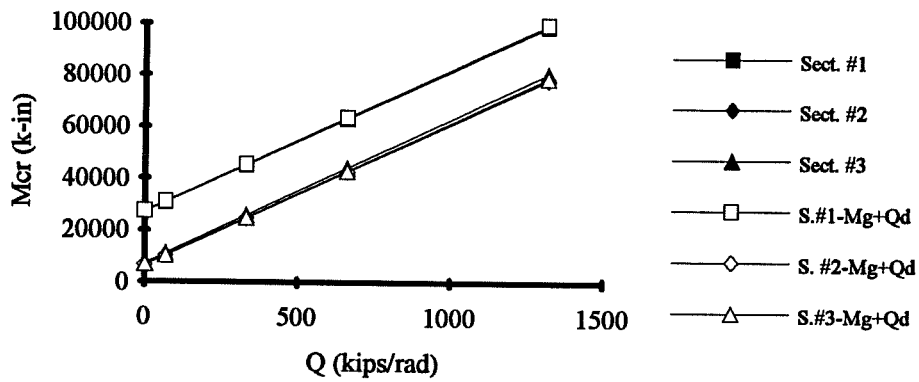
**Figure 6.16a : Mcr versus Q for ANSYS results with approximation
"Mg + Qd" for 25 foot span with constant moment.**
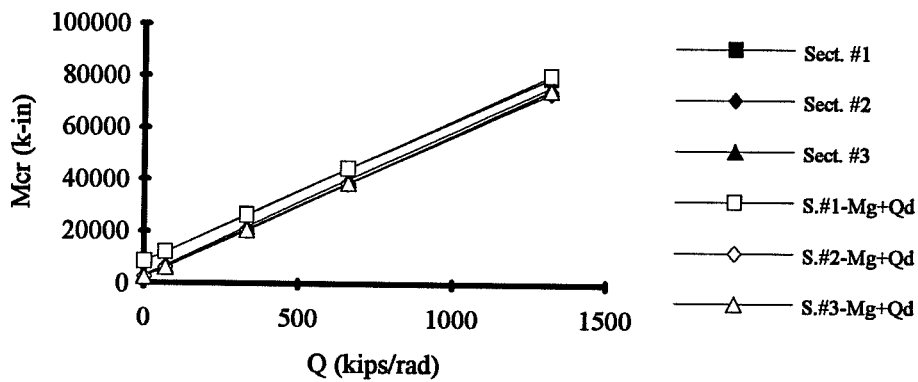
**Figure 6.16b : Mcr versus Q for ANSYS results with approximation
"Mg + Qd" for 50 foot span with constant moment.**
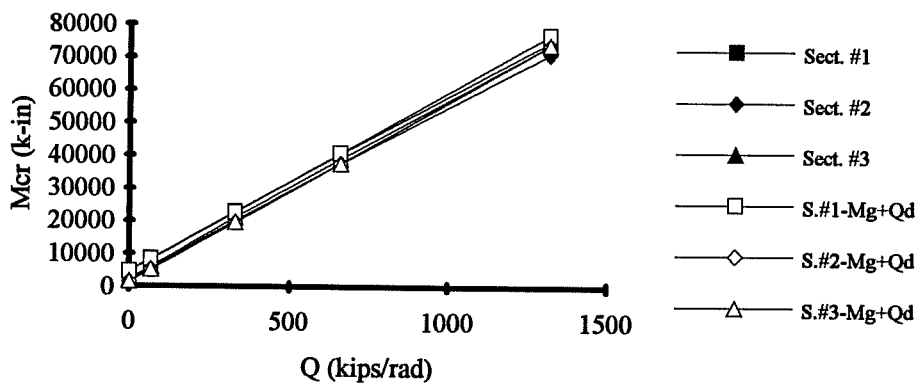
**Figure 6.16c : Mcr versus Q for ANSYS results with approximation
"Mg + Qd" for75 foot span with constant moment.**

In comparing the plots for the Errera solution with the approximate solution in Equation 6.8, it is apparent that the Errera solution is nearly linear. It is worthwhile to isolate the different terms in the Errera solution in order to determine why the equation, which appears very complex, is nearly linear. The approximate solution uses "Qd" to approximate the contribution of the deck. The Errera solution (modified) has been shown again in Equation 6.9a. The terms in Equation 6.9a have been expressed as simple variables A, B, C, and D in Equation 6.9b, and the equation has been normalized by the buckling capacity of the girder with no deck as a bracing element (M_{AASHTO}) in Equation 6.9c.

$$M_{cr} = \sqrt{\left(M_{AASHTO}\right)^2 + \left[\frac{Qd^2}{2}\,\frac{\pi^2 E(2I_{yc})}{L_b^2} + QGJ + \frac{Q^2 d^2}{4}\right]} + \frac{Qd}{2} \qquad (6.9a)$$

$$M_{cr} = \sqrt{\left(M_{AASHTO}\right)^2 + [A + B + C]} + D \qquad (6.9b)$$

$$\frac{M_{cr}}{M_{AASHTO}} = \sqrt{1 + \left[\frac{A}{\left(M_{AASHTO}\right)^2} + \frac{B}{\left(M_{AASHTO}\right)^2} + \frac{C}{\left(M_{AASHTO}\right)^2}\right]} + \frac{D}{\left(M_{AASHTO}\right)} \qquad (6.9c)$$

Equation 6.9c has been plotted in Figures 6.17a, 6.17b, and 6.17c for section #1 with respective lengths of 25, 50, and 75 feet. The figures show graphs of M_{cr}/M_{AASHTO} versus Q. The curve for Equation 6.9c has been denoted as "full equation" in the figures. In addition to plotting the full equation, the figures also show curves which correspond to Equation 6.9c with the four individual cases of setting A, B, C, and D equal to zero. By comparing the curves with the various parameters set equal to zero, it is possible to determine the effect of the parameter on the buckling capacity of the girder system.

The term "B" has little effect on the estimate from the equation. This can be observed by the very small difference in Equation 6.9 when the B-term is taken as zero when compared to the full equation. The term "A" does have a small effect for the 25 foot length, however, for the length of 50 and 75 feet the curve when the A term is neglected is very close to the full equation.
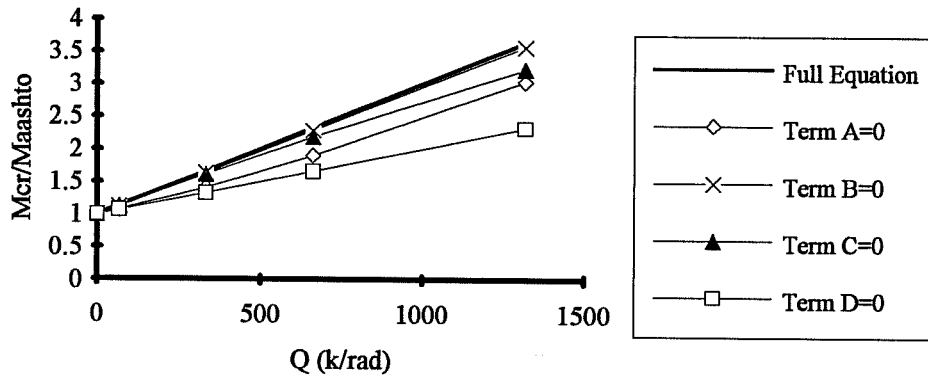
Figure 6.17a : Effect of different terms in Errera solution for section #1.
Constant moment - 25 foot span
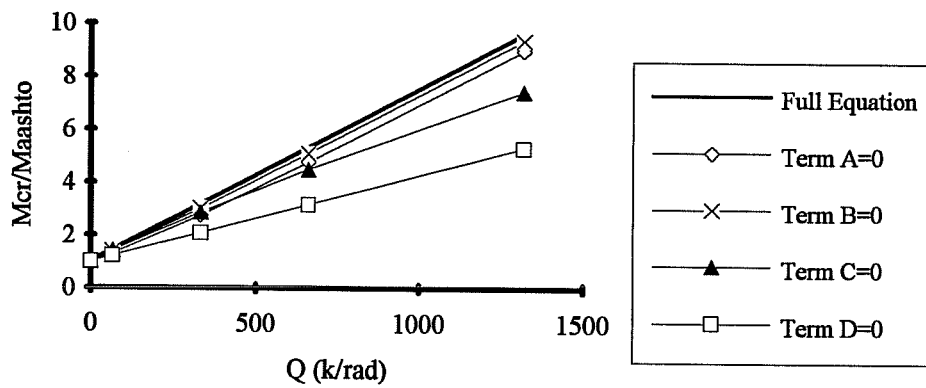
Figure 6.17b : Effect of different terms in Errera solution for section #1.
Constant moment - 50 foot span
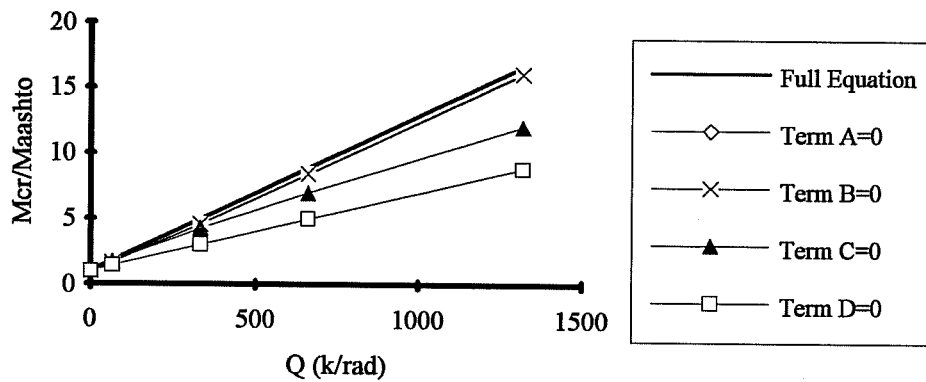
Figure 6.17c : Effect of different terms in Errera solution for section #1.
Constant moment - 75 foot span

For the 75 foot length, the curve with "A" equal to zero can not be distinguished from the curve with "B" equal to zero. Neglecting the "C"-term has a significant effect for all three lengths considered; particularly for longer girder spans. The "D"-term has the largest effect on the capacity. For all three lengths which were considered, neglecting the "D"-term caused a large reduction in the equation prediction.

For longer span girders it is understandable why Qd provides a good approximation for the contribution of the deck. The capacity is dominated by the two terms $Qd/2$ outside the radical and $Q^2d^2/4$ within the radical, which would essentially yield a buckling estimate of Qd. For shorter girders, the buckling capacity of the girder is somewhat larger so the relative increase from the deck would be smaller, however the $Qd/2$ term and the $Q^2d^2/4$ term still dominate the capacity.

ANSYS results were presented in Section 5.1.1 for shallow and deep sections which had girder lengths of 75 feet. These cross-sections were considered in order to study the effect of girder depth on the ability of the deck to act as a bracing element. These ANSYS results can now be compared to the Errera solution. Figures 6.18a, 6.18b, and 6.18c show plots of M_{cr} versus Q for the shallow sections #1, #2, and #3, respectively. The Errera solution is plotted along with ANSYS results. The Errera solution does a very good job of predicting the buckling capacity for shear rigidities up to about 660 kips/rad. The solution does diverge slightly from the finite element results for larger values of the shear rigidity, however, the solution is still relatively close. The Errera solution also worked very well with the deep section as shown in Figures 6.19a, 6.19b, and 6.19c.

Graphs of the approximate solution $M_{AASHTO} + Qd$ are shown for the shallow girders in Figures 6.20a, 6.20b, and 6.20c; and for the deep girders in Figures 6.21a, 6.21b, and 6.21c. For both the shallow and deep girders, the approximate solution does a very good job of estimating the buckling capacity. The approximation is slightly unconservative for the highest values of the shear rigidity considered ($Q=1320$), however, even in these cases the approximation is close.

The comparisons have been made in this section which have shown that the Errera solution had very good agreement with the finite element results for doubly-symmetric girders subjected to constant moment. The Errera solution with a slight modification also provided good estimates for singly-symmetric sections as long as the value of the variable "e" was taken as the distance from the plane of decking to midheight of the girders (d/2). In addition, very good
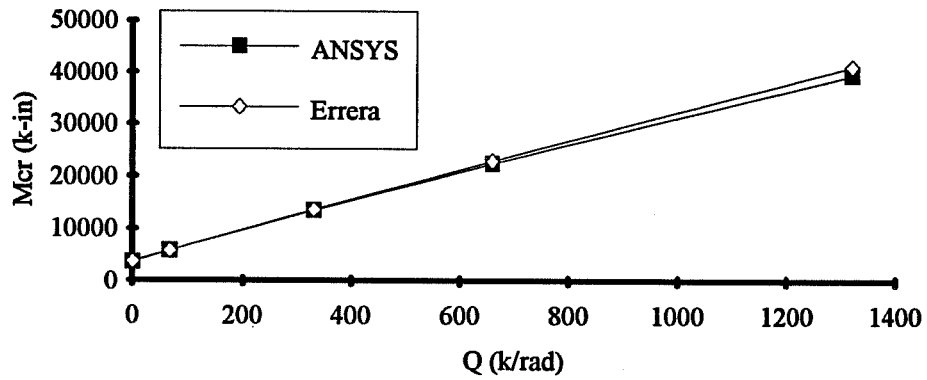
Figure 6.18a : Mcr verus Q for shallow #1 - comparison between ANSYS results and Errera solution - constant moment and 75 foot span.
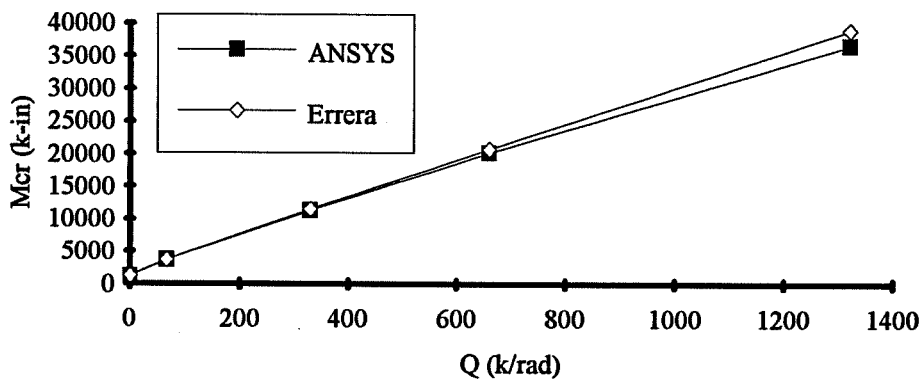
Figure 6.18b : Mcr verus Q for shallow #2 - comparison between ANSYS results and Errera solution - constant moment and 75 foot span.
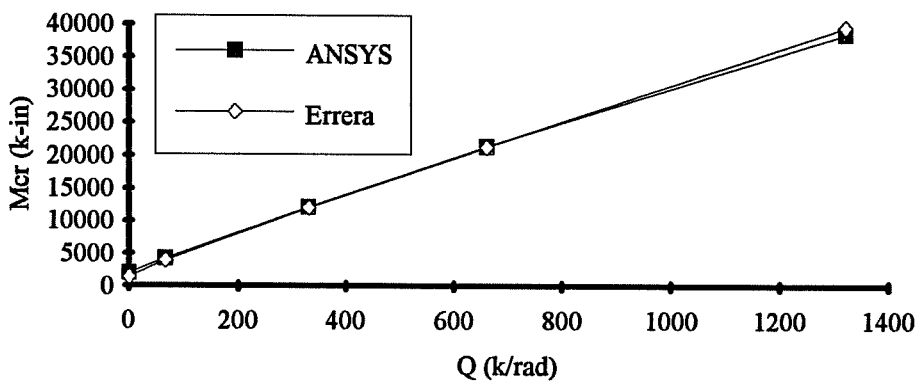
Figure 6.18c : Mcr verus Q for shallow #3 - comparison between ANSYS results and Errera solution - constant moment and 75 foot span.
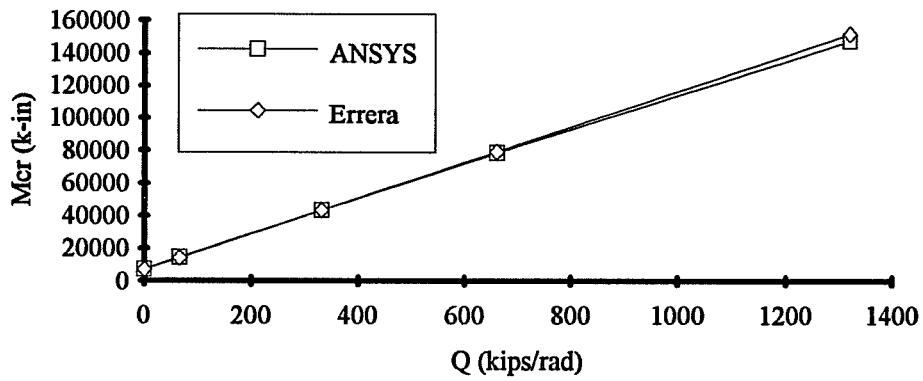
**Figure 6.19a : Mcr verus Q for deep #1 - comparison between ANSYS results
and Errera solution - constant moment and 75 foot span.**
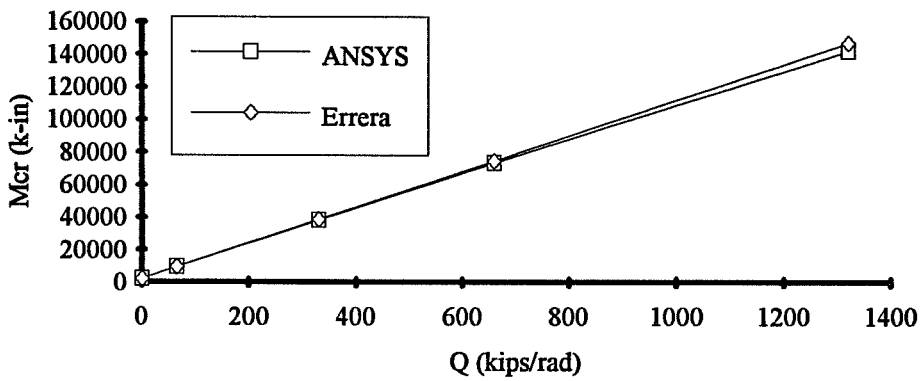
**Figure 6.19b : Mcr verus Q for deep #2 - comparison between ANSYS results
and Errera solution - constant moment and 75 foot span.**
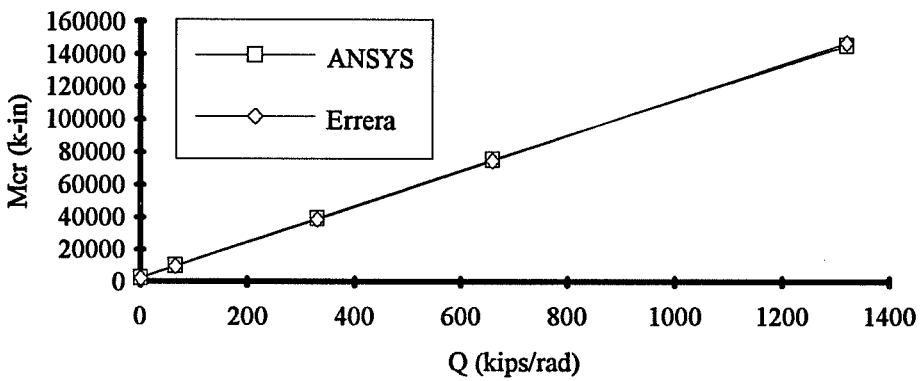
**Figure 6.19c : Mcr verus Q for deep #3 - comparison between ANSYS results
and Errera solution - constant moment and 75 foot span.**
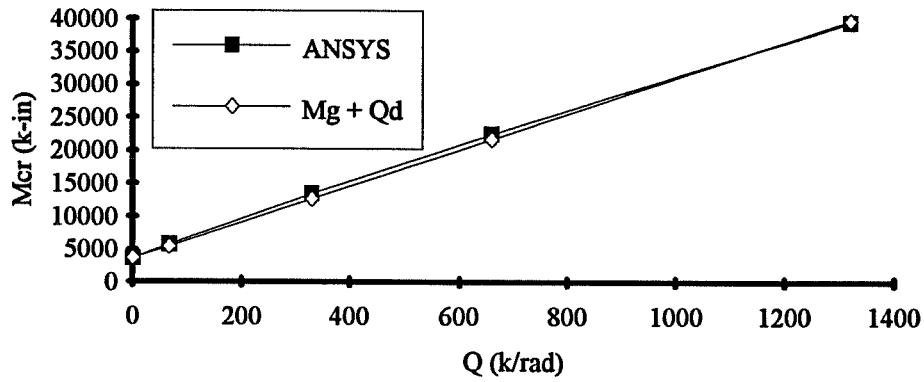
Figure 6.20a : Mcr verus Q for shallow #1 - comparison between ANSYS results and approximation "Mg + Qd" - constant moment and 75 foot span.
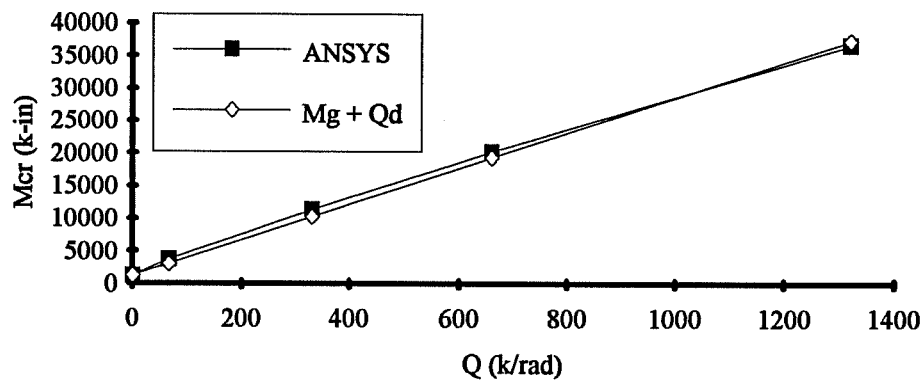
Figure 6.20b : Mcr verus Q for shallow #2 - comparison between ANSYS results and approximation "Mg + Qd" - constant moment and 75 foot span.
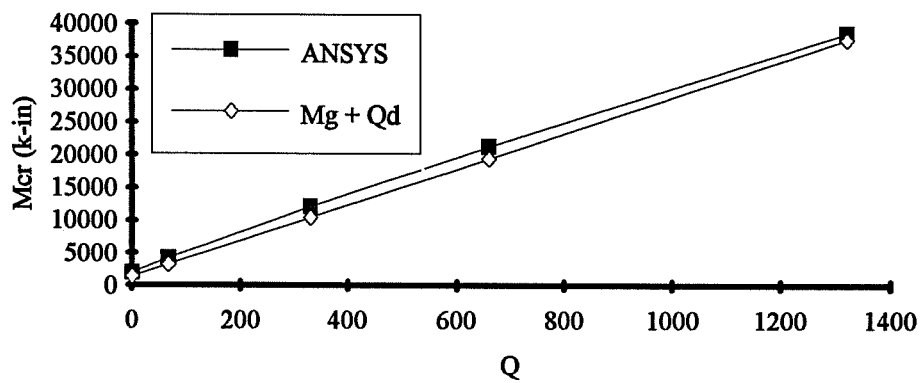
Figure 6.20c : Mcr verus Q for shallow #3 - comparison between ANSYS results and approximation "Mg + Qd" - constant moment and 75 foot span.
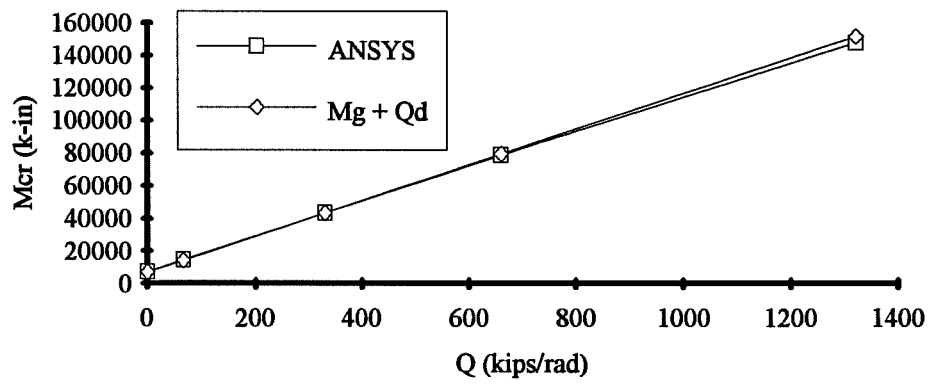
Figure 6.21a : Mcr verus Q for deep #1 - comparison between ANSYS results and approximation "Mg + Qd" - constant moment and 75 foot span.
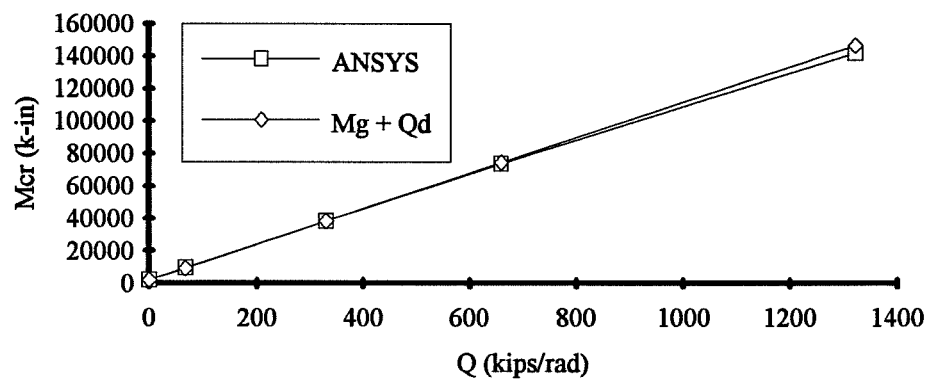
Figure 6.21b : Mcr verus Q for deep #2 - comparison between ANSYS results and approximation "Mg + Qd" - constant moment and 75 foot span.
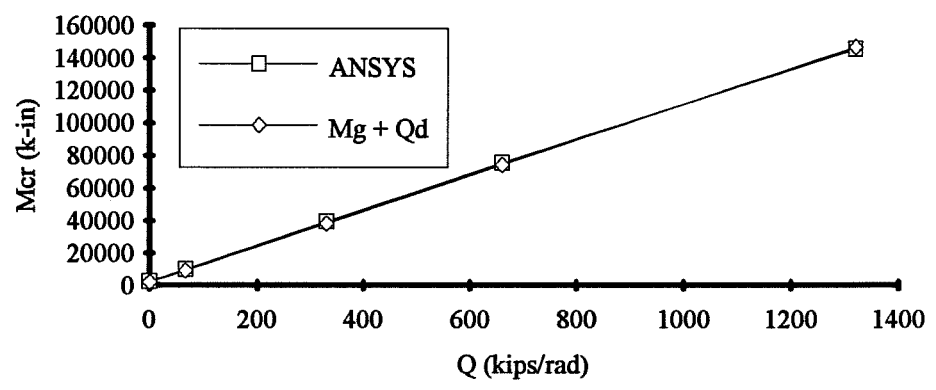
Figure 6.21c : Mcr verus Q for deep #3 - comparison between ANSYS results and approximation "Mg + Qd" - constant moment and 75 foot span.

estimates of the buckling load were obtained using the simple approximation $M_{AASHTO} + Qd$ for the buckling capacity of girders braced by a shear diaphragm.

6.3 Buckling of Girders Subjected to Moment Gradient

The previous section showed that the contribution of the deck in increasing the buckling capacity of girders subjected to constant moment was somewhat linear and dependent on the girder depth, and was not significantly affected by girder length or other cross-sectional properties. This section will present the results of girders subjected to a moment gradient caused by transverse loading applied at midheight of the girders. The transverse loading consisted of either a point load applied at midspan or a uniformly distributed load.

This section has been divided into two sub-sections. The first sub-section will present the ANSYS results for girders subjected to a moment gradient, followed by a sub-section which compares the finite element results with the energy based solution as well as approximate solutions.

### 6.3.1 Buckling Capacity of Girders Subjected to Moment Gradient

Figures 6.22a, 6.22b, and 6.22c show the plots of the buckling moment for the respective sections #1, #2, and #3 versus the deck shear rigidity. The loading consists of a point load applied at midheight centerline of the girders. Each plot shows the results for girder spans of 25, 50, and 75 feet. The curves in the plots show a noticeable reduction in slope for increasing shear rigidity. This is different than what was observed for the constant moment cases which showed a much more gradual reduction in the slope with increasing shear rigidity of the deck. In many cases the buckling load for cases with moment gradient are actually less than the buckling capacity for cases with uniform moment. This reduction in slope for girders with a moment gradient can be explained by the location of the center of twist. The results in Chapter 4 showed that the center of twist for girders subjected to moment gradient was higher on the cross-section of the girder with increasing shear rigidity of the shear diaphragm, which would make the deck less effective as a bracing element. The center of twist for girders subjected to constant moment, on the other hand, approached the bottom flange, which would explain the much more gradual reduction in slope.

If the capacity of the unbraced girders, M_g, is subtracted from M_{cr}, the increase in moment due to the deck (M_{deck}) can be obtained. Figures 6.23a, 6.23b, and 6.23c show the plots
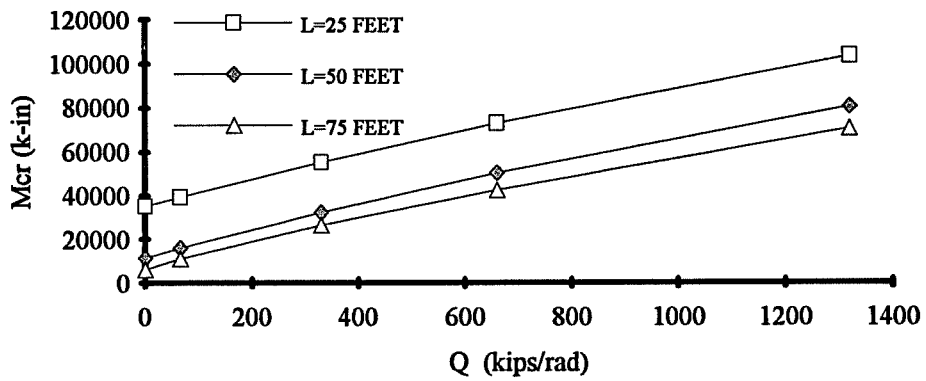
Figure 6.22a: Mcr versus Q for section #1 with midspan point load applied at midheight.
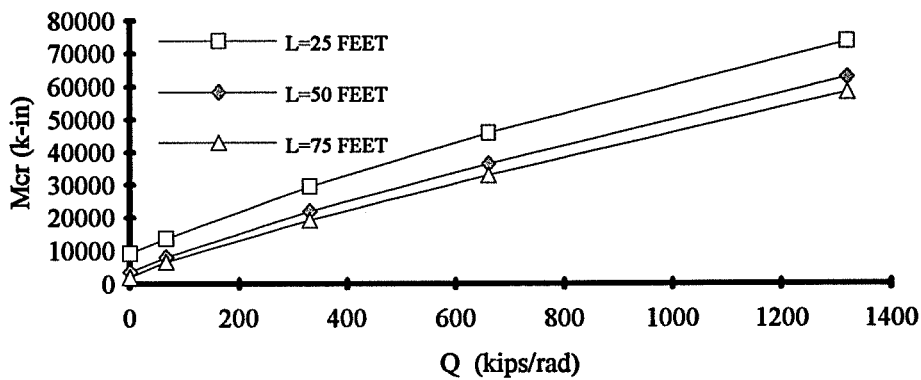
Figure 6.22b: Mcr versus Q for section #2 with midspan point load applied at midheight.
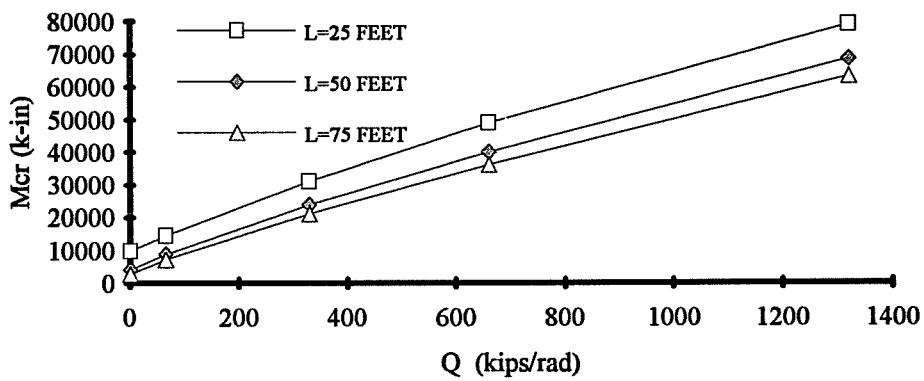
Figure 6.22c: Mcr versus Q for section #3 with midspan point load applied at midheight.
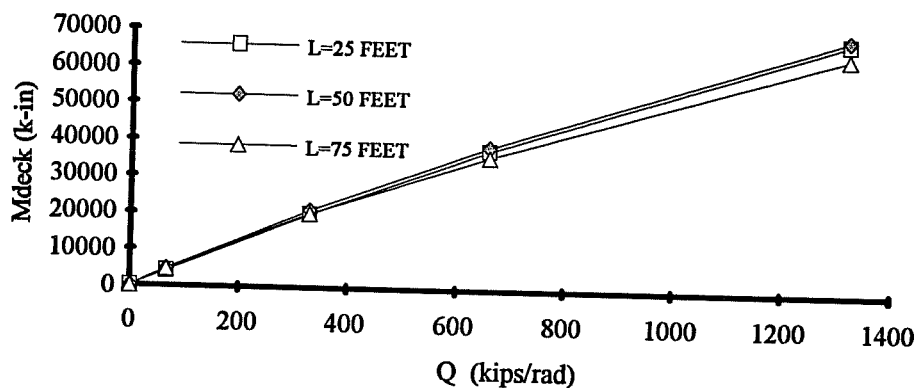
Figure 6.23a: Mdeck versus Q for section #1 with midspan point load applied at midheight.
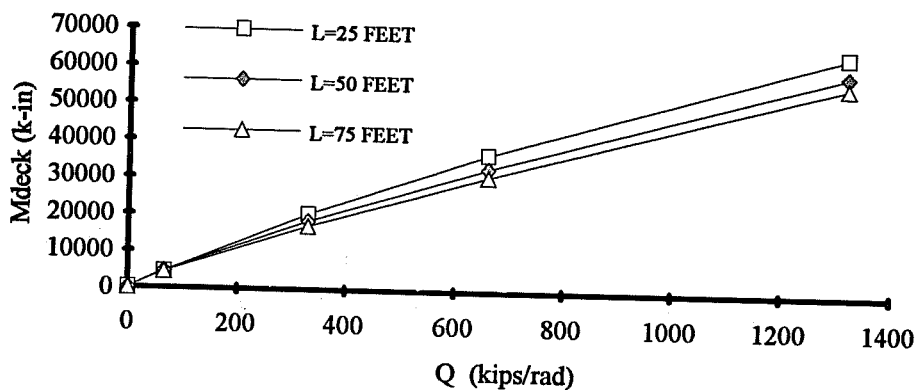
Figure 6.23b: Mdeck versus Q for section #2 with midspan point load applied at midheight.
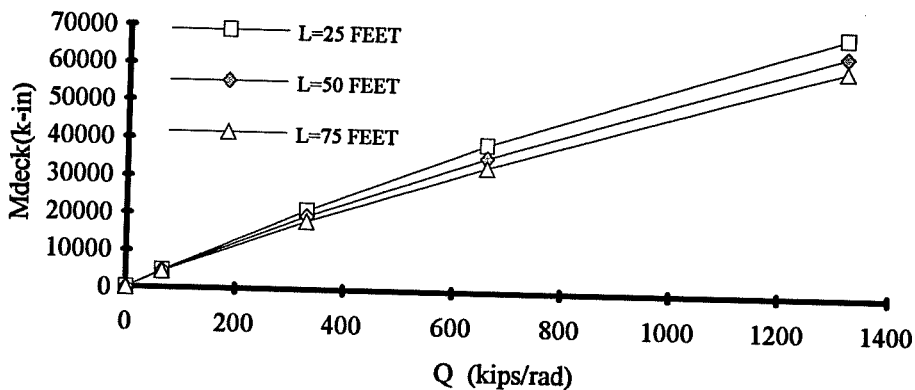
Figure 6.23c Mdeck versus Q for section #3 with midspan point load applied at midheight.

of M_{deck} versus Q for the load cases involving a point load at the centerline midheight. The curves with M_{deck} versus Q for a distributed load at midheight are shown in Figures 6.24a, 6.24b, and 6.24c. In each of the different plots, the curves are not coincident like the curves observed for the constant moment cases. There is a larger decrease in the slope of the curves for the longer span girders. The results presented in Chapter 4 showed that for a given deck shear stiffness, the center of twist for a longer span girder was closer to the top flange than for a shorter span girder, which would make the deck less effective.

Another comparison can be made if the curves of M_{deck} versus Q are plotted on the same graph for the three different cross-sections for a given length. This is shown for a point load at midspan for the three respective lengths in Figures 6.25a, 6.25b, and 6.25c. The corresponding curves for a distributed load at midheight are shown in Figures 6.26a, 6.26b, and 6.26c. When the girders were subjected to constant moment, the curves for the three different cross-sections were essentially coincident for a given length because the center of twist in these cases were located near the bottom flange. The curves these figures, on the other hand, are distinctively different depending on the section. Section #2, which had the lowest lateral stiffness, had the largest decrease in slope in the plot of the M_{deck} versus Q. The behavior of section #1 and #3 is somewhat unusual for the 25 foot long girders. Section #1 has a larger compression flange than section #3, so it is reasonable to assume that the buckling capacity of the section would be larger. This is what has been observed in the graphs which have been presented previously. The curves in Figure 6.25a, however, show that when the 25 foot long girders are subjected to a point load at midheight, the curve for the singly-symmetric section #3 plots above the curve for section #1. For a distributed load, the curves for section #1 and #3 in Figure 6.26a are essentially coincident. The reason for this is unclear. For the 50 and 75 foot lengths, section #3 had a larger reduction in slope than section #2 with increasing shear rigidity.

6.3.2 Comparison of Moment Gradient Results with Closed Formed Solutions

Modifications were performed to the Errera solution in Section 5.2.2 in order to arrive at an expression which would predict the buckling capacity of both doubly and singly-symmetric sections braced by a shear diaphragm at the top flange. The solution which resulted is shown in the following expression:
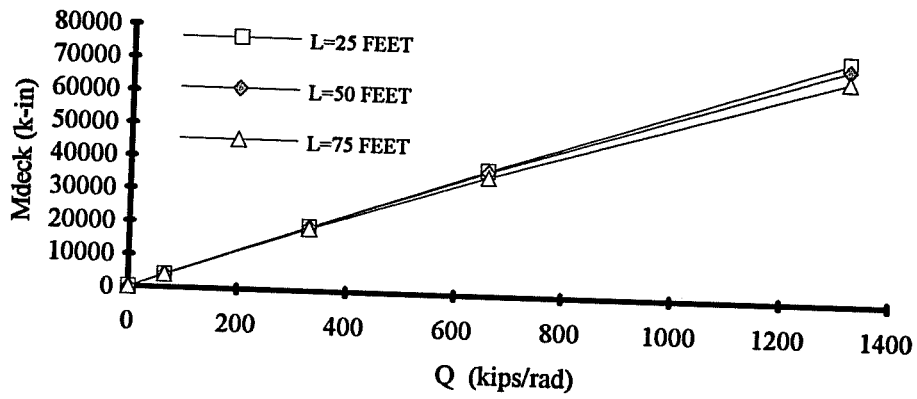
Figure 6.24a Mdeck versus Q for section #1 with distributed load at midheight.
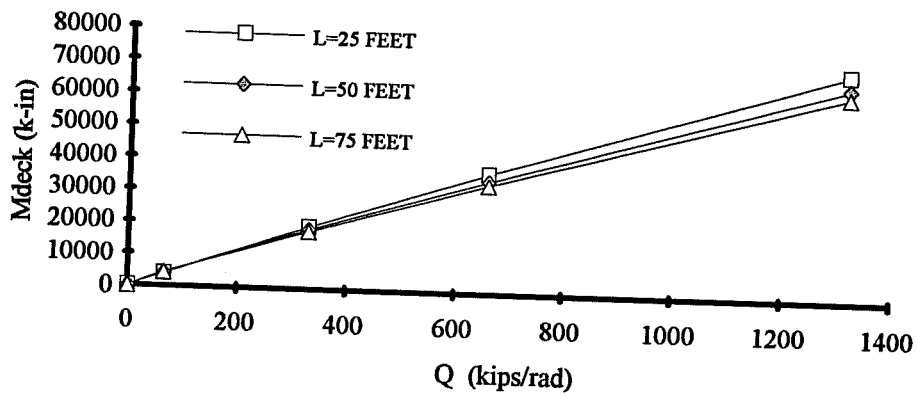
Figure 6.24b Mdeck versus Q for section #2 with distributed load at midheight.
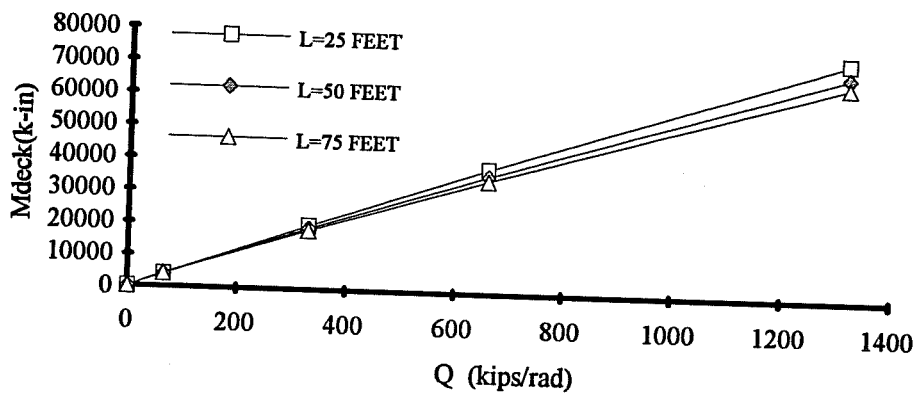
Figure 6.24c Mdeck versus Q for section #3 with distributed load at midheight.
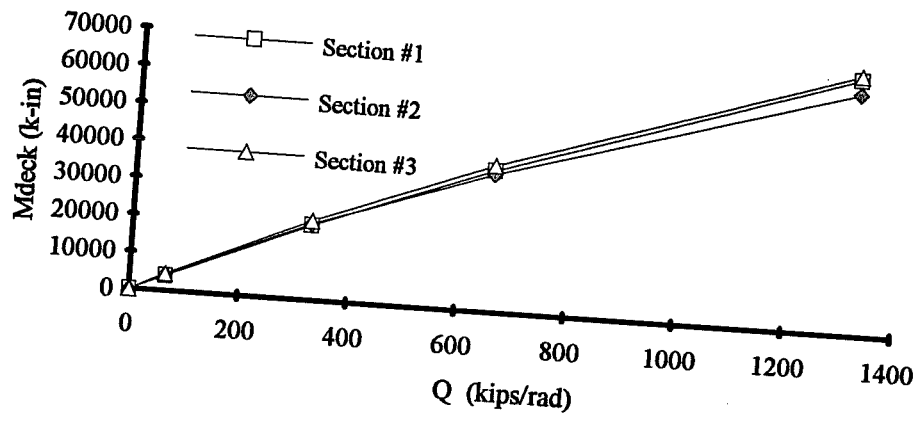
Figure 6.25a Mdeck versus Q for 25 foot span with midspan point load applied at midheight.
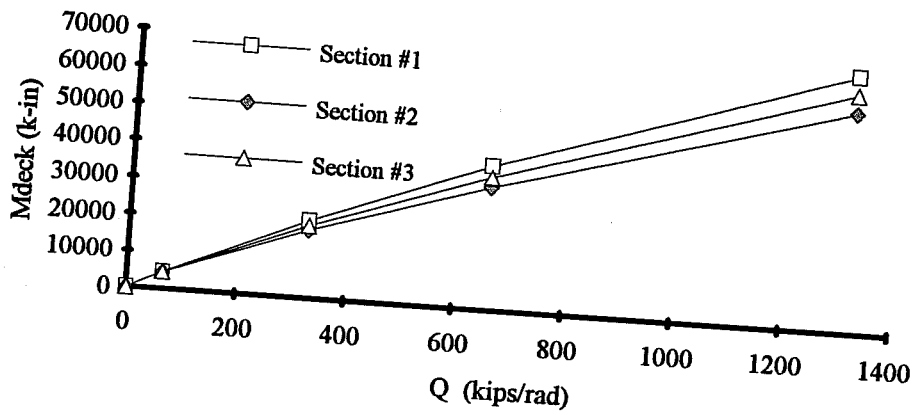
Figure 6.25b Mdeck versus Q for 50 foot span with midspan point load applied at midheight.
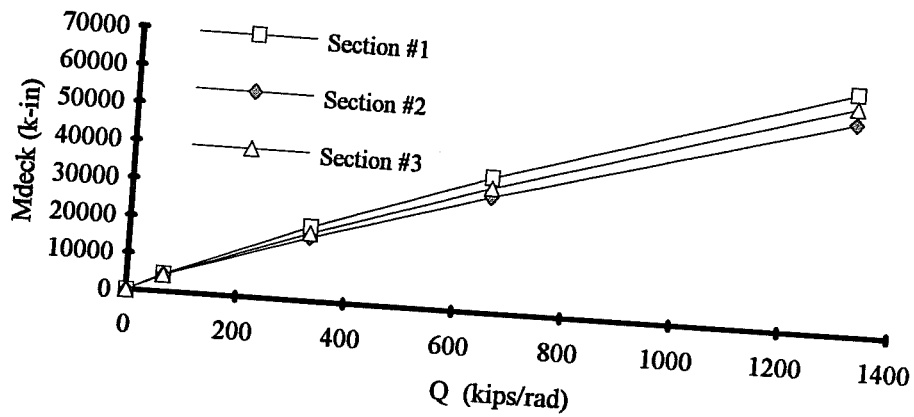
Figure 6.25c Mdeck versus Q for 75 foot span with midspan point load applied at midheight.
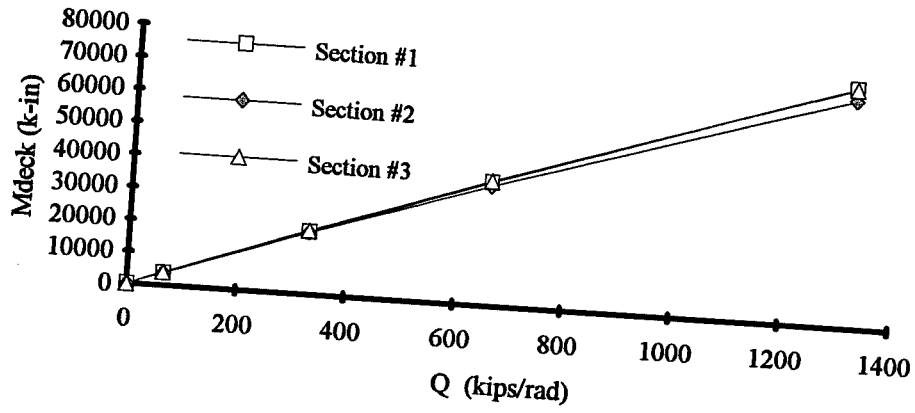
Figure 6.26a : Mdeck versus Q for 25 foot span with distributed load applied at midheight.
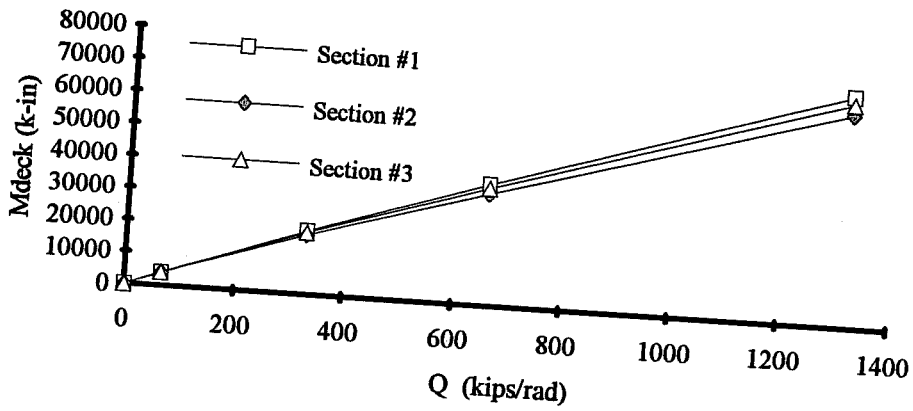
Figure 6.26b : Mdeck versus Q for 50 foot span with distributed load applied at midheight.
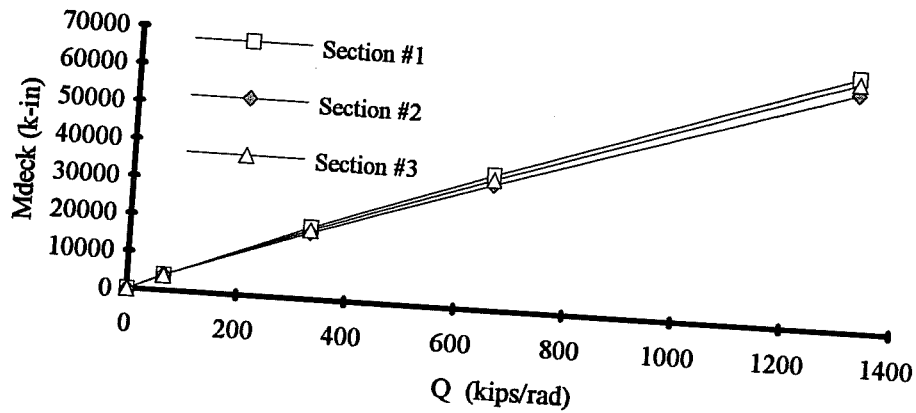
Figure 6.26c : Mdeck versus Q for 75 foot span with distributed load applied at midheight.

$$M_{cr} = \sqrt{(M_{AASHTO})^2 + \left[\frac{Qd^2}{2}\frac{\pi^2 E(2I_{yc})}{L_b^2} + QGJ + \frac{Q^2 d^2}{4}\right]} + \frac{Qd}{2} \qquad (6.10)$$

This expression worked very well for girders subjected to a constant moment. The purpose of this section is to check the validity of the expression for girders subjected to a moment gradient. It was outlined in Chapter 2 that it is unclear how to handle moment gradients with the energy based solution. Lawson and Nethercot [16] suggested using traditional C_b values on the entire Errera expression. In order to determine how C_b values should be used with the energy based solution, the finite element results with midheight loading were compared with three different cases of the C_b on Equation 6.10:

a) C_b applied to the entire Equation 6.10,

b) use $(C_b M_{AASHTO})^2$ for the girder capacity in Equation 6.10, and

c) no C_b.

The resulting expressions are shown in Equations 6.11a, 6.11b, and 6.11c

$$M_{cr} = C_b\left[\sqrt{(M_{AASHTO})^2 + \left[\frac{Qd^2}{2}\frac{\pi^2 E(2I_{yc})}{L_b^2} + QGJ + \frac{Q^2 d^2}{4}\right]} + \frac{Qd}{2}\right] \qquad (6.11a)$$

$$M_{cr} = \sqrt{(C_b M_{AASHTO})^2 + \left[\frac{Qd^2}{2}\frac{\pi^2 E(2I_{yc})}{L_b^2} + QGJ + \frac{Q^2 d^2}{4}\right]} + \frac{Qd}{2} \qquad (6.11b)$$

$$M_{cr} = \sqrt{(M_{AASHTO})^2 + \left[\frac{Qd^2}{2}\frac{\pi^2 E(2I_{yc})}{L_b^2} + QGJ + \frac{Q^2 d^2}{4}\right]} + \frac{Qd}{2} \qquad (6.11c)$$

Comparisons are made with midheight loading in the finite element studies so as to eliminate load height effects.

Figures 6.27a, 6.27b, and 6.27c show the M_{cr} versus Q for section #1 with a point load at the centerline midheight for lengths of 25, 50, and 75 feet, respectively. In addition to the ANSYS results, the modified Errera solution with the three different C_b cases are plotted in each figure. All three plots show that applying the C_b to the entire modified Errera solution is unconservative. For the 25 foot length girders, there is a discernable difference between applying the C_b to just the girder buckling capacity and the case with no C_b. For the longer girders, however, applying the C_b to the girder capacity does not differ very much from the case without the C_b. This is because the capacity of the girder within the radical is relatively small for longer girders when compared to the contribution of the deck. The modified Errera solution doesn't do as good of a job at estimating the buckling capacity as was observed for the constant moment case. The equation does a reasonable job for the 25 and 50 foot lengths, however, it is unconservative for the 75 foot length at higher values of the shear stiffness.

Figures 6.28a, 6.28b, and 6.28c show the plots of M_{cr} versus Q for section #2 with a point load at the centerline midheight for respective lengths of 25, 50, and 75 feet. The corresponding plots for the singly-symmetric section #3 are shown in Figures 6.29a, 6.29b, and 6.29c. When the plots for section #2 and #3 are compared with those from section #1, the Errera solution overestimates the buckling capacity for even relatively low values of the shear rigidity. There is also very little difference between the cases with the C_b on the girder versus no C_b.

The reason the energy based solution does not estimate the buckling capacity of girders subjected to a moment gradient as well as for constant moment probably stems from the drastic change in the buckled shape that the deck causes. Recalling from Chapter 4, when the deck was provided as a bracing element for girders subjected to a moment gradient, the center of twist was very high on the girder. The higher the center of twist is on the girder, the less effective the deck is as a bracing element. This also accounts for why section #2 experienced the largest reduction in slope of the M_{deck} versus Q curves. Section #2 had the lowest lateral stiffness, and the center of twist was closer to the top flange than on the other two sections for a given deck rigidity.

When the girders were subjected to constant moment, on the other hand, the center of twist always tended to the bottom flange for all three of the sections considered. Since the center of twist approached the same point, the deck was essentially equally effective for all three girder cross-sections.
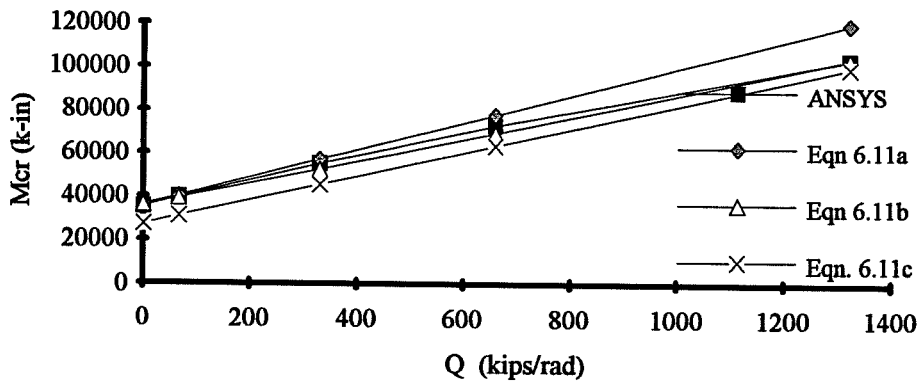
Figure 6.27a : Mdeck versus Q for section #1 with 25 foot span and point load applied at midheight - variable Cb position on Errera solution.
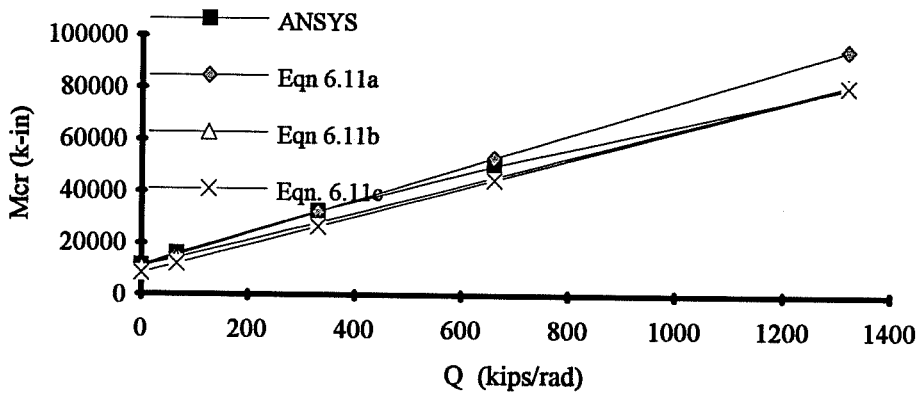
Figure 6.27b : Mdeck versus Q for section #1 with 50 foot span and point load applied at midheight - variable Cb position on Errera solution.
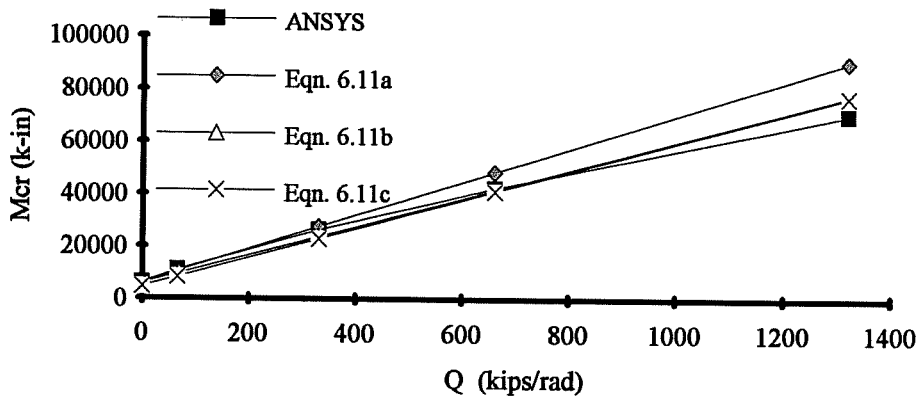
Figure 6.27c : Mdeck versus Q for section #1 with 75 foot span and point load applied at midheight - variable Cb position on Errera solution.
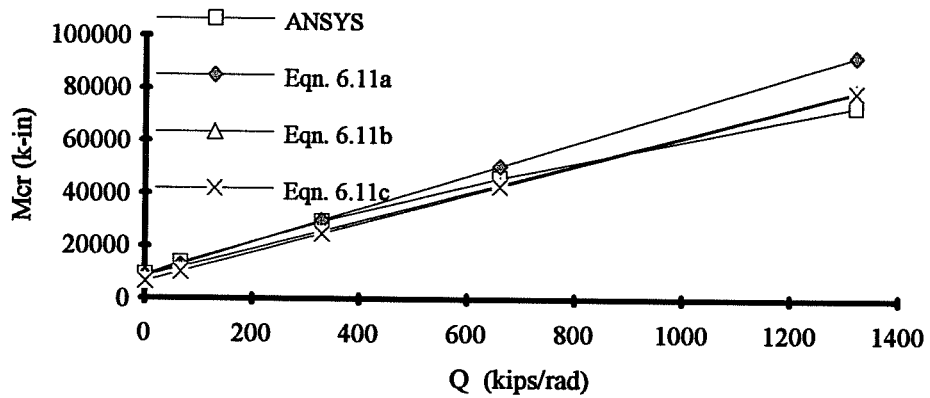
Figure 6.28a : Mcr versus Q for section #2 with 25 foot span and point load applied at midheight - variable Cb position on Errera solution.
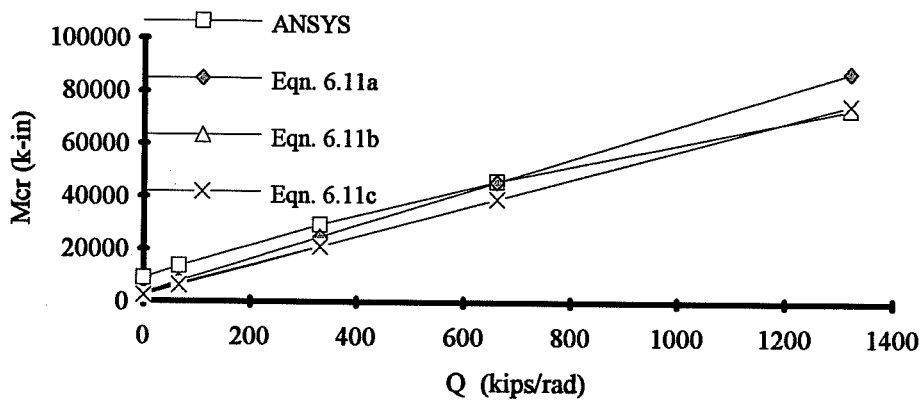
Figure 6.28b : Mcr versus Q for section #2 with 50 foot span and point load applied at midheight - variable Cb position on Errera solution.
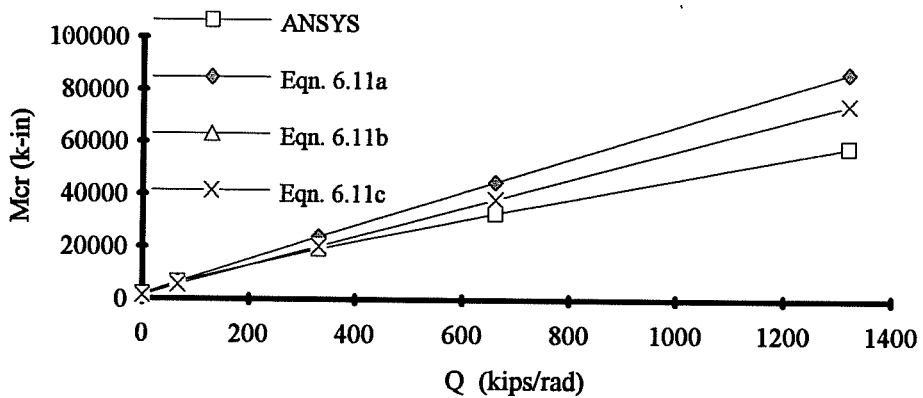
Figure 6.28c : Mcr versus Q for section #2 with 75 foot span and point load applied at midheight - variable Cb position on Errera solution.
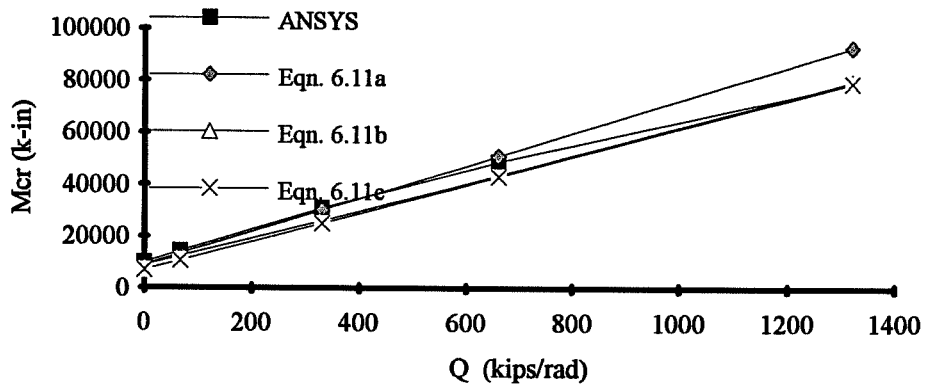
Figure 6.29a : Mcr versus Q for section #3 with 25 foot span and point load applied at midheight - variable Cb position on Errera solution.
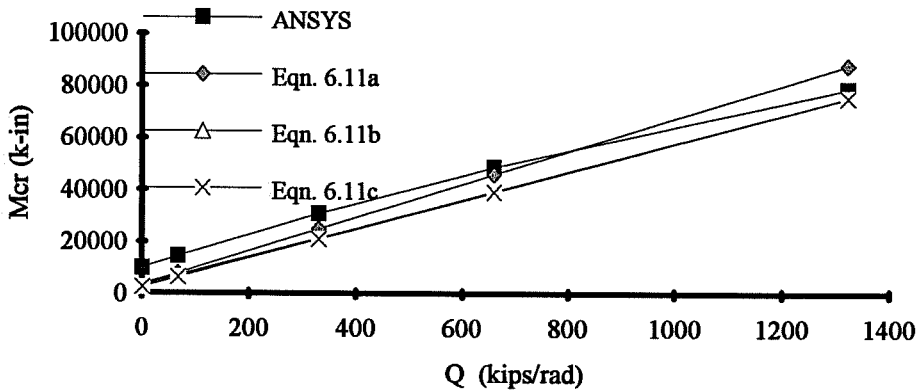
Figure 6.29b : Mcr versus Q for section #3 with 50 foot span and point load applied at midheight - variable Cb position on Errera solution.
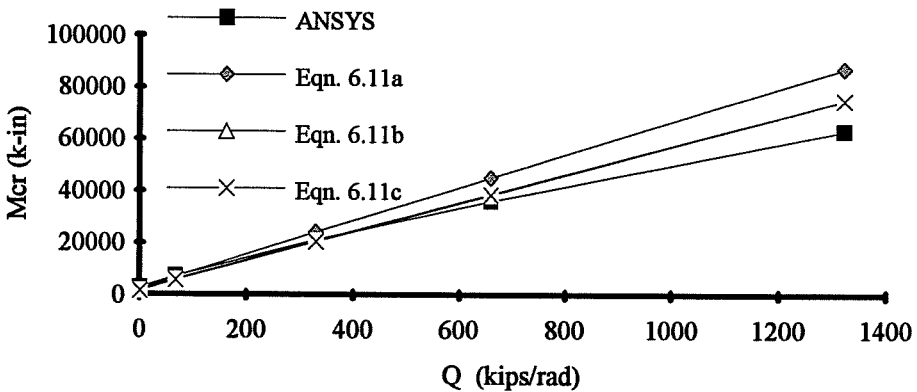
Figure 6.29c : Mcr versus Q for section #3 with 75 foot span and point load applied at midheight - variable Cb position on Errera solution.

It was shown in the last section that for constant moment, the following recommendation by Errera [11] as well as Nethercot and Trahair [18] provided good estimates of the buckling capacity:

$$M_{cr} = M_{AASHTO} + Q\ d$$

The figures shown in this section thus far have indicated that for moment gradients, using a C_b factor on the girder capacity in the Errera solution was the most logical design approach. Equation 6.8 could therefore be modified by applying a C_b factor to M_{AASHTO} which produces the expression shown in the following expression:

$$M_{cr} = C_b M_{AASHTO} + Q\ d \tag{6.12}$$

For loading consisting of a midheight point load at midspan, Figures 6.30a, 6.30b, and 6.30c show a comparison of the approximate solution $M_{cr} = (C_b\ M_g + Qd)$ for section #2 with respective lengths of 25, 50, and 75 feet. The approximate solution does a reasonable job for the 25 foot length girder in Figure 6.30a, however it is unconservative for lengths of 50 and 75 feet for most of the shear rigidities considered.

Better results could be obtained if a more conservative estimate was used for the deck contribution. A more conservative approximation can be obtained if the component of the deck is reduced slightly. Equation 6.13 shows an expression in which the component from the deck has been reduced by a factor of 3/4.

$$M_{cr} = C_b M_{AASHTO} + \frac{3}{4}\ Q\ d \tag{6.13}$$

Figures 6.31a, 6.31b, and 6.31c show a comparison of the ANSYS results with Equation 6.13 for section #2 with respective lengths of 25, 50, and 75 feet. The girders were subjected to a point load at the centerline midheight. Recalling from Figures 6.25a, 6.25b, and 6.25c, when the girders were subjected to a moment gradient, the deck was the least effective for section #2. The approximate solution is slightly conservative when compared to the finite element results; however, it does a good job at estimating the buckling capacity. The approximation is slightly more conservative for the other two sections, but it still gives reasonable estimates of the buckling capacity. Figures 6.32a, 6.32b, and 6.32c show the curves of M_{cr} versus Q for section #3 with
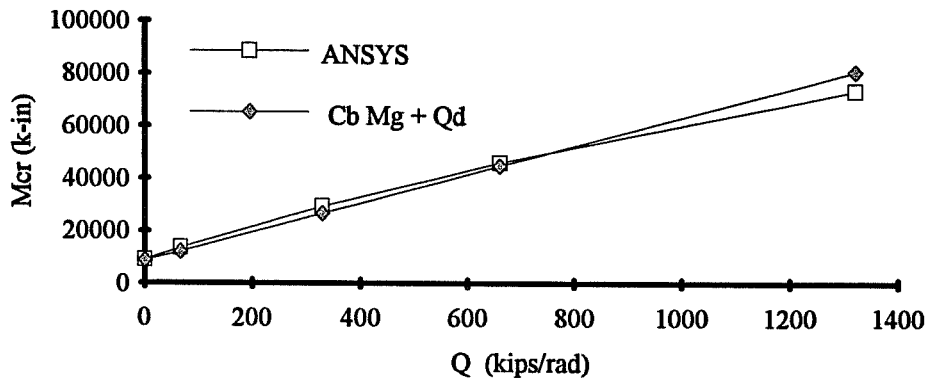
Figure 6.30a : Mcr versus Q for section #2 with 25 foot span and point load applied at midheight - ANSYS results and approximation Cb Mg + Qd.
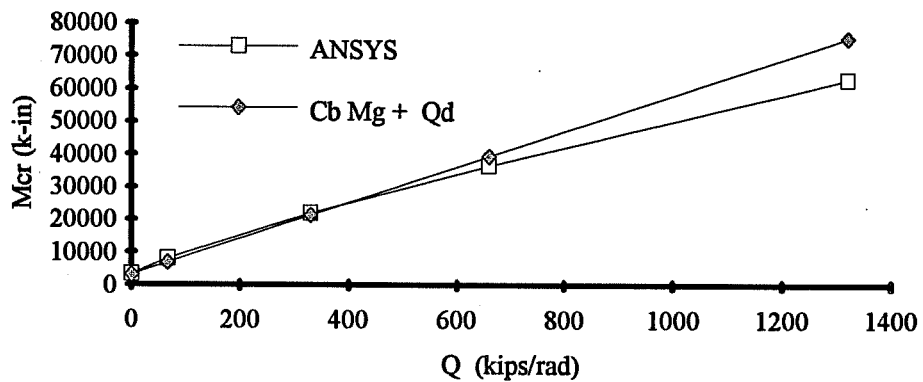
Figure 6.30b : Mcr versus Q for section #2 with 50 foot span and point load applied at midheight - ANSYS results and approximation Cb Mg + Qd.
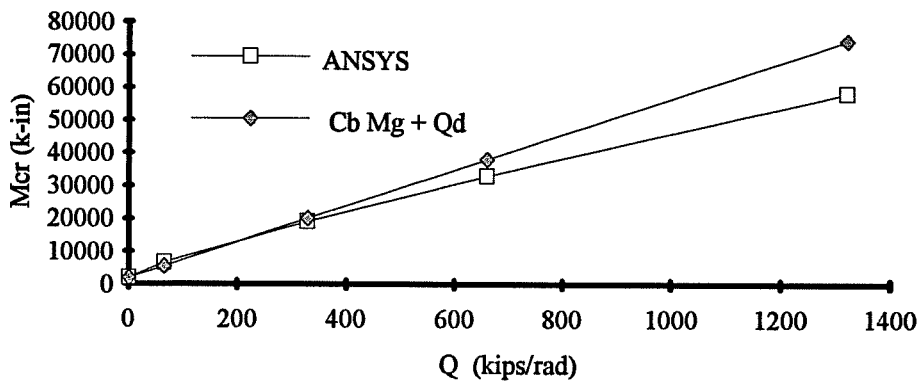
Figure 6.30c : Mcr versus Q for section #2 with 75 foot span and point load applied at midheight - ANSYS results and approximation Cb Mg + Qd.
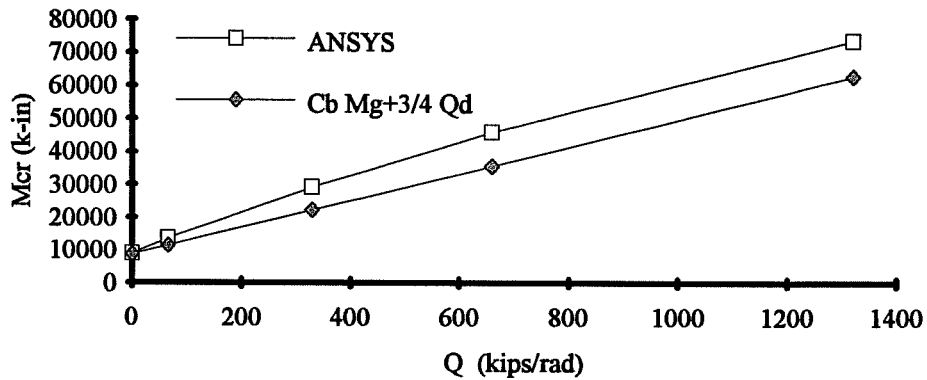
Figure 6.31a : Mcr versus Q for section #2 with 25 foot span and point load applied at midheight - ANSYS results and approximation - Cb Mg + (3/4)Qd.
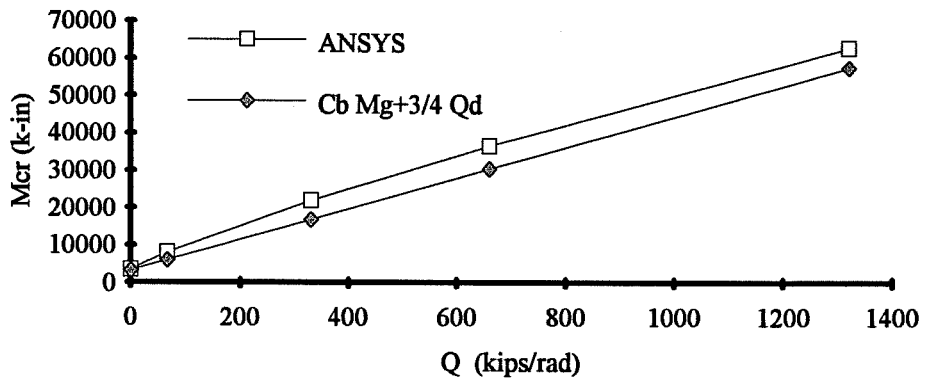
Figure 6.31b : Mcr versus Q for section #2 with 50 foot span and point load applied at midheight - ANSYS results and approximation - Cb Mg + (3/4)Qd.
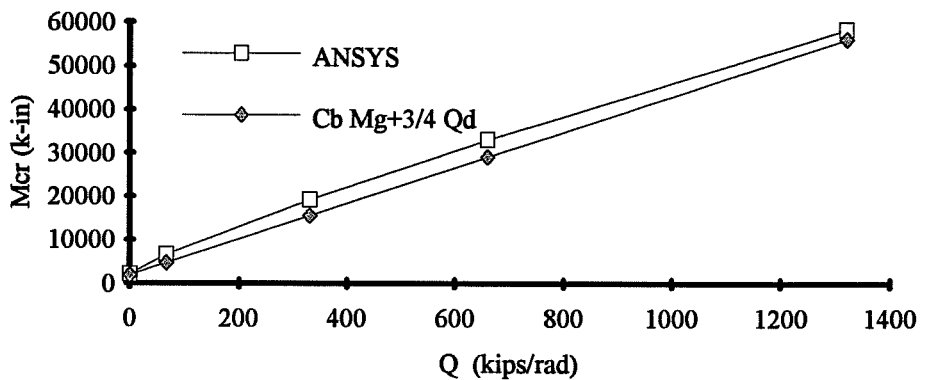
Figure 6.31c : Mcr versus Q for section #2 with 75 foot span and point load applied at midheight - ANSYS results and approximation - Cb Mg + (3/4)Qd.
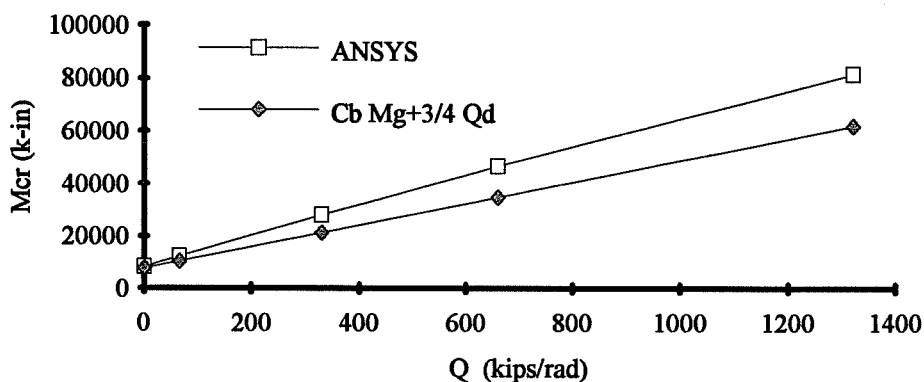
Figure 6.32a : Mcr versus Q for section #3 with 25 foot span and point load applied at midheight - ANSYS results and approximation - Cb Mg + (3/4)Qd.
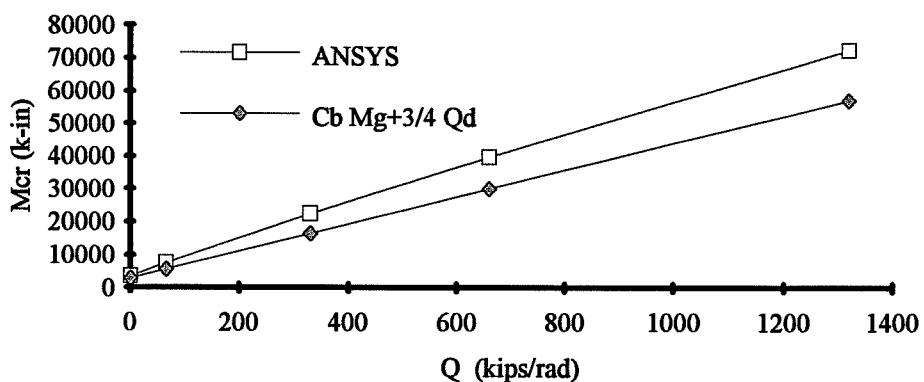
Figure 6.32b : Mcr versus Q for section #3 with 50 foot span and point load applied at midheight - ANSYS results and approximation - Cb Mg + (3/4)Qd.
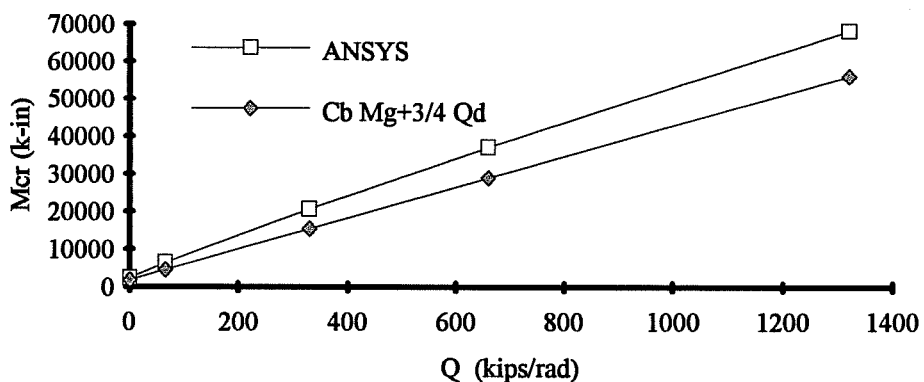
Figure 6.32c : Mcr versus Q for section #3 with 75 foot span and point load applied at midheight - ANSYS results and approximation - Cb Mg + (3/4)Qd.

respective lengths of 25, 50, and 75 feet. The girders are subjected to a distributed load at centerline midheight.

In general, this section has shown that the effectiveness of the deck is reduced when the girders are subjected to moment gradients. In most cases, the Errera solution was unconservative with respect to the finite element results, especially when C_b factors are applied to the entire expression. Reasonable estimates of the buckling capacity were obtained, however, by using the approximation $M_{cr} = C_b M_{AASHTO} + (3/4) Qd$.

6.4 Effects of Load Height on Buckling Capacity

It was mentioned in Chapter 2 that the height transverse loads are applied on the cross-section has a significant effect on the buckling load. The effects of load height on the buckling capacity of girders without a shear diaphragm were presented in Chapter 4, along with solutions which accounted for the effects of load height in singly-symmetric and doubly-symmetric sections. This section presents the finite element results for transverse loads applied at the top flange. The transverse loading consisted of either a point load applied at midspan or a uniformly distributed load.

This section has been divided into two sub-sections. The first sub-section will present the ANSYS results for girders braced by a shear diaphragm, subjected to transverse loading at the top flange. This will be followed by a sub-section which compares the finite element results with an energy based solution from Lawson and Nethercot [16] and also approximate solutions.

6.4.1 Buckling Capacity of Girders Subjected to Top Flange Loading

This section presents the ANSYS results for girders braced by a shear diaphragm which are subjected to top flange loading. Figures 6.33a, 6.33b, and 6.33c show the plots of M_{cr} versus Q for the respective sections #1, #2, and #3, which are subjected to a point load at the midspan top flange. The results for girder spans of 25, 50, and 75 feet are shown in each figure. There is a noticeable reduction in the slope of the curve as the shear rigidity is increased. The curves also diverge slightly with increasing shear rigidity.

In order to determine the effect load height has on the effectiveness of the deck to act as a bracing element, the results will be compared with the results for loading applied at midheight. The capacity of the unbraced girders (Q=0) was subtracted from M_{cr} to obtain the increase in moment capacity due to the deck (M_{deck}). Figures 6.34a, 6.34b, and 6.34c show plots
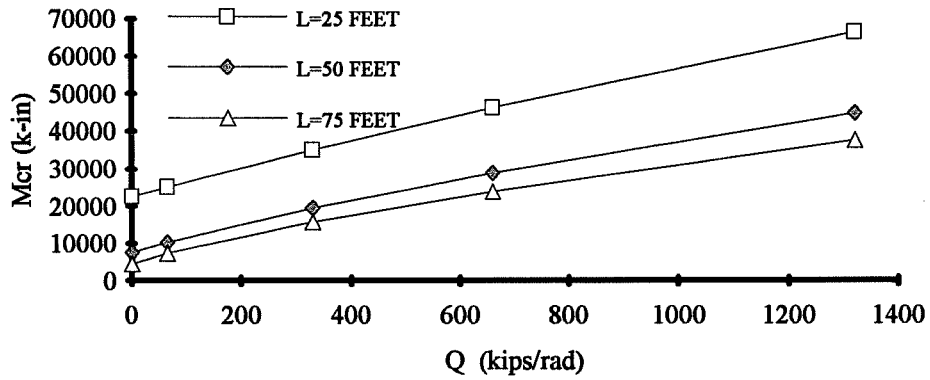
Figure 6.33a: Mcr versus Q for section #1 with midspan point load applied at top flange.
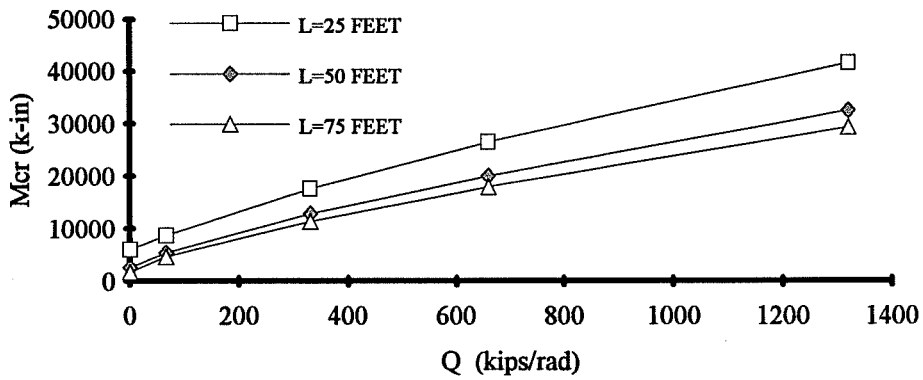
Figure 6.33b: Mcr versus Q for section #2 with midspan point load applied at top flange.
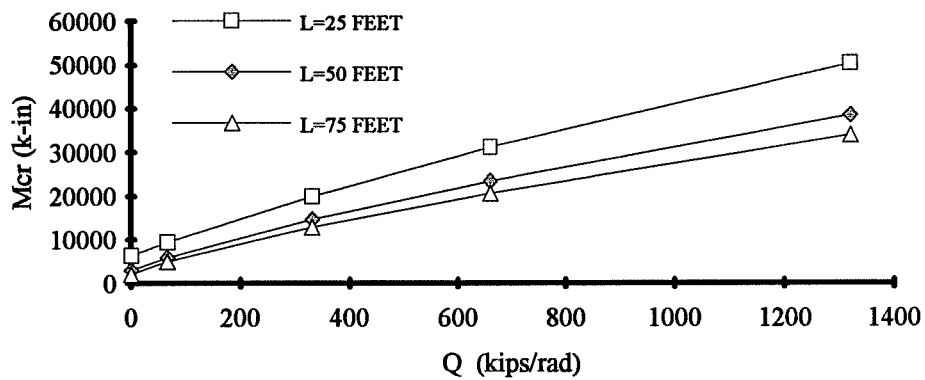
Figure 6.33c: Mcr versus Q for section #3 with midspan point load applied at top flange.
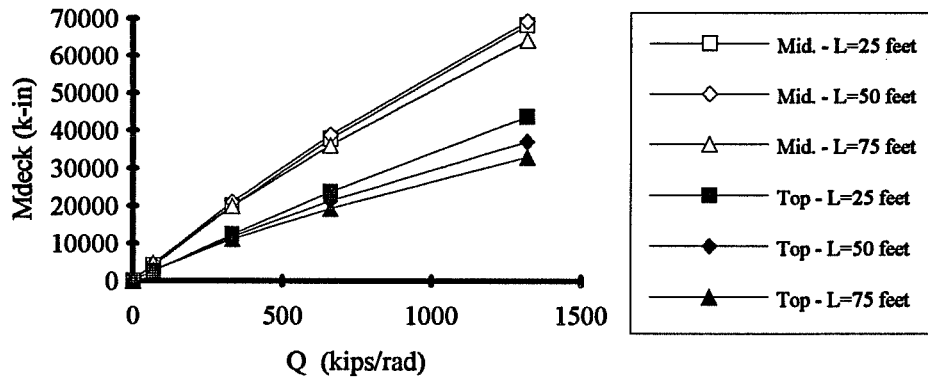
Figure 6.34a: Mdeck versus Q for section #1 with midspan point load applied at midheight and top flange.
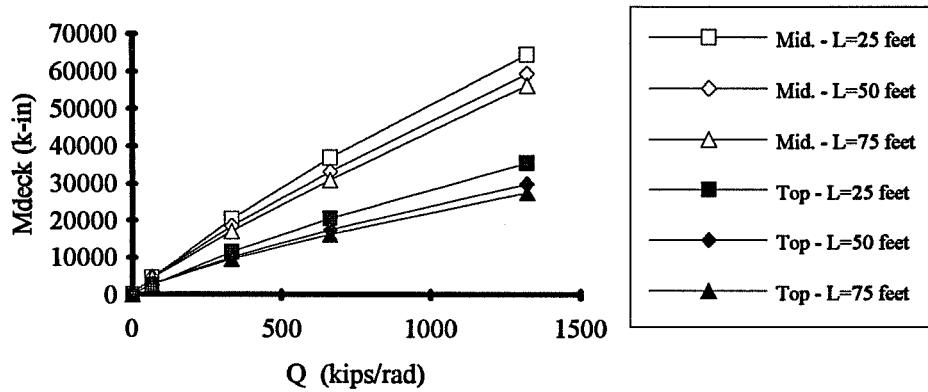
Figure 6.34b: Mdeck versus Q for section #2 with midspan point load applied at midheight and top flange.
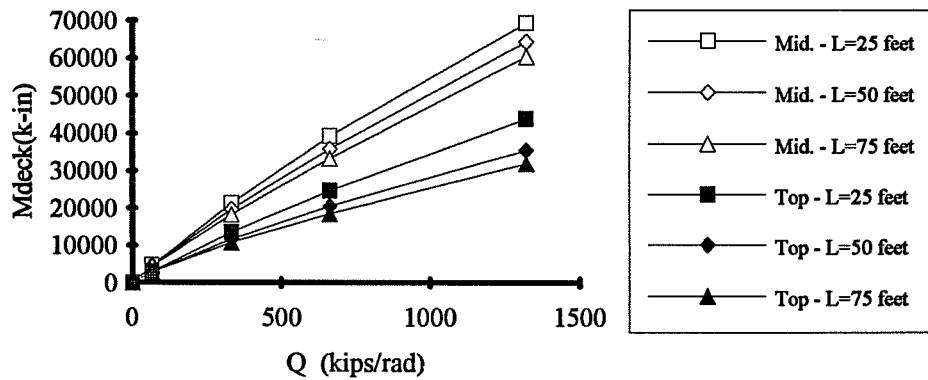
Figure 6.34c: Mdeck versus Q for section #3 with midspan point load applied at midheight and top flange.

of M_{deck} versus Q for the three different lengths which were considered for sections #1, #2, and #3. The graphs show results for a point load which has been applied at midspan at two different load heights. Unfilled markers were used for the curves with the load applied at midheight. The corresponding marker was filled for cases with the load at the top flange. There is a very large reduction in the effectiveness of the deck when the load is applied at the top flange. It is unclear in Figure 6.34a why the curve for a 25 foot length girder with midheight loading plots below the corresponding 50 foot curve; however, the general trend in the rest of the graphs is that the deck is less effective for longer length girders. Figures 6.35a, 6.35b, and 6.35c show the behavior of sections #1, #2, and #3 with a distributed load at the top flange. For a given load height the curves for different girder lengths do not diverge as much as was observed for a point load at midspan.

In general, top flange loading makes the deck significantly less effective as a bracing element when compared to midheight loading. The deck is less effective as the span of the girders is increased. Effects of top flange loading were similar for the two types of loading considered, however, the reduction in effectiveness of the deck as a bracing element with increasing span length was not as severe for a distributed load when compared to a load consisting of a point load at midspan.

6.4.2 Comparison of Moment Gradient Results with Closed Formed Solutions

Chapter 4 showed that the equations in the SSRC guide do a very good job of estimating load height effects on simply-supported girders with no intermediate bracing. The task of this section, however, is to find either a closed formed solution or an approximate solution which does an adequate job of predicting the buckling capacity of girders braced by a shear diaphragm and subjected to transverse loading applied at the top flange.

It was shown in Section 6.3 that the Errera solution produced unconservative approximates of the buckling load with respect to the ANSYS results for girders braced by a shear diaphragm which are subjected to moment gradients. The accuracy of the Errera solution would be further reduced with top flange loading due to load height effects. It is necessary, therefore to find a different solution to account for load height effects. Lawson and Nethercot [16] presented an energy based solution which assumes the twist and lateral translation of the beam vary sinusoidally along the beam. The expression is shown in Equation 6.14. The variables in Equation 6.14 were
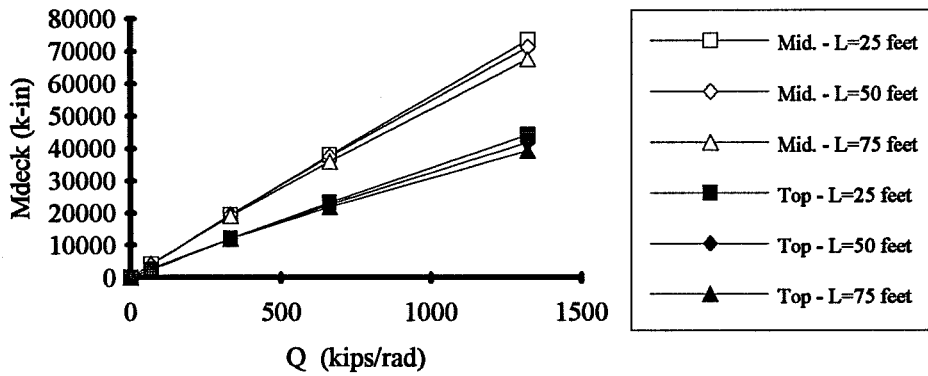
Figure 6.35a: Mdeck versus Q for section #1 with distributed load applied at midheight and top flange.
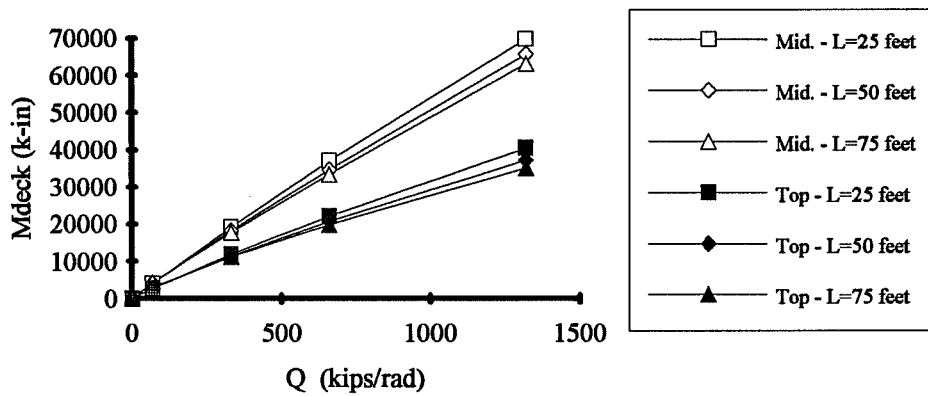
Figure 6.35b: Mdeck versus Q for section #2 with distributed load applied at midheight and top flange.
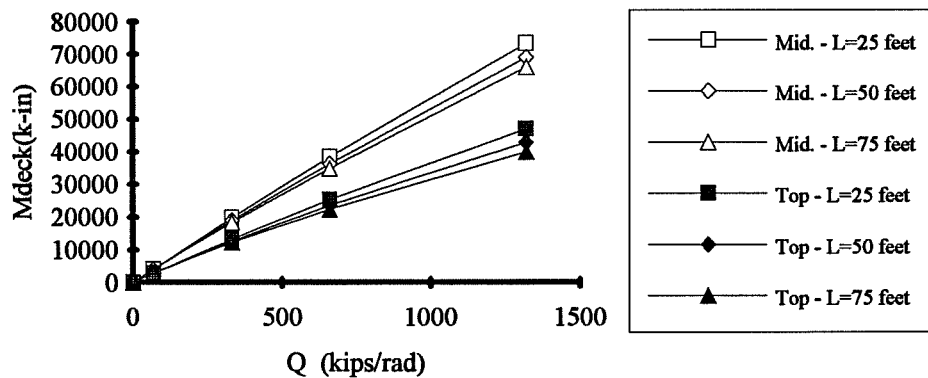
Figure 6.35c: Mdeck versus Q for section #3 with distributed load applied at midheight and top flange.

$$M_{cr} = C_b d \left[\frac{-P_e g}{2} + \frac{Q(1-g)}{2} + \sqrt{\left(\frac{-P_e g}{2} + \frac{Q(1-g)}{2} \right)^2 - \frac{Q^2}{4} + \left(\frac{P_e}{2} + \frac{Q}{2} \right) \left(\frac{P_e}{2} + 2P_T + \frac{Q}{2} \right)} \right] \qquad 6.14$$

outlined in Chapter 2. The C_b accounts for the effects of moment gradient while the parameter g accounts for load height effects. Lawson and Nethercot recommended using traditional C_b values for the moment gradient, and the following values for g:

<div align="center">

Point Load at Midspan: g = 0.55

Distributed Load   g = 0.45

</div>

It should be noted that these values for g are the same as the values recommended for the variable C_2 which accounts for load height in the 3rd edition of the SSRC Guide [14] (outlined in Chapter 2).

Figures 6.36a, 6.36b, and 6.36c show the graphs of M_{cr} versus Q for Equation 6.14 and the ANSYS results for a point load at the midspan top flange of section #1 with respective lengths of 25, 50, and 75 feet. Equation 6.14 is plotted with and without the C_b value. It was shown in Section 6.3, that in the equation to estimate the buckling load, a C_b should be used on the contribution of the girder, but no C_b should be used for the contribution from the deck. The curves with the C_b on the entire expression reemphasize this point here because the buckling moment is considerably overestimated with the C_b on the deck expression. With no C_b at all, the equation is conservative for section #1 for most of the cases considered with the exception of the larger values of the deck shear rigidity on the 75 foot long girder. This is not always the case, however, for girders with a smaller lateral stiffness. Figures 6.37a, 6.37b, and 6.37c show M_{cr} versus Q for Equation 6.14 and the ANSYS results for section #2 with respective lengths of 25, 50, and 75 feet. The girders have been subjected to a point load at the midspan top flange. Without the C_b, the equation is conservative for the 25 foot long girder, however, for longer length girders, it is unconservative at higher values of the shear rigidity. Similar results were observed for girders loaded with a distributed load. Figures 6.38a, 6.38b, and 6.38c show the curves of M_{cr} versus Q for Equation 6.14 and the ANSYS results for section #2 with different lengths and a distributed load applied at the top flange.

The reason the equation from Lawson and Nethercot does not give a good estimate of the buckling load is because the buckled shape that was assumed in the derivation is incorrect. Energy based derivations are upper bound solutions. If the correct buckled shape is assumed the

Figure 6.36a: Mcr versus Q for section #1 with 25' span and midspan point load applied at top flange - ANSYS results and Equation 6.14.

Figure 6.36b: Mcr versus Q for section #1 with 50' span and midspan point load applied at top flange - ANSYS results and Equation 6.14.

Figure 6.36c: Mcr versus Q for section #1 with 75' span and midspan point load applied at top flange - ANSYS results and Equation 6.14.
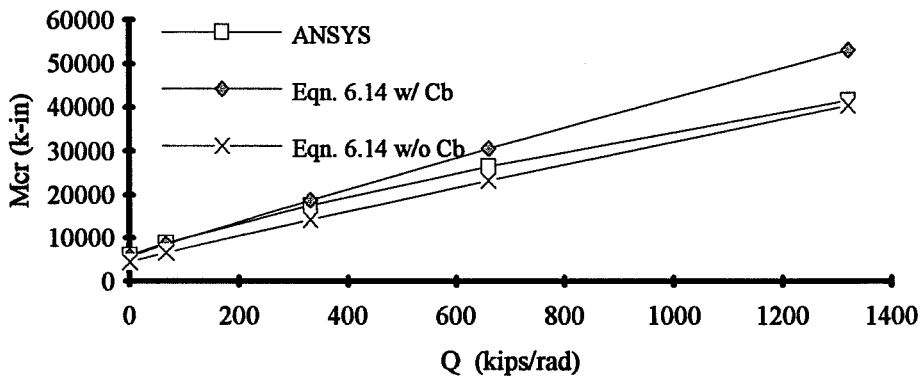
Figure 6.37a: Mcr versus Q for section #2 with 25' span and midspan point load
applied at top flange - ANSYS results and Equation 6.14.

Figure 6.37b: Mcr versus Q for section #2 with 50' span and midspan point load
applied at top flange - ANSYS results and Equation 6.14.

Figure 6.37c: Mcr versus Q for section #2 with 75' span and midspan point load
applied at top flange - ANSYS results and Equation 6.14.

Figure 6.38a: Mcr versus Q for section #2 with 25 foot span and a distributed load applied at top flange - ANSYS results and Equation 6.14.

Figure 6.38b: Mcr versus Q for section #2 with 50 foot span and a distributed load applied at top flange - ANSYS results and Equation 6.14.

Figure 6.38c: Mcr versus Q for section #2 with 75 foot span and a distributed load applied at top flange - ANSYS results and Equation 6.14.

solution will be "exact", however, if the wrong buckled shape is assumed, the solution will be unconservative. The results in chapter 5 showed that the buckled shape for girders subjected to a moment gradient is significantly different than a sine curve. The equation will therefore give unconservative predictions.

In addition to Equation 6.14, Lawson and Nethercot also recommended the following expression which is a simplified form of Equation 6.14 for diaphragm braced girders subjected to top flange loading:

$$M_{cr} = C_b d \left[\frac{P_e}{2} \left(\frac{1}{1-g} - 2g \right) + Q(1-g) + \frac{P_T}{(1-g)} \right] \tag{6.15}$$

The previous results have already shown that the C_b should not be applied to the deck component, however, the rest of the equation will be checked with the ANSYS results. The values which will be used for g are 0.55 for a point load and 0.45 for a distributed load. Figures 6.39a, 6.39b, and 6.39c show plots of Equation 6.15 versus the ANSYS results for section #2 with respective lengths of 25, 50, and 75 feet. The girders have been subjected to a point load at the top flange. The results for section #2 subjected to a distributed load at the top flange are shown in Figures 6.40a, 6.40b, and 6.40c. The equation produces a reasonable estimate for the 25 foot span, however, it is unconservative for the 50 and 75 foot long girders. It is somewhat surprising that the equation overestimates the capacity of the unbraced girder (Q=0), even though the C_b value was neglected.

Results presented in Chapter 4 showed that the SSRC equations for C_b^* did a very good job of estimating the effects of load height for simply supported girders with no intermediate bracing. A logical design equation for girders braced by a shear diaphragm would be to use the C_b^* predicted by the SSRC equations on the capacity of the unbraced girder (AASHTO equation), and then add on a component for the deck. When girders were subjected to constant moment, the contribution of the deck was approximated as Qd, which was suggested by Errera and also Nethercot with Trahair. Section 6.3 showed that when girders were subjected to transverse loading at midheight, the deck contribution could be estimated as 3/4 Qd. With the loading applied at the top flange, a possibility is to estimate the deck contribution as 1/2 Qd. This would actually be the average of what Lawson and Nethercot used for the deck contribution in Equation 6.14 which was 0.45 ~ 0.55 Qd depending on the load type. The following equation would result:

Figure 6.39a: Mcr versus Q for section #2 with 25' span and a midspan point load applied at top flange - ANSYS results and Equation 6.15.
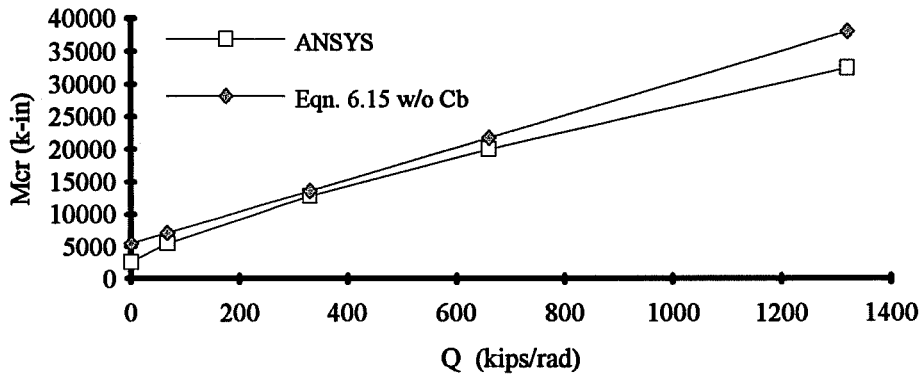
Figure 6.39b: Mcr versus Q for section #2 with 50' span and a midspan point load applied at top flange - ANSYS results and Equation 6.15.
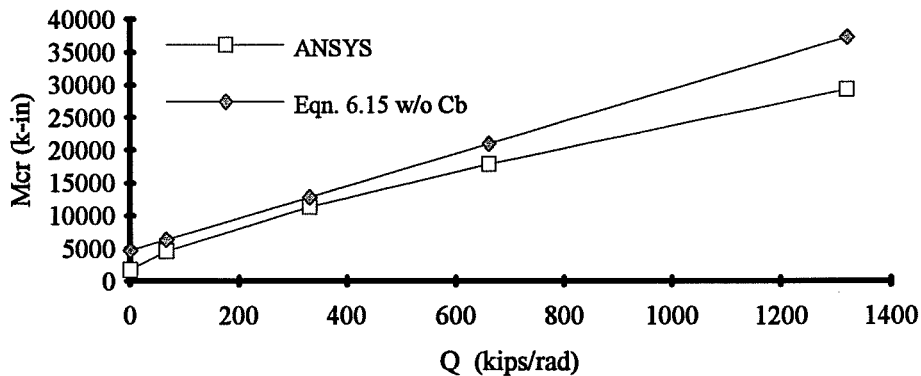
Figure 6.39c: Mcr versus Q for section #2 with 75' span and a midspan point load applied at top flange - ANSYS results and Equation 6.15.

Figure 6.40a: Mcr versus Q for section #2 with 25' span and a distributed load applied at top flange - ANSYS results and Equation 6.15.

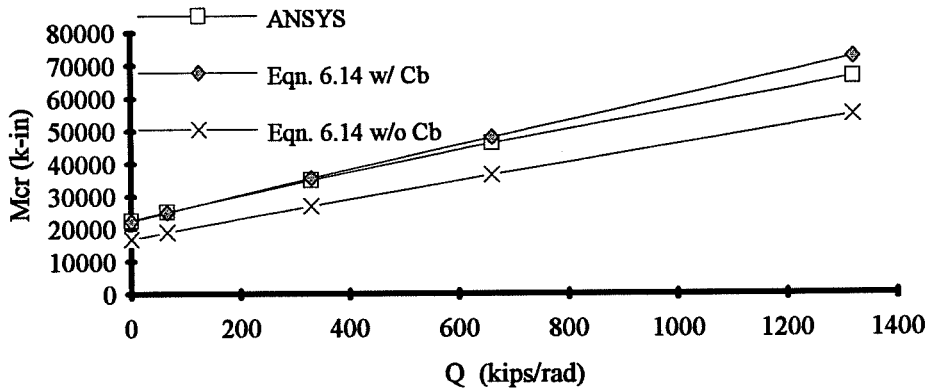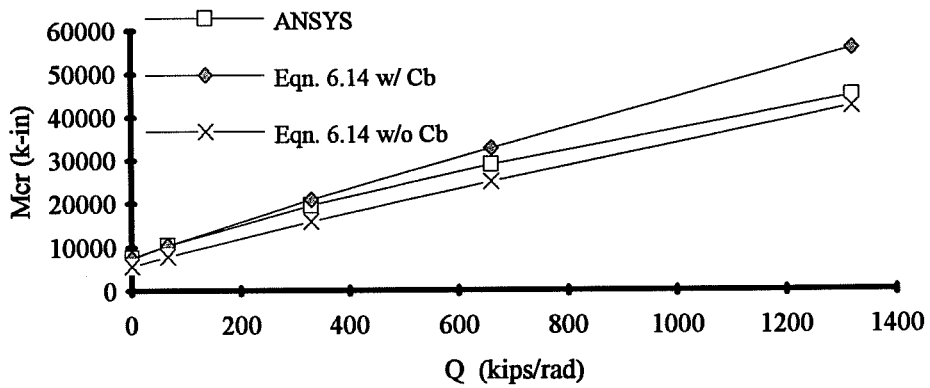**Figure 6.40b: Mcr versus Q for section #2 with 50' span and a distributed load applied at top flange - ANSYS results and Equation 6.15.**
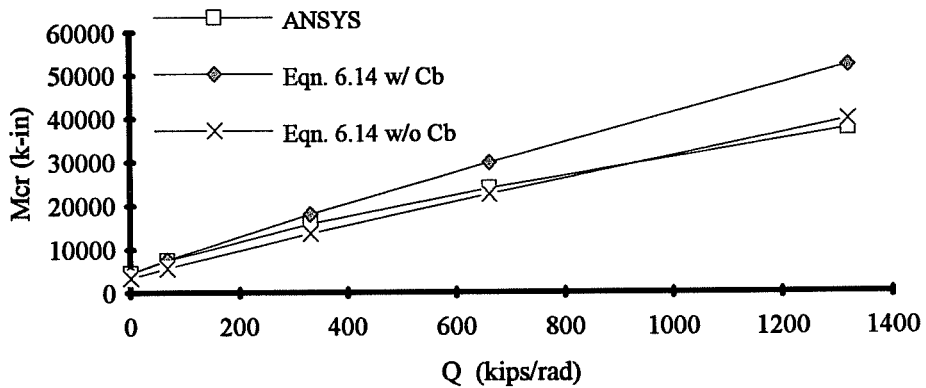

Figure 6.40c: Mcr versus Q for section #2 with 75' span and a distributed load applied at top flange - ANSYS results and Equation 6.15.

$$M_{cr} = C_b{}^* M_{AASHTO} + \frac{Qd}{2} \tag{6.16}$$

Figure 6.41a, 6.41b, and 6.41c show plots of M_{cr} versus Q for Equation 6.16 and the ANSYS results for section #1 with respective lengths of 25, 50, and 75 feet. The girders are subjected to a point load at the midspan top flange. The corresponding curves for girders subjected to distributed load are shown for section #1 in Figures 6.42a, 6.42b, and 6.42c. Equation 6.16 produces a reasonable estimate of the buckling capacity of section #1. The estimate does get slightly unconservative for higher values of the shear rigidity for longer spans as shown in Figure 6.41c for the 75 foot long girder and a loading consisting of a point load. For the other cases involving section #1, however, Equation 6.16 does a very good job.

When girders with a lower lateral stiffness are considered, the approximate solution becomes slightly more unconservative. Figure 6.43a, 6.43b, and 6.43c show plots of M_{cr} versus Q for section #2 with a point load at the midspan top flange. The corresponding curves for a distributed loading are shown in Figures 6.44a, 6.44b, and 6.44c. The curves for the 50 and 75 foot long girders which have a point load applied at midspan top flange show that the estimate is unconservative for higher values of the shear rigidity (660 ~ 1320 kips/rad). The equation does a much better job for the girders which are subjected to a uniform distributed load, which would be more representative of the type of loading that bridge girders would be subjected to during construction. The estimate only becomes slightly unconservative for the 75 foot long girder and a shear rigidity of 1320 kips/rad.

Figures 6.45a, 6.45b, and 6.45c show plots of M_{cr} versus Q for the singly-symmetric section #3 subjected to a point load at the midspan top flange. The corresponding curves for a distributed load at the top flange are shown in Figures 6.46a, 6.46b, and 6.46c. Equation 6.16 does a reasonable job of estimating the buckling load for the singly-symmetric girders. The equation is slightly unconservative at higher values of the shear rigidity for the 75 foot long girder subjected to a point load at the midspan top flange, however, it does a good job in the other cases.

The accuracy of Equation 6.16 was also checked with the shallow and deep sections which were used in Chapter 4 and also in Section 6.2. The girders had lengths of 75 feet, and the were subjected to a distributed load at the top flange.
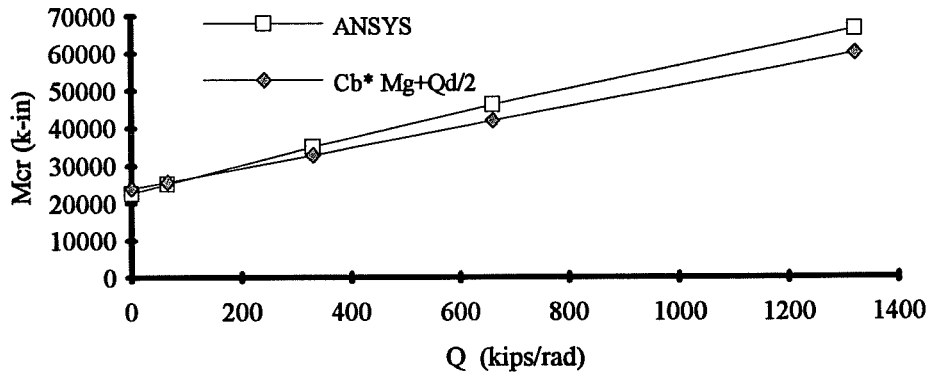
Figure 6.41a : Mcr versus Q for ANSYS results with Equation 6.16 for
section #1 with 25 foot span with point load at top flange.
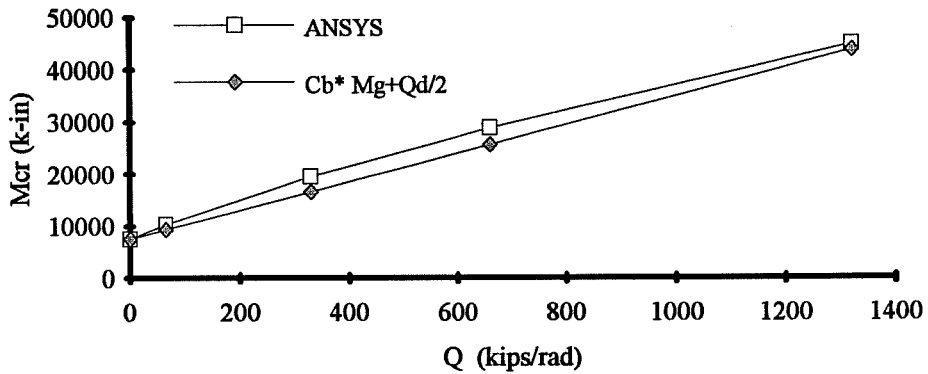
Figure 6.41b : Mcr versus Q for ANSYS results with Equation 6.16 for
section #1 with 50 foot span with point load at top flange.
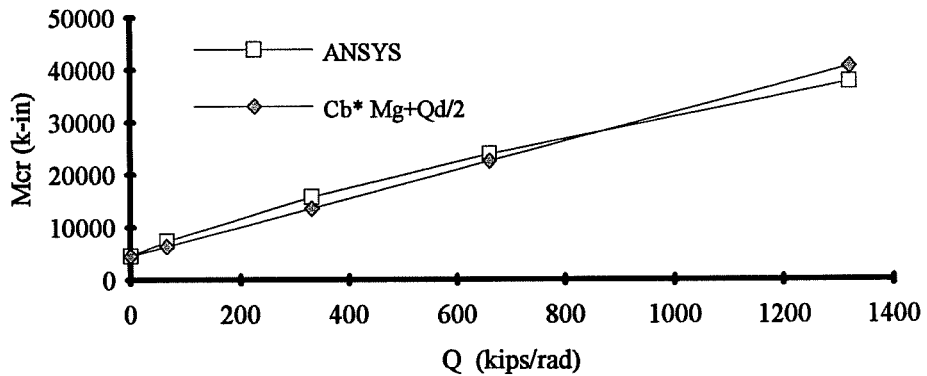
Figure 6.41c : Mcr versus Q for ANSYS results with Equation 6.16 for
section #1 with 75 foot span with point load at top flange.
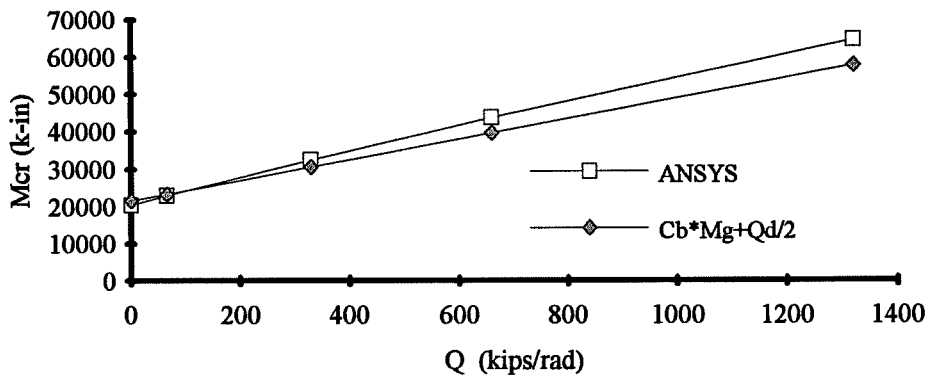
Figure 6.42a: Mcr versus Q for section #1 with 25' span and a distributed load applied at top flange - ANSYS results and Eqn 6.16.
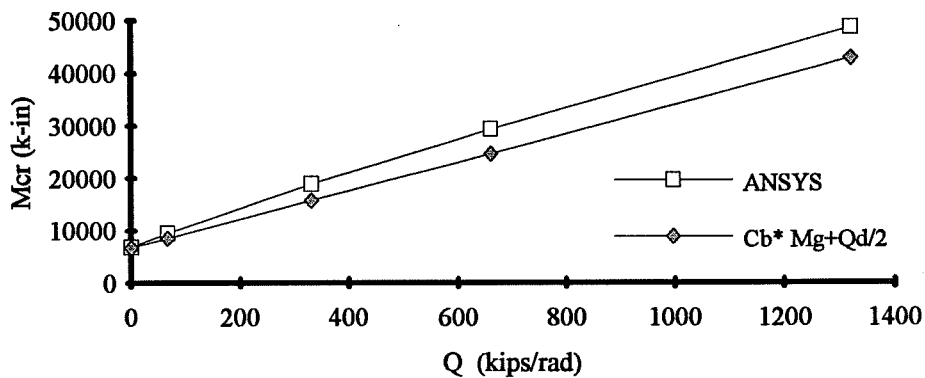
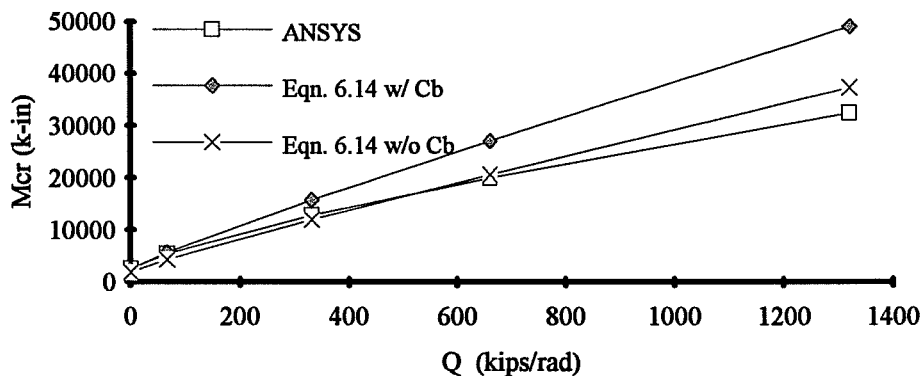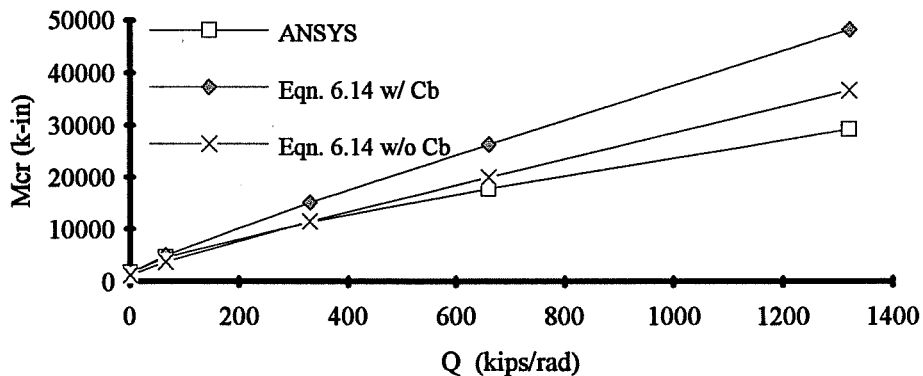**Figure 6.42b: Mcr versus Q for section #1 with 50' span and a distributed load applied at top flange - ANSYS results and Eqn 6.16.**
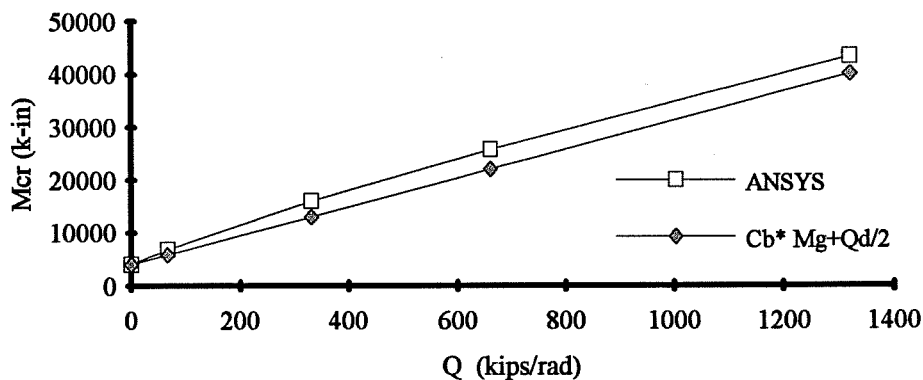
Figure 6.42c: Mcr versus Q for section #1 with 75' span and a distributed load applied at top flange - ANSYS results and Eqn 6.16.
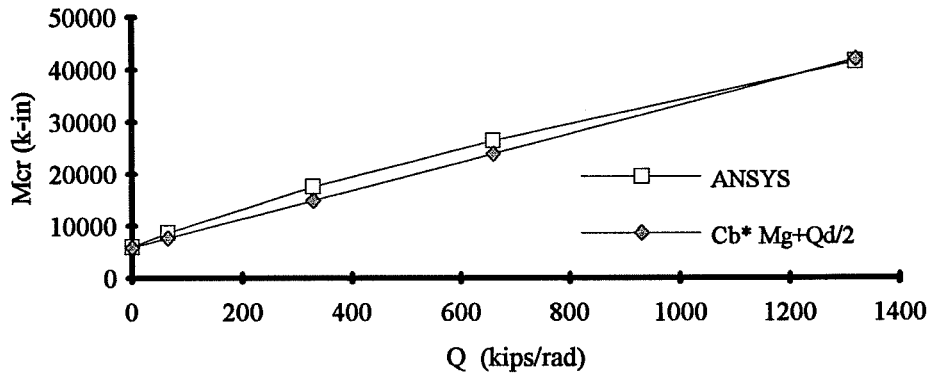
Figure 6.43a: Mcr versus Q for section #2 with 25' span and a point load
applied at CL top flange - ANSYS results and Eqn. 6.16.
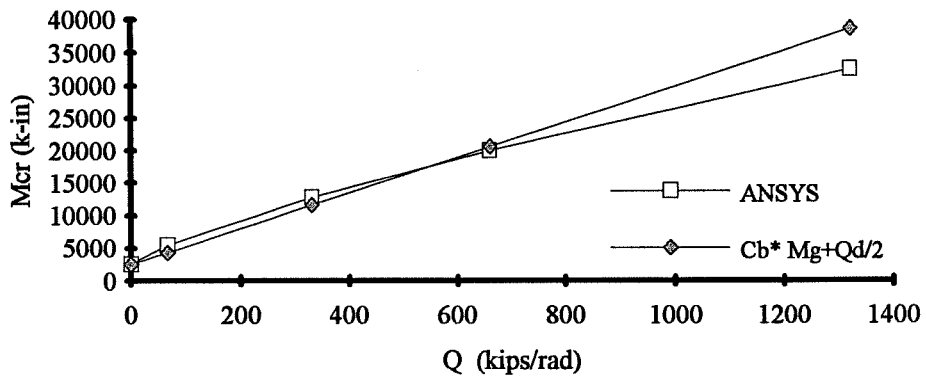
Figure 6.43b: Mcr versus Q for section #2 with 50' span and a point load
applied at CL top flange - ANSYS results and Eqn. 6.16.
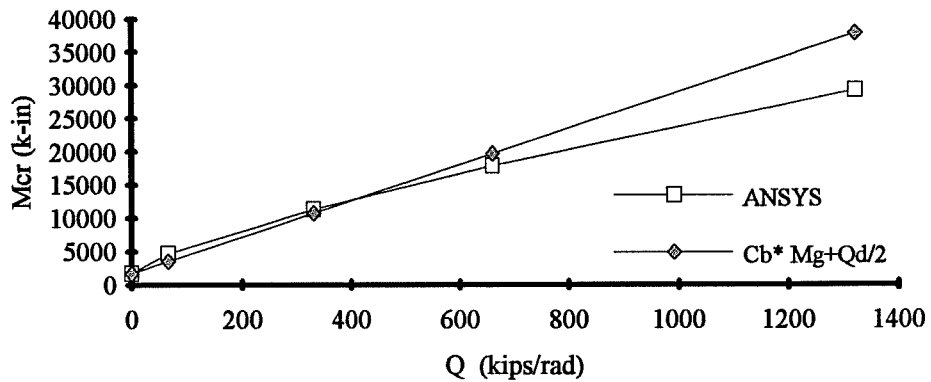
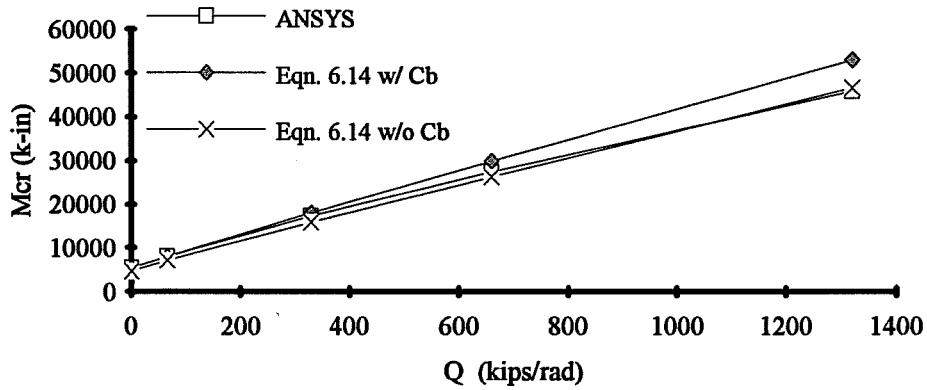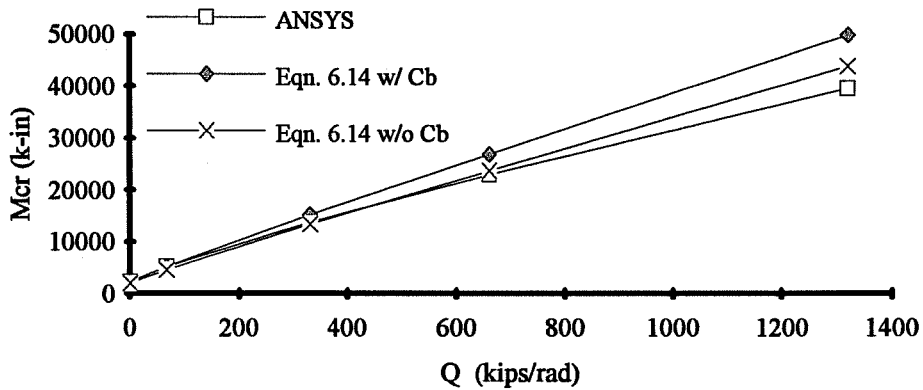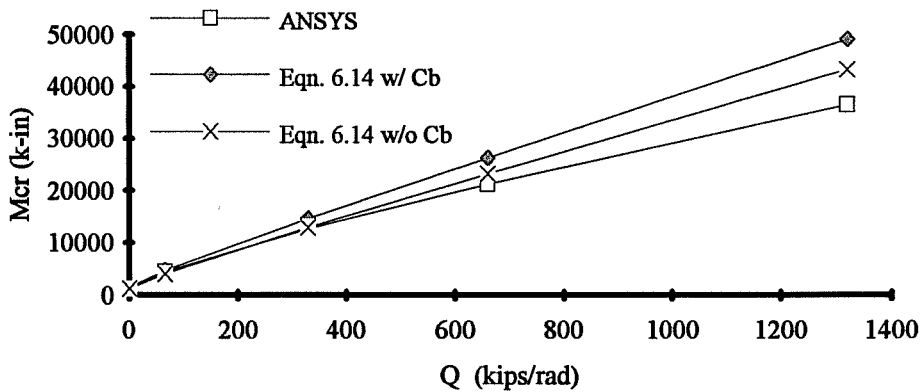Figure 6.43c: Mcr versus Q for section #2 with 75' span and a point load
applied at CL top flange - ANSYS results and Eqn. 6.16.
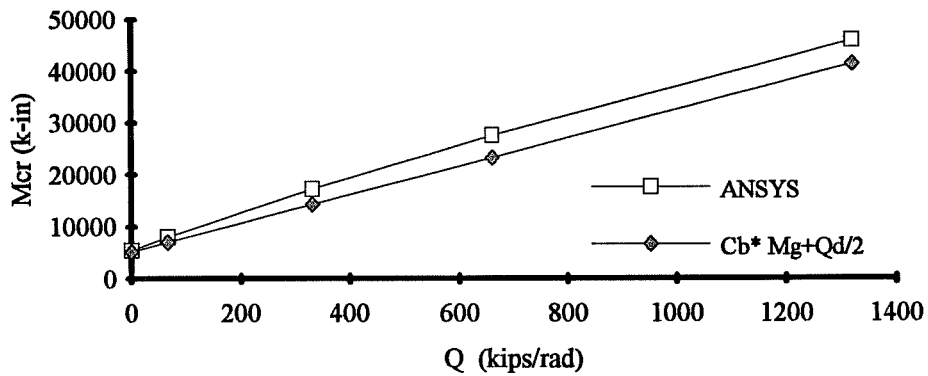
Figure 6.44a: Mcr versus Q for section #2 with 25' span and a distributed load applied at top flange - ANSYS results and Eqn. 6.16.
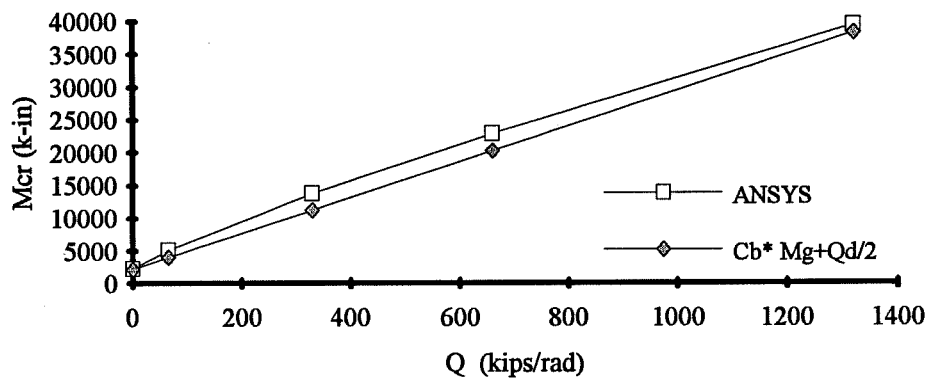
Figure 6.44b: Mcr versus Q for section #2 with 50' span and a distributed load applied at top flange - ANSYS results and Eqn. 6.16.
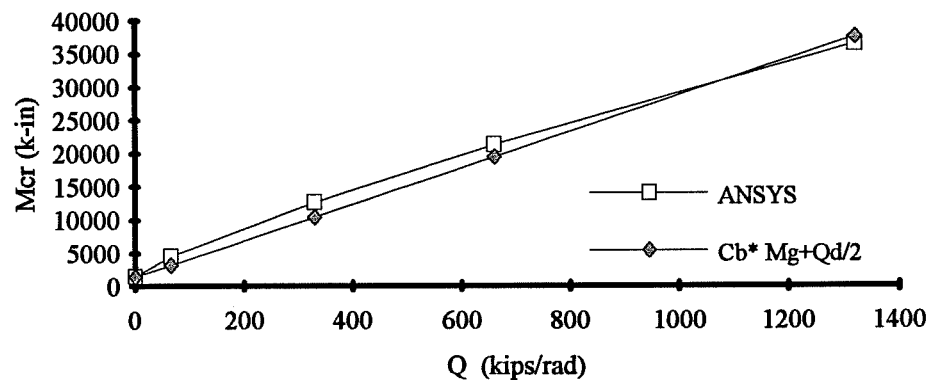
Figure 6.44c: Mcr versus Q for section #2 with 75' span and a distributed load applied at top flange - ANSYS results and Eqn. 6.16.
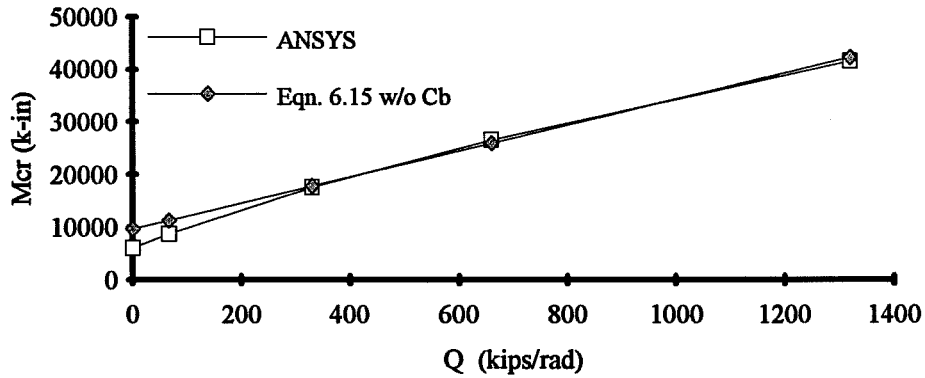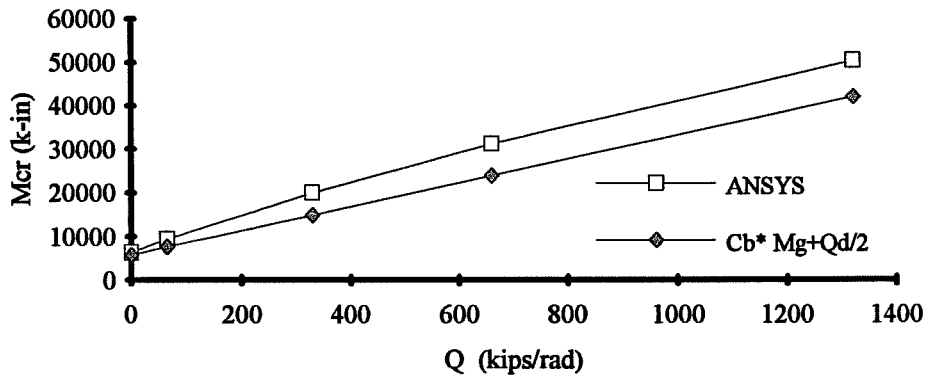
Figure 6.45a: Mcr versus Q for section #3 with 25' span and a point load applied at CL top flange - ANSYS results and Eqn. 6.16.
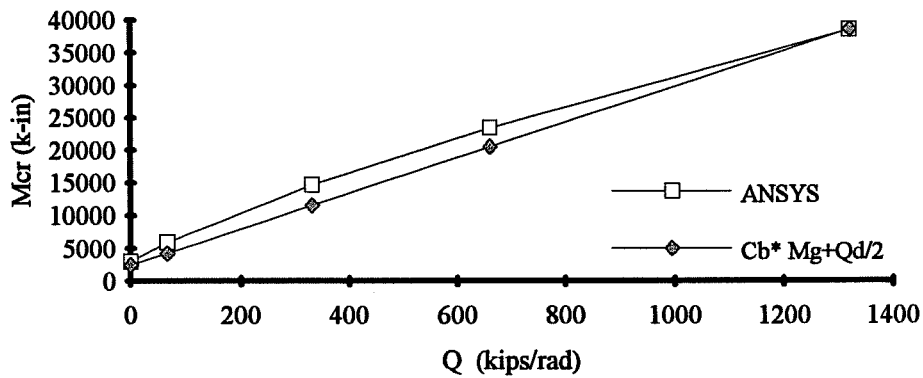
Figure 6.45b: Mcr versus Q for section #3 with 50' span and a point load applied at CL top flange - ANSYS results and Eqn. 6.16.
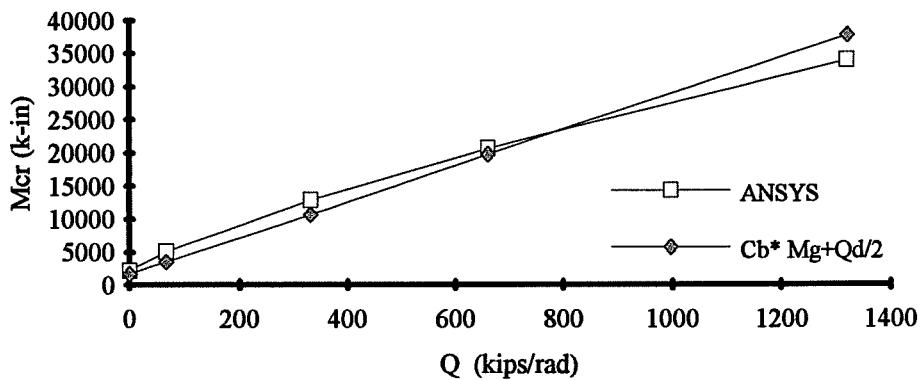
Figure 6.45c: Mcr versus Q for section #3 with 75' span and a point load applied at CL top flange - ANSYS results and Eqn. 6.16.
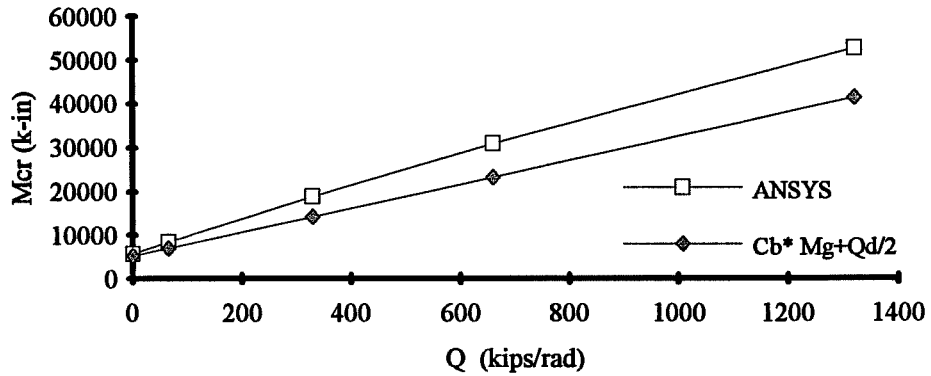
Figure 6.46a: Mcr versus Q for section #3 with 25' span and a distributed load applied at top flange - ANSYS results and Eqn. 6.16.
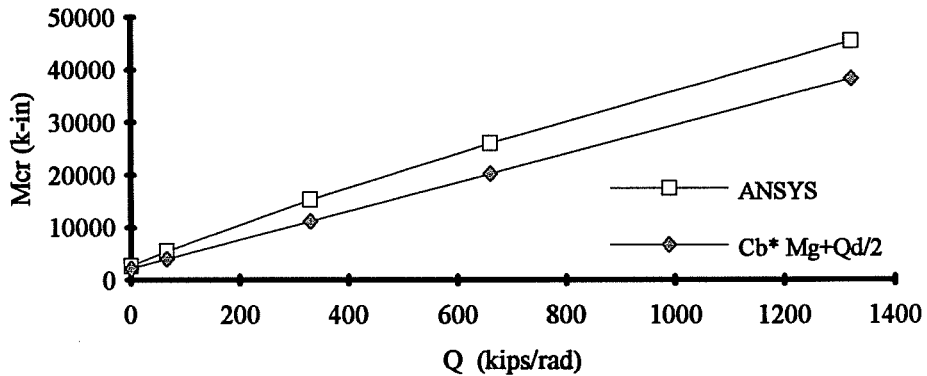
Figure 6.46b: Mcr versus Q for section #3 with 50' span and a distributed load applied at top flange - ANSYS results and Eqn. 6.16.
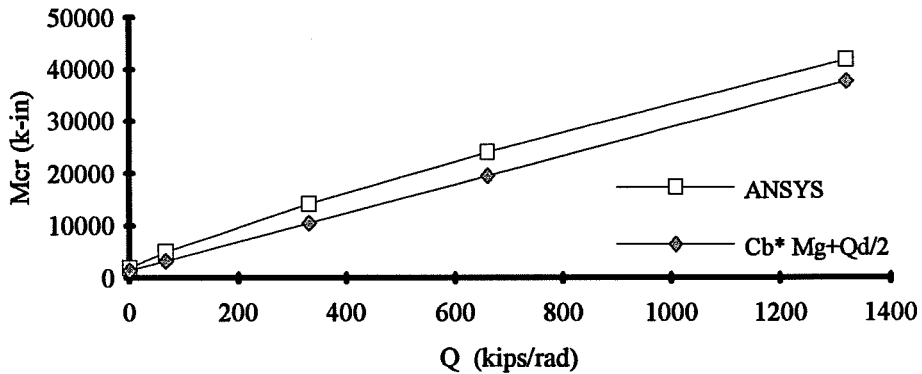
Figure 6.46c: Mcr versus Q for section #3 with 75' span and a distributed load applied at top flange - ANSYS results and Eqn. 6.16.

Figures 6.47a, 6.47b, and 6.47c show the plots of M_{cr} versus Q for the ANSYS results and Equation 6.15 for the respective sections shallow #1, #2, and #3. The equation is relatively conservative for these girders. The results for M_{cr} versus Q for the sections deep #1, #2, and #3 in the respective Figures 6.48a, 6.48b, and 6.48c. The estimates from the equation plot closer to the ANSYS results for the deep girders than was observed for the shallow girders. The equation is slightly unconservative for larger values of the shear rigidity for the section deep #2, however, the equation does a very good job of predicting the buckling capacity.

In general, Equation 6.16 provides a relatively straight forward method of predicting the buckling capacity of beams with top flange loading and bracing provided by a shear diaphragm. The other solutions which were presented are more complex and in most cases were found to be unconservative with respect to the finite element studies. Equation 6.16 was an easy expression to use and in most cases was found to produce conservative estimates of the buckling capacity.

6.5 Summary

This chapter has presented finite element results for a variety of loading conditions, and comparisons were made with existing closed-formed solutions as well as other approximate solutions. The ability of a shear diaphragms to brace a number of girder cross-sections subjected to constant moment were presented first. These results showed that the increase in buckling moment with increasing shear rigidity was approximately linear. In addition, it was found that the increase in buckling moment that the deck is responsible for was not very sensitive to the girder span, and was essentially a linear function of the girder depth.

The Errera energy solution had good agreement with the finite element results for doubly-symmetric girders subjected to constant moment. With a slight modification, the Errera solution provided good estimates for singly-symmetric sections when the value of the variable "e" in the equation was taken as half the girder depth. It was also shown that very accurate estimates of the buckling capacity of girders braced by a shear diaphragm could be obtained with the simple approximation $M_{AASHTO} + Qd$.

When girders were subjected to a moment gradient, the effectiveness of the deck was reduced. In most cases, the Errera solution was unconservative with respect to the finite element results, especially when C_b factors are applied to the entire expression. Reasonable estimates of
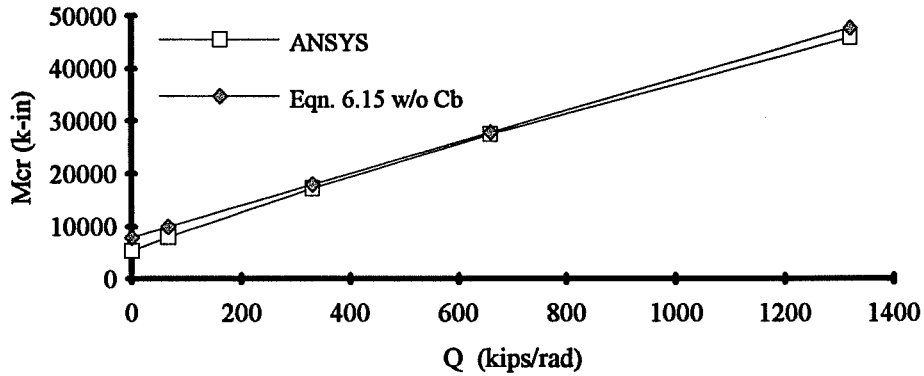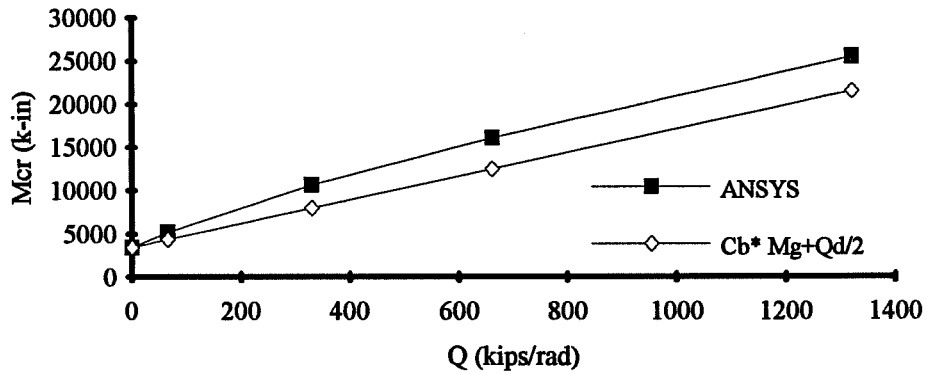
Figure 6.47a: Mcr versus Q for Shallow #1 with 75' span and a distributed load applied at top flange - ANSYS results and Eqn. 6.16.
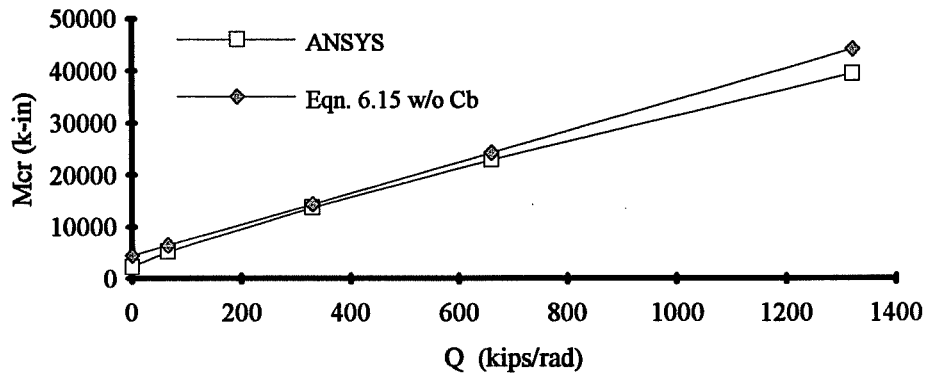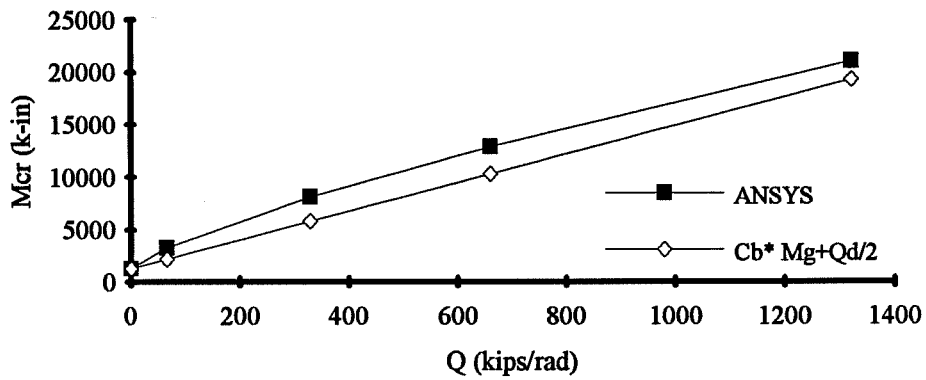

Figure 6.47b: Mcr versus Q for Shallow #2 with 75' span and a distributed load applied at top flange - ANSYS results and Eqn. 6.16.
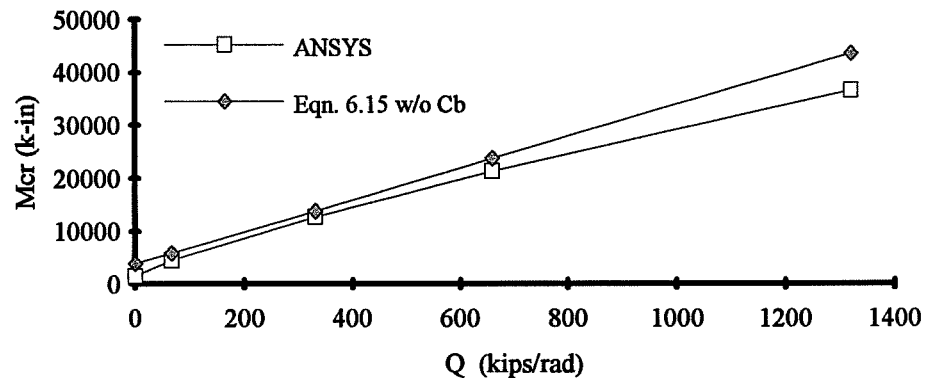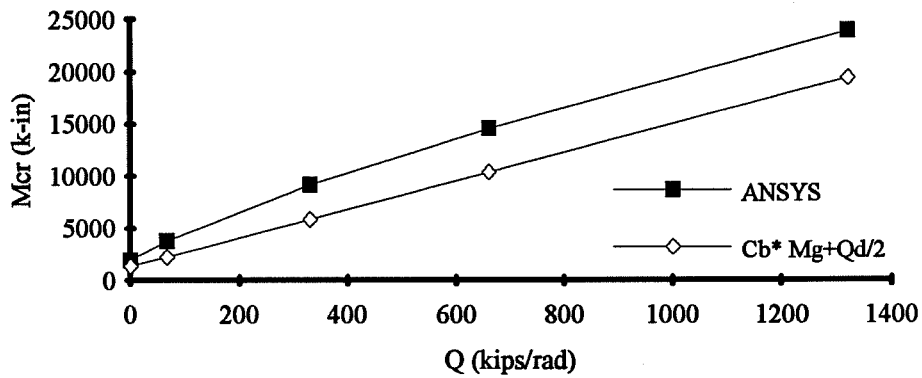

Figure 6.47c: Mcr versus Q for Shallow #3 with 75' span and a distributed load applied at top flange - ANSYS results and Eqn. 6.16.
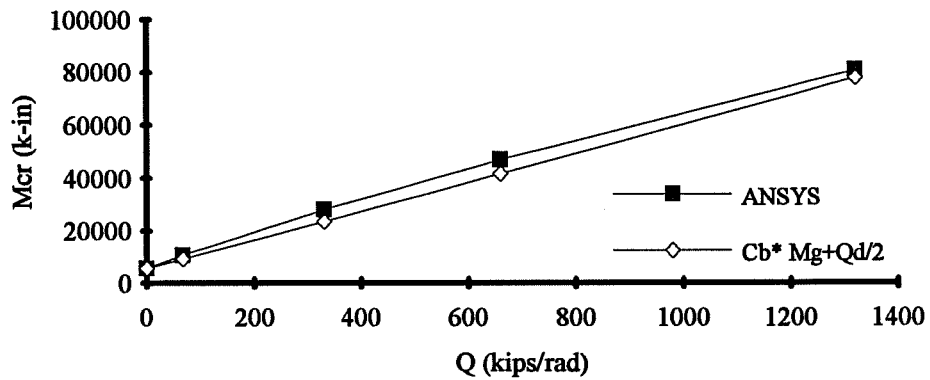
Figure 6.48a: Mcr versus Q for Deep #1 with 75' span and a distributed load applied at top flange - ANSYS results and Eqn. 6.16.
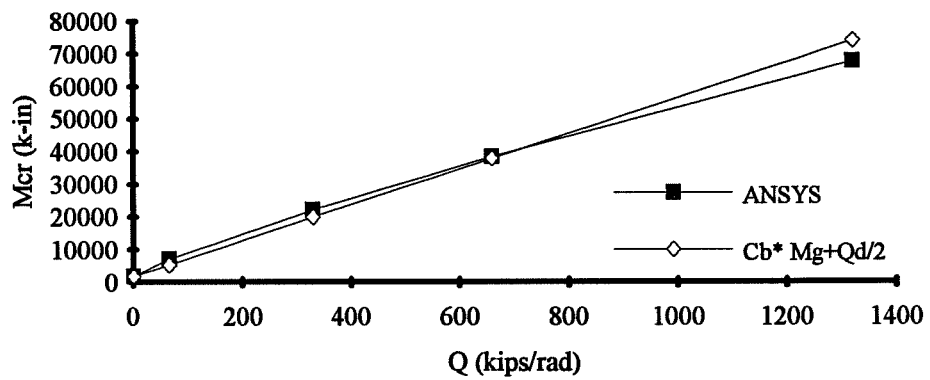
Figure 6.48b: Mcr versus Q for Deep #2 with 75' span and a distributed load applied at top flange - ANSYS results and Eqn. 6.16.
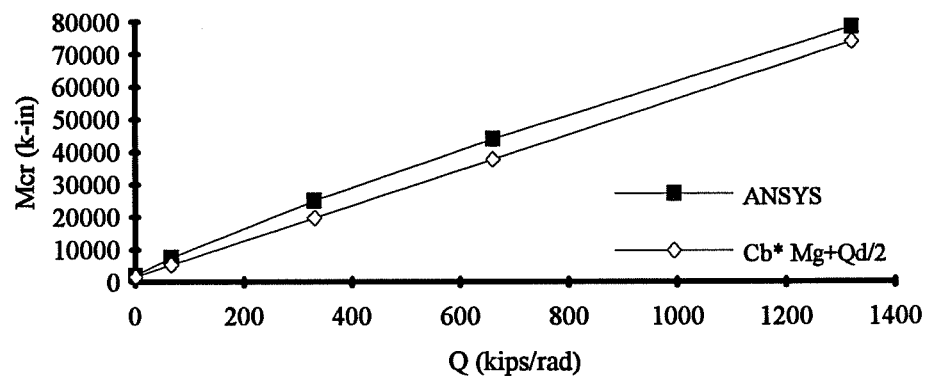
Figure 6.48c: Mcr versus Q for Deep #3 with 75' span and a distributed load applied at top flange - ANSYS results and Eqn. 6.16.

the buckling capacity were obtained, however, by using the approximation $M_{cr} = C_b M_{AASHTO} + (3/4) Qd$.

The effectiveness of the deck was reduced further when the girders were subjected to top flange loading. The deck was slightly less effective as the span of the girders is increased. Reasonable estimates of the buckling capacity were obtained with the simple approximation $M_{cr} = C_b^* M_{AASHTO} + (1/2)Qd$. This equation provides a simple expression which is conservative for most of the cases which were considered.

CHAPTER 7

Buckling Capacity of Partially-Stiffened
Simply Supported Girders Braced by a Shear Diaphragm

7.1 Introduction

Chapters 5 and 6 presented some of the finite element results for girders which had closely-spaced transverse stiffeners. The close spacing of stiffeners was used to increase the shear buckling and bend buckling capacity of the girder webs. Actual bridge girders, however, will have a larger stiffener spacing.

The accuracy of the approximate solutions recommended in Chapter 6 will be checked in this chapter on girders with less stiffened webs. Two different web thicknesses were considered in this chapter. In one case, a thin web (0.33 in.) was used with stiffeners spaced at 1.4 times the web depth. These webs will be referred to as "partially stiffened". The thin web was selected in order to determine the effect of web bend buckling and shear buckling on the effectiveness of the deck to brace the girders. In addition, a thick web (0.625 in.) with stiffeners only at the supports and under the point load was also considered. These webs will be referred to as "unstiffened". The thicker webs were selected in order to compare the results with the Chapter 6 results to determine the effect of the web stiffeners which prevent cross-sectional distortion on the buckling capacity.

The applied loading in this chapter consists of a point load applied at the midspan of the girders. The load was applied at midheight and also at the girder top flange.

Section 7.2 will present buckling modes for girders with partially stiffened and unstiffened webs. The effect of bend buckling and shear buckling on girder webs will be outlined in Section 7.3. Section 7.4 will present finite element results which show the effect of a shear diaphragm on the buckling load of girders with partially stiffened webs which are subjected to transverse loading applied at midheight. The results for partially stiffened webs with transverse loading applied at the top flange will be presented in Section 7.5. The results will be summarized in Section 7.6.

7.2 Buckling Modes of Partially-Stiffened Girders with Diaphragm Bracing

Chapter 5 presented finite element results which showed the effect of a shear diaphragm on the buckling modes of simply-supported girders. The girders which were considered in Chapter

214

5 and 6 had a compact web (d/t_w = 86) with transverse stiffeners spaced at 18.75 inches. The closely spaced stiffeners and thick web were used to eliminate web buckling resulting from shear and/or bending stresses. In addition to preventing web buckling, the closely spaced transverse stiffeners also reduce web distortions by increasing the out of plane bending stiffness of the web. Since web distortions were eliminated, the ability of the deck to brace the girder against lateral-torsional buckling could be isolated. It is important, however, to determine the influence of web slenderness and stiffener spacing upon the accuracy of the design equations.

Two different web thicknesses were considered in this portion of the study. Figure 7.1 shows three sections which have been used extensively in the studies reported in the previous chapters. Sections #1, #2, and #3 were also used in this portion of the study, however stiffeners were provided only at the supports and at midspan, where the load was applied. In addition, the sections shown in Figure 7.2 were also considered. These sections have identical flange sizes as sections #1, #2, and #3, however the web has a thickness of only 0.33 inches. For the doubly-symmetric sections, this web has a slenderness ratio equal to 53.75 / 0.33 = 163. Assuming a yield stress of 50 ksi, 0.33 inches is the minimum thickness that the AASHTO Specification [1] would allow for the doubly-symmetric sections without providing a longitudinal stiffener. The thickness is slightly smaller than the AASHTO minimum thickness for the singly-symmetric section without a longitudinal stiffener. Transverse stiffeners were spaced at 75 inches which gives an aspect ratio of the shear panel to web depth of d_o/D = 1.4. These sections will be designated as Slender #1, #2, and #3.

Figures 7.3a-7.3e show plots of the lateral displacement of the top flange, mid-height web, and bottom flange along the 25 foot girder length of the unstiffened section #1 (0.625 in. web thickness) with increasing deck shear rigidity. The girders have been subjected to a point load at midheight of the centerline of the girders. The displacements have been normalized by the lateral displacement of the top flange at midspan. A sine curve has also been plotted in these figures. With no deck as a bracing element (Figure 7.3a), the lateral displacement of the top flange along the girder length is very similar to the sine curve. With increasing shear rigidity of the deck, the lateral displacement of the top flange deviates slightly from a sine curve, however, it is still very close. The center of twist of this section is near the bottom flange for all deck shear rigidities, which is indicated by the very small lateral displacement of the bottom flange.

With no web distortion, the lateral displacements of the nodes of the web lie along a straight line between the two flanges. When a girder experiences lateral-torsional buckling and
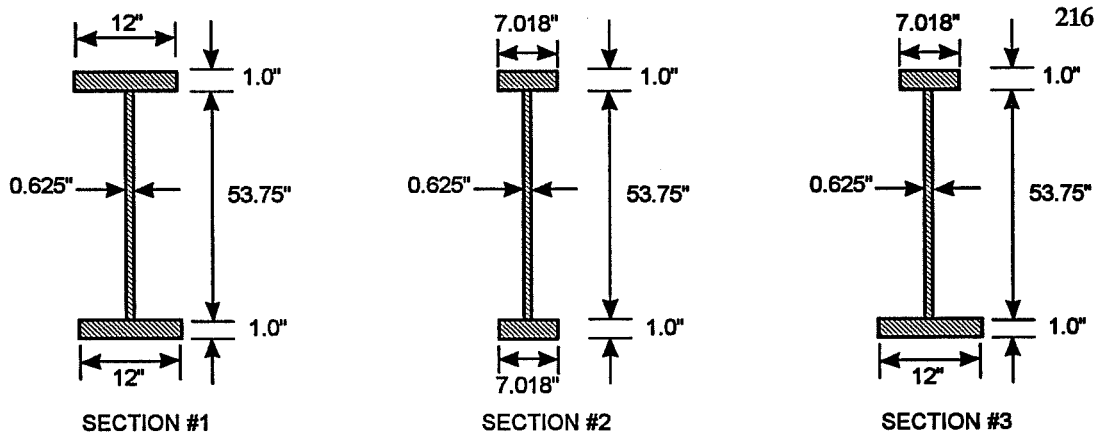
Figure 7.1 Cross-sections with compact web considered in computational study.
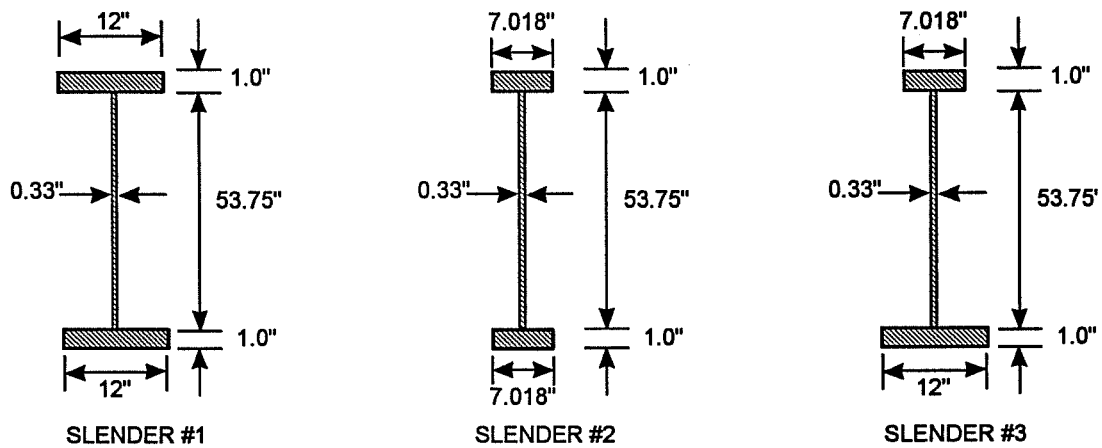
Figure 7.2 Cross-sections with slender web considered in computational study.
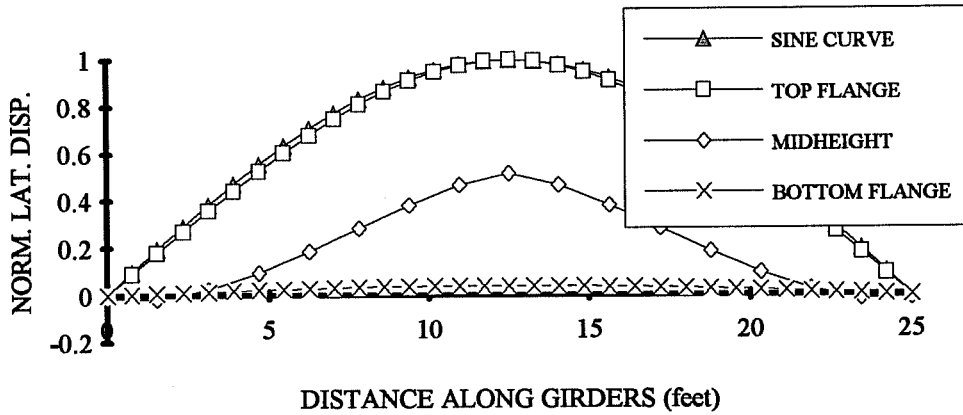
Figure 7.3a: Lateral displacement of unstiffened girder vs sine curve for section #1
L=25', P @ CL midheight, Q=0.
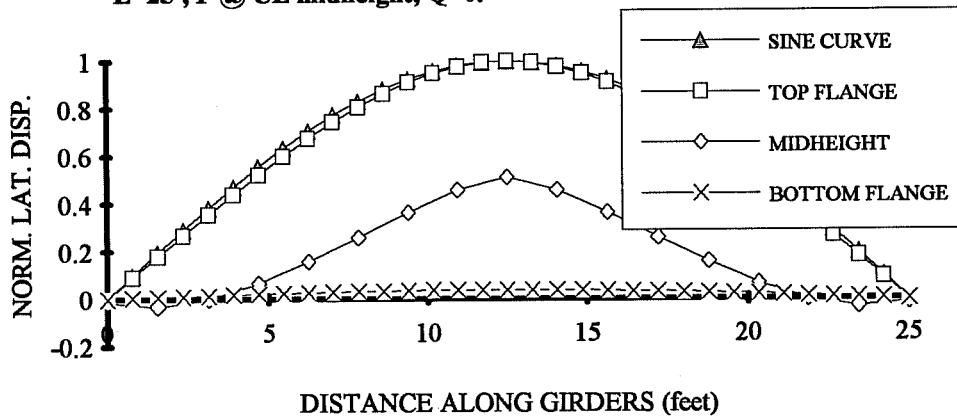
Figure 7.3b: Lateral displacement of unstiffened girder vs sine curve for section #1
L=25', P @ CL midheight, Q=66.
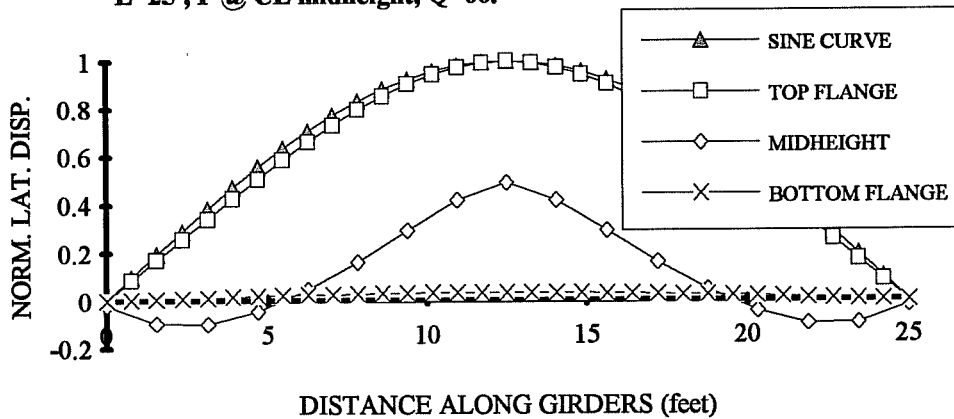
Figure 7.3c: Lateral displacement of unstiffened girder vs sine curve for section #1
L=25', P @ CL midheight, Q=330.
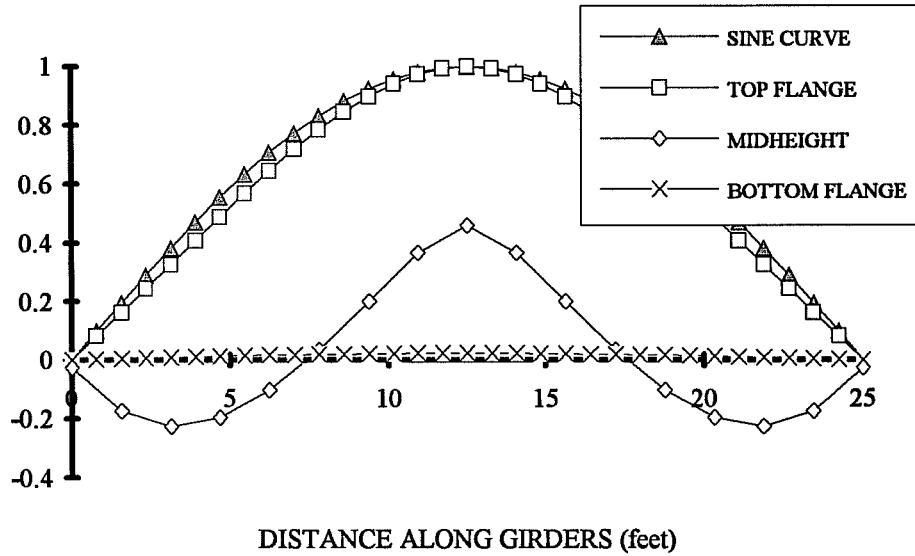
**Figure 7.3d: Lateral displacement of unstiffened girder vs sine curve for section #1
L=25', P @ CL midheight, Q=660.**
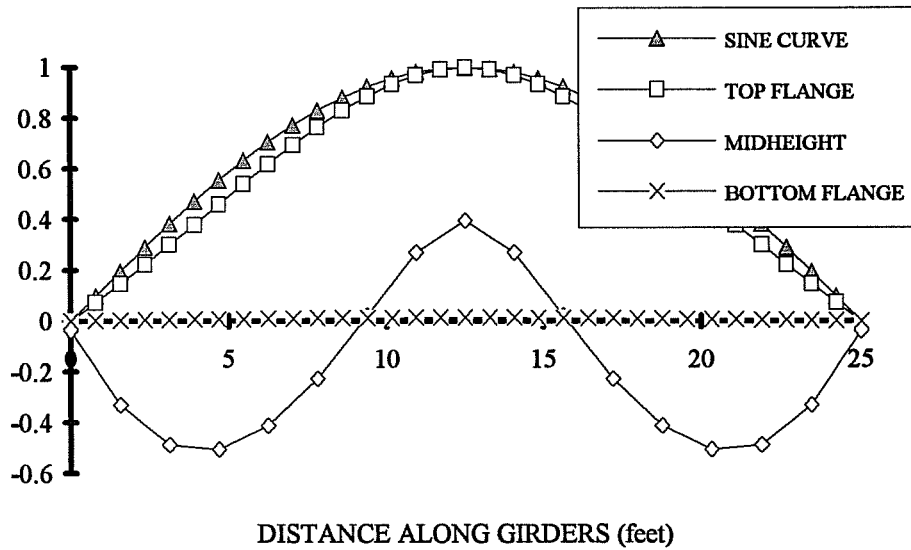
**Figure 7.3e: Lateral displacement of unstiffened girder vs sine curve for section #1
L=25', P @ CL midheight, Q=1320.**

does not have any web distortion, the lateral displacement of the midheight node of a web should lie midway between the top and bottom flange. In Figures 7.3a-7.3e, there was a significant amount of web distortion when the deck shear rigidity was increased. The web distortion was caused by shearing stresses, and was not as significant for longer girder spans since the shear at the lateral torsional buckling load for the longer spans was significantly smaller. For larger values of the deck shear rigidity, the "web distortion" was due to web buckling. In these cases, the buckling mode is a combination of web shear buckling with lateral torsional buckling of the girder cross-section.

Figures 7.4a-7.4e show plots of the lateral displacement of the top flange, mid-height web, and bottom flange with increasing deck shear rigidity along the 25 foot girder with the cross-section of Slender #2. The center of twist of the cross-section moved higher up on the girder cross-section with increasing deck shear rigidity which is evidenced by the increasing negative displacement of the bottom flange. The web experienced distortions at relatively low values of the deck shear rigidity, and had buckled at a deck shear rigidity of 330 k/rad. The web buckling became more severe with increasing deck shear rigidity, and for rigidities of 660 and 1320 k/rad, the web buckling controlled the buckling mode.

It will be shown in Sections 7.4 and 7.5 that when the webs experience web shear and/or bend buckling, the buckling capacity of the section does not increase significantly with increasing deck shear rigidity since the webs control the buckling mode. It is necessary, therefore, to isolate web buckling due to shear or bending stress, from ordinary web distortions. Web buckling will be outlined in Section 7.3.

7.3 Web Buckling of Partially-Stiffened Girders

Web buckling can be caused by either shearing stress or bending stress. If adequate transverse stiffeners are provided to develop a tension field, there is a significant amount of post-shear buckling strength. Webs experiencing bend buckling also have some post-buckling strength, however it is typically not as significant as in the case of shear buckling.

AASHTO Section 10.50d imposes restrictions on the web slenderness to control bend buckling during construction. AASHTO Section 10.50e limits the maximum non-composite shear from dead load to the shear buckling load of the web. The maximum increase in the lateral-torsional buckling capacity provided by the deck should therefore be limited by the buckling capacity of the girder webs.
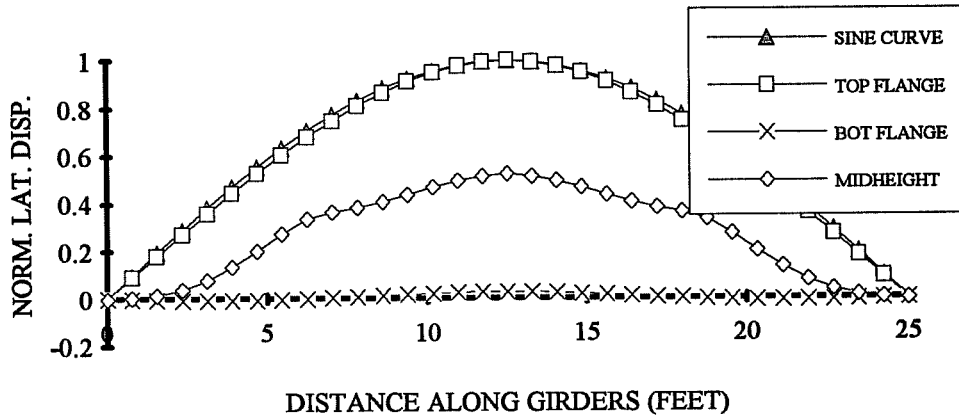
Figure 7.4a: Lateral disp. of partially stiffened girder vs sine curve for slender #2, L=25', P @ CL midheight, Q=0.
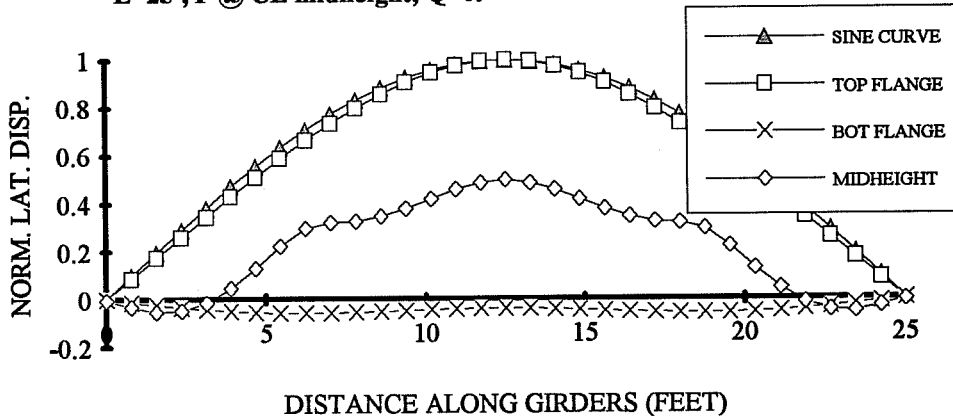
Figure 7.4b: Lateral disp. of partially stiffened girder vs sine curve for slender #2, L=25', P @ CL midheight, Q=66.
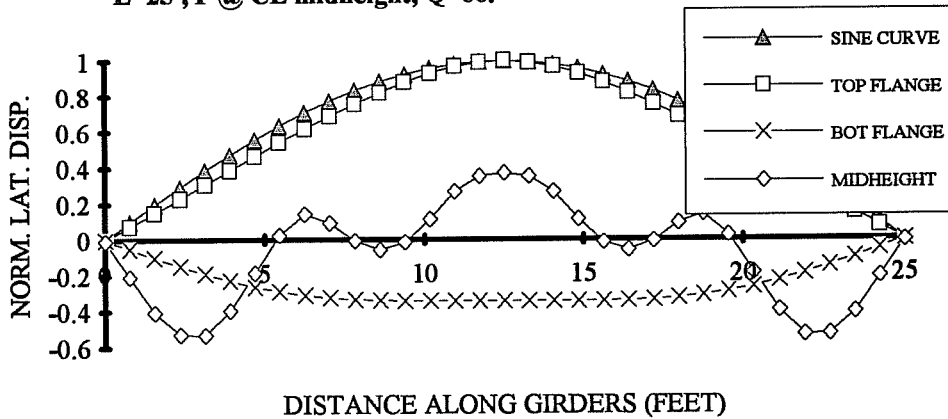
Figure 7.4c: Lateral disp. of partially stiffened girder vs sine curve for slender #2, L=25', P @ CL midheight, Q=330.
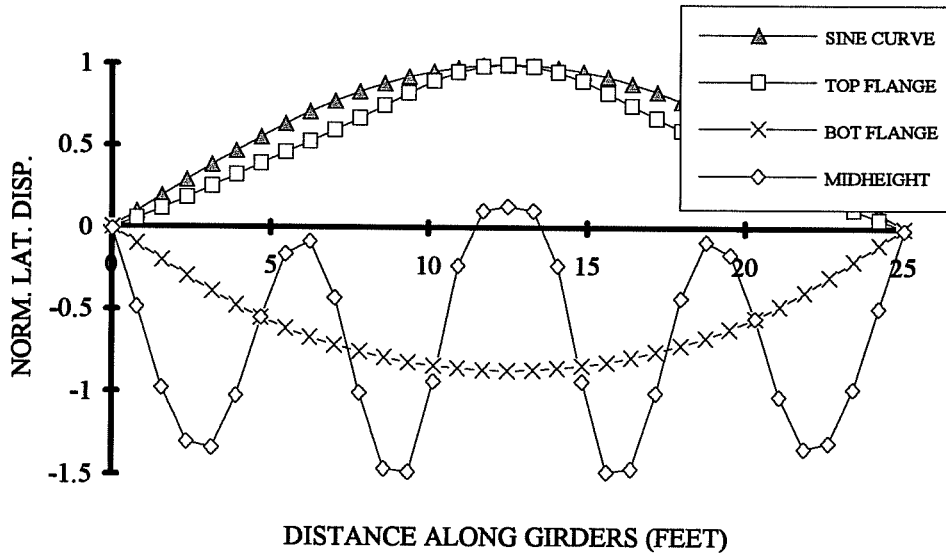
Figure 7.4d: Lateral disp. of partially stiffened girder vs sine curve for slender #2, L=25', P @ CL midheight, Q=660.
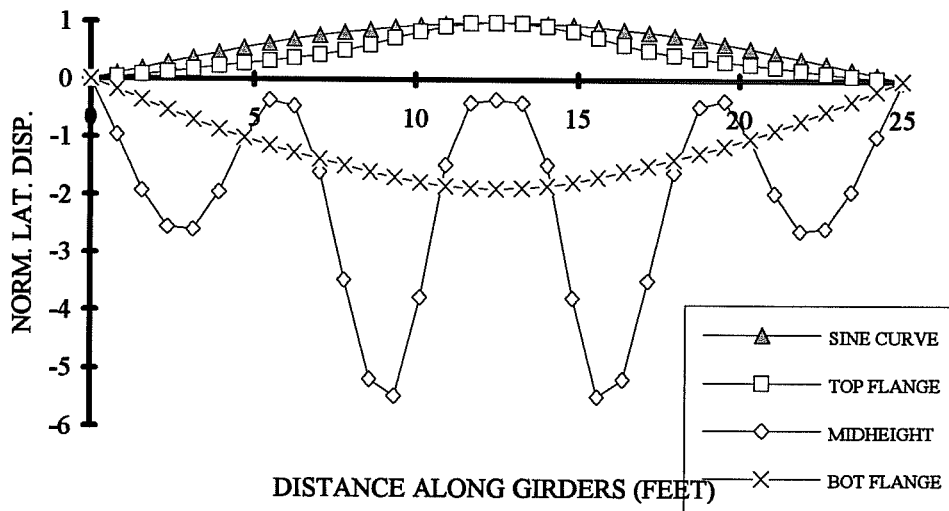
Figure 7.4e: Lateral displacement of partially stiffened girder vs sine curve for section L=25', P @ CL midheight, Q=1320.

The AASHTO specification controls the bend buckling in Section 10.48.4.1, which makes use of the moment reduction factor R_b given by the following expression:

$$R_b = 1 - 0.002 \left(\frac{D_c \, t_w}{A_{fc}}\right) \left[\frac{D_c}{t_w} - \frac{\lambda}{\sqrt{\frac{M_r}{S_{xc}}}}\right]$$ (7.1)

where:

D_c = depth of the web in compression,

t_w = web thickness,

A_{fc} = area of the compression flange,

λ = factor relating to plate buckling coefficient (explained below)

M_r = applied bending moment

S_{xc} = section modulus with respect to the compression flange.

Bend buckling of the web causes an increase in the stress in the compression flange. The R_b factor therefore limits the bending moment to prevent yielding of the girder in the advent of web bend buckling. The last term in brackets in Equation 7.1 can be used as a limit for bend buckling if it is set equal to zero which is shown in the following expression:

$$\frac{D_c}{t_w} - \frac{\lambda}{\sqrt{\frac{M_r}{S_{xc}}}} = 0$$ (7.2a)

The equation can be rearranged to obtain a form of the classical plate buckling formula, which is shown as follows:

$$\frac{M_r}{S_{xc}} = \sigma_{cr} = \frac{\lambda^2}{\left(\frac{D_c}{t_w}\right)^2}$$ (7.2b)

The classic plate buckling equation typically takes the form of Equation 7.2c. The variables in Equation 7.2c are as follows: σ_{cr} is the buckling stress, E is the modulus of elasticity (29000000 psi for steel), k is the plate buckling coefficient (depends on the state of stress and plate boundary

$$\sigma_{cr} = \frac{\pi^2 E k}{12(1-v^2) \left(\frac{b}{t_w}\right)^2} \tag{7.2c}$$

conditions), v is Poisson's ratio (0.3 for steel), b is the depth of the plate, and t_w is the plate thickness. The webs of singly-symmetric sections can be handled using Equation 7.2c by replacing the plate depth "b" by two times the depth of the web in compression. The plate buckling coefficient which would be used in this case would correspond to the state of bending stress resulting from symmetric bending (i.e. D_c = D/2). Substituting in Equation 7.2c for π, E = 29000000 psi, v = 0.3, and b = $2D_c$, results in the following:

$$\sigma_{cr} = \frac{6.55 x 10^6 \; k}{\left(\frac{D_c}{t_w}\right)^2} \tag{7.2d}$$

Referring back to the expression shown in Equation 7.2b which resulted from the AASHTO Specification , the parameter λ can have one of the following values:

> 12500 for members with a compression flange area less than the tension flange area,

> 15400 for members with a compression flange area equal to or greater than the tension flange area.

By comparing Equations 7.2b and 7.2d, the following correlation can be made:

$$6.55 x 10^6 \; k = \lambda^2 \tag{7.2e}$$

The resulting plate buckling coefficients for the corresponding values of λ can then be found.

$$\lambda = 12500 \; : \; k = 23.8$$
$$\lambda = 15400 \; : \; k = 36.2$$

The minimum buckling coefficient for a plate subjected to symmetrical bending stress with all edges simply supported and free to rotate is 23.9 which essentially matches the value calculated for λ = 12500. The minimum buckling coefficient corresponding to clamping of the top and bottom web edges is 39.6. The increase in the plate buckling coefficient when the boundary conditions at the top and bottom of the web are changed from simply supported to clamped is therefore equal to 39.6 - 23.9 = 15.7. The buckling coefficient which was calculated for λ = 15400

considers partial restraint from the flanges by making use of 78 % of the difference between clamped edges and simply supported edges. This is shown in the following expression:

$$k_{\lambda=15400} = 23.9 + 0.78x(39.6 - 23.9) = 36.2.$$ (7.2f)

Equation 7.2b can be rewritten to solve for the maximum moment allowed to prevent bend buckling as follows:

$$M_r = \left[\frac{\lambda^2}{\left(\frac{D_c}{t_w}\right)^2} \right] S_{xc}$$ (7.2g)

The moment resulting from Equation 7.2g is the useful limit that the deck can be counted on to increase the lateral-torsional buckling capacity of the girder without incurring web bend buckling. The limit will be calculated for doubly-symmetric sections and sections with a compression flange bigger than the tension flange using a $\lambda = 15400$, while singly-symmetric sections with a small compression flange will have a limit based on $\lambda = 12500$.

Shear buckling is controlled in the AASHTO specification in Section 10.48.8.1 using Equation 7.3a.

$$V_u = C \; V_p$$ (7.3a)

V_p in Equation 7.3a is equal to the plastic shear capacity of the web and is given by the expression:

$$V_p = 0.58 \; F_y \; D \; t_w$$ (7.3b)

The variables in Equation 7.b are F_y which is the yield capacity of the web material, D which is the web depth, and t_w which is the web thickness. The parameter C is an expression which accounts for shear buckling in the web. For elastic buckling, C is given by:

$$C = \frac{4.5x10^7 \; k}{\left(\frac{D}{t_w}\right)^2 F_y}$$ (7.3c)

Since the expressions above are for elastic shear buckling, the capacity should be independent on the yield stress of the material. This is the case since the yield stress, F_y, in the denominator of Equation 7.3c for C, cancels with the F_y in the expression for V_p when the two are multiplied in Equation 7.3a. The variable k in Equation 7.3c is the plate buckling coefficient for shear and can be calculated with the following expression:

$$k = 5 + \frac{5}{\left(\frac{d_o}{D}\right)^2}$$ (7.3d)

Equation 7.3e shows the equation which results for elastic shear buckling of the web.

$$V_u = 0.58 \ D \ t_w \left[\frac{4.5 x 10^7 \ k}{\left(\frac{D}{t_w}\right)}\right]$$ (7.3e)

Since the applied loading consisted of a point load at midspan, the moment corresponding to web shear buckling can be calculated as $M_{cr} = V_u \ (L/2)$. This will indicate the useful limit that the deck can be relied on to increase the lateral-torsional buckling capacity of the girders without causing shear buckling.

7.4 Finite Element Results for Partially Stiffened Girders with Point Load Applied at Midheight

Finite element results were presented in Chapter 6 for fully stiffened girders with a compact web. These computational results were compared with existing closed formed solutions. It was shown in Chapter 6, however, that good estimates of the buckling load could be obtained using simple design approximations like Equation 7.4 for girders with transverse loading applied at midheight.

$$M_{cr} = C_b M_{AASHTO} + \frac{3}{4} Qd$$ (7.4)

The variables in Equation 7.4 are as follows: M_{cr} is the lateral torsional buckling moment of the deck and girder system, C_b is the modifier for moment gradient, M_{AASHTO} is the buckling

moment of the unbraced girder and can be calculated using the AASHTO equation (10-102c) for buckling between cross-frames, Q is the shear rigidity of the deck, and d is the depth of the girder.

Equation 7.4 will be plotted along with the ANSYS results for girders with partially stiffened webs. The finite element results for the fully-stiffened girders from Chapter 6 will also be plotted as a reference. The results for the girders with the 0.625 inch web will be presented first. Although these girders had stiffeners at the supports and also midspan, they will be referred to as "unstiffened", while the girders from Chapter 6 which had stiffeners every 18.75 inches will be referred to as "fully stiffened". Moments causing web shear buckling or bend buckling will be indicated in the figures when the limits fall in the range of the lateral-torsional buckling capacity of the girders.

Figures 7.5a, 7.5b, and 7.5c show plots of M_{cr} versus Q for the doubly-symmetric section #1 with respective lengths of 25, 50 , and 75 feet. There is a significant reduction in the buckling capacity of the 25 foot long unstiffened girder, even for the case with no deck as a bracing element. A large portion of this reduction may be caused by load effects. The applied load is around 400 kips, and an extremely large bearing stiffener is required in order to prevent local effects. There is much better correlation between the stiffened and unstiffened girders for the 50 and 75 foot spans; the approximate formula is slightly conservative in both of these cases.

The results for section #2 are shown in Figures 7.6a, 7.6b, and 7.6c for respective lengths of 25, 50, and 75 foot spans. For larger values of the deck shear rigidity, the design approximation is slightly unconservative with respect to the unstiffened 25 foot span girder, however it is still very close. The approximation does a good job of estimating the buckling capacity of the 50 and 75 foot span girders.

Figures 7.7a, 7.7b, and 7.7c show plots of M_{cr} versus Q for the singly-symmetric section #3 with respective lengths of 25, 50, and 75 feet. The design approximation is slightly unconservative for large shear rigidities with the 25 foot span, however, bend buckling of the web would control the capacity of the section. Since the compression flange is smaller than the tension flange, the bend buckling limit corresponds to $\lambda = 15400$. This limit is shown as the horizontal line in the figures. The increase in the lateral-torsional buckling capacity provided by the deck would be limited by the bend buckling capacity for all three lengths.

In the following three groups of graphs, the results for the thin web (0.33 in.) will be referred to as the "slender" web, while the results for the fully stiffened thick web (0.625 in.) will be referred to as the "fully-stiffened" web. Figure 7.8a, 7.8b, and 7.8c show plots of M_{cr} versus Q

Figure 7.5a: Mcr versus Q for section #1 with 25' span and a point load applied at CL midheight- ANSYS results and Estimate.

Figure 7.5b: Mcr versus Q for section #1 with 50' span and a point load applied at CL midheight- ANSYS results and Estimate.

Figure 7.5c: Mcr versus Q for section #1 with 75' span and a point load applied at CL midheight- ANSYS results and Estimate.

Figure 7.6a: Mcr versus Q for section #2 with 25' span and a point load applied at CL midheight- ANSYS results and Estimate.

Figure 7.6b: Mcr versus Q for section #2 with 50' span and a point load applied at CL midheight- ANSYS results and Estimate.

Figure 7.6c: Mcr versus Q for section #2 with 75' span and a point load applied at CL midheight- ANSYS results and Estimate.

Figure 7.7a: Mcr versus Q for section #3 with 25' span and a point load applied at CL midheight- ANSYS results and Estimate.

Figure 7.7b: Mcr versus Q for section #3 with 50' span and a point load applied at CL midheight- ANSYS results and Estimate.

Figure 7.7c: Mcr versus Q for section #3 with 75' span and a point load applied at CL midheight- ANSYS results and Estimate.
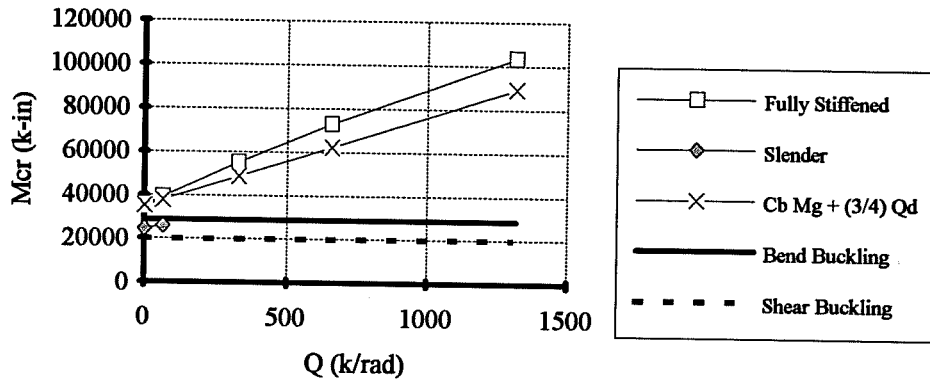
**Figure 7.8a: Mcr versus Q for fully stiff. section #1 and part. stiff slender #1
L= 25', P @ CL midheight- ANSYS results and Estimate.**
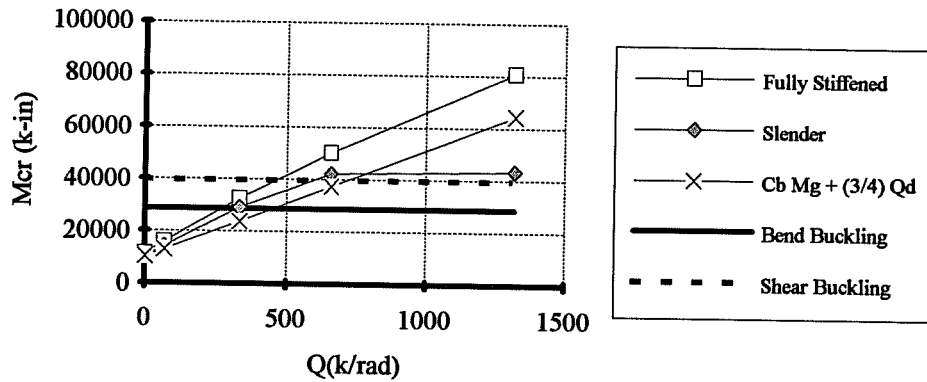
**Figure 7.8b: Mcr versus Q for fully stiff. section #1 and part. stiff slender #1
L= 50', P @ CL midheight- ANSYS results and Estimate.**
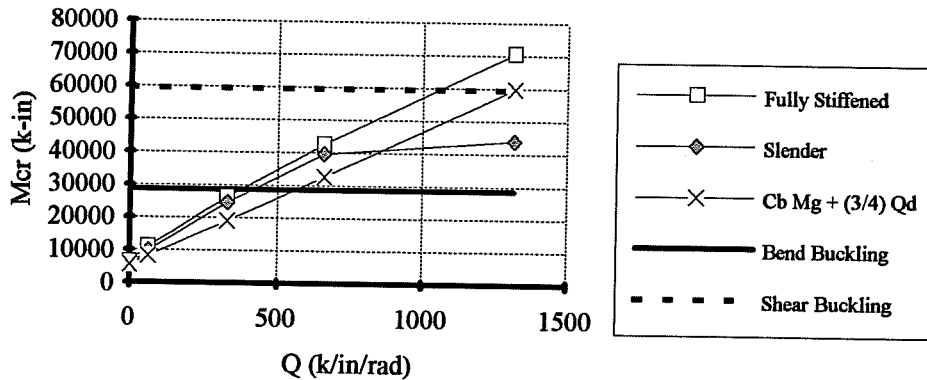
**Figure 7.8c: Mcr versus Q for fully stiff. section #1 and part. stiff slender #1
L= 75', P @ CL midheight- ANSYS results and Estimate.**

for the doubly-symmetric section slender #1 with respective lengths of 25, 50, and 75 feet. In addition to the ANSYS results and the design approximation, the limits for shear buckling and bend buckling for the 0.33 in. thick web have also been plotted. The curve for the unstiffened 25 foot long girder only had two points due to severe web buckling at a shear rigidity of 66 k/rad. There was actually significant web buckling with no deck which is evidenced by the large reduction in capacity when compared to the fully stiffened compact web. The capacity of the section in this case would be controlled by the AASHTO limit on shear buckling which occurred at a moment slightly smaller than 20000 k-in. For girder spans of 50 and 75 feet, the design approximation is conservative for the slender web for deck shear rigidities less than 660 kips/rad, however, buckling of the web causes the curve of the ANSYS results to posses a sharp plateau. The AASHTO limits on bend buckling would limit the capacity of the girder.

The results for girders with cross-sections slender #2 are shown in Figures 7.9a, 7.9b, and 7.9c for respective lengths of 25, 50, and 75 feet. For values of the shear rigidity less than 330 k/rad the design approximation does a very good job of predicting the capacity of the slender web girder. Buckling of the slender web causes the ANSYS curve to have a plateau. The AASHTO limits for web buckling would control the capacity of the section. Similar results were observed for the girders with spans of 50 and 75 feet, except that the ANSYS results level out at larger values of moment. In these cases, the shear rigidity of the deck has very little influence on the buckling load since web buckling controls the capacity.

Figures 7.10a, 7.10b, and 7.10c show plots of M_{cr} versus Q for the singly-symmetric girders slender #3 with respective spans of 25, 50, and 75 feet. For the 25 foot long girder, the design approximation does a very good job of approximating the capacity of the slender web girder for values of the shear rigidity less than 330 kips/rad; however, the web buckled for higher values of the shear rigidity. The AASHTO limit on bend buckling would control the bending capacity of the section. The limit on bend buckling also controlled the capacity of the 50 and 75 foot long girders. In most of the cases considered, the AASHTO limit on bend buckling is conservative. This is probably due to the moment gradient in the panel.

In general, the approximate formula for loading at midheight did a very good job of estimating the capacity of the partially stiffened girders. For the slender web girders, the capacity was typically controlled by the bend buckling capacity of the section.

**Figure 7.9a: Mcr versus Q for fully stiff. section #2 and part. stiff slender #2
L= 25', P @ CL midheight- ANSYS results and Estimate Eqn. 7.4.**
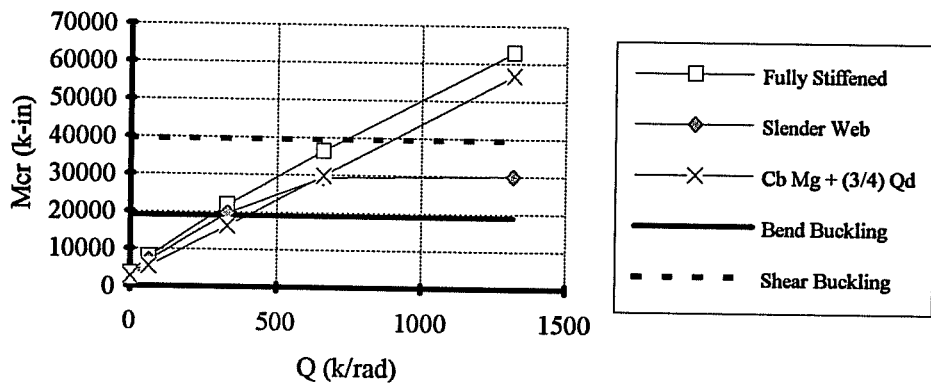
**Figure 7.9b: Mcr versus Q for fully stiff. section #2 and part. stiff slender #2
L= 50', P @ CL midheight- ANSYS results and Estimate Eqn.7.4.**
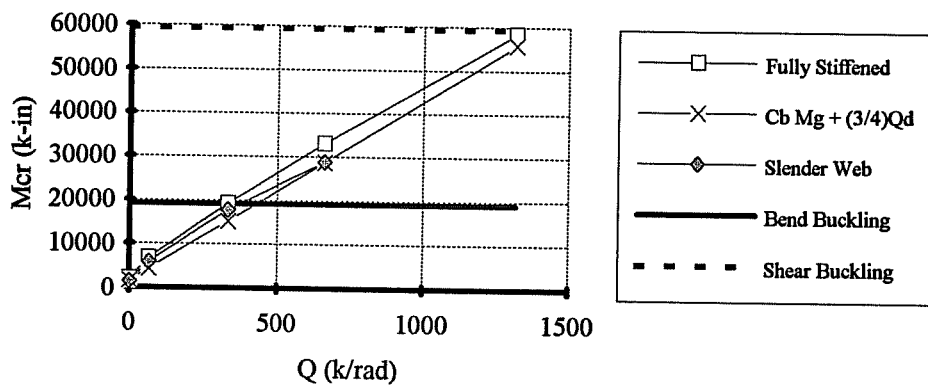
**Figure 7.9c: Mcr versus Q for fully stiff. section #2 and part. stiff slender #2
L= 75', P @ CL midheight- ANSYS results and Estimate Eqn.7.4.**
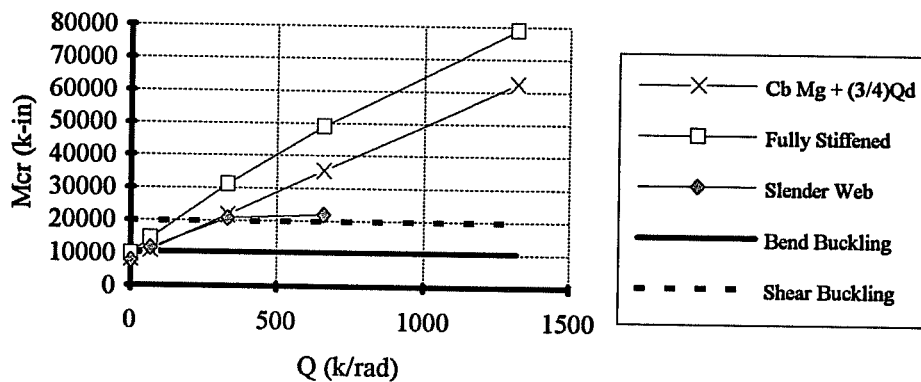
Figure 7.10a: Mcr versus Q for fully stiff. section #3 and part. stiff slender #3 L= 25', P @ CL midheight- ANSYS results and Estimate Eqn. 7.4.
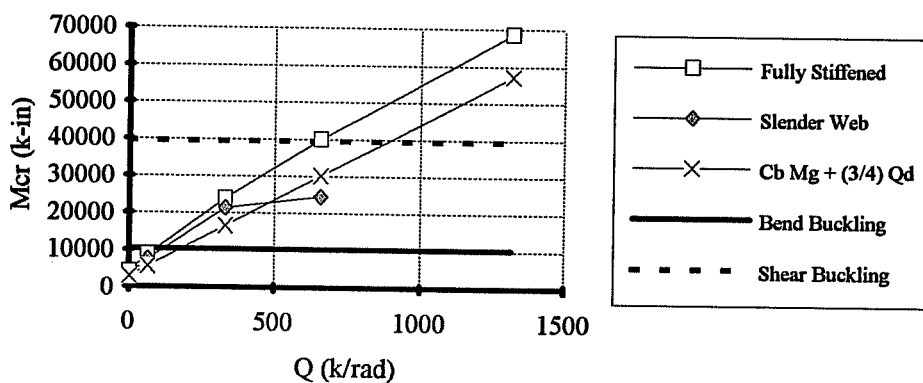
Figure 7.10b: Mcr versus Q for fully stiff. section #3 and part. stiff slender #3 L= 50', P @ CL midheight- ANSYS results and Estimate Eqn.7.4.
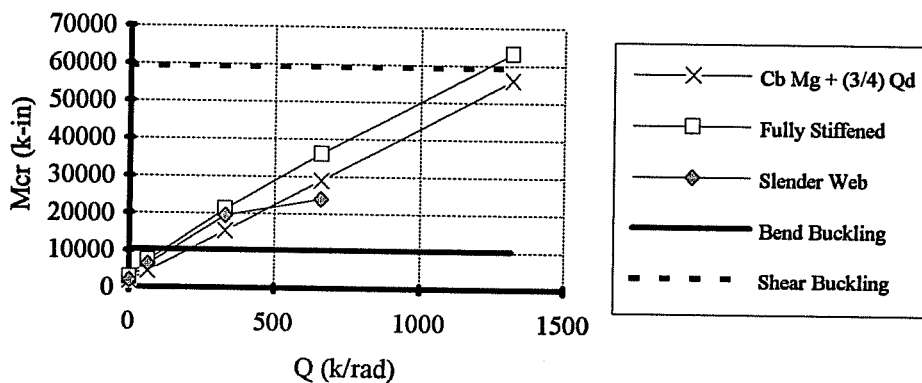
Figure 7.10c: Mcr versus Q for fully stiff. section #3 and part. stiff slender #3 L= 75', P @ CL midheight- ANSYS results and Estimate Eqn.7.4.

7.5 Finite Element Results for Partially Stiffened Girders with Top Flange Loading

This section presents the ANSYS results for partially stiffened girders subjected to transverse loading applied at the top flange. It was shown in Chapter 6 that good estimates of the buckling load with top flange loading could be obtained using the design approximation shown in Equation 7.5.

$$M_{cr} = C_b^* \, M_{AASHTO} + \frac{1}{2} \, Qd \qquad (7.5)$$

The variables in Equation 7.5 are the same as presented for Equation 7.4 with the exception of C_b^* which is the moment magnifier for top flange loading and can be calculated using the method in the SSRC Guide which was outlined in Chapters 2 and 4.

Figures 7.11a and 7.11b show Equation 7.5 plotted along with ANSYS results for the section slender #2. Equation 7.5 generally overestimated the buckling load of the partially stiffened and unstiffened webs. In order to account for effects of web distortions, the contribution of the deck was reduced by changing the factor on the deck term from 1/2 to 3/8. The resulting equation is shown in Equation 7.6.

$$M_{cr} = C_b^* \, M_{AASHTO} + \frac{3}{8} \, Qd \qquad (7.6)$$

Equation 7.6 will be plotted along with the ANSYS results for girders with partially stiffened webs. The results for the girders with the 0.625 inch web will be presented first. Similar to the previous section, moments causing web shear buckling or bend buckling will be indicated in the figures when the limits fall in the range of the lateral-torsional buckling capacity of the girders. The results from Chapter 6 with the heavily stiffened girders will be shown as a reference in the plots presented in this section. These girders will be referred to as "stiffened", while the partially stiffened girders with the 0.625 inch web will be referred to as "unstiffened".

Plots of M_{cr} versus Q for top flange loading on the doubly-symmetric section #1 are shown in Figures 7.12a, 7.12b, and 7.12c for respective lengths of 25, 50, and 75 feet. The shear and bend buckling load far exceed the lateral torsional buckling load for the stocky webs, so the these limits do not show up in the graphs. The unstiffened girder with a 25 foot length falls significantly below the curve for the fully stiffened girder, however the design approximation does a good job of estimating the buckling capacity. The large difference between the stiffened and
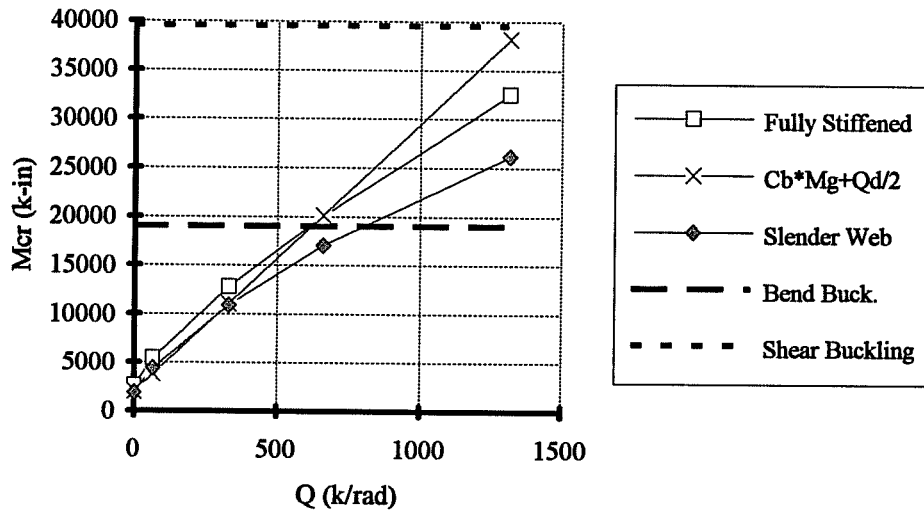
**Figure 7.11a: Mcr versus Q for fully stiff. section #2 and part. stiff slender #2
L= 50', P @ CL top flange- ANSYS results and Estimate Eqn. 7.5.**
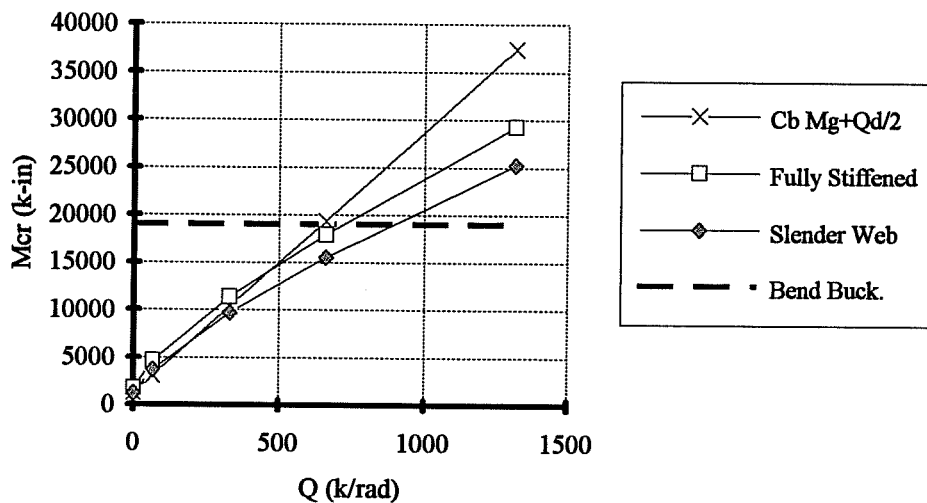
**Figure 7.11b: Mcr versus Q for fully stiff. section #2 and part. stiff slender #2
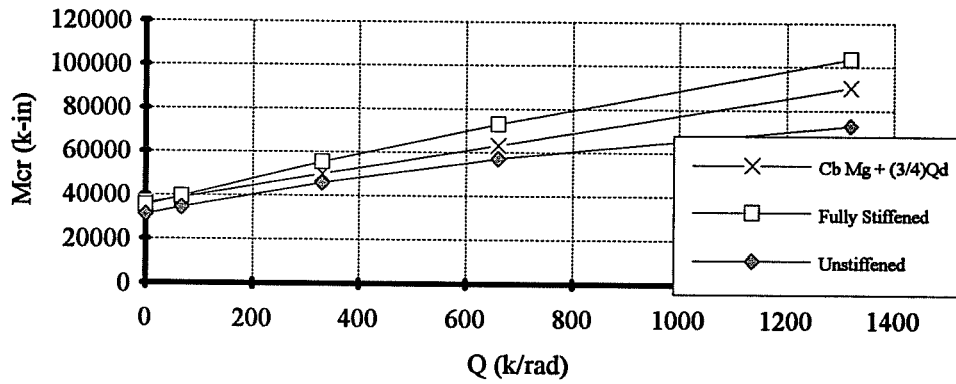L= 75', P @ CL top flange- ANSYS results and Estimate Eqn. 7.5.**
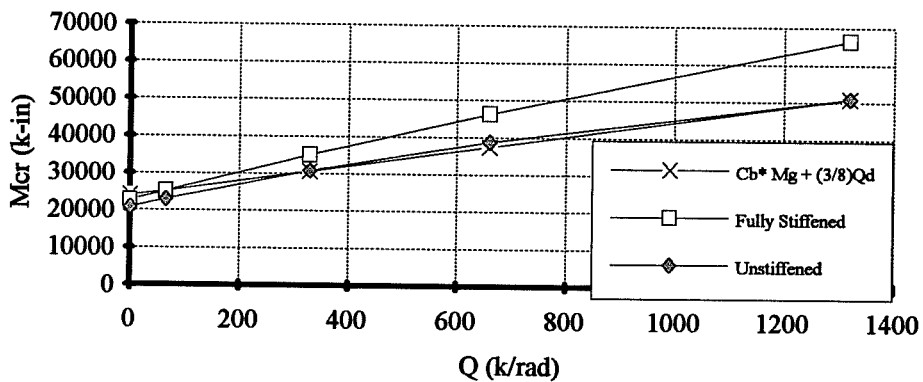
Figure 7.12a: Mcr versus Q for section #1 with 25' span and a point load applied at CL top flange - ANSYS results and Estimate.
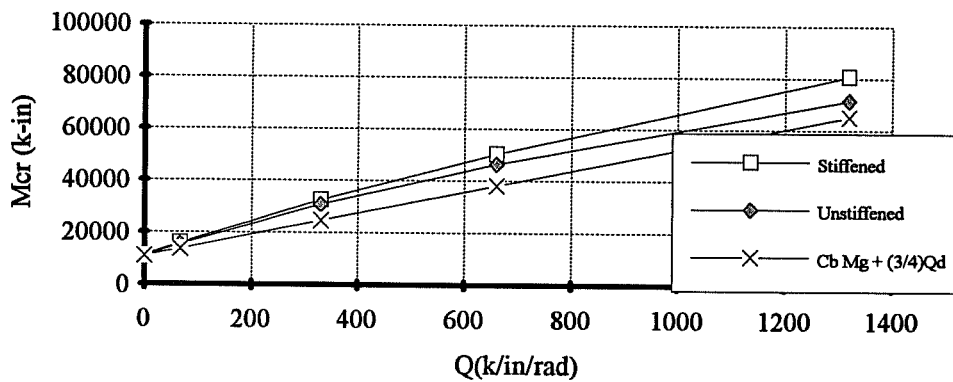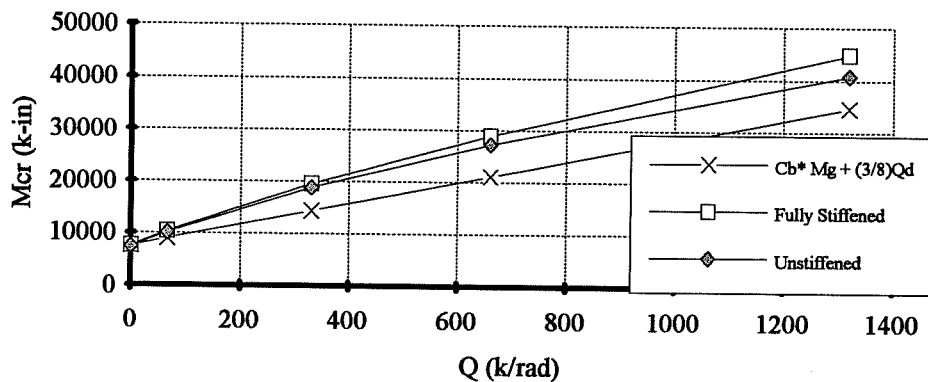

Figure 7.12b: Mcr versus Q for section #1 with 50' span and a point load applied at CL top flange- ANSYS results and Estimate.
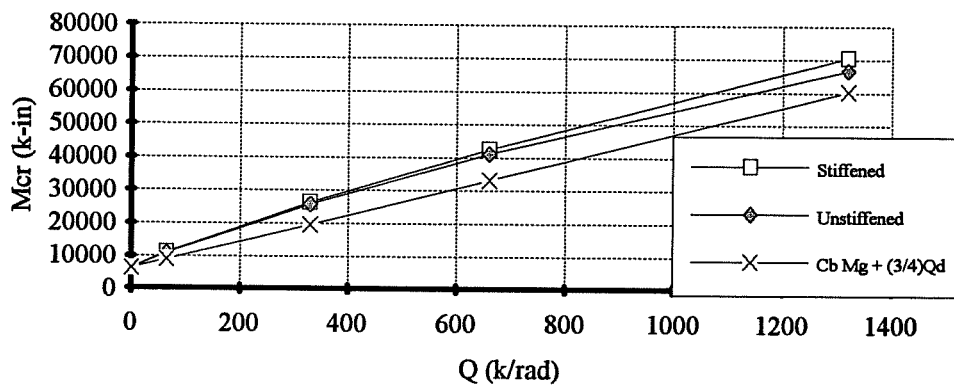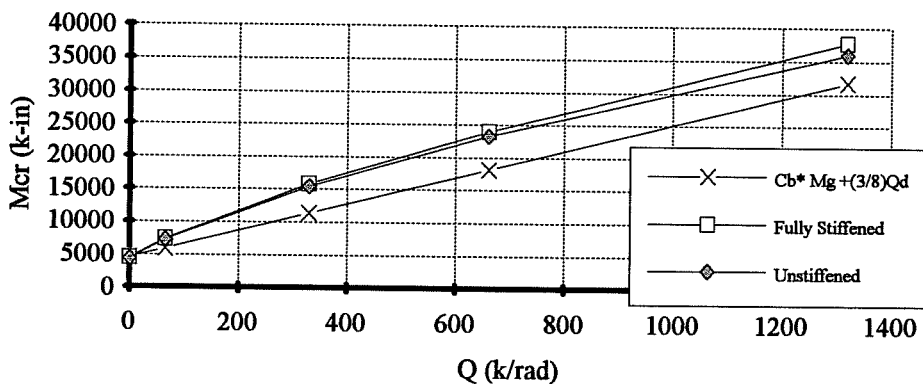

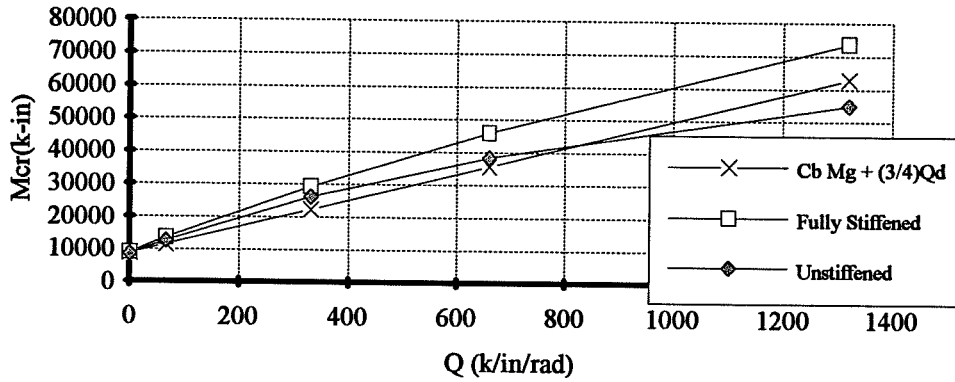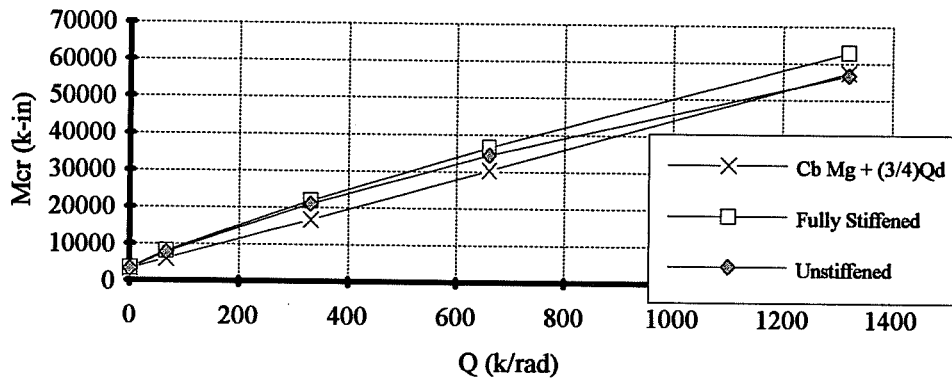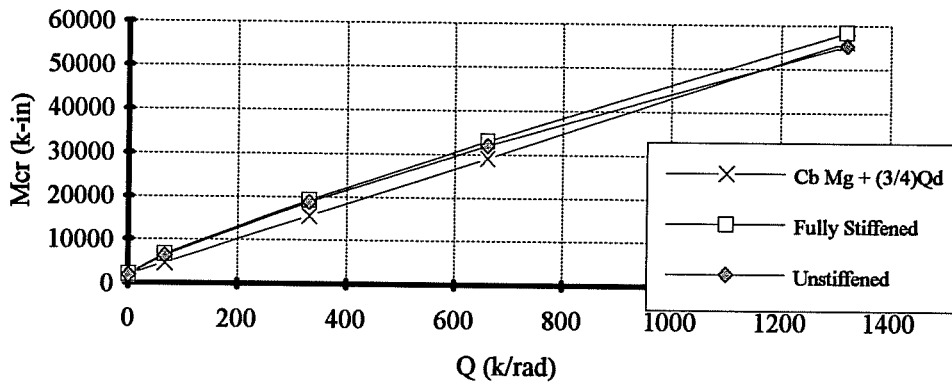**Figure 7.12c: Mcr versus Q for section #1 with 75' span and a point load applied at CL top flange- ANSYS results and Estimate.**

unstiffened case may be similar to the situation that was observed for the same cross-section in Section 7.4 which may have been caused by local effects around the load point. For the 50 and 75 foot long girders, the design approximation is conservative and falls well below both the curves for the unstiffened and stiffened girders.

Figures 7.13a, 7.13b,and 7.13c show plots of M_{cr} versus Q for top flange loading on section #2 with respective lengths of 25, 50, and 75 feet. For the 25 and 50 foot long spans, the design approximation is slightly conservative up until shear rigidities of 1320. For the 75 foot long span, the approximation is slightly unconservative for large shear rigidities, however it is very close.

The ANSYS results for the top flange loading on the singly-symmetric section #3 are shown in Figures 7.14a, 7.14b, and 7.14c for respective lengths of 25, 50, and 75 feet. Although the design approximation is slightly conservative, it does a good job of estimating the capacity of the girders for all three lengths.

In the remaining graphs in this section, the results for the thin web (0.33 in.) will be referred to as the "slender" web, while the results for the fully stiffened thick web (0.625 in.) will be referred to as the "fully-stiffened" web. Figure 7.15a, 7.15b, and 7.15c show plots of M_{cr} versus Q for the doubly-symmetric section slender #1 with respective lengths of 25, 50, and 75 feet. The curves for the limits for shear buckling and bend buckling have been plotted where applicable. The curve for the 25 foot long girder with the slender web had a very small slope due to web buckling. The capacity of the section in this case would be controlled by the AASHTO limit on shear buckling which occurred at a moment of approximately 19000 kip-in. The approximate solution was slightly conservative for the 50 and 75 foot long spans.

Figures 7.16a, 7.16b, and 7.16c show plots of M_{cr} versus Q for the doubly-symmetric section slender #2 with respective lengths of 25, 50, and 75 feet. For each of the three girder spans, the design approximation does a good job of estimating the buckling capacity of the system for deck shear rigidities less than about 660 kips/rad. For larger values of the deck shear rigidity, the girder webs begin to buckle which causes a reduction in the slope of the curves. This is not a problem, however, since the AASHTO limit on bend buckling would control the capacity of the section for all three girder lengths.

The results for the singly-symmetric girder with cross-section slender #3 are shown in Figures 7.17a, 7.17b, and 7.17c, for respective lengths of 25, 50, and 75 feet. The design approximation does a good job of estimating the buckling capacity for lower values of the shear
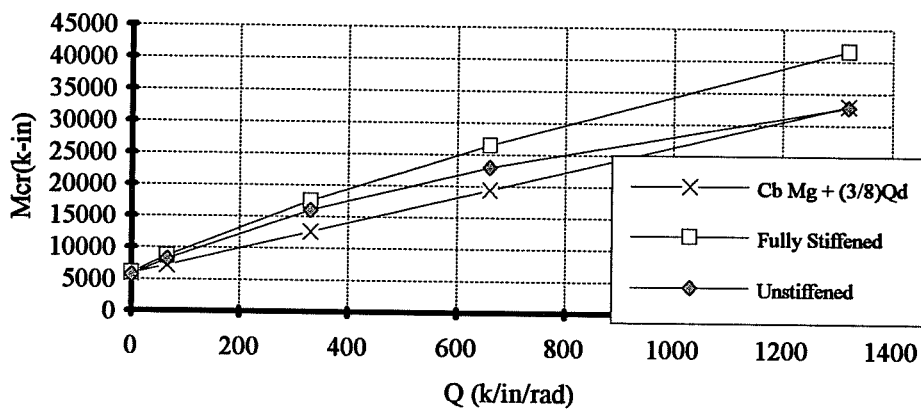
Figure 7.13a: Mcr versus Q for section #2 with 25' span and a point load applied at CL top flange - ANSYS results and Estimate.
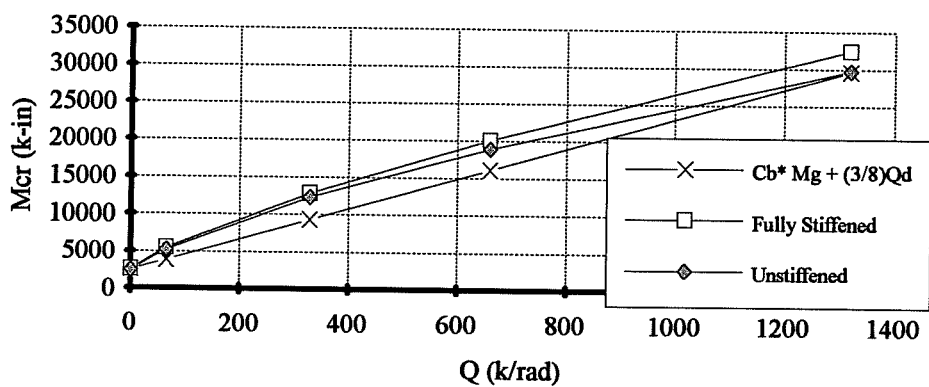
Figure 7.13b: Mcr versus Q for section #2 with 50' span and a point load applied at CL top flange- ANSYS results and Estimate.
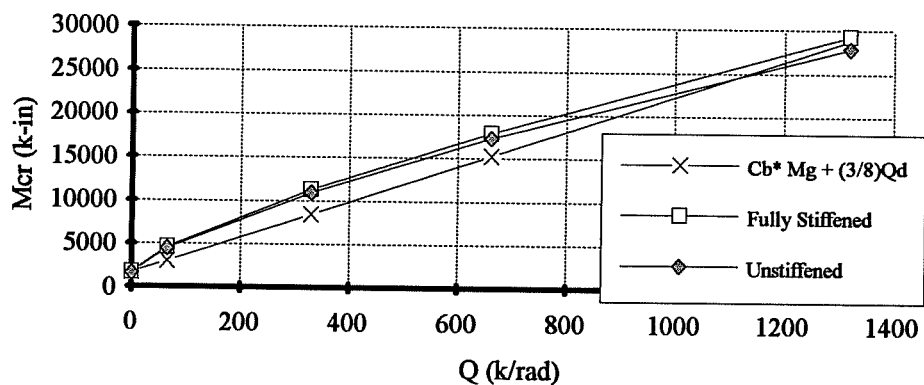
Figure 7.13c: Mcr versus Q for section #2 with 75' span and a point load applied at CL top flange- ANSYS results and Estimate.
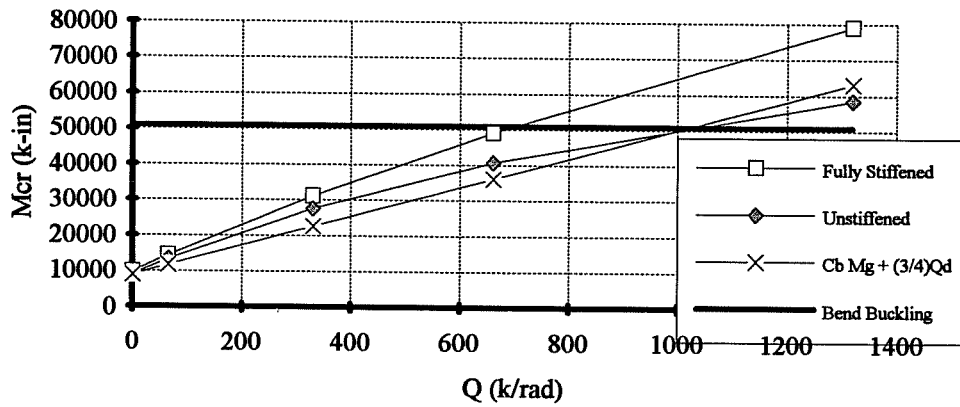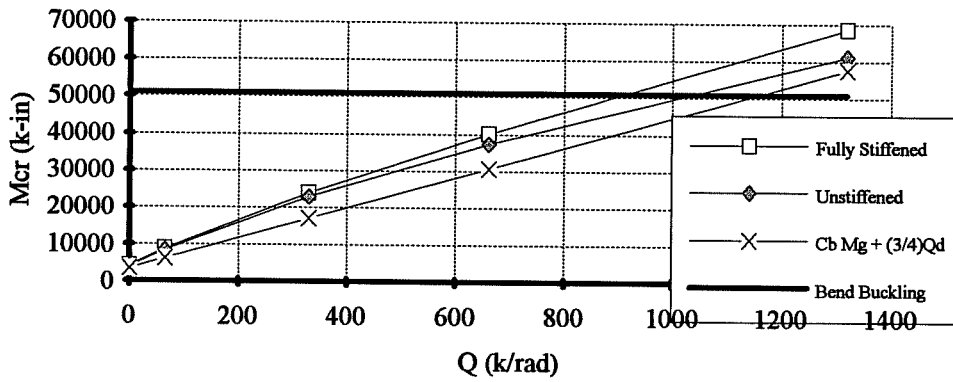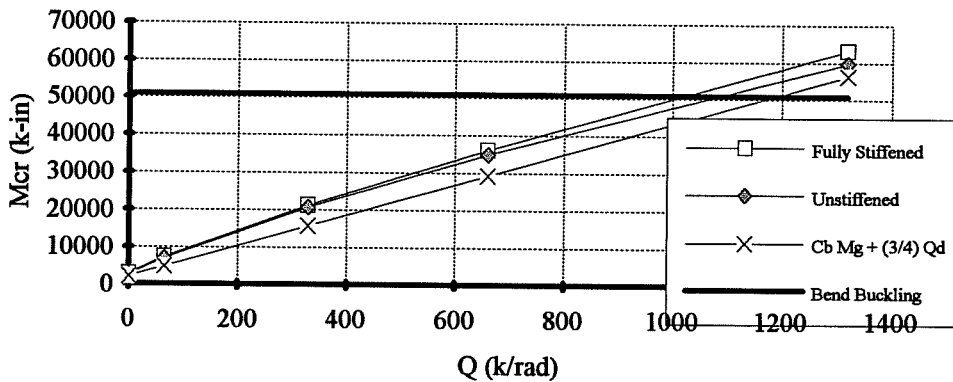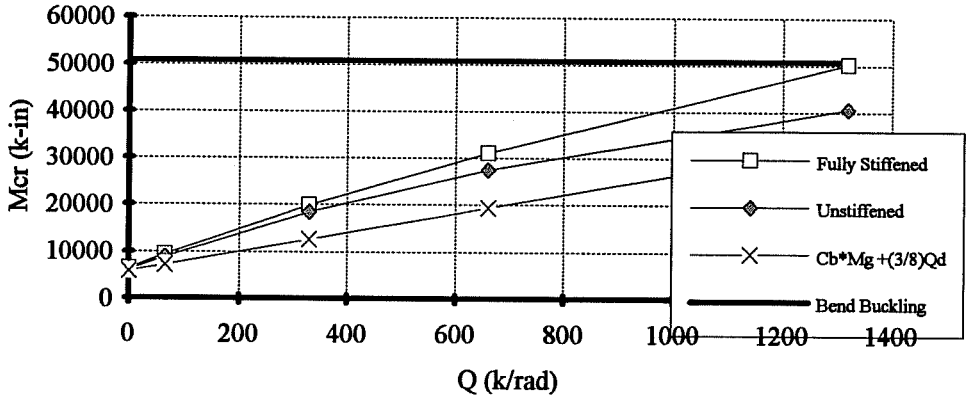
Figure 7.14a: Mcr versus Q for section #3 with 25' span and a point load applied at CL top flange - ANSYS results and Estimate.
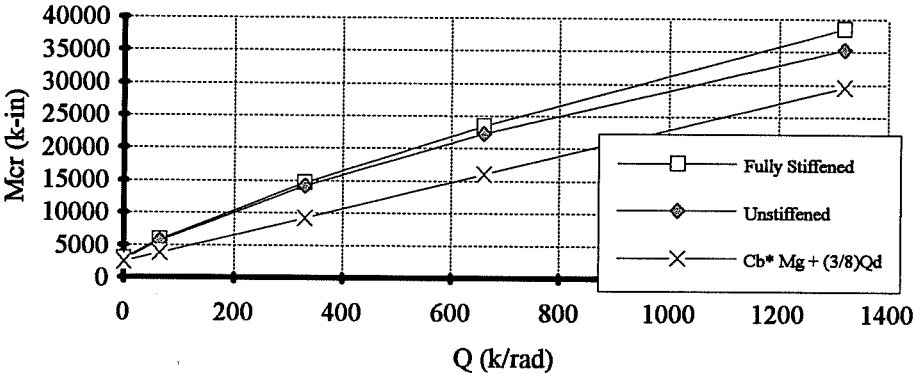
Figure 7.14b: Mcr versus Q for section #3 with 50' span and a point load applied at CL top flange- ANSYS results and Estimate.
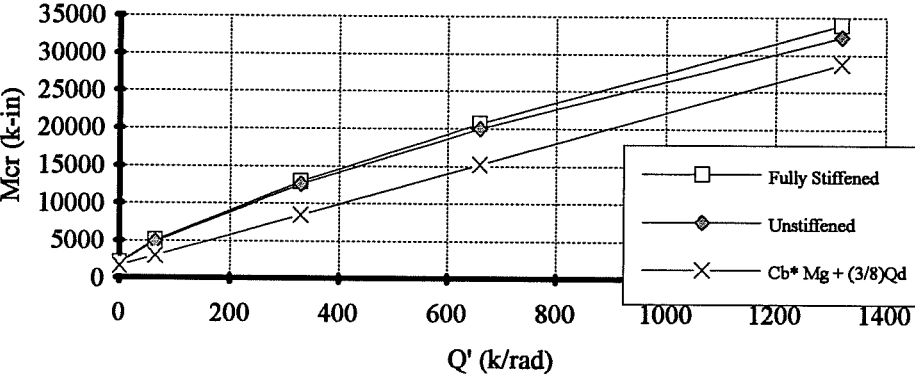
Figure 7.14c: Mcr versus Q for section #3 with 75' span and a point load applied at CL top flange- ANSYS results and Estimate.
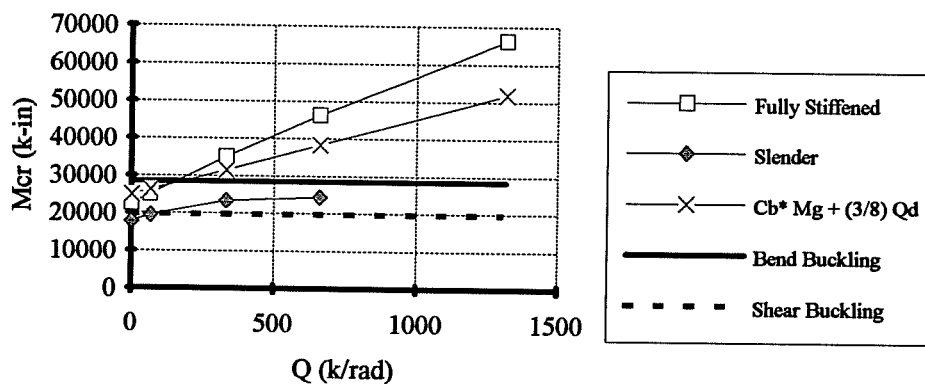
Figure 7.15a: Mcr versus Q for fully stiff. section #1 and part. stiff slender #1
L= 25', P @ CL top flange- ANSYS results and Estimate.
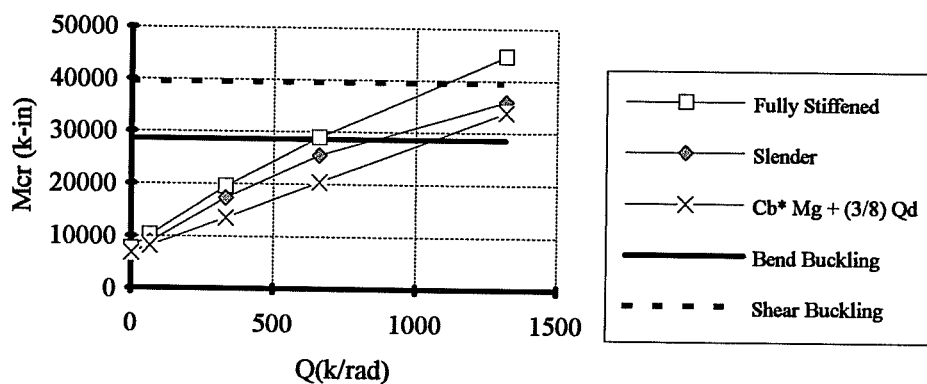
Figure 7.15b: Mcr versus Q for fully stiff. section #1 and part. stiff slender #1
L= 50', P @ top flange- ANSYS results and Estimate.
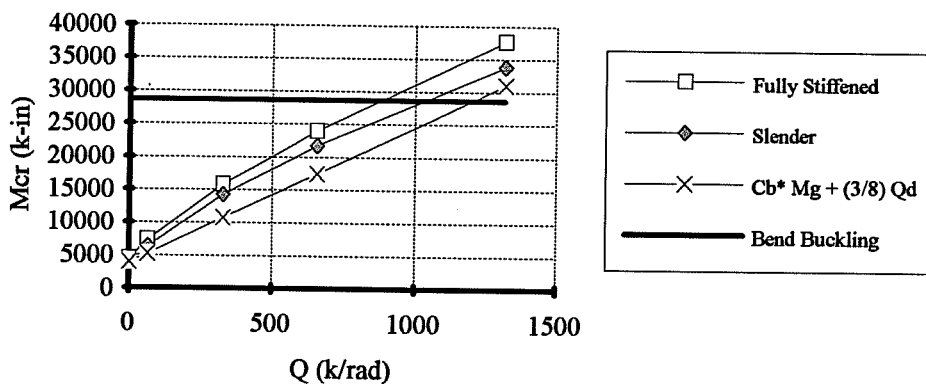
Figure 7.15c: Mcr versus Q for fully stiff. section #1 and part. stiff slender #1
L= 75', P @ CL top flange- ANSYS results and Estimate.
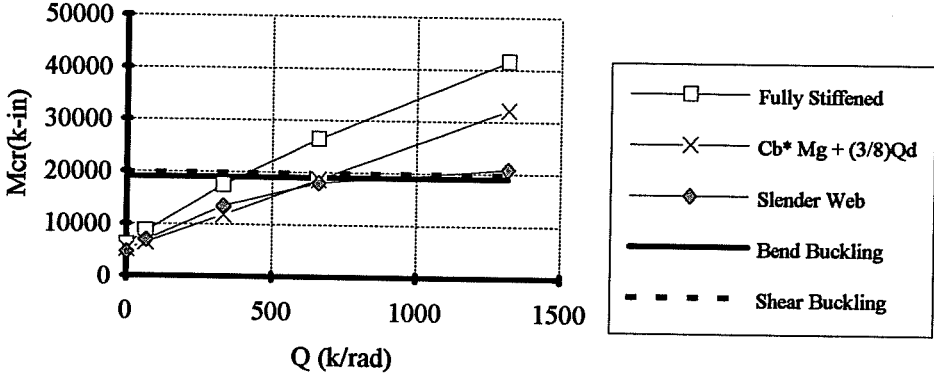
Figure 7.16a: Mcr versus Q for fully stiff. section #2 and part. stiff slender #2
L= 25', P @ CL top flange- ANSYS results and Estimate Eqn. 7.6.
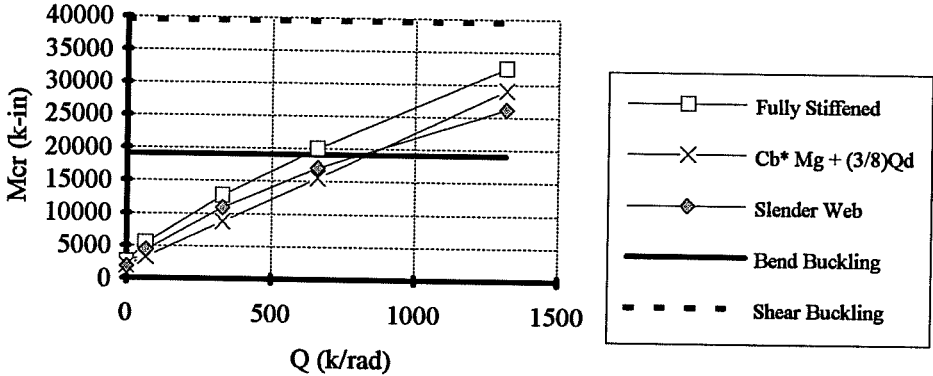
Figure 7.16b: Mcr versus Q for fully stiff. section #2 and part. stiff slender #2
L= 50', P @ CL top flange- ANSYS results and Estimate Eqn. 7.6.
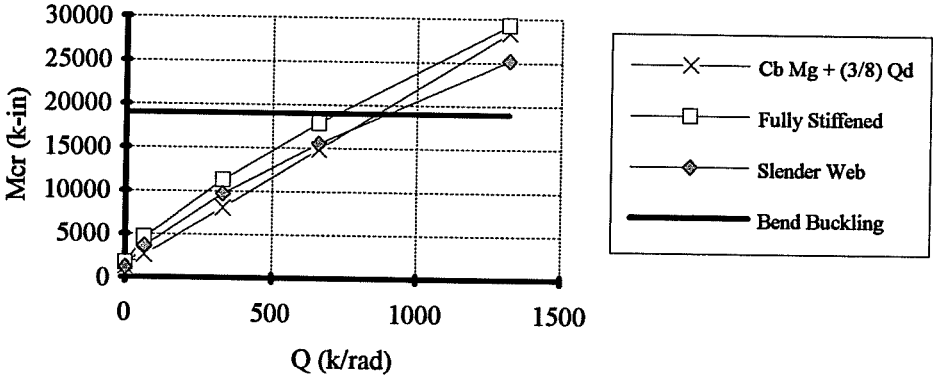
Figure 7.16c: Mcr versus Q for fully stiff. section #2 and part. stiff slender #2
L= 75', P @ CL top flange- ANSYS results and Estimate Eqn. 7.6.
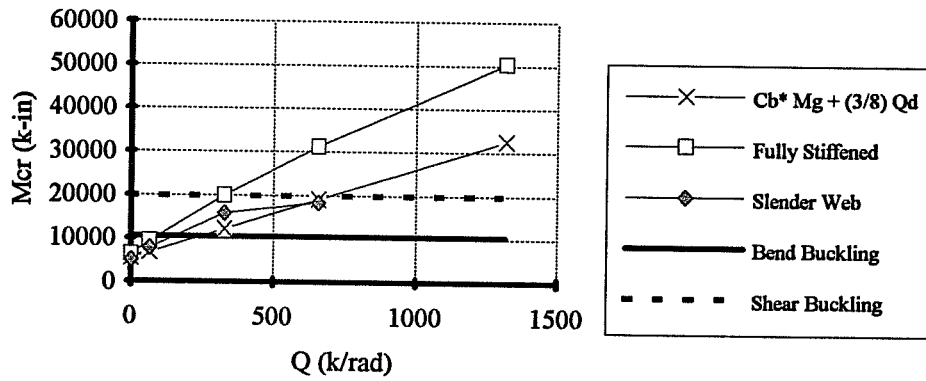
Figure 7.17a: Mcr versus Q for fully stiff. section #3 and part. stiff slender #3 L= 25', P @ CL top flange- ANSYS results and Estimate Eqn. 7.6.
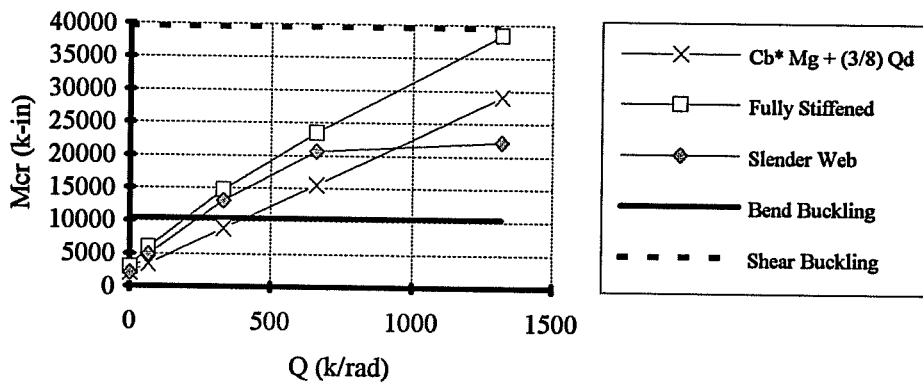
Figure 7.17b: Mcr versus Q for fully stiff. section #3 and part. stiff slender #3 L= 50', P @ CL top flange- ANSYS results and Estimate Eqn. 7.6.
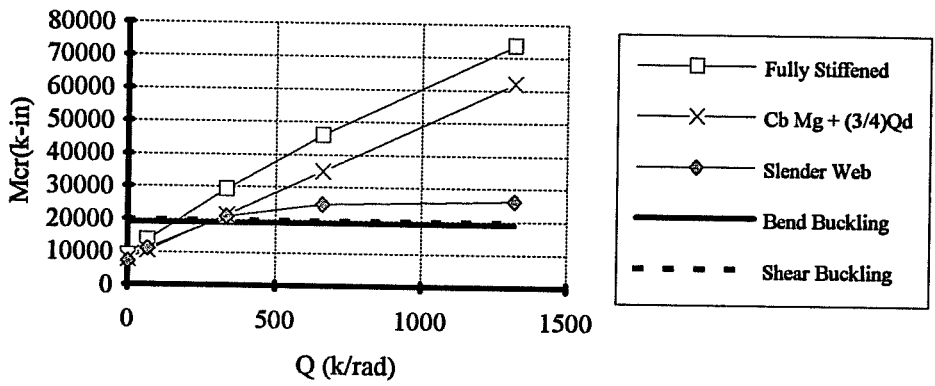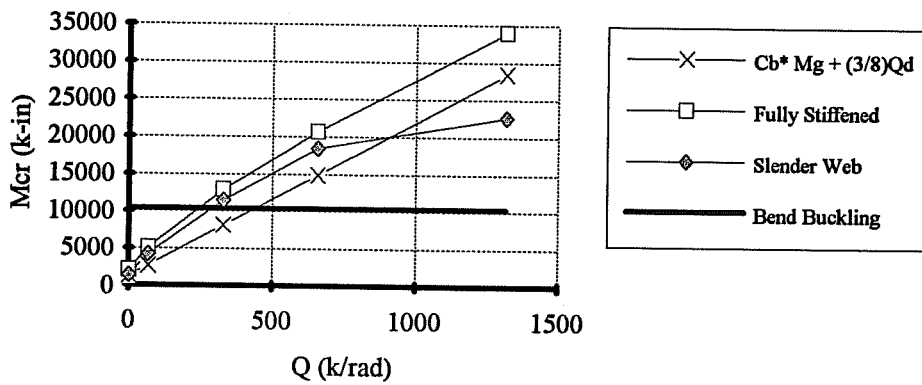

Figure 7.17c: Mcr versus Q for fully stiff. section #3 and part. stiff slender #3 L= 75', P @ CL top flange- ANSYS results and Estimate Eqn. 7.6.

rigidity until the web begins to buckle. The capacity would be limited by the bend buckling capacity of the section which is quite conservative for the 50 and 75 foot long girders.

7.6 Summary of Results on Partially Stiffened Girders

The finite element results which were presented in this chapter considered two web thicknesses: 0.625 in. and 0.33 in. The thicker web just met the AASHTO limits for compactness, while the slender web just met the extreme limit for webs without a longitudinal stiffener. The compact web was essentially unstiffened, while the slender web had transverse stiffeners spaced at 1.4 times the web depth. The finite element results for the girders with the unstiffened and partially-stiffened webs were compared with results from the girders from Chapters 5 and 6 which had a 0.625 in. thick web with stiffeners spaced at 18.75 in.

The lateral-torsional buckling capacity of the unstiffened compact web and the partially-stiffened slender web were lower than the capacity for the fully-stiffened compact web. The loss in capacity with the unstiffened webs and partially-stiffened webs was caused by two factors: cross sectional distortion, and web shear and bend buckling. In order to account for the loss in capacity due to web buckling, the maximum increase in the lateral-torsional buckling capacity provided by the deck was limited by the buckling capacity of the girder webs.

For many of the cases which were considered with relatively small values of the deck shear rigidity, the buckling mode was not clearly defined as either web buckling or lateral-torsional buckling, but was actually a combination of the two different types of buckling. In most of these cases, the web deformation was labeled as "web distortion". In general, the deck was less effective as a bracing element due to the web distortion. For transverse loading applied at midheight, the approximate solution, $M_{cr} = C_b M_{AASHTO} + (3/4) Qd$, produced reasonable estimates of the buckling capacity of the girders for most of the cases which were considered. For top flange loading, however, it was necessary to reduce the contribution of the deck from the solution used on fully-stiffened webs in order to account for cross-sectional distortion. The resulting expression consisted of $M_{cr} = C_b^* M_{AASHTO} + (3/8) Qd$, which typically resulted in conservative estimates of the buckling load. In the cases in which web buckling controlled the buckling mode, the AASHTO limits on web shear or bend buckling worked very well at limiting the capacity of the girder.

CHAPTER 8

Buckling Capacity of Continuous Girders Braced by a Shear Diaphragm

8.1 Introduction

This chapter will present finite element results for continuous girders braced by a shear diaphragm at the top flange. The results presented thus far have dealt with simply-supported girders braced by a shear diaphragm. The behavior of girders which were simply supported was relatively easy to understand since only one flange was in compression and the lateral-torsional buckling mode generally involved a large lateral translation of the compression flange. The buckling modes of continuous girders, on the other hand, are more complex because both flanges are prone to large lateral translations since each flange is subjected to compression at different regions along the girder length.

The main purpose of this chapter is to gain a better understanding of buckling of continuous girders with the top flange restrained. Lateral-torsional buckling of the support section of bridge girders, however, is not critical during the construction phase. The critical stage of the support section for buckling occurs in the completed bridge when the design traffic load is applied. The material presented in this chapter, however, will be applicable to the design of the support sections for lateral-torsional buckling since the top flange of the girders will be braced by the concrete deck at the critical stage.

This chapter has been divided into five sections. The effect of a shear diaphragm on the buckled shape of continuous girders will be outlined in Section 8.2. Buckling of girders with the top flange rigidly restrained laterally will be presented in Section 8.3. Finite element results which show the effect of a shear diaphragm connected to the top flange on the buckling capacity of continuous girders will be presented in Section 8.4. Finally, the results for continuous girders will be summarized in Section 8.5.

8.2 Buckling Modes of Continuous Girders with Diaphragm Bracing

The studies on simply supported girders demonstrated that for many loading conditions, when the deck was introduced as a bracing element, there was a significant change in the buckling mode. Changes in the buckling mode, usually reduced the effectiveness of the deck to act as a bracing element. It is very important, therefore, to study the effect that the deck has on the

244

buckling mode of continuous girders. The study of continuous girders will make use of the three girder cross-sections which have been used extensively in the previous chapters. The three sections are shown in Figure 8.1. Two different spacings of transverse stiffeners were considered. In one of the modeling schemes, transverse stiffeners were spaced at 18.75 inches, which will be referred to as the "fully stiffened" case. In addition, transverse stiffeners were also placed only at the locations of cross-frames, which will be referred to as the "unstiffened" case.

Buckling of continuous girders is more complex than for simply supported girders due to the distribution of moment along the girder length. Figure 8.2 shows a three-span continuous girder which has been subjected to a uniform distributed load. Interior spans of the continuous girder were modeled with rotations fixed at both ends, while the exterior spans were modeled as a propped cantilever. Both of these cases are shown below the three-span girder in Figure 8.2. In all cases considered, the girders were free to warp at the supports.

With no deck as a bracing element, the top flange will usually dominate the buckled shape. Even though the maximum compressive stress in the top flange is usually significantly smaller than the compressive stress in the bottom flange at the support, the top flange often controls the buckled shape due to a longer laterally "unsupported" length and smaller moment gradient.

This is demonstrated in Figure 8.3a which shows the lateral displacement of the top flange, midheight, and the bottom flange for section #1 with a 75 foot span and the in-plane boundary conditions of a propped cantilever. The webs of the girders were fully stiffened, and there were no cross-frames or deck for bracing within the span. The applied loading consisted of a uniform distributed load applied at the top flange. The bottom flange displaced laterally a small amount, while the top flange displacement was significantly larger.

When bracing is provided by a shear diaphragm at the top flange, there is a significant change in the buckled shape of the girders with increasing deck shear rigidity. The deck is very effective at restraining the top flange of the girder from displacing laterally, however it has very little effect on the bottom flange. As the shear rigidity of the deck is increased, the buckling mode will change from being dominated by the top flange to being dominated by the lateral displacement of the bottom flange. This is demonstrated in Figure 8.3b which shows the lateral displacement of the top flange, midheight, and bottom flange of the same girder considered in Figure 8.3a. In this case, however, a deck with a shear rigidity of 1320 k/rad was used as a
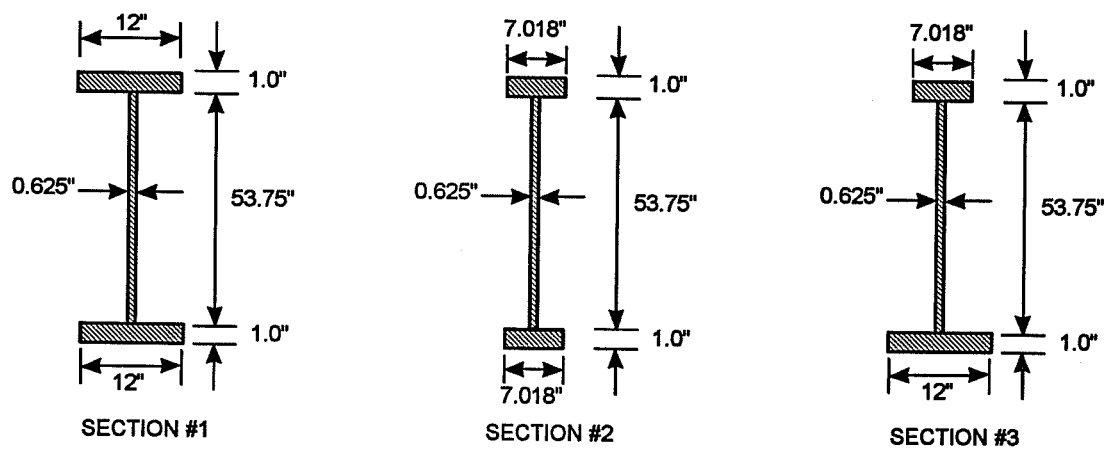
Figure 8.1 Cross-sections with compact web considered in computational study.

$$\frac{9}{128} \, wL_e^2$$

$$\frac{wL_e^2}{8}$$
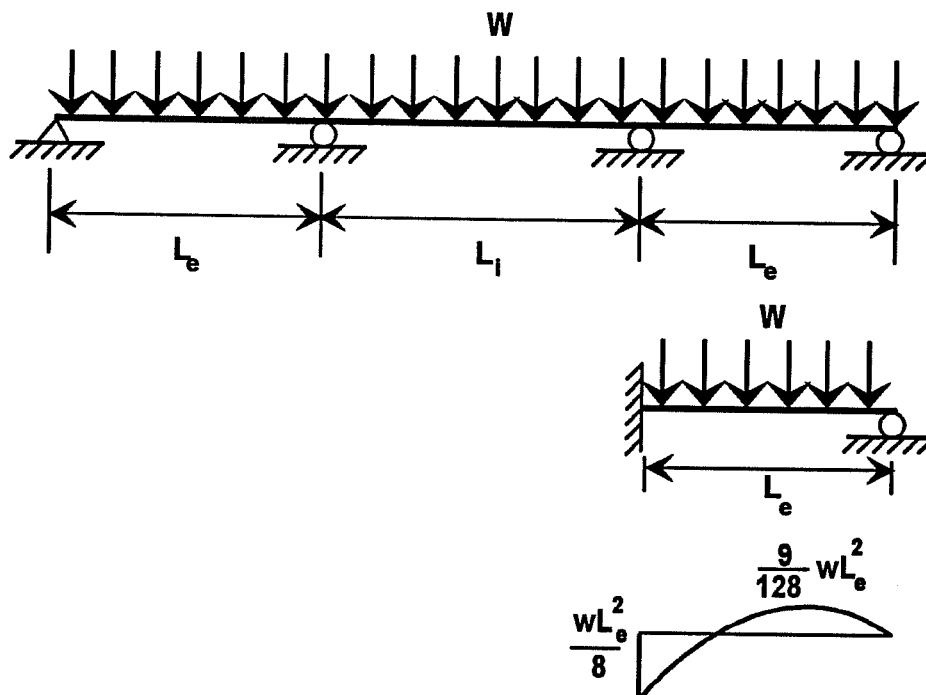
**CASE #1: Exterior span modeled
as a propped cantilever.**

$$\frac{wL_i^2}{24}$$

$$\frac{wL_i^2}{12}$$

$$\frac{wL_i^2}{12}$$
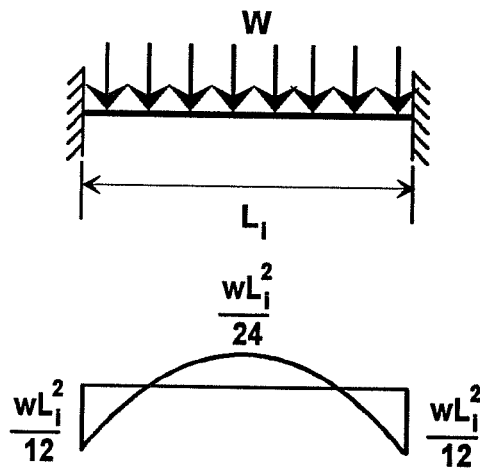
**CASE #2: Interior span modeled
with both ends fixed.**

Figure 8.2 Modeling of continuous girders.
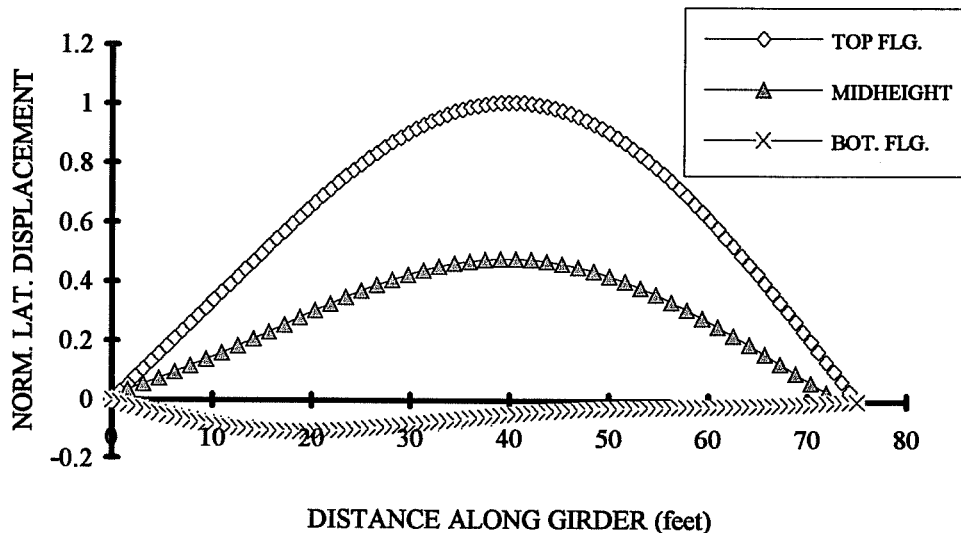
Figure 8.3a Lateral displacement of section #1, fully stiff. propped cantilever
L=75', Q=0, w @ top flange.
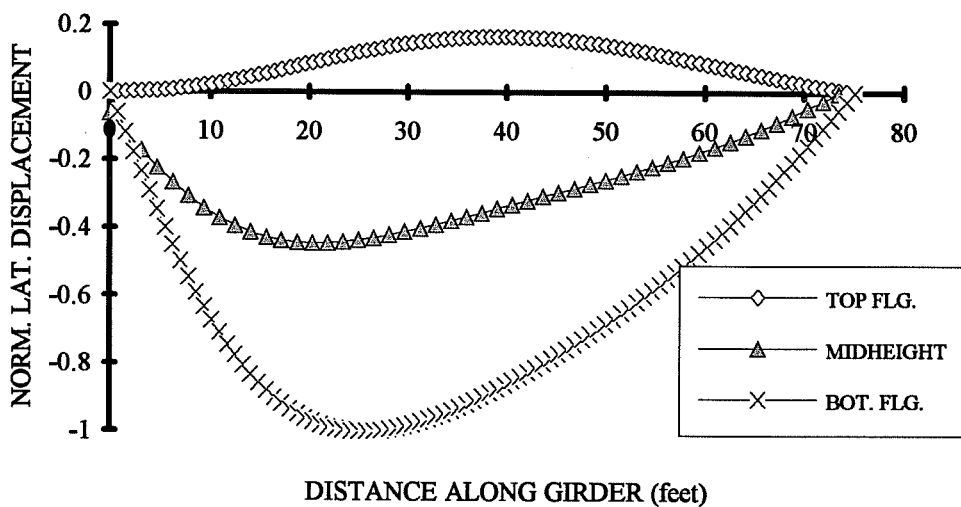
Figure 8.3b Lateral displacement of section #1, fully stiff. propped cantilever
L=75', Q=1320, w @ top flange.

bracing element. The buckling mode is dominated by the lateral displacement of the bottom flange, while the displacement of the top flange is relatively small.

When discrete bracing was introduced to the system, similar behavior was observed for increasing deck shear rigidities. Figure 8.4a shows the lateral displacements for section #2 with boundary conditions of a propped cantilever and cross-frames at the third points; however there was no deck for bracing. The girder was subjected to a distributed load at the top flange, and the web of the girder was fully stiffened. The buckling mode is controlled by the lateral displacement of the top flange near midspan and also at the exterior support (support with zero moment). The lateral displacement of the bottom flange, on the other hand, is relatively small. When the deck is introduced as a bracing element, the buckling mode changes significantly. This is demonstrated in Figure 8.4b for the same girder considered in Figure 8.4a, except that a deck with a shear rigidity of 66 k/rad was used for bracing. The rigidity of the deck is actually relatively small, however, the effect on the buckled shape is significant. The lateral displacement of the top flange is reduced a great deal while the lateral displacement of the bottom flange at the fixed end dominates the buckling mode. With increasing shear rigidity of the deck, the lateral displacement of the top flange would be reduced further, however, the displacement of the bottom flange would essentially be unaffected.

Similar results were observed for girders with both ends fixed against in-plane rotations. Figure 8.5a shows the lateral displacements for the singly-symmetric section #3 with both ends fixed against in-plane rotation. The web was fully-stiffened. There was no deck provided for bracing, however, there is a cross-frame at midspan. The buckling mode is dominated by the lateral displacement of the top flange, while the bottom flange has very little lateral displacement. When the deck was introduced as a bracing element, the buckling mode changed considerably with increasing deck shear rigidity. Figure 8.5b shows a plot of the lateral displacement for the same section #3 considered in Figure 8.5a, however, a deck shear rigidity of 330 k/rad was employed. For this deck shear rigidity, the top and bottom flange essentially buckled simultaneously which is evidenced by nearly identical maximum lateral displacements of the two flanges. When the deck rigidity was further increased, the lateral displacement of the top flange was further restrained while the bottom flange was unrestrained. This is shown in Figure 8.5c which shows results for the same girder system used in Figures 8.5a and 8.5b, however, the deck shear rigidity was increased to 1320 k/rad. In this case, the lateral displacement of the bottom flange dominated the buckling mode, while the lateral displacement of the top flange was relatively small. In Section
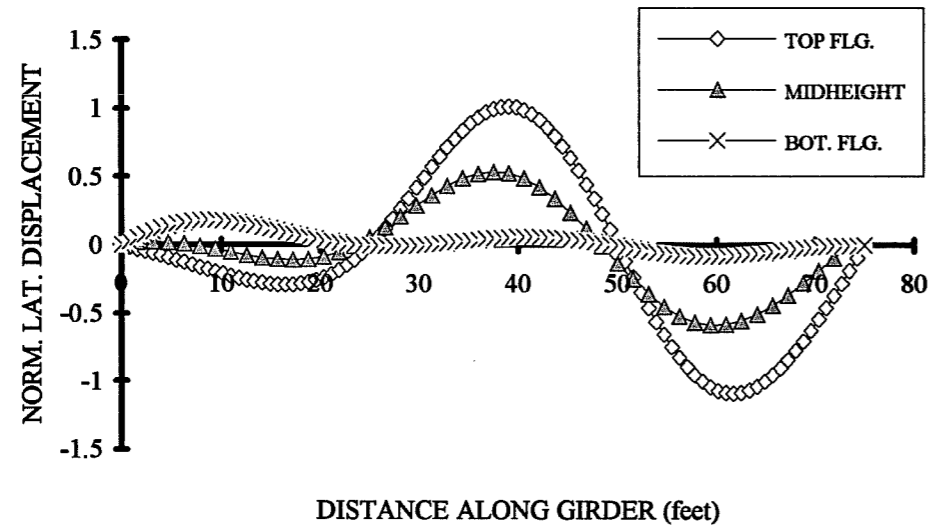
Figure 8.4a Lateral displacement of section #2, fully stiff. propped cantilever
L=75', Lb=25', Q=0, w @ top flange.
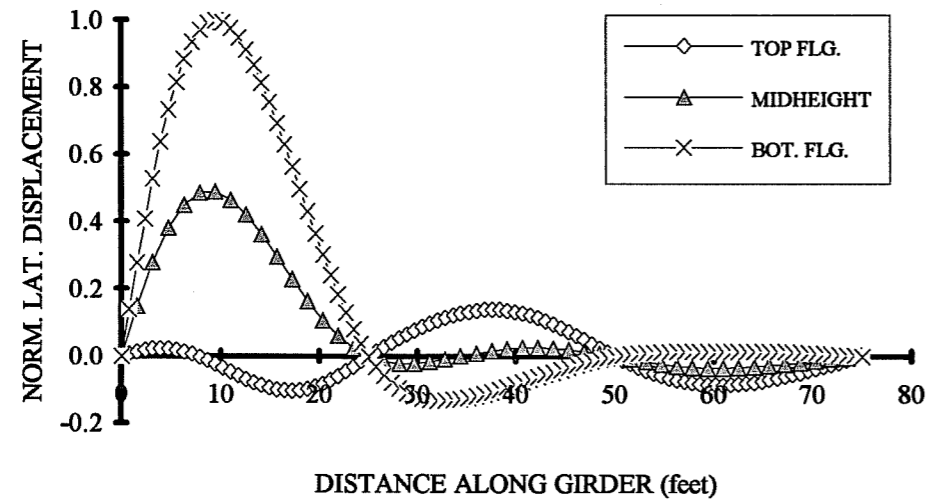
Figure 8.4b Lateral displacement of section #2, fully stiff. propped cantilever
L=75', Lb=25', Q=66, w @ top flange.
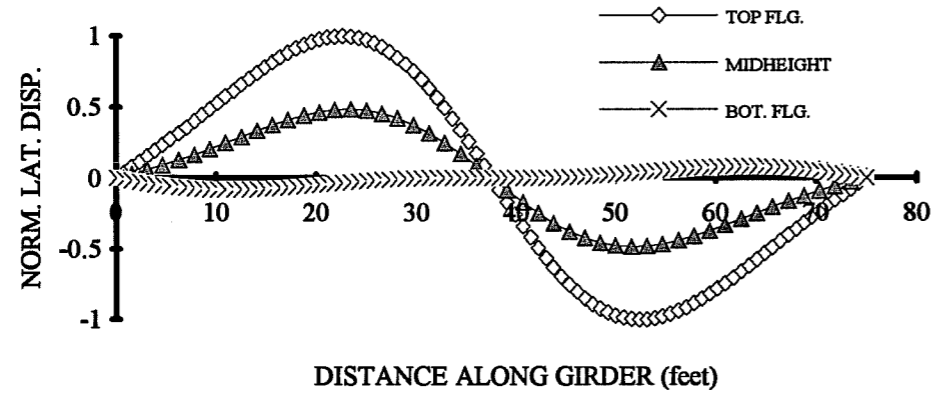
Figure 8.5a Lateral displacement of section #3, fully stiff. fixed-ended girder
L=75', Lb=37.5', Q=0, w @ top flange.
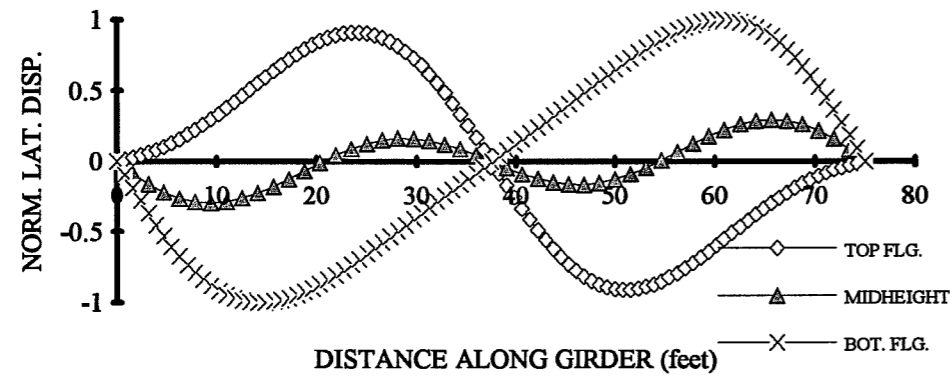
Figure 8.5b Lateral displacement of section #3, fully stiff. fixed-ended girder
L=75', Lb=37.5', Q=330, w @ top flange.
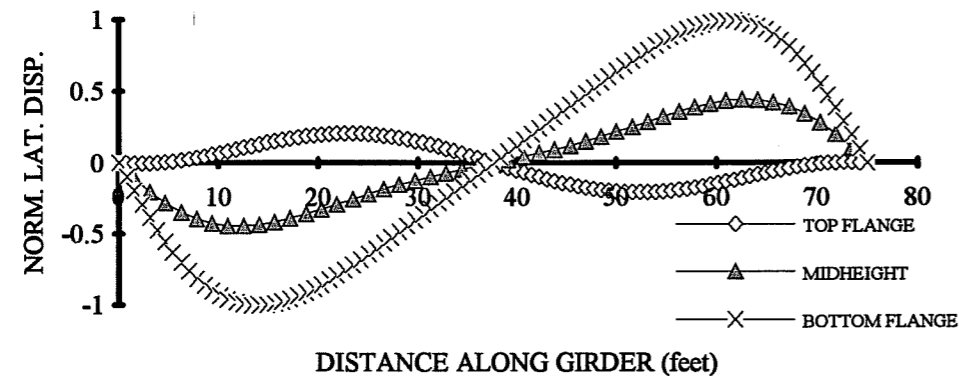
Figure 8.5c Lateral displacement of section #3, fully stiff. fixed-ended girder
L=75', Lb=37.5', Q=1320, w @ top flange.

8.4 the finite element results will show that when the top flange controls the buckling mode, increasing the deck shear rigidity causes a corresponding increase in the buckling capacity.

The buckling modes for girders with unstiffened webs versus stiffened webs were similar in terms of the displaced shapes of the flanges. For cases with no deck or cases with relatively small deck shear rigidities, the buckling mode was dominated by the top flange, while the bottom flange experienced relatively small lateral displacements. When the shear rigidity was increased, however, the bottom flange displacements typically dominated the buckling mode and the top flange displacements were relatively small.

Although the behavior of the buckled shapes of the flanges did not change a great deal, the webs of the unstiffened girders did experience a significant amount of distortion as the shear rigidity of the deck was increased. This is shown in Figure 8.6a for the singly-symmetric section #3 with ends fixed against in-plane rotations. The web of the girder in Figure 8.6a is unstiffened, and the girder has cross-frames at the third points and a deck shear rigidity of 1320 k/rad. The overall buckling mode is controlled by the lateral displacement of the bottom flange. In addition there is a significant amount of web distortion near the supports and also at the cross-frames at the third points. The influence of the transverse stiffeners upon web distortion are shown in Figure 8.6b which shows the lateral displacement of the midheight web nodes for the unstiffened and fully stiffened 0.625 in. thick webs at a deck shear rigidity of 1320 k/rad. Web distortions in the fully stiffened web are controlled with the closely spaced stiffeners, however, the unstiffened web has a significant amount of distortion. The distortions in the unstiffened web are most prevalent at the supports and also at the cross-frames at the third points (25 feet and 50 feet). Although the web distortions in the unstiffened web in Figures 8.6a and 8.6b may not be due to buckling of the web, bend buckling and shear buckling must be considered as a limit to the girder capacity. In order to control web buckling, the increase in lateral-torsional buckling capacity that the deck causes must be limited to the web shear and bend buckling capacity. These limits will be identical to the those applied to the girders with the partially stiffened and unstiffened webs in Chapter 7.

8.3 Buckling Capacity of Continuous Girders with Full Lateral Restraint of Top Flange

The results which were covered in Section 8.2 showed that the buckling mode of continuous girders can change significantly when the deck is used as a bracing element. The top flange will control the buckling capacity of the section for many cases when the deck is not used
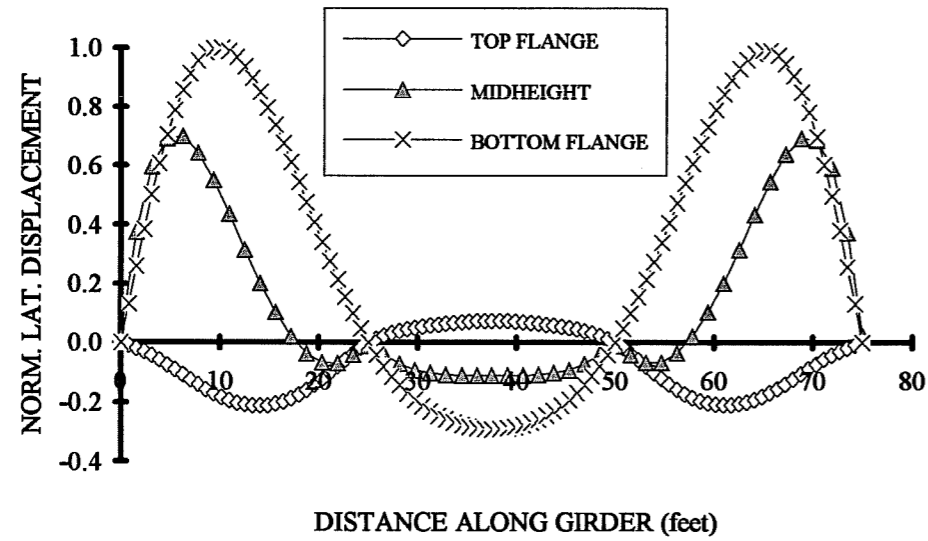
Figure 8.6a Lateral displacement of section #1, unstiffened fixed-ended girder
L=75', Lb=25', Q=1320, w @ top flange.
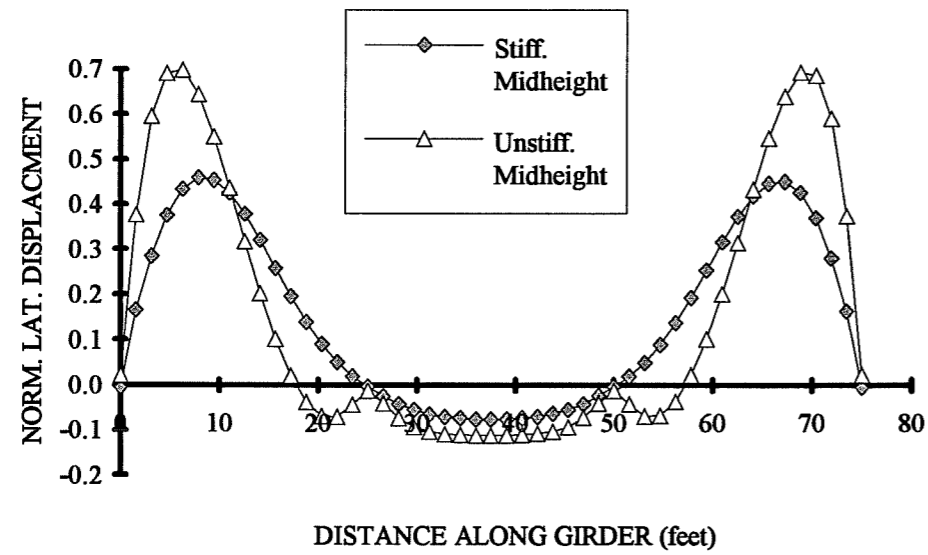
Figure 8.6b Comparing lateral disp. of section #1 midheight nodes, fixed-ended girder
Fully stiff. vs. unstiffened webs, L=75', Lb=25', Q=1320, w @ top flange.

for bracing, or when a deck with a small shear rigidity is utilized. When a deck with sufficient shear rigidity is employed, on the other hand, the buckling mode will change and the buckling capacity will be controlled by the bottom flange.

In cases in which the buckled shape of the girders was controlled by the bottom flange, the girders behave in a manner similar to girders with the top flange restrained from lateral displacement along the girder length. It was mentioned in Chapter 2 that Yura [25] has presented a formula for the moment gradient factor, C_b, for continuous girders which have the top flange rigidly braced from lateral displacement along the girder length and transverse loading applied at the top flange. In this case, the buckling mode only involves lateral displacement of the bottom flange. The equation for the C_b value is shown in the following expression:

$$C_b = 3.0 - \frac{2}{3}\left(\frac{M_1}{M_0}\right) + \frac{8}{3}\frac{M_{cl}}{\left(M_0 + M_1^*\right)} \qquad M_1^* \text{ is explained below} \qquad (8.1)$$

The buckling moment which the C_b in Equation 8.1 is to be applied to is the moment at the fixed end. Equation 8.1 is for a girder segment with full bracing at the ends, subjected to a moment causing compression in the bottom flange at one or both ends. M_0 and M_1 are the two end moments, while M_{cl} is the moment at the centerline of the beam segment. In the equation, M_0 will always cause compression in the bottom flange, while M_1 may or may not cause bottom flange compression. If both end moments cause compression in the bottom flange, the value of M_1 in the denominator of the last term is taken as zero. The M_1 which would be taken as zero if both end moments cause compression in the bottom flange has been marked with an asterisk. The C_b resulting from Equation 8.1 is to be applied to the buckling moment of the girder treating the bottom flange as the compression flange (i.e. apply the C_b to M_{AASHTO} treating the bottom flange as the compression flange).

In order to check the accuracy of Equation 8.1, finite element analyses were conducted on girders with the top flange rigidly restrained along the girder length from lateral movement with a distributed load applied at the top flange. The in-plane boundary conditions which were used consisted of a propped cantilever and also both ends fixed from rotation. The corresponding C_b value from the ANSYS results can be calculated using Equation 8.2.

The value of $M_{Top\ Fix}$ which is used in Equation 8.2 is the buckling moment for a girder with the top flange supported laterally along the entire girder length and a distributed load applied

$$C_{b \; ANSYS} = \frac{M_{Top \; Fix}}{M_{Constant \; Moment}} \qquad (8.2)$$

at the top flange. The value of the buckling moment for $M_{Top \; Fix}$ is the maximum moment causing compression in the bottom flange. For a propped cantilever, $M_{Top \; Fix}$ corresponds to "$W_{cr} L^2/ 8$", with W_{cr} defined as the distributed load causing buckling, while L is equal to the girder span. For a girder with both ends fixed from in-plane rotation, the value of $M_{Top \; Fix}$ corresponds to "$W_{cr} L^2/ 12$". The value of $M_{Constant \; Moment}$ corresponds to the buckling moment causing uniform compression in the bottom flange. $M_{Constant \; Moment}$ was obtained in the finite element studies by subjecting a simply supported girder, with no deck for bracing, to a constant moment which caused compression in the bottom flange.

Table 8.1 shows a comparison of Equation 8.1 and the ANSYS results for girders with boundary conditions of a propped cantilever and the lateral displacement of the top flange rigidly supported along the girder span. The web of the girder was fully stiffened and there were three different cases of discrete bracing considered (cross-frame locations). Three different cross-frame locations were considered because these change the unbraced length of the bottom flange. Since the unbraced length changes, $M_{Constant \; Moment}$ changes and the moment gradient also changes.

Table 8.1 Comparison of C_b Values from ANSYS Results and Eqn. 8.1 for Fully-Stiffened Propped Cantilevers				
Case	Section #1	Section #2	Section #3	Eqn. 8.1
No X	5.34	5.26	5.45	4.33
X @ CL	4.14	3.80	4.14	3.33
X @ 3rd Pts.	3.08	2.94	3.08	2.41

For the fully stiffened webs, Equation 8.1 is conservative with respect to the finite element studies. This is shown by the smaller C_b values predicted by the equation when compared to the values from ANSYS. The reason that the C_b values become smaller as discrete bracing is added can be better understood by referring to Figure 8.7. The moment ($M_{Constant \; Moment}$) which is in the denominator of Equation 8.2 increases significantly as discrete bracing is added since the
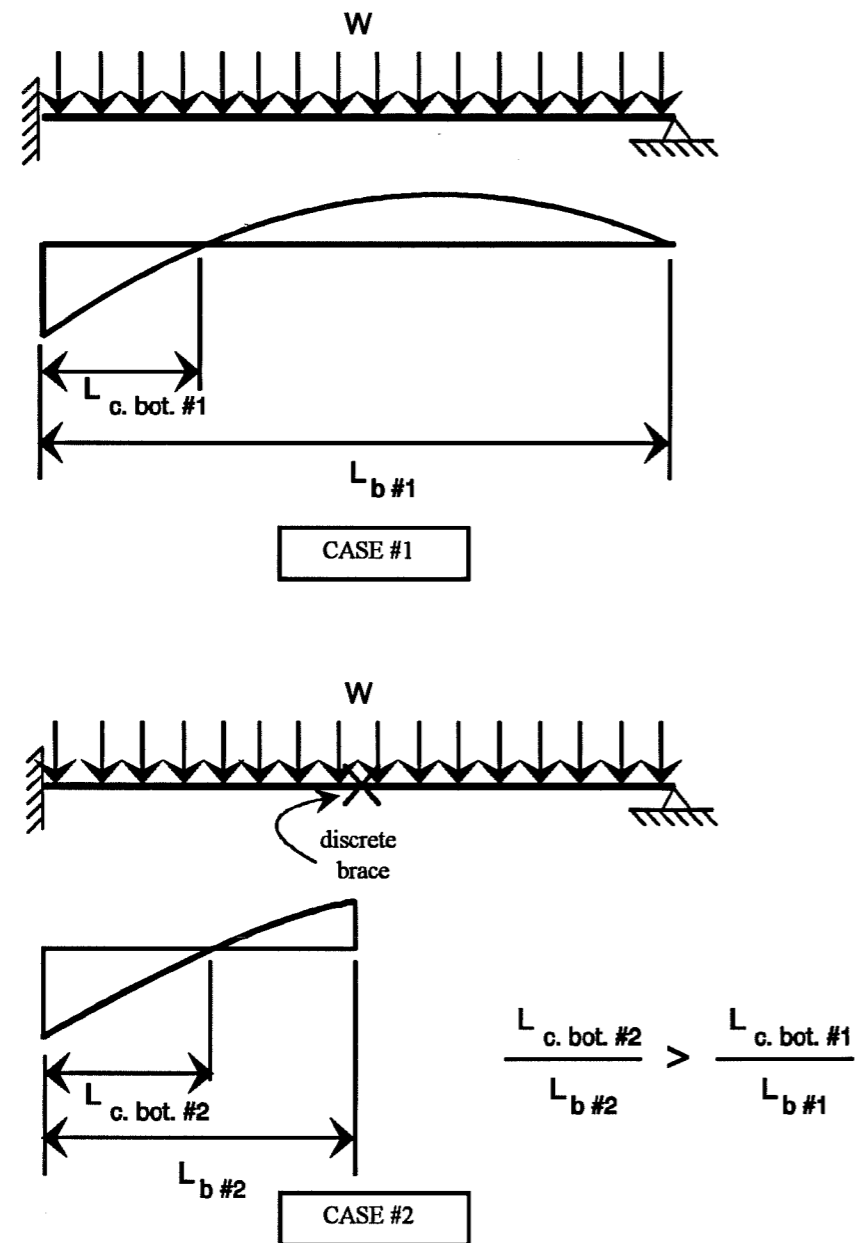
Figure 8.7 Effect of discrete bracing on $M_{top\ fix}$

buckling moment is a function of the inverse of the unbraced length squared. The moment in the numerator of Equation 8.2 also increases, however, the relative increase is not as large as the constant moment case. The reason for this is because, while the "unbraced" length of the bottom flange is reduced when a cross-frame is added at midspan, the percent of the "unbraced" length which is subjected to compression goes up significantly. Consequently, C_b is reduced when discrete bracing is added which reduces the unbraced length of the bottom flange.

Table 8.2 shows the corresponding ANSYS values for the propped cantilever girders with an unstiffened web. The predictions from Equation 8.1 are slightly conservative for the unstiffened webs, however there is a reduction in the C_b values when compared to the corresponding values for the fully stiffened web in Table 8.1. The reduction in the C_b values for the unstiffened girders is due to web distortion.

Table 8.2 Comparison of C_b Values from ANSYS Results and Eqn. 8.1 for Unstiffened Propped Cantilevers				
Case	Section #1	Section #2	Section #3	Eqn. 8.1
No X	4.74	5.07	4.87	4.33
X @ CL	3.41	3.62	3.49	3.33
X @ 3rd Pts.	2.43	2.75	2.50	2.41

Table 8.3 shows a comparison of the ANSYS values of C_b and Equation 8.1 for the girders with ends fixed against rotation and fully stiffened webs. Equation 8.1 is not as conservative for the fully stiffened girders with the fixed ends as was observed for the propped cantilevers, however, it is still conservative for the cases considered.

Table 8.3   Comparison of C_b Values from ANSYS Results and Eqn. 8.1
for Fully-Stiffened Girders with Ends Fixed Against Rotation

Case	Section #1	Section #2	Section #3	Eqn. 8.1
No X	3.01	3.55	3.04	3.00
X @ CL	4.13	3.94	4.15	3.67
X @ 3rd Pts.	3.31	3.21	3.32	2.78

Table 8.4 shows a comparison of the ANSYS values of C_b and Equation 8.1 for the girders with ends fixed against rotation and unstiffened webs. Equation 8.1 is conservative with respect to the finite element results for the unstiffened section #2 for the cases with no cross-frames and for cross-frames at the third points. The equation predicts a C_b slightly larger than the ANSYS results for section #2 with a cross frame at midspan, however the difference is small. The equation is unconservative, however, with respect to all three cases of discrete bracing for the unstiffened sections #1 and #3. The reason that there is such a large reduction between the ANSYS results for stiffened and unstiffened webs for the fixed ended girders is probably due to web distortion.

Table 8.4   Comparison of C_b Values from ANSYS Results and Eqn. 8.1
for Unstiffened Girders with Ends Fixed Against Rotation

Case	Section #1	Section #2	Section #3	Eqn. 8.1
No X	2.75	3.38	2.79	3.00
X @ CL	3.19	3.65	3.28	3.67
X @ 3rd Pts.	2.39	2.91	2.49	2.78

The ANSYS results which were tabulated in Tables 8.1-8.4 represent the best that the deck can provide. So as to avoid unsafe estimates of the buckling capacity, Equation 8.1 should be reduced in order to obtain conservative estimates for the unstiffened webs.

If 75% of the full equation (Equation 8.1) is used, the following expression results:

$$C_b = 2.25 - \frac{1}{2}\left(\frac{M_1}{M_0}\right) + \frac{2\,M_{cl}}{(M_0 + M_1^*)} \qquad (8.3)$$

The variables have the same definitions as defined for Equation 8.1. This equation does not reduce to $C_b = 1.0$ for the constant moment case, and in some instances, the reduced C_b shown in Equation 8.3 many produce conservative estimates of the C_b value for the support section. Adding bracing to the top flange, however, should not reduce the buckling capacity of the girder, so a lower limit of the buckling capacity (of the bottom flange at the support section) could be established by the C_b for the girder with no deck for bracing. This would make use of the modified Kirby-Nethercot formula which is used in the AISC manual and is shown in Equation 8.4. The equation would be applied between cross-frames.

$$C_b = \frac{12.5 M_{max}}{2.5 M_{max} + 3 M_2 + 4 M_{cl} + 3 M_4} \qquad (8.4)$$

The use of Equation 8.4 and the definition of the various moments was outlined in Chapter 2. The limiting C_b value using Equation 8.4 would be for the region of the girder with moment causing compression in the bottom flange.

Table 8.5 shows a comparison of the various C_b Equations along with the ANSYS results for propped cantilevers with unstiffened webs. The estimate from Equation 8.1 has been labeled "Full C_b", while the Equation 8.3 which makes use of 75% of Equation 8.1 has been labeled "Reduced C_b". The lower limit for the C_b which results from the modified Kirby-Nethercot formula (Equation 8.4) has been labeled "Unbraced C_b". The reduced equation is conservative for the propped cantilever. A lower limit C_b from the unbraced girder could therefore be used for the cases of a cross-frame at midspan and also with cross-frames at the third points.

Table 8.5 Comparison of C_b Values from ANSYS Results and Equations for Unstiffened Propped Cantilevers						
Case	Section #1	Section #2	Section #3	Eqn. 8.1 Full C_b	Eqn. 8.3 Reduced C_b	Eqn. 8.4 Unbraced C_b
No X	4.74	5.07	4.87	4.33	3.25	2.08
X @ CL	3.41	3.62	3.49	3.33	2.50	2.63
X @ 3rd Pts.	2.43	2.75	2.50	2.41	1.81	2.30

Table 8.6 shows a comparison of the various C_b Equations along with the ANSYS results for girders with ends fixed from rotations and unstiffened webs. The reduced equation gives conservative estimates of the buckling capacity of the girders with the ends fixed which were considered. The C_b equation for the unbraced girder could be used for the girder with no cross frames between the supports and also for cross frames at the third points.

Table 8.6 Comparison of C_b Values from ANSYS Results and Equations for Girders with Ends Fixed From Rotation						
Case	Section #1	Section #2	Section #3	Eqn. 8.1 Full C_b	Eqn. 8.3 Reduced C_b	Eqn. 8.4 Unbraced C_b
No X	2.75	3.38	2.79	3.00	2.25	2.38
X @ CL	3.19	3.65	3.28	3.67	2.75	2.38
X @ 3rd Pts.	2.39	2.91	2.49	2.78	2.08	2.42

Finite element results were presented in this section for girders with the top flange rigidly supported from lateral displacement. Since the top flange could not buckle, the bottom flange controlled the buckling mode at the supports fixed from rotation.

For fully-stiffened girders, the equation recommended by Yura [25] produced reasonable estimates of the C_b values when compared to the finite element results. When unstiffened webs were considered, however, web distortions reduced the buckling capacity. Although the equation

from Yura was still slightly conservative for the cases considered with unstiffened webs, in many cases metal deck forms would not be able to supply adequate lateral restraint to provide near-lateral-fixity on the top flange. The equation from Yura was therefore reduced by a factor of 75% to account for web distortion. In order to avoid overly-conservative estimates of the C_b with the reduced equation, a lower limit for the C_b equation may be established as the C_b for the unbraced girder for the region around the support. This would make use of a solution such as the modified Kirby-Nethercot formula.

8.4 Buckling Capacity of Continuous Girders with Shear Diaphragm at the Top Flange

The results which were presented in Section 8.3 showed that the C_b formula presented by Yura [25] produced good estimates of the buckling capacity of girders with fully stiffened webs and the top flange fully restrained from lateral displacement. The equation was reduced by 25% to account for distortions of unstiffened webs. A lower limit for the reduced C_b equation with top flange braced could be established as the C_b for the unbraced girder using the modified Kirby-Nethercot formula.

It was shown in Section 8.2 that in many cases, girders braced by a shear diaphragm behave in a manner similar to girders with the top flange fully restrained from lateral displacement along the girder length. In these instances the expression for the reduced C_b in Equation 8.3 may be useful for predicting the buckling capacity of these girders. This section will present finite element results which show the effect of a shear diaphragm on the buckling capacity of continuous girders and compare the results with the reduced C_b equation. The results will concentrate on girders with unstiffened webs.

The girders which were considered had boundary conditions of propped cantilevers and also girders with both ends fixed. Three different cases of discrete bracing were considered: no cross-frames within the span, a cross-frame at midspan, and cross-frames at the third points of the girders. Before the finite element results are compared with the solution, the behavior of the different girder cross-sections in terms of the buckling capacity, M_{cr}, with increasing shear rigidity of the deck, Q, are presented. The girders were subjected to a distributed load, "w", applied at the top flange. The value of M_{cr} corresponds to the maximum moment along the span when the girders buckle. The maximum moment for the girders considered will occur at the supports where in-plane rotations were prevented. For the propped cantilevers, the moment at the fixed support is $WL^2/8$, while the maximum moment for girders with the ends fixed from rotation is $WL^2/12$.

Figures 8.8a, 8.8b, and 8.8c show graphs of M_{cr} versus Q for the three different cases of cross-frame locations for the propped cantilevers with unstiffened webs. The overall behavior which was exhibited is similar in each of the different plots. For smaller values of the shear rigidity, the buckling capacity of the girder system increases with increasing values of the shear rigidity. The curves reach a plateau, however, beyond which there is very little increase in the buckling moment with increasing deck shear rigidity. This behavior can be best understood by referring back to the results on the changing buckling mode which were presented in Section 8.2. For values of the shear rigidity which were relatively small, the buckling mode was controlled by the lateral deformation of the top flange near the midspan of the girder. For larger values of the shear rigidity, the bottom flange began controlling the buckling mode due to large compressive stresses at the fixed supports. When the top flange controls the buckling mode, increasing the shear rigidity of the deck causes relatively large increases in the buckling capacity of the girder since the buckling mode imposes shearing deformations in the deck. When the bottom flange controls the buckling mode, increasing the deck shear rigidity will have very little effect on the buckling capacity of the girder, since the deck is not significantly "engaged" when the girders buckle. When the bottom flange begins to control the buckling mode, the solution should approach the solution with the top flange rigidly supported laterally.

The behavior of the singly-symmetric section #3 in Figures 8.8a-8.8c is interesting. Section #3 has a large bottom flange which is the same size as the doubly-symmetric section #1, and a smaller top flange which is the same size of the doubly-symmetric section #2. When the top flange dominates the buckling for smaller values of the deck shear rigidity, the buckling capacity of the singly-symmetric section #3 is very close to the capacity of section #2. As the shear rigidity is increased, and the bottom flange begins to dominate the buckling mode, the capacity of the singly-symmetric section #3 begins to approach the capacity of section #1.

Figures 8.9a, 8.9b, and 8.9c show graphs of M_{cr} versus Q for the three different cases of cross-frame locations for the girders with both ends fixed and unstiffened webs. The behavior is very similar to that which was observed for the propped cantilevers. For smaller values of the deck shear rigidity, increases in the shear rigidity caused the buckling capacity of the girders to increase. When lateral displacements of the bottom flange began dominating the buckling mode, however, the curves of M_{cr} versus Q reached a plateau past which increasing the deck shear rigidity had very little effect on the buckling moment. The behavior of the singly-symmetric section was also similar to the behavior observed for the propped cantilever. For lower values of
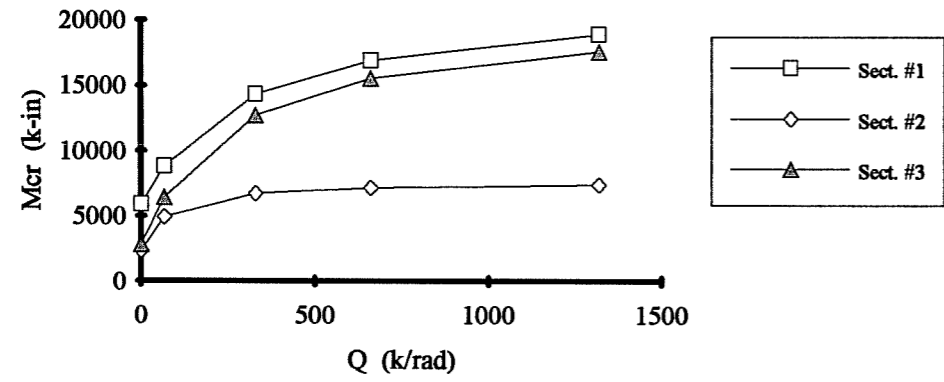
Figure 8.8a: Mcr versus Q for unstiffened propped cantilevers, no cross-frames.
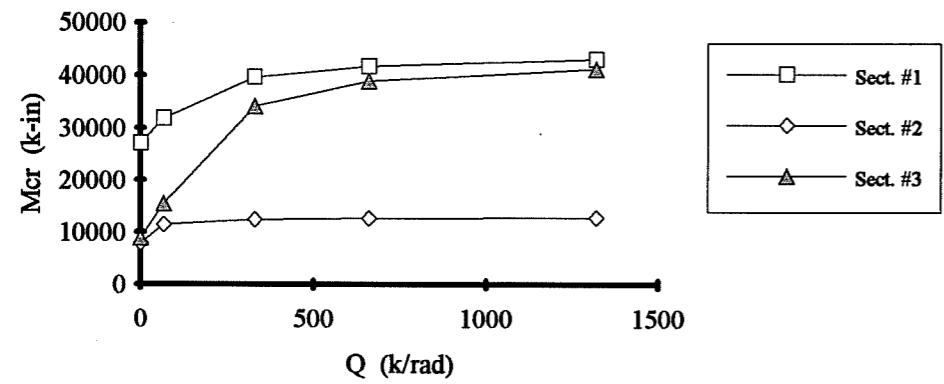
Figure 8.8b: Mcr vs. Q for unstiffened propped cantilevers, cross-frame @ midspan.
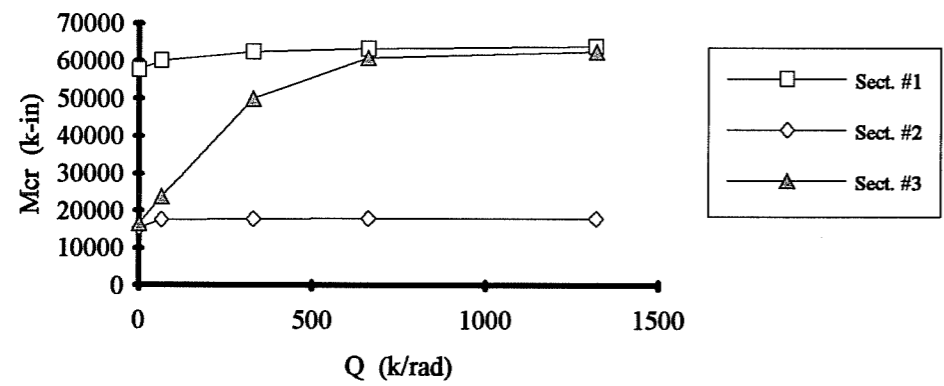
Figure 8.8c: Mcr vs. Q for unstiff. propped cantilevers, cross-frames @ third points.
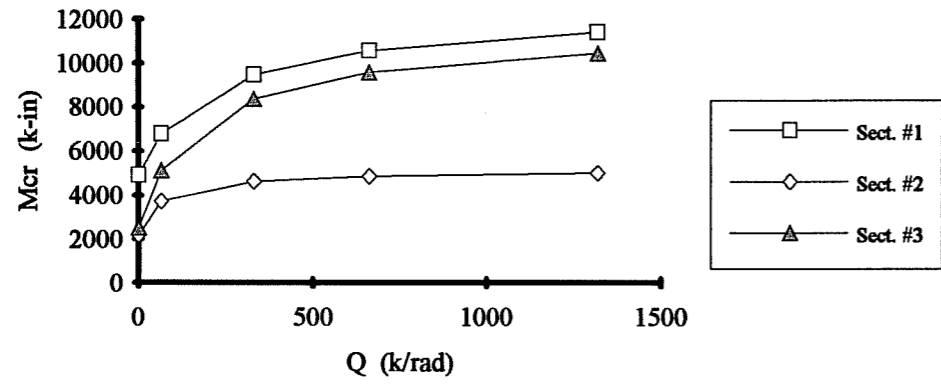
Figure 8.9a: Mcr versus Q for unstiffened fixed-ended girders, no cross-frames.
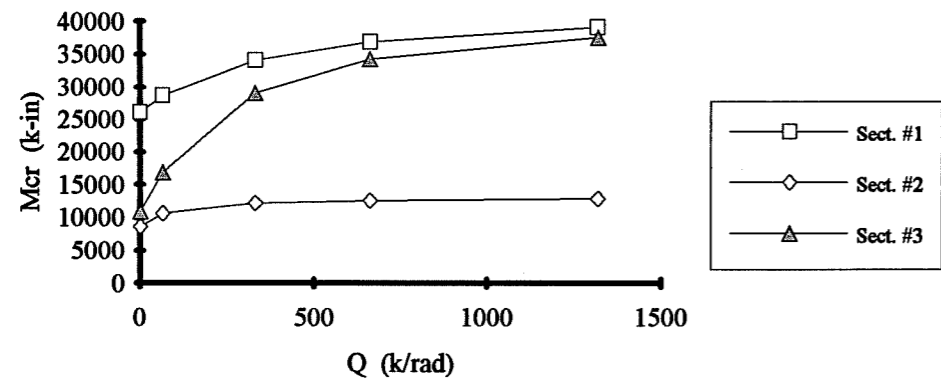
Figure 8.9b: Mcr vs. Q for unstiffened fixed-ended girders, cross-frame @ midspan.
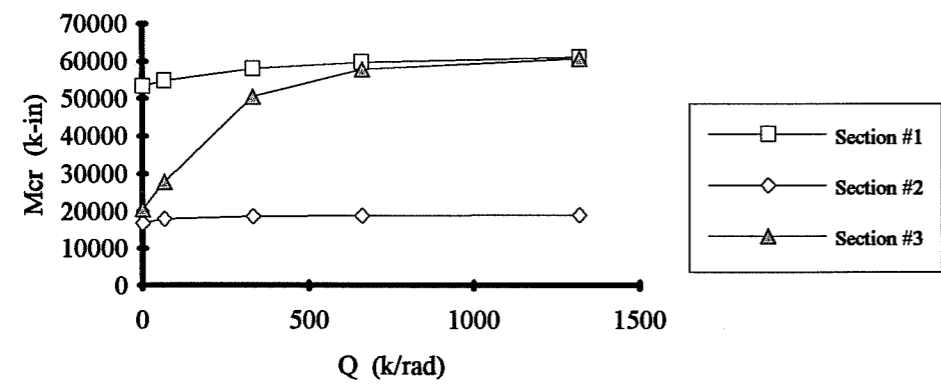
Figure 8.9c: Mcr vs. Q for unstiff. fixed-ended girders, cross-frames @ third points.

the shear rigidity, which is a region in which the top flange controlled the buckling mode, the buckling capacity of the section was very close to the capacity of section #2 which had the smaller flanges. As the deck shear rigidity was increased, the larger bottom flange began to control the buckling mode, and the capacity of section #3 approached to the capacity of section #1 which had the larger flanges.

A comparison can be made between the reduced C_b equation (Equation 8.3) and the ANSYS results for girders braced by a shear diaphragm at the top flange. The C_b from the ANSYS results can be computed as follows:

$$C_{b\ ANSYS} = \frac{M_{cr\ Deck\ Braced}}{M_{Constant\ Moment}} \tag{8.5}$$

Equation 8.5 is similar to Equation 8.2, except $M_{Top\ Fix}$ has been replaced with $M_{cr\ Deck\ Braced}$ which is equal to the maximum moment at buckling for the girders braced by a shear diaphragm at the top flange. For the propped cantilevers this corresponds to $W_{cr}\ L^2/8$, in which W_{cr} is the distributed load which causes buckling, and L is the span length. The corresponding moment for girders with both ends fixed is equal to $W_{cr}\ L^2/12$. The value of $M_{Constant\ Moment}$ corresponds to the buckling moment causing uniform compression in the bottom flange. $M_{Constant\ Moment}$ was obtained in the finite element studies by subjecting a simply supported girder, with no deck for bracing, to a constant moment which caused compression in the bottom flange.

Figures 8.10a, 8.10b, and 8.10c are graphs of C_b versus Q for the three different cases of discrete bracing of the unstiffened propped cantilevers with a distributed load at the top flange. In addition to the ANSYS results for the three girders, the value of the reduced C_b from Equation 8.3 is shown as the heavy solid line. The C_b value from Equation 8.4 (modified Kirby-Nethercot formula) has also been plotted as the heavy dashed line. The dashed line from Equation 8.4 has been labeled as "unbraced girder" because it represents the value of C_b, with no deck for bracing, for the region of the girder from the fixed support to the first discrete brace. This region has been shown in Figure 8.11. For relatively large values of the deck shear rigidity, the C_b values from the ANSYS results exceed the values predicted using Equation 8.3 and 8.4. For relatively small values of the deck shear rigidity, however, the C_b values from the ANSYS results fall below the line labeled "unbraced girder". This may be alarming at first glance, and therefore requires some explanation. This may be best explained by referring to Figures 8.12a, 8.12b, and 8.12c, which
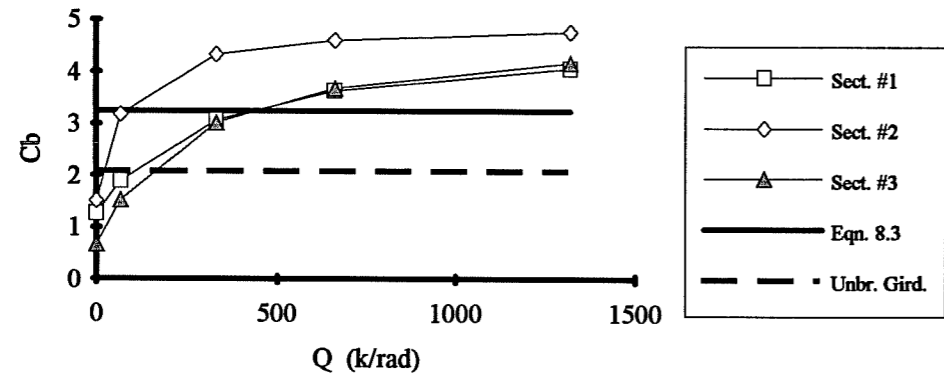
Figure 8.10a: Cb vs. Q for unstiff. propped cantilevers, no cross-frames, w @ top flange. ANSYS results versus Cb Equations.
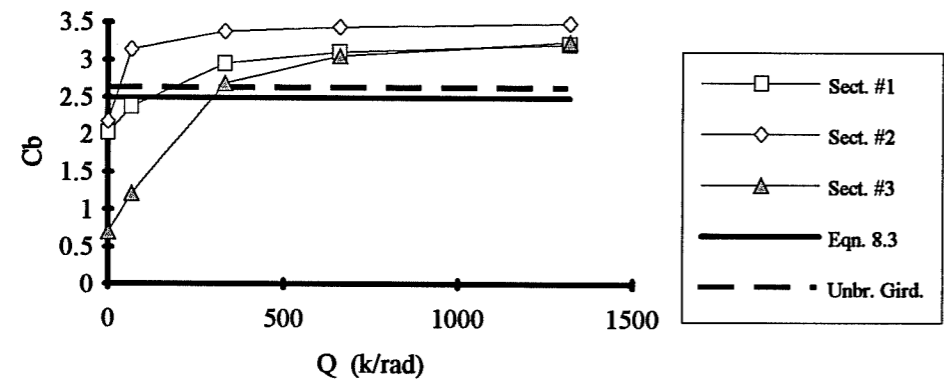
Figure 8.10b: Cb vs. Q for unstiff. propped cantilevers, cross-frames @ midspan, w @ top flange. ANSYS results versus Cb Equations.
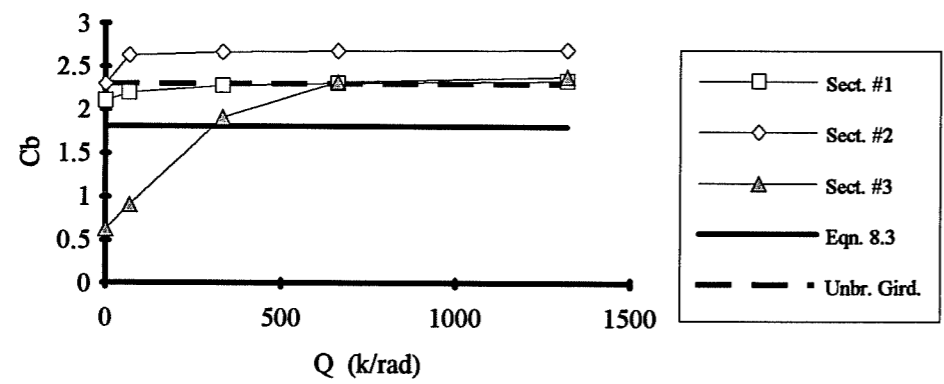
Figure 8.10c: Cb vs. Q for unstiff. propped cantilevers, cross-frames @ third points, w @ top flange. ANSYS results versus Cb Equations.

$$\frac{wL^2}{12}$$
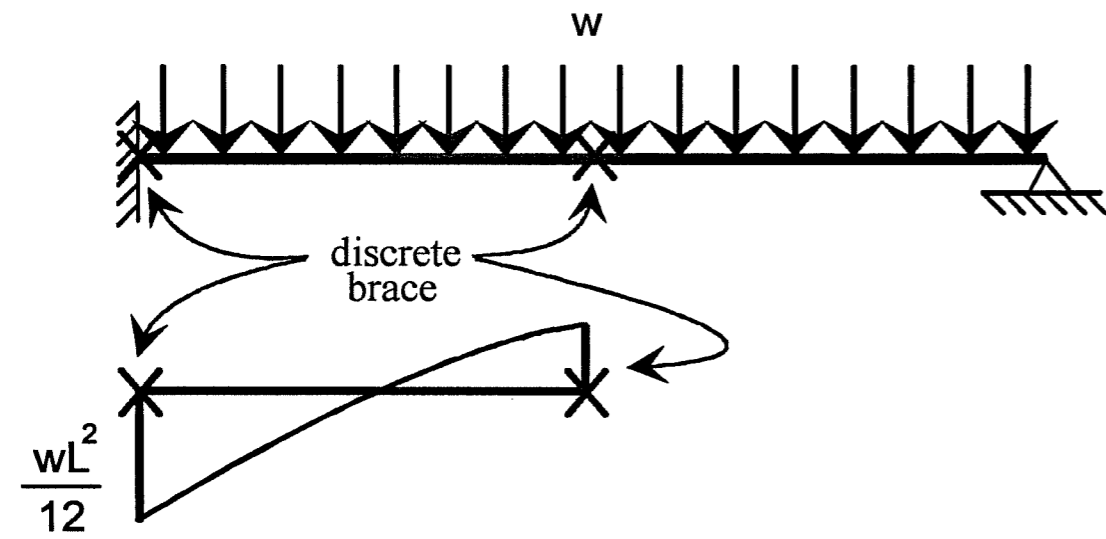
C_b for "unbraced" girders is calculated using modified Kirby-Nethercot on this region.

Figure 8.11 Calculation of C_b for "unbraced girder."
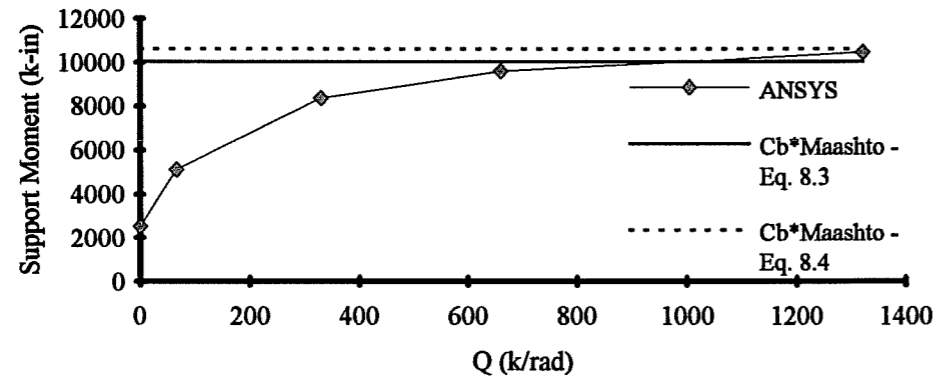
Figure 8.12a: ANSYS support moment vs. Q for unstiffened fixed-ended girders, no cross-frames, w @ top flange. ANSYS results versus Cb Equations.
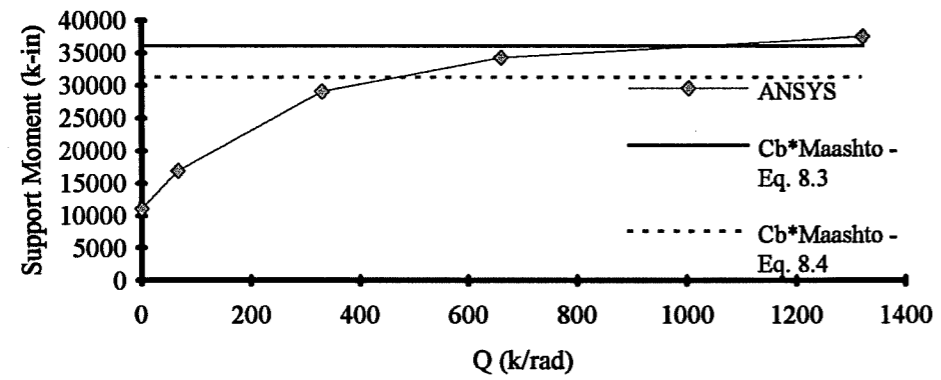
Figure 8.12b: ANSYS support moment vs. Q for unstiffened fixed-ended girders, cross-frames @ midspan, w @ top flange. ANSYS results vs Cb Eqns.
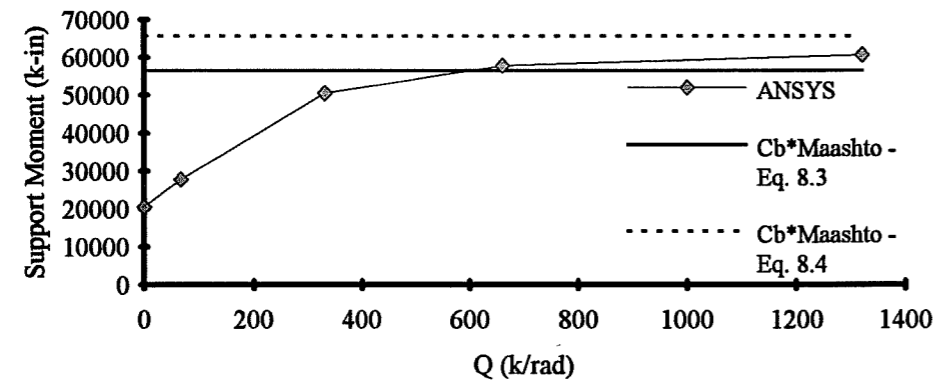
Figure 8.12c: ANSYS support moment vs. Q for unstiffened fixed-ended girders, cross-frames @ third points, w @ top flange. ANSYS results vs Cb Eqns.

show plots of the support moment at buckling versus the deck shear rigidity for section #3 with ends fixed from rotation. The girders in Figures 8.12a-8.12c were loaded with a distributed load applied at the top flange. In addition to the ANSYS results, values of $C_b M_{AASHTO}$ have been plotted using Equations 8.3 and 8.4 to calculate C_b. The value of the AASHTO moment was calculated treating the bottom flange as the compression flange. For smaller values of the deck shear rigidity, the moment at the support falls below the values calculated with $C_b M_{AASHTO}$ using Equation 8.3 and 8.4. Recalling from Figures 8.3-8.5, for relatively small values of the shear rigidity, the top flange controlled the buckling capacity of the section. Since the top flange controlled the buckling capacity, the buckling moment calculated using $C_b M_{AASHTO}$ will be larger than the support moment since the bottom flange has not buckled. When the shear rigidity of the deck is large enough to brace the top flange so that the bottom flange at the support controls the buckling mode, the support moment should reach the $C_b M_{AASHTO}$ values.

It should be noted that in a design for a continuous girder, buckling of the bottom flange in the region at the support would be compared with the capacity of the top flange at midspan so that the low values of C_b would not be a problem.

Referring back to Figures 8.10a-8.10c, for the case with no deck (Q=0) or decks with small shear rigidities, the C_b value from the ANSYS results for section #3 is relatively small compared to the C_b values for the other two sections. The reason for the small C_b for section #3 is because for low deck rigidities, the small top flange is controlling the buckling capacity, however the C_b is calculated based on constant moment on the larger bottom flange. The ANSYS C_b values for section #2 are considerably larger than for the other two sections. This is similar to the results observed in Section 8.3 with the top flange fully restrained, however, the reason for this is not clear.

It was mentioned in Section 8.3 that a lower limit on the reduced C_b calculated using Equation 8.3 could be established based on the C_b for the "unbraced" girder which was calculated using Equation 8.4. The C_b of the unbraced girder could then be used when the heavy solid line plots below the heavy dashed line. This would be the case in Figures 8.10b, and 8.10c, for which the reduced C_b falls below the value calculated using Equation 8.4.

Figures 8.13a, 8.13b, and 8.13c are graphs of C_b versus Q for the three different cases of discrete bracing for the unstiffened girders with both ends fixed from rotation and a distributed load applied at the top flange. The plots are similar to the results found for the propped cantilevers. For small values of the deck shear rigidity, the plots fall below the capacity of the
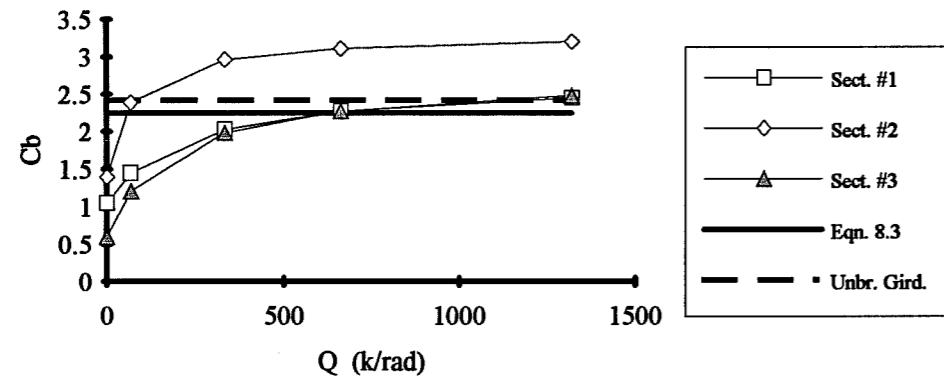
Figure 8.13a: Cb vs. Q for unstiffened fixed-ended girders, no cross-frames, w @ top flange. ANSYS results versus Cb Equations.
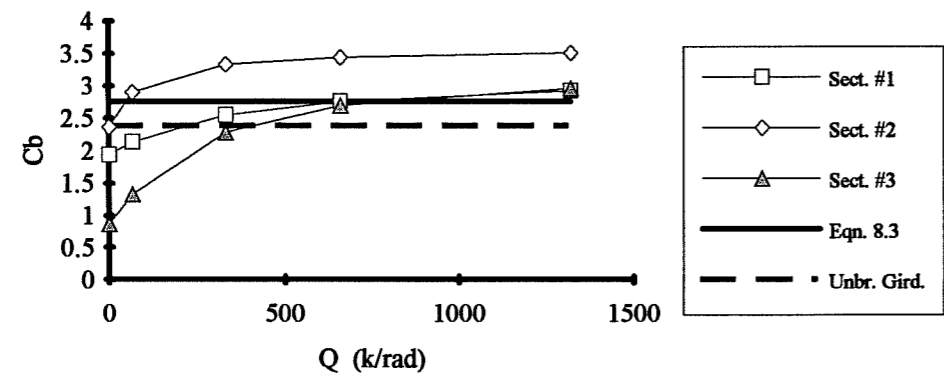
Figure 8.13b: Cb vs. Q for unstiff. fixed-ended girders, cross-frames @ midspan, w @ top flange. ANSYS results versus Cb Equations.
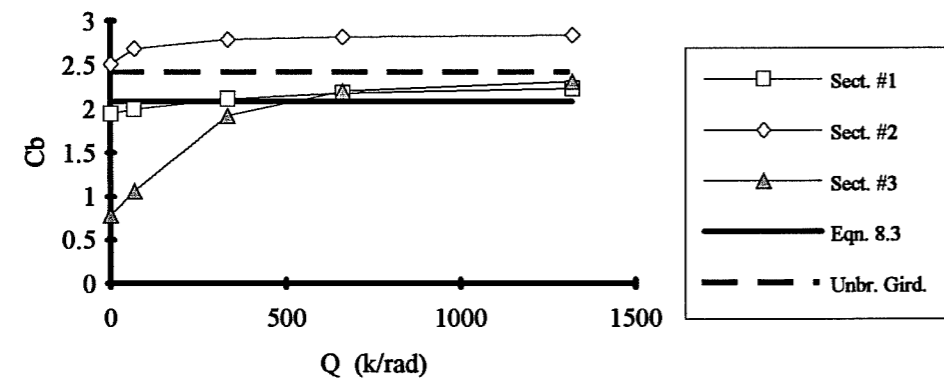
Figure 8.13c: Cb vs. Q for unstiff. fixed-ended girders, cross-frames @ third points, w @ top flange. ANSYS results versus Cb Equations.

"unbraced" girder. This is because the buckling capacity is controlled by the top flange in these regions of the graph. The curves exhibited a plateau for larger values of the shear rigidity which is a region in which the bottom flange controlled the buckling capacity.

For each of the cases of discrete bracing, the reduced C_b equation is conservative with respect to the ANSYS results for values of the shear rigidity larger than approximately 660 k/rad. The reduced C_b equation falls below the dashed line for the unbraced girder for the cases in Figures 8.13a, and 8.13c. In these two instances, the C_b for the unbraced girder could be substituted for the reduced C_b, however the C_b for the unbraced girder does overestimate the values predicted by ANSYS for cross-frames at the third points. The C_b of the unbraced girder is approximately 10 percent larger than the ANSYS values for a deck shear rigidity of 660 k/rad. Web shear buckling and bend buckling were checked for the unstiffened web, however, neither of these buckling phenomenon were responsible for the lower capacity. The reason for the lower buckling capacity is probably due to distortions of the unstiffened web.

8.5 Summary of Results on Continuous Girders Braced by a Shear Diaphragm at the Top Flange

The behavior of continuous girders braced by a shear diaphragm were slightly more complex than the results presented in previous chapters for simply supported girders. For relatively small values of the deck shear rigidity, the buckling mode is generally dominated by the lateral displacement of the top flange near midspan. For larger values of the deck shear rigidity, the buckling mode changes and the lateral displacements of the bottom flange due to large compressive stresses near fixed supports control the buckling mode.

When the buckling mode is dominated by the top flange, increases in the deck shear rigidity cause corresponding increases in the buckling capacity of the girder. When the bottom flange controls the buckling capacity, however, changes in the deck shear rigidity do not significantly influence the buckling capacity. In these instances, the girder behaves in a manner similar to a girder with the top flange continuously restrained from lateral displacement along the span. A reduced form of an equation presented by Yura for the C_b factor for girders with the top flange continuously restrained from lateral displacement produced conservative estimates of the buckling capacity when compared to finite element results. In some instances, the reduced equation was overly-conservative, and a lower limit was established based on the C_b factor for the unbraced girder in the region around the fixed support. Web distortions can significantly reduce

the buckling capacity of the girders, and in some instances the C_b factors for the unbraced girders can overestimate the buckling capacity.

CHAPTER 9

Proposed Design Method

9.1 Introduction

The previous chapters have presented finite element results for eigenvalue analyses for simply-supported girders and continuous girders braced by a shear diaphragm at the top flange. These finite element results have been compared to closed form solutions as well as approximate solutions. This chapter presents an overview of the recommended solutions which have resulted from the previous chapters and outlines the use of the various solutions.

Section 9.2 presents an overview of the design recommendations for deck stiffness for girders braced by a shear diaphragm at the top flange. Examples will be presented in Section 9.3 which demonstrate the design method for simply supported and continuous girders braced by a shear diaphragm.

It was shown in Chapter 1 that a bracing system must satisfy stiffness and strength criteria. The bifurcation solutions which have been presented in the previous chapters give an indication of the stiffness requirements for bracing by a shear diaphragm, however strength requirements have not been established. In order to determine strength requirements, large-displacement analyses must be conducted. Section 9.4 of this chapter will present finite element results large-displacement analyses which give an indication of the effect of imperfections on the displacement behavior and forces which develop in the deck. Finally, the chapter is summarized in Section 9.5.

9.2 Design Recommendations

The previous chapters have covered a wide variety of problems and proposed several solutions for girders with a deck (shear diaphragm) for bracing. The girders which were considered had a wide variety of cross-sectional properties and dimensions. Although girders were considered which had "fully-stiffened" webs, these girders are not practical. Therefore, the recommendations will be based on girders with partially-stiffened and unstiffened webs. Based on the studies in the previous chapters, the following recommendations can be made:

> The lateral-torsional buckling capacity of girders with transverse loading applied at midheight can be predicted using Equation 9.1a, while the capacity of girders with transverse loading applied at the top flange can be estimated using Equation 9.1b.

$$M_{cr} = C_b M_{AASHTO} + \frac{3}{4} Qd \qquad\qquad (9.1a)$$

$$M_{cr} = C_b{}^* M_{AASHTO} + \frac{3}{8} Qd \qquad\qquad (9.1b)$$

where: M_{cr} = bucking moment of the girder and deck system,

C_b = factor for moment gradient,

$C_b{}^*$ = factor to account for load height,

M_{AASHTO} = buckling moment calculated using the AASHTO formula,

Q = shear rigidity of the deck, and

d = depth of the girder.

The capacity of the girders should be limited to the web shear and/or bend buckling capacity. Equations for both of these phenomenon are covered in the AASHTO specification [1]. The design examples which will be presented in this chapter will make use of Equation 9.1b for top flange loading, however, the use of Equation 9.1a is essentially the same.

9.3 Design Examples

This chapter presents design examples which demonstrate the use of the design recommendations. In-depth calculations will be presented in the first example, however, later examples will only cover the essential calculations.

The first example consists of the 4 girder bridge shown in Figure 9.1. The bridge is from the design tables for short-span bridges with composite rolled beams from the American Iron and Steel Institute (AISI) [2]. The girders are 50 feet long and consist of W33x130 rolled beams which are spaced 10 feet on center. The girders will act composite with the concrete slab in the finished bridge, however the steel girders must support the entire construction load which consists of a factored dead load moment of 614 k-ft. The existing bridge was designed with cross-frames spaced at 16.67 feet, which is very conservative since the AASHTO lateral-torsional buckling formula estimates the capacity at 2295 k-ft (>614 k-ft.) with this cross-frame spacing. The steel girders could have supported the construction load with a single cross-frame at midspan for which the
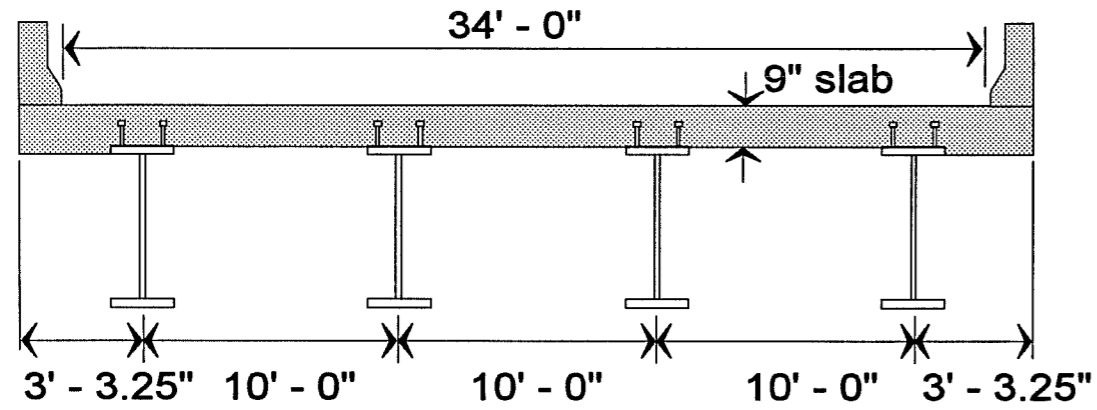
ORIGINAL BRIDGE DESIGN:

Girder Span: 50'

Beams: Rolled Beams - W33 x 130

4 Cross-Frames Spaced at 16.67'

Unfactored Dead Load Moment = 471.9 k'

Unfactored Dead Load Shear = 37.8 k

Factored D. L. Moment = 1.30 x 471.9 k' = 614 k'

Factored D. L. Shear = 1.30 x 37.8 k = 49.1 k

Design Problem: Determine what shear rigidity
is required for the stay-in-place
forms in order to provide adequate
bracing to eliminate the 2 intermediate
cross-frames within the span.

Figure 9.1 Bridge used in Design Example #1.

AASHTO buckling formula estimates the capacity at 1125 k-ft (>614 k-ft.). A single brace at midspan would give a cross-frame spacing of 25 feet and meet the current maximum limit for spacing of cross-frames in the AASHTO specification.

The purpose of the problem is to determine what shear rigidity is required for the stay-in-place deck forms so that the two intermediate cross-frames may be eliminated, which would produce a 50 foot spacing between the cross-frames at the supports. The factored dead load moment for the problem is 614 k-ft. The cross-section of the W33x130 section is shown in Figure 9.2, which also shows some of the section properties.

Chapter 7 presented the results for girders with partially-stiffened and unstiffened webs. It was necessary to limit the increase in the buckling load which resulted from the deck to the web shear or bend buckling capacity. The first step in this problem will be to check the web buckling capacity against the factored dead load moment of 614 k-ft and a factored dead load shear of 49.1 kips. The bend buckling capacity is calculated using Equation 9.2. Since the girders are doubly-symmetric, the value of λ will be taken as 15400 (as apposed to 12500 for singly-symmetric girders with the small flange in compression). The cross-sectional properties can be found on Figure 9.2. The resulting capacity for bend buckling is shown in Equation 9.3.

$$M_r = \left[\frac{\lambda^2}{\left(\frac{D_c}{t_w}\right)^2} \right] S_{xc} \tag{9.2}$$

$$M_r = \left[\frac{(15400)^2}{\left(\frac{16.12\,in}{0.58\,in}\right)^2} \right] 406\,in^3 \left(\frac{1}{12\frac{in}{ft}\,1000\frac{lb}{kip}} \right) = 10400 \; kip\,ft \tag{9.3}$$

The bend buckling capacity of 10400 kip-ft is much greater than the dead load moment of 614 kip-ft. The equation for shear buckling is shown in Equations 9.4. The web is relatively stocky for this problem and had a slenderness ratio (d/t_w) of 56. For a yield stress of 50000 psi for the steel, this puts the web in the range to base the web capacity on shear yielding. The resulting capacity in shear is shown in Equation 9.5.

$$V_u = 0.58 \; D \; t_w \; F_y \tag{9.4}$$
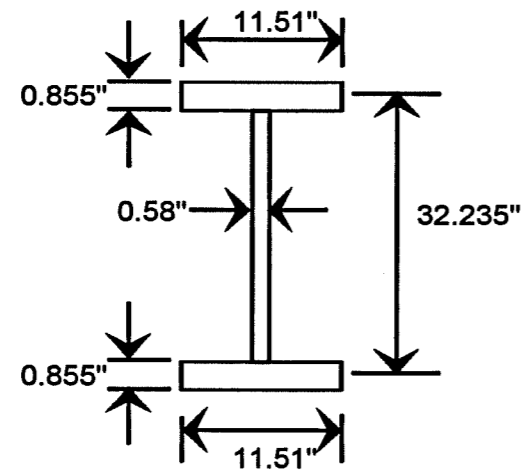
Section Properties:

$I_y = 218 \ \text{in}^4$

$I_{yc} = 109 \ \text{in}^4$

$J = 7.37 \ \text{in}^4$

$w_g = 130 \ \text{lb/ft}$

$C_w = 56600 \ \text{in}^6$

$S_{xc} = 406 \ \text{in}^3$

$D_c = d/2 = 16.12 \ \text{in}$

Figure 9.2 Girder section properties for Design Example #1.

$$V_u = 0.58\ (32.235in)\ (0.58in)\ (50000\ psi)\left(\cfrac{1}{1000\ \cfrac{lb}{kips}}\right) = 542\ kips \qquad (9.5)$$

Shear buckling and bend buckling are not a problem for this web.

Two separate stages must be considered during construction. During the casting of the concrete deck, the girder with the metal form system for bracing will be relied on to support the entire construction load. In the first stage of construction, however, the girders must be able to support their self-weight and a small portion of the construction load. The amount of the construction load that the girders must support will be taken as 10 lb/ft^2. The total applied load that the girders must be able to support in the initial construction stage with an unbraced length of 50 feet is given by the following calculations.

Girder self-weight : $w_g = 130$ lb/ft

$w_{c.l.}$ = construction load =10 lb/ft^2 x tributary width of girder.

$w_{c.l.}$ = 10 lb/ft^2 x 10 ft. = 100 lb/ft

w_{gird} = 1.30 x (130 lb/ft + 100 lb/ft) = 300 lb/ft = 0.300 k/ft

The moment that the girder must support is therefore equal to $M_{gird} = w_{gird}\ L^2/8$.

M_{gird}= (0.300 k/ft)x(50 ft.)^2/8 = 94 k-ft.

The capacity of the girder is calculated using the AASHTO equation for lateral-torsional buckling which is shown in Equation 9.6.

$$M_{AASHTO} = 91x10^6 \left(\frac{I_{yc}}{L_b}\right)\sqrt{0.772\ \frac{J}{I_{yc}} + 9.87\left(\frac{d}{L_b}\right)^2} \qquad (9.6)$$

Making use of the section properties shown in Figure 9.2, the calculation of the buckling capacity using the AASHTO buckling equation is shown in Equation 9.7.

$$M_{AASHTO} = 91 x 10^6 \left(\frac{109 \ in^4}{600 \ in} \right) \sqrt{0.772 \frac{7.37 \ in^4}{109 \ in^4} + 9.87 \left(\frac{32.235 \ in}{600 \ in} \right)^2} \left(\frac{1}{12 \frac{in}{ft} 1000 \frac{lb}{kip}} \right) = 391 \ kip\text{-}ft \quad (9.7)$$

It was shown in Chapter 4 that in many cases, load height effects for girders with intermediate cross-frames can be accounted for by using $C_b^* = 1.0$. In this case, however, the girder is subjected to top flange loading and there are no intermediate cross-frames, so load height effects should be considered. It should be noted that only the construction loading would cause top flange loading; the resultant of the girder self-weight would be applied at the center of gravity. Midheight loading will be neglected for the self-weight, however, and the entire load the girder must support will be assumed to be applied at the top flange. The equations for load height from the SSRC guide [13] can be used to calculate the effects of load height. Equation 9.8a shows the expression for 'W' which is a measure of the girder warping stiffness. The section properties J and C_w can be obtained from Figure 9.2.

$$W = \frac{\pi}{L} \sqrt{\frac{E \ C_w}{G \ J}} \quad (9.8a)$$

The resulting calculation is shown in Equation 9.8b.

$$W = \frac{\pi}{109 \ in} \sqrt{\frac{(29000 \ ksi) \ (56600 \ in^4)}{11154 \ ksi \ 7.37 \ in^4}} = 0.74 \quad (9.8b)$$

The girder is subjected to a distributed load, so the equation for the term 'B' is shown in Equation 9.9a, while the calculation is shown in Equation 9.9b.

$$Uniform \ Distributed \ Load \quad B = 1 - 0.154 \ W^2 + 0.535 \ W \quad (9.9a)$$

$$B = 1 - 0.154 \ (0.74)^2 + 0.535 \ (0.74) = 1.31 \quad (9.9b)$$

The load height factor C_b^* for top flange loading is then calculated as the ratio of C_b to 'B'. C_b is the factor to account for moment gradient and for a distributed load the SSRC Guide recommends a value of 1.12. The calculation of C_b^* is shown in Equation 9.10.

$$C_b^* = \frac{C_b}{B} = \frac{1.12}{1.31} = 0.85 \qquad (9.10)$$

The resulting moment capacity of the section is equal to $C_b^* M_{AASHTO}$ which is shown in Equation 9.11.

$$M_r = C_b^* M_{AASHTO} = 0.85 \ x \ 391 \ kip\text{-}ft = 334 \ kip\text{-}ft \qquad (9.11)$$

The capacity of the girders with a 50 foot long unbraced length and top flange loading is equal to 334 kip-ft. This is greater than M_{gird} = 94 kip-ft which was calculated above, so the girders can easily support their self-weight plus a portion of the construction load.

The increase in the buckling capacity that is required from the deck can now be calculated by substituting the factored design moment, M_u, for M_{cr} and rewriting Equation 9.1b which is shown in Equation 9.12. The resulting expression for $Q_{req'd}$ is shown in Equation 9.13.

$$\frac{3}{8} Qd = M_u - C_b^* M_{AASHTO} \qquad (9.12)$$

$$Q_{req'd} = \frac{8}{3d}(M_u - C_b^* M_{AASHTO}) = \frac{8}{3 x 2.70 \ ft} (614 \ kipft - 334 \ kipft) = 277 \frac{k}{rad} \qquad (9.13)$$

A deck shear rigidity of 277 k/rad provides enough bracing to the girder to eliminate the cross-frames between the supports. The distance between the cross-frames is therefore equal to 50 feet which is twice the maximum spacing of 25 feet in the current AASHTO specification [1].

Results were presented in Chapter 1 which were typical of the shear rigidities measured in the experimental phase of this study. These values have been shown again in Table 9.1a and 9.1b in order to provide representative values of the bridge deck. The values of the shear rigidity in Table 9.1a have an "unstiffened" support angle, while the values in Table 9.1b have a "stiffened" support angle.

Table 9.1a Shear Rigidity for Bridge Deck Systems - Unstiffened Support Angle				
Deck	Span (feet - inches)	Q_{deck} (k/rad)	Q_{conn} (k/rad)	Q_{sys} (k/rad)
LSM2224	8' - 11.5"	1129	1637	668
LSM1716	12' - 10"	3234	1143	844
LSM1516	12' - 10"	4543	1143	913
BOS816	10' - 0"	3240	1467	1010
BO8.5P	7' - 8"	4324	1913	1326
BUBF14	8' - 6"	4488	1725	1246

Table 9.1b Shear Rigidity for Bridge Deck Systems - Stiffened Support Angle				
Deck	Span (feet - inches)	Q_{deck} (k/rad)	Q_{conn} (k/rad)	Q_{sys} (k/rad)
LSM2224	8' - 11.5"	1129	4502	903
LSM1716	12' - 10"	3234	3143	1594
LSM1516	12' - 10"	4543	3143	1858
BOS816	10' - 0"	3240	4033	2005
BO8.5P	7' - 8"	4324	5261	2373
BUBF14	8' - 6"	4488	4745	2306

The values of the shear rigidity in Tables 9.1a and 9.1b were from a shear test with a single deck panel. The "effective width" which was used to calculate the shear rigidities in Table 9.1a and 9.1b was s/2, where "s" is the span of the deck. The bridge in the first design example had 4 girders which would result in three deck panels. Equation 9.14 was first presented in

Chapter 1 for calculating the "effective width" or "tributary width" for the girders in a bridge with "n" girders. The "effective width" is the width of decking which provides bracing to a single girder.

$$effective\ width\ =\ w\ =\ \frac{(n-1)}{n}\ s \qquad (9.14)$$

With 4 girders the resulting effective width is given in Equation 9.15

$$effective\ width\ =\ w\ =\ \frac{(4-1)}{4}\ s\ =\ 0.75s \qquad (9.15)$$

The shear rigidity of the decks shown in Tables 9.1a and 9.1b can be modified to reflect what the rigidity would be in a multi-girder bridge by multiplying the tabulated shear rigidity by the ratio of the effective width from Equation 9.14 to the width used for the deck tests which was 0.5s. The modifying factor, α, is shown in Equation 9.16 for the bridge under consideration.

$$modifying\ factor\ =\ \alpha\ =\frac{0.75s}{0.5s}\ =1.5 \qquad (9.16)$$

Therefore, for the bridge in the first design example, shear rigidities which would be provided by the metal deck forms in Tables 9.1a and 9.1b can be obtained by multiplying the tabulated shear rigidities by 1.5. The smallest shear rigidity in Table 9.1a was 668 k/rad for the LSM2224 deck. For the 4-girder bridge, the shear rigidity would be 1.5 x 668 k/rad = 1002 k/rad. This is significantly larger than the value of 277 k/rad which is what was calculated using the design equations. Since the LSM2224 deck had the smallest shear rigidity from the experimental results, any of the metal deck forms in Tables 9.1a and 9.1b would provide adequate bracing for the girders.

A finite element analysis was conducted on the bridge girders for the first design example with a deck shear rigidity of 277 k/rad. The eigenvalue buckling load for the girder system was 870 k-ft. which is greater than the design moment of 614 k-ft. For the problem considered, the design equations produced conservative estimates of the buckling capacity.

It should be noted that in an actual design, the effective shear modulus, G', would be calculated using the formulas in the manual from the Steel Deck Institute (SDI) [17] or perhaps the recommended values from the deck manufacturer. The shear rigidity of the deck would then be calculated by multiplying the effective shear modulus by the effective width given by Equation 9.15. The shear rigidity of the deck system would then be calculated by combining the shear

rigidity of the deck with that of the connection as outlined in Chapter 1 (as well as in Reference 21). For the purposes of these design examples, however, the values will be compared with the values of the shear rigidity which were measured experimentally. In these cases a modifying factor will need to be computed based on the ratio of the effective width over 0.5s.

The second example consists of the 4 girder bridge shown in Figure 9.3. The bridge is from the design tables for short-span bridges with composite plate girders from the American Iron and Steel Institute (AISI). The girders are 100 feet long and the cross-section of the girders are shown in Figure 9.4. The girders were spaced 12.5 feet on center and were designed to act composite with the concrete slab in the finished bridge. The bridge design called for cross-frames spaced at 25 feet, which matches the maximum spacing allowed in the current AASHTO specification [1].

The purpose of this problem is to determine what shear rigidity is required for the stay-in-place deck forms so that two of the three intermediate cross-frames could be eliminated which would produce a 50 foot spacing between the cross-frames. The factored dead load moment for the problem is 3526 k-ft.

The first step in this problem will be to check the web buckling capacity against the factored dead load moment of 3526 k-ft and a factored dead load shear of 108.5 kips. The calculation of the bend buckling capacity is shown in Equation 9.17. Since the girders are singly-symmetric and the small flange is in compression, the value of λ is taken as 12500. The cross-sectional properties can be found on Figure 9.4.

$$M_r = \left[\frac{(12500)^2}{\left(\frac{33.4\,in}{0.5625\,in}\right)^2} \right] 1182\,in^3 \left(\frac{1}{12\frac{in}{ft}\ 1000\frac{lb}{kip}}\right) = 4365\ kip\ ft \qquad (9.17)$$

The resulting capacity of 4365 kip-ft is greater than the dead load moment of 3526 kip-ft, so bend buckling is not a problem during construction.

The web slenderness ratio (d/t_w) for this girder is 102 so Equations 9.18a and 9.18b are used to estimate the web shear buckling capacity.

Figure 9.3 Bridge used in Design Example #2.
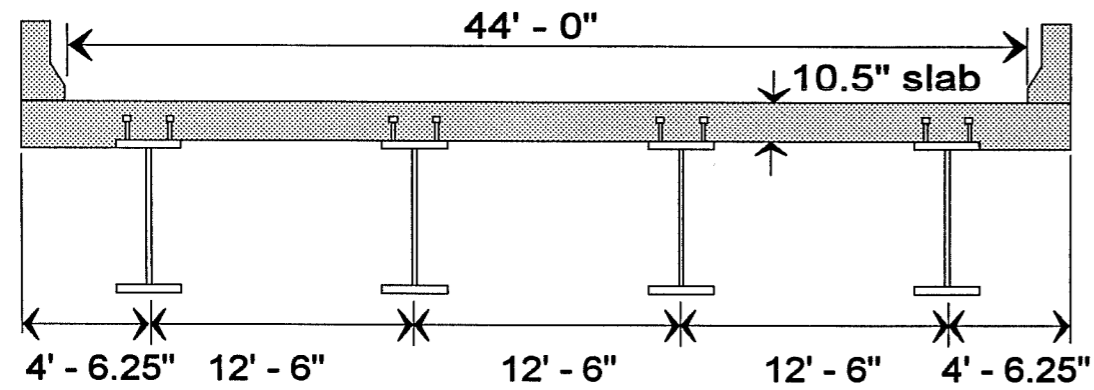
ORIGINAL BRIDGE DESIGN:

Girder Span: 100'
5 Cross-Frames Spaced at 25.0'
Unfactored Dead Load Moment = 2712.5 k'
Unfactored Dead Load Shear = 108.5 k
Factored D. L. Moment = 1.30 x 2712.5 k' = 3526.25 k'
Factored D. L. Shear = 1.30 x 108.5 k = 141.1 k

Design Problem: Determine what shear rigidity
                   is required for the stay-in-place
                   forms in order to provide adequate
                   bracing to eliminate 2 of the 3
                   intermediate cross-frames within
                   the span, producing a 50' spacing
                   between cross-frames.

Section Properties:

$I_y = 783$ in^4

$I_{yc} = 229$ in^4

$J = 30.9$ in^4

$w_g = 243$ lb/ft

$S_{xc} = 1182$ in^3

$D_c = 33.4$ in

Figure 9.4 Girder section properties for Design Example #2.

$$V_u = 0.58 \, D \, t_w \left[\frac{4.5 x 10^7 \, k}{\left(\frac{D}{t_w} \right)^2} \right] \qquad \text{(9.18a)}$$

$$k = 5 + \frac{5}{\left(\frac{d_o}{D} \right)^2} \qquad \text{(9.18b)}$$

In the definition of the web buckling coefficient, k, d_o is the spacing between transverse stiffeners. The girders for this problem had transverse stiffeners near the supports spaced at 6.67 feet, so the ratio of d_o/D equal to 6.67/(4.75) = 1.40. The resulting value of k is 7.5. The calculation of the shear buckling capacity is shown in Equation 9.19.

$$V_u = 0.58 \, (57.3125 in) \, (0.5625 in) \left[\frac{4.5 x 10^7 \, x \, 7.5}{\left(\frac{57.3125 in}{0.5625 in} \right)^2} \right] \left(\frac{1}{1000 \, \frac{lb}{kips}} \right) = 608 \, kips \qquad \text{(9.19)}$$

The shear buckling capacity is 608 kips which is greater than 108.5 kips which is the factored dead load.

As mentioned in the first design problem, two separate stages must be considered during construction. In the first stage of construction, the girders must be able to support their self-weight and an estimated part of the construction load of 10 lb/ft^2. The total load applied that the girders must be able to support in the initial construction stage with an unbraced length of 50 feet (girder span of 100 feet) is therefore given by the following calculations.

Girder self-weight : w_g = 243 lb/ft

$w_{c.l.}$ = construction load = 10 lb/ft^2 x tributary width of girder.

$w_{c.l.}$ = 10 lb/ft^2 x 12.5 ft. = 125 lb/ft

w_{gird} = 1.30 x (243 lb/ft + 125 lb/ft) = 480 lb/ft = 0.480 k/ft

The moment that the girder must support is therefore equal to $M_{gird} = w_{gird} \, L^2/8$.

$$M_{gird} = (0.480 \text{ k/ft}) \times (100 \text{ ft.})^2 / 8 = 600 \text{ k-ft.}$$

The capacity of the girder is calculated using the AASHTO equation for lateral-torsional buckling with an unbraced length of 50 feet. The resulting capacity of the girder is $M_{AASHTO} = 1274$ kip-ft. Finite element results were presented in Chapter 4 which showed that the effects of top flange loading in girders with intermediate bracing could be accounted for by using a C_b^* factor equal to 1.0. Since this problem has a cross-frame at midspan, a C_b^* factor of 1.0 will be used to account for load height effects. It should be noted that a finite element analysis was conducted on the girder in this design example with a distributed load applied at the top flange and a cross-frame at midspan. The resulting value of C_b^* was equal to 1.20, so the assumption of $C_b^* = 1.0$ in this problem is conservative.

The capacity of the girder with top flange loading was estimated at $C_b^* M_{AASHTO} = 1.0 \times 1274$ k-ft. which is greater that $M_{gird} = 600$ k-ft. The girder can therefore support the self-weight and a small portion of the construction loading without a problem.

The increase in the buckling capacity that is required from the deck can now be calculated by substituting the factored design moment, M_u, for M_{cr} and rewriting Equation 9.1b. The calculation of the required shear rigidity $Q_{req'd}$ is shown in Equation 9.20.

$$Q_{req'd} = \frac{8}{3d}(M_u - C_b^* M_{AASHTO}) = \frac{8}{3 \times 4.77 \, ft} (3526 \, kipft - 1274 \, kipft) = 1257 \frac{k}{rad} \quad (9.20)$$

A deck shear rigidity of 1257 k/rad provides enough bracing to the girder to eliminate the cross-frames at 25 feet and 75 feet along the 100 foot girders. The distance between the cross-frames is therefore equal to 50 feet which is twice the maximum spacing of 25 feet in the current AASHTO specification [1].

Referring back to the values of the experimental shear rigidities in Tables 9.1a and 9.1b, the shear rigidity for the deck LSM1716 with the unstiffened connection was 844 k/rad. The girder spacing for this design example was 12 ft. - 6 in., whereas the span of the deck LSM1716 was 12 ft - 10 in. This deck should give a reasonable estimate of the stiffness with a slightly shorter span. Recalling that the alpha factor for a four girder bridge was 1.5 for the experimental shear rigidities. The shear rigidity of the deck LSM1716 is therefore estimated at 1.5 x 844 k/rad = 1266 k/rad. This shear rigidity is slightly greater than the $Q_{req'd}$, however a slightly larger value would probably be desirable for a larger factor of safety. One possible alternative would be to stiffen the connection so that a value closer to the corresponding shear rigidities in Table 9.2 would

apply. For the deck LSM1716, the experimental shear rigidity with a fully-stiffened connection was 1594 k/rad. If the alpha factor of 1.5 is applied to this deck rigidity, the corresponding shear rigidity is equal to 2390 k/rad which is significantly greater than $Q_{req'd}$ of 1257 k/rad.

It should be noted that a finite element analysis was conducted on the girders from the second design example using a deck shear rigidity of 1257 k/rad and the resulting bifurcation load was 7500 k-ft which is significantly greater than the design moment of 3526 k-ft. The resulting buckling mode was controlled by web bend buckling. For this particular problem, the design approach was quite conservative.

The last design example will consider a bridge with continuous girders. The bridge layout is shown in Figure 9.5a and 9.5b. This is a 6-girder bridge which was prepared by AISC Marketing as a preliminary design study for the Akers Mill Road bridge over Interstate Highway 75 in Marietta, Georgia [6]. The bridge had three spans, with exterior spans of 140 feet and 115 feet, while the center span was 200 feet. This example will concentrate on the design of bracing for the center 200 foot span. The original design made use of cross-frames spaced at 25 feet, which consisted of 7 intermediate cross-frames.

Figure 9.6 shows the actual layout of flange transitions along the 200 foot span. There were five flange transitions along the girder length. In order to simplify the design, the larger sections at the support were conservatively neglected in this design and the cross-section at the second transition were used at the supports. These "support" sections are referred to as "end 1" and "end 2" and were assumed to extend over the first 25 feet of the bridge measured from the supports. It was mentioned in Chapter 8, that lateral-torsional buckling will typically not control at the support section during construction. The critical stage for the support section occurs at a later stage in the finished bridge.

The simplified bridge is shown in Figure 9.7 complete with the factored dead load design moments at the supports and at midspan. For this particular design problem, a metal deck with the shear rigidity matching the value in Table 9.1 for the LSM1716 value of 844 (using s/2), is to be used for the formwork for this bridge. The purpose of the design problem is to determine what cross-frame spacing would be required to adequately brace the girders during the construction loading.

The first step in this problem will be to check the web buckling capacity against the factored dead load moments and shears. The calculation of the bend buckling capacity is shown in Equation 9.21a for the midspan section and in Equations 9.21b and 9.21c for the support
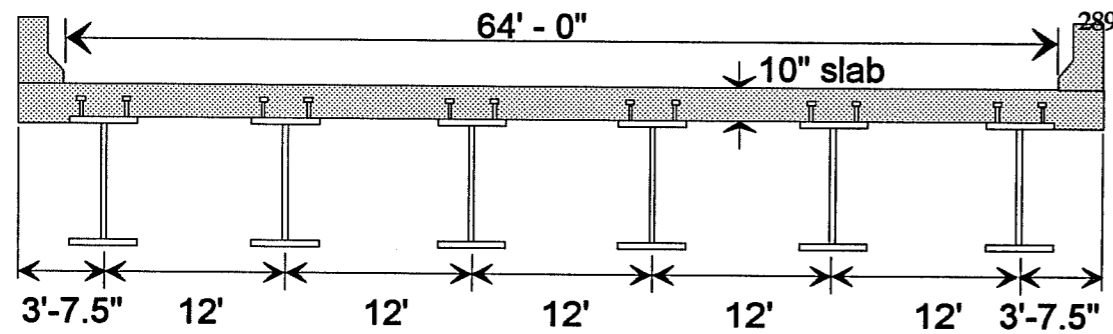
ORIGINAL BRIDGE DESIGN:

Girder Span: 200'

9 Cross-Frames Spaced at 25.0'

Design Shears and Moments, see Figure 9.6

Design Problem: Assuming a shear rigidity of 1409 k/rad for the metal deck forms (see text for explanation), determine what spacing is required for intermediate cross-frames to supplement the stay-in-place metal deck forms in providing adequate bracing during the construction stage.

Figure 9.5a Cross-section of bridge used in Design Example #3.
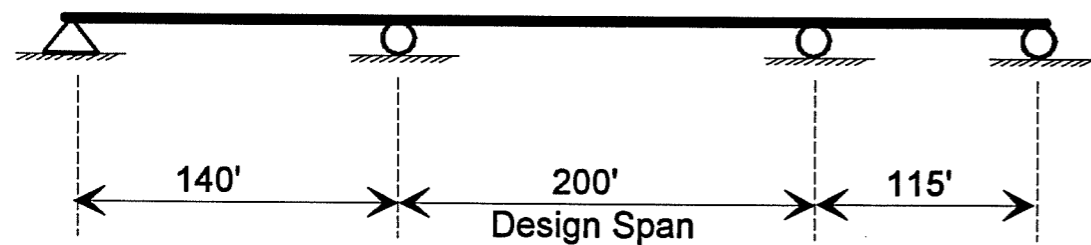
Figure 9.5b Layout of actual bridge modeled in Design Example #3.

top
flange
size:

length:

bottom
flange
size:

length:
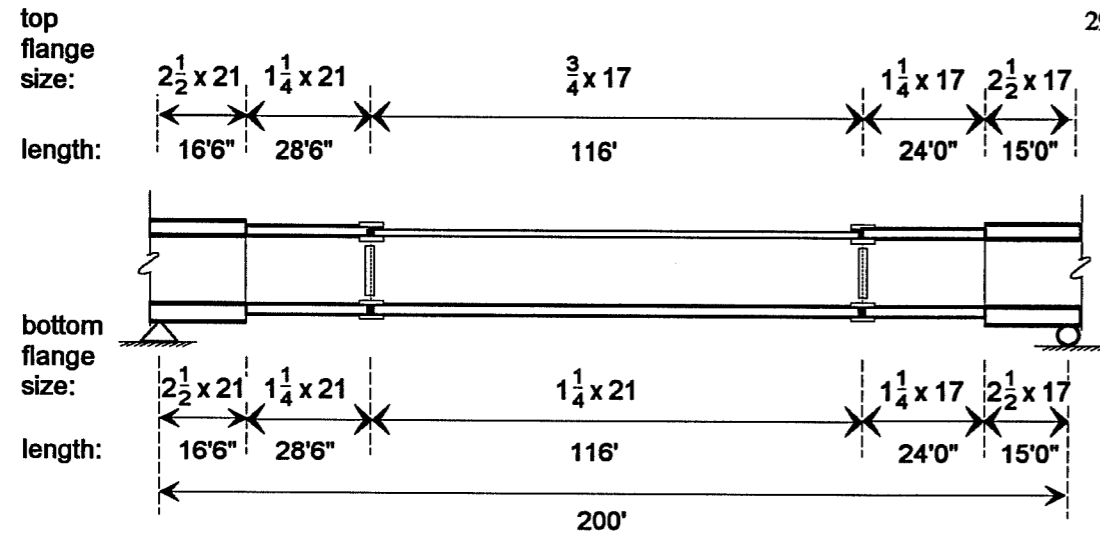
Figure 9.6 Flange transitions of 200' span in actual bridge.

top
flange
size:

length:

bottom
flange
size:

length:
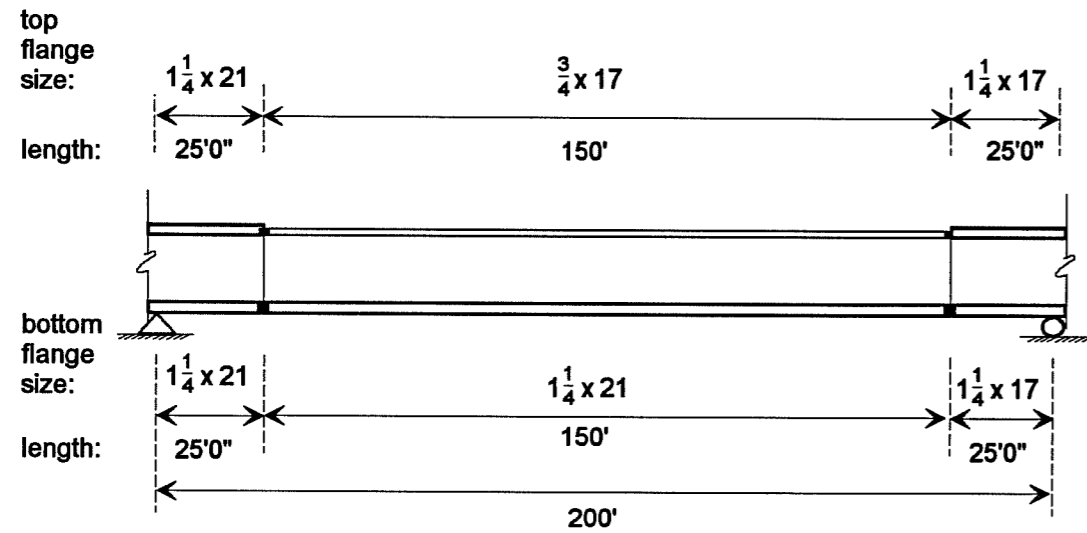
factored moment:	9667 k'	4235 k'	7914 k'
factored shear:	273 k		255 k

Figure 9.7 Simplified bridge used for Design Example #3.

sections. Since the girders are singly-symmetric at midspan and the small flange is in compression, the value of λ is taken as 12500. The sections are doubly-symmetric at the supports so λ is taken as 15400 in these cases. The cross-sectional properties can be found on Figure 9.8.

$$M_r = \left[\frac{(12500)^2}{\left(\frac{45.1\,in}{0.5\,in}\right)^2} \right] 1675\,in^3 \left(\frac{1}{12\frac{in}{ft}\ 1000\frac{lb}{kip}}\right) = 2681\ kip\,ft < 4235\,kip\,ft \quad (9.21a)$$

$$M_r = \left[\frac{(15400)^2}{\left(\frac{40.625\,in}{0.5\,in}\right)^2} \right] 2658\,in^3 \left(\frac{1}{12\frac{in}{ft}\ 1000\frac{lb}{kip}}\right) = 7957\ kip\,ft < 9667\,kip\,ft \quad (9.21b)$$

$$M_r = \left[\frac{(15400)^2}{\left(\frac{40.625\,in}{0.5\,in}\right)^2} \right] 2252\,in^3 \left(\frac{1}{12\frac{in}{ft}\ 1000\frac{lb}{kip}}\right) = 6742\ kip\,ft < 7914\,kip\,ft \quad (9.21b)$$

The factored dead load moments exceed the web bend buckling capacity at all three of the sections which were checked. It was found in Chapter 6, that web bucking reduced the effectiveness of the deck to provide bracing to the girder. The actual flange sizes at the support, would reduce the stresses significantly, so web bend buckling at the support would not be a problem. At midspan, however, the girder may have a problem with web buckling. It should be noted that the current AASHTO specifications allow bend bucking of the web during the construction stage. The moment is controlled in these cases, however, by using a factor R_b. For this particular problem, it may be desirable to provide a longitudinal stiffener to prevent web buckling.

The shear buckling capacity at the supports should also be checked. The girder has a web slenderness of 162.6 and the stiffeners at the supports are spaced at 0.74d. The resulting value of the plate buckling coefficient, k, is 13.9. The shear buckling capacity, V_u, was calculated as 560 kips which was greater than the largest factored shear of 274 kips which occurs at the first support. Shear buckling is therefore not a problem.

Cross-frames would have to be provided near the support sections to control lateral-torsional buckling during the critical stage which would occur in the finished bridge. Therefore, cross-frames would be provided 25 feet from the two supports. The purpose of this problem is
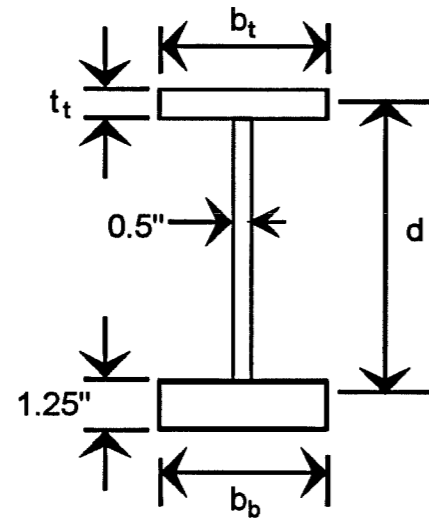
	End #1	Midspan	End #2
SECTION DIMENSIONS			
b_t (in)	21	17	17
b_b (in)	21	21	17
t_t (in)	1.25	.75	1.25
d (in)	81.25	81	81.25
SECTION PROPERTIES			
I_y (in^4)	1929	819	1024
I_{yc} (in^4)	965	307	512
J (in^4)	30.7	16.8	25.5
w_g (lb/ft)	315	252	281
S_{xc} (in^3)	2658	1675	2252
D_c (in)	40.63	45.1	40.63

Figure 9.8 Cross-sectional dimensions and properties for Design Example #3 plate girder.

to determine how many cross-frames would be required for the middle 150 feet between the two cross-frames near the supports.

The deck which is to be employed has a shear rigidity of 844 k/rad (from Table 9.1a for LSM1716 based on width of 0.5s). This is a six girder bridge so the effective width is shown in Equation 9.22.

$$effective\ width\ =\ w\ =\ \frac{(6-1)}{6}\ s\ =\ 0.83s \qquad (9.22)$$

The modifying factor, α, for the deck is shown in Equation 9.23 for the bridge under consideration.

$$modifying\ factor\ =\ \alpha\ =\frac{0.83s}{0.5s}\ =1.67 \qquad (9.23)$$

Therefore, for the 6-girder bridge in this design example, a comparable deck to the LSM1716 with the unstiffened connection would provide a shear rigidity of 1.67 x 844 k/rad = 1409 k/rad in this bridge.

It was mentioned in Chapter 4, as well as in the previous design example, that effects of top flange loading could be handled in girders with intermediate cross-frames by using a $C_b^* = 1.0$. In this design, a $C_b^* =1.0$ will be used on the girder capacity so that the AASHTO equation for lateral-torsional buckling directly estimates the capacity of the girders.

Using the AASHTO equation for lateral-torsional buckling, the capacity of the support sections were calculated based on the spacing of cross-frames in this region which was 25 feet. The buckling capacity of the sections at the first support was 21097 kip-ft. which is significantly greater than the factored dead load moment of 9667 kip-ft. The AASHTO equation predicted a buckling capacity at the other support of 11295 kip-ft which is greater than the factored dead load moment of 7914 kip-ft. Recalling from Chapter 8, the C_b values for the moment at the support sections would make the capacity significantly larger, however these C_b equation are not required. It should also be noted that the actual support section is considerably larger than the section used. This demonstrates that lateral-torsional buckling at the support section will not be critical during the construction stage. The C_b equations presented in Chapter 8 would be applicable to check the

capacity of the support section at the critical stage since the top flange would be braced by the hardened concrete deck.

Although the construction stage is not critical for lateral-torsional buckling at the support section, this stage is critical for buckling of the midspan section. The midspan factored design moment is 4235 kip-ft. The moment that the girder must provide can be calculated by subtracting the moment component which results from the deck (3/8 Qd) from the factored design moment. This is shown in Equation 9.24.

$$M_{rreq'd} = M_u - \frac{3}{8} Q d = 5235 \, kipft - \frac{3}{8} \, x(1407 \frac{kip}{rad}) x 6.75 ft = 674 \, kipft \qquad (9.24)$$

During the casting of the concrete deck, the girder must provide a buckling capacity between cross-frames of 674 kip-ft. The AASHTO equation for lateral-torsional buckling produces a buckling capacity of 674 kip-ft. when an unbraced length of 90 feet is used.

Before selecting a cross-frame spacing however, it is necessary to check the construction stage at the erection of the girders. In this case, the girders must be able to support their self-weight plus a construction load of approximately 10 lb/ft^2. In order to estimate the moment from the self-weight, the weight per foot of the two support sections and the midspan section were averaged. The factored erection loads are as follows:

$$W_g = \frac{315\frac{lb}{ft} + 252\frac{lb}{ft} + 281\frac{lb}{ft}}{3} = 284 \, \frac{lb}{ft} = 0.284 \, \frac{kip}{ft} \qquad (9.25a)$$

$$construction \; load = 10\frac{lb}{ft} \, x \, 12 \, ft = 120\frac{lb}{ft} = 0.120\frac{kip}{ft} \qquad (9.25b)$$

$$w_{gird} = 1.30 \, x \left(0.284\frac{kip}{ft} + 0.120\frac{kip}{ft} \right) = 0.525 \, \frac{kip}{ft} \qquad (9.25c)$$

The midspan moment due to the construction loading was estimated by modeling the girder as a beam with both ends fixed for which the midspan moment is $M_{gird \; CL} = w_{gird} \, L^2/24$, and increasing the moment by 10%.

$$M_{girdCL} = 1.10 \; x \; \frac{w_{gird}L^2}{24} = 1.10 \; x \; \frac{0.525\frac{kip}{ft} \; (200 ft)^2}{24} = 962 \; k \, ft \qquad (9.26)$$

This controls the required girder capacity since it is larger than the moment requirement when the deck is in place and the full construction load is applied. For an unbraced length of approximately 72 feet, the AASHTO formula for lateral torsional buckling produces a capacity of 962 kip-ft. If two cross-frames are used for the "midspan" region, the unbraced length would be reduced to 50 feet. For an unbraced length of 50 feet, the AASHTO formula produces an estimate of 1830 kip-ft for the lateral-torsional buckling load. With the full construction load, the capacity of the girder and deck system in the midspan region is equal to $M_{AASHTO} + 3/8 \; Qd$ which is shown in the following expression:

$$M_r = 1830 k\text{-}ft. + \frac{3}{8} x (1407 \frac{k}{rad}) x (6.75 ft.) = 5391 k\text{-}ft. > 4235 k\text{-}ft. \quad O.K. \qquad (9.27)$$

The girder capacity therefore satisfies the two stages of loading during construction. The total number of intermediate cross-frames in this example is therefore reduced from 7 cross-frames to 4 cross-frames.

9.4 Large-Displacement Results

The design examples for bracing by metal deck forms which have been presented in Section 9.3 have only considered stiffness requirements developed using bifurcation-type analyses. In order for a bracing solution to be complete, however, the deck must also be designed for strength requirements. While deck strength requirements will not be established in this dissertation, it is necessary to give an indication of the effect girder imperfections have on the stiffness and strength requirements for girders braced by a shear diaphragm. A large-displacement analyses is necessary in order to give an indication of the effect of imperfections.

Results from four large-displacement analyses will be presented in this section. The doubly-symmetric section #1 which was shown in the previous chapters was used in each of the analyses conducted. The girder had a 50 foot span and was subjected to a midspan point load applied at the centerline of the top flange. Transverse web stiffeners were positioned only at the supports and under the point load. Table 9.2 shows the characteristics of the four different analyses which were conducted. Two different deck shear rigidities were considered: 660 k/rad

and 1320 k/rad. The maximum sweep allowed for plate girders in the Bridge Welding Code(ANSI/AASHTO/AWS D1.5-88) [7] can be calculated using the following expression:

$$\text{Maximum Sweep (in inches)} = \left(\frac{\text{Span in feet}}{10}\right) x \frac{1}{8} \qquad (9.28)$$

Since the girders in the analyses have a 50 foot span, the maximum sweep resulting from the above equation would be 5/8 inch. If the top flange is assumed to have this maximum sweep while the bottom flange is perfectly straight, the twist at midspan would be 0.654 degrees. This imperfection was considered as well as a 1 degree twist at midspan.

Table 9.2 Girders Considered in Large Displacement Analyses		
Case	Deck Shear Rigidity, Q (k/rad)	Initial Twist of Cross-section (deg)
1	660	0.654
2	660	1
3	1320	0.654
4	1320	1

Since two different deck shear rigidities were considered, the girder system had two different bifurcation moments which are shown in Table 9.3. The bifurcation moment is the maximum moment at midspan and was found from an eigenvalue analysis.

Table 9.3 Bifurcation Moment (@ midspan)	
Deck Shear Rigidity (k/rad)	Bifurcation Moment (k-in)
660	27326
1320	40773

Based on the recommendations which resulted from the eigenvalue analyses presented in previous chapters, the buckling capacity of the girders would be estimated using the expression,

Based on the recommendations which resulted from the eigenvalue analyses presented in previous chapters, the buckling capacity of the girders would be estimated using the expression, $M_{cr} = C_b^* M_{AASHTO} + 3/8 \, Qd$. For section #1 with top flange loading, $C_b^* M_{AASHTO}$ is equal to 7576 k-in ($C_b^* = 0.9$). The resulting estimates of the buckling moment for the girders braced by the deck systems are as follows:

$Q = 660 \text{ k/rad}$: $M_{cr} = 21127$ k-in.

$Q = 1320 \text{ k/rad}$: $M_{cr} = 34677$ k-in.

For each of the four cases which were considered in the large-displacement analyses, the solutions experienced convergence problems at loads below the moments predicted by the approximate solution: $M_{cr} = C_b^* M_{AASHTO} + 3/8 \, Qd$. For the two cases with deck shear rigidities of 660 k/rad, the solutions converged at a moment of 19138 k-in which is 70% of the bifurcation moment (27326 k-in), however, the solution could not reach convergence at higher moments. For the two cases with a deck shear rigidity of 1320 k/rad, the solutions converged at a moment of 20386 k-in which is 50% of the bifurcation moment (40773 k-in), however, the solution could not reach convergence at higher moments.

The reason for the convergence problems in these analyses is unclear. A possible explanation for the convergence problems may have to do with the imperfection-sensitivity of the twin girder and diaphragm system. Plaut [20] referred to some cases with bracing of columns in which the imperfection-sensitivity of the problem reduced the buckling capacity of the column to less than 50% of the predicted bifurcation load of a perfect column. Thompson and Hunt [22] also provide a discussion on problems with imperfection-sensitivity. It is not clear whether the convergence problems for the beams braced by a shear diaphragm are due to imperfection-sensitivity, however, this does require further investigation.

Although the problems had trouble converging, the results which were obtained will still give an indication of the effect of imperfections on the displacement behavior and resulting brace forces in the deck. Figure 9.9 shows a plot of the midspan moment in the girder versus twist at midspan. The midspan moment has been normalized by M_g, which is the buckling capacity of the girder with no deck for bracing ($C_b^* M_{AASHTO} = 7576$ k-in). The cases with the deck shear rigidities of 1320 k/rad controlled the midspan twist much better than the cases with a deck shear rigidity of 660 k/rad. The girders with the larger deck shear rigidity, however, would be designed to carry a larger load. Figure 9.10 shows a plot of the buckling moment versus the twist at midspan, however, in this case the buckling moment has been normalized by the corresponding
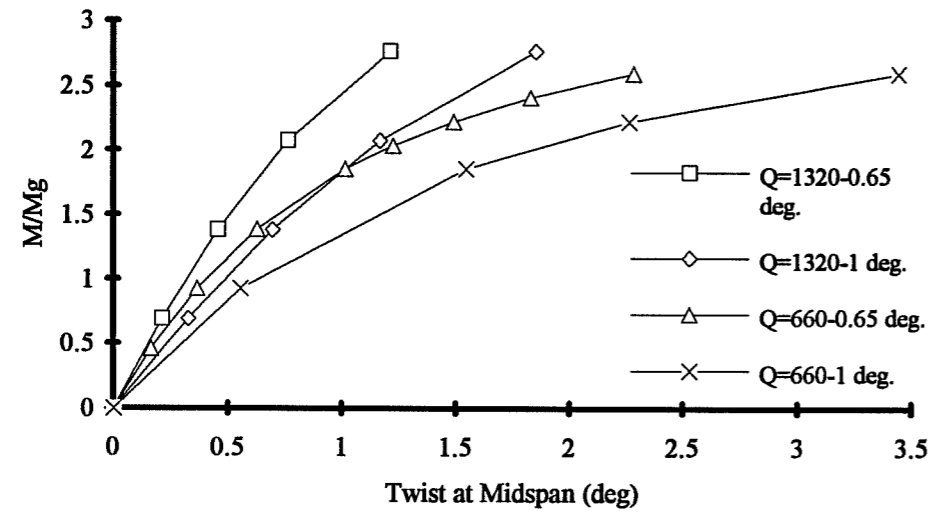
**Figure 9.9 M/Mg versus midspan twist for section #1 with a 50 foot span.
Point load at midspan top flange.**
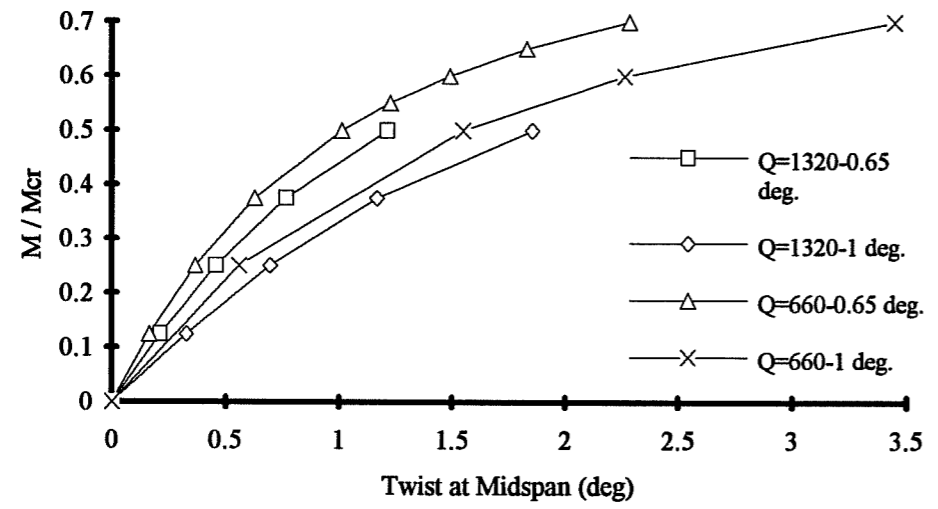
**Figure 9.10 M/Mcr versus midspan twist for section #1 with a 50 foot span
Point load at midspan top flange.**

(M/M_{cr}), the curves for Q=660 k/rad have smaller midspan twists than the curves with Q=1320 k/rad.

An interesting comparison can be made if the twist at midspan is normalized by the initial imperfection. This has been done in Figure 9.11 which shows a plot of M / M_{cr} versus θ / θ_o. The curves for a given deck shear rigidity plot directly on top of one another which indicates that the twist is linearly dependent on the initial imperfection. In addition, there is not much of a difference between the curves for shear rigidities of 660 k/rad and 1320 k/rad. For both values of the shear rigidity, for $M/M_{cr} = 0.5$, the twist at the midspan is more than $2.5\theta_o$, which indicates that excessive displacements may be of concern.

It is also necessary to provide an indication of the increase in the forces in the deck due to the imperfections. Figure 9.12 shows the forces which result on a "panel" from the finite element analyses when the top flange of the girders deflect laterally. The forces result in a couple at each end of the panel as well as a shear. In order to gain an understanding of the brace forces relative to the capacity of the actual deck a method of comparison must be developed. Figure 9.13 shows a sketch of the testing frame which was used to perform the shear tests in the experimental portion of this study. Below the testing frame is a free body diagram of the beam of the testing frame. The forces from the deck which are transverse to the beams of the testing frame have been represented as a restraining moment, M_{rd}. If the restraining moment is divided by the cover width of the panel ("a" in Figure 9.13), the restraining moment per foot of deck can be obtained. This has been denoted as M^*_{rd}, and can be calculated with the following expression:

$$M^*_{rd} = \frac{\frac{P}{2}L}{a} \tag{9.30}$$

The shear rigidity of the deck from experimental studies is typically based on a secant stiffness at 40% of the ultimate load [9]. The load "P" which would be used in Equation 9.30 would therefore be 40% of the ultimate capacity of the deck form. As an indicator of the deck capacity from the shear tests of the deck capacity, M^*_{rd} is evaluated for the following decks:

    22 gage - cellular deck - 9 ft. span - 8 ft. cover width - $P_{ult} = 2.8$ kips

        $M^*_{rd} = (((0.4*2.8 \text{ kips})/2)*216")/(8 \text{ ft.}) = 15.1$ kip-in/ft

    16 gage - conventional deck - 7.75 ft. span - 8 ft. cover width - $P_{ult}=8.6$ kips

        $M^*_{rd} = (((0.4*8.6 \text{ kips})/2)*216")/(8 \text{ ft.}) = 46.4$ kip-in/ft
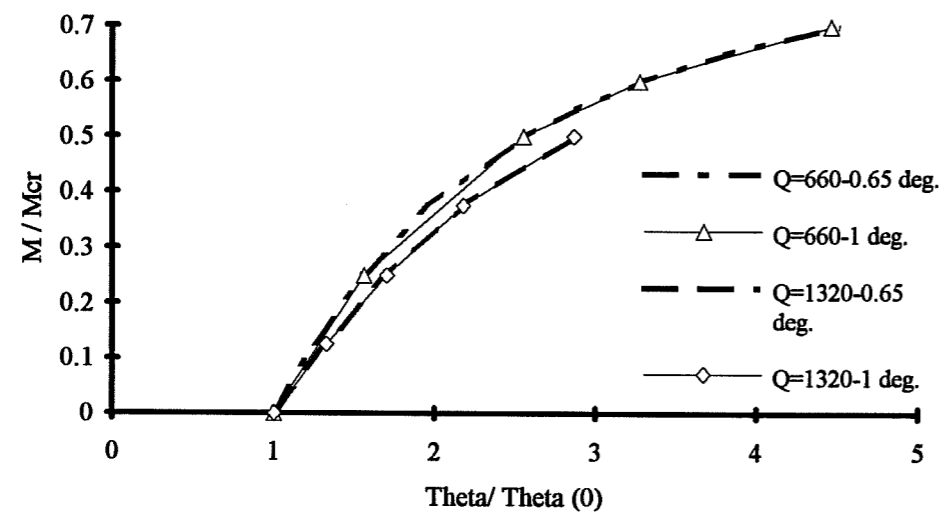
Figure 9.11 M/Mcr versus normalized midspan twist for section #1 with
a 50 foot span and a top flange point load at midspan.
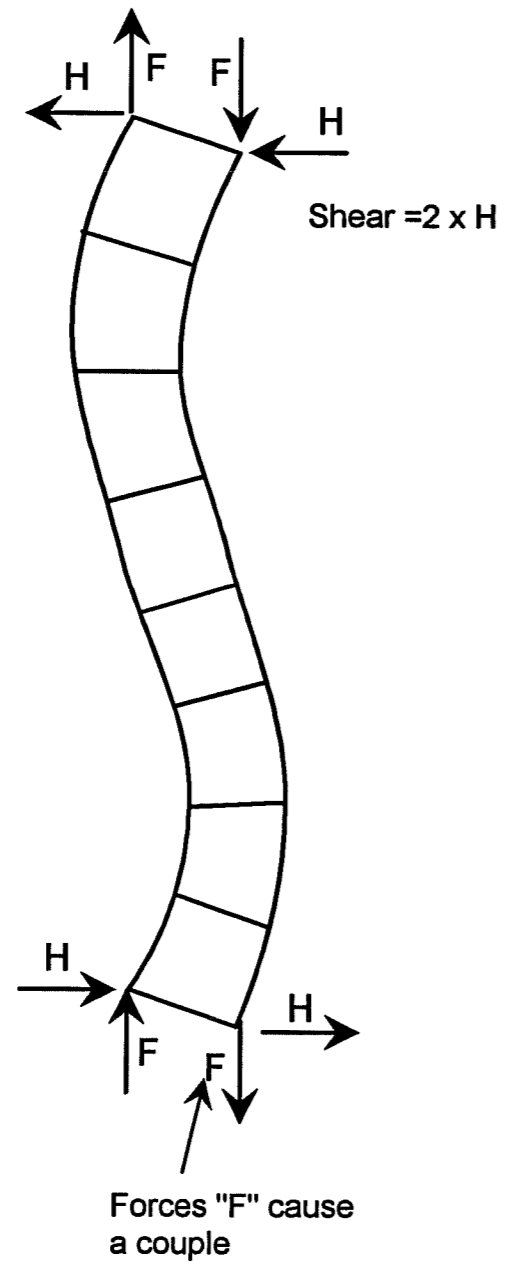
Figure 9.12 Forces on the deck panel when top
flange displaces laterally.
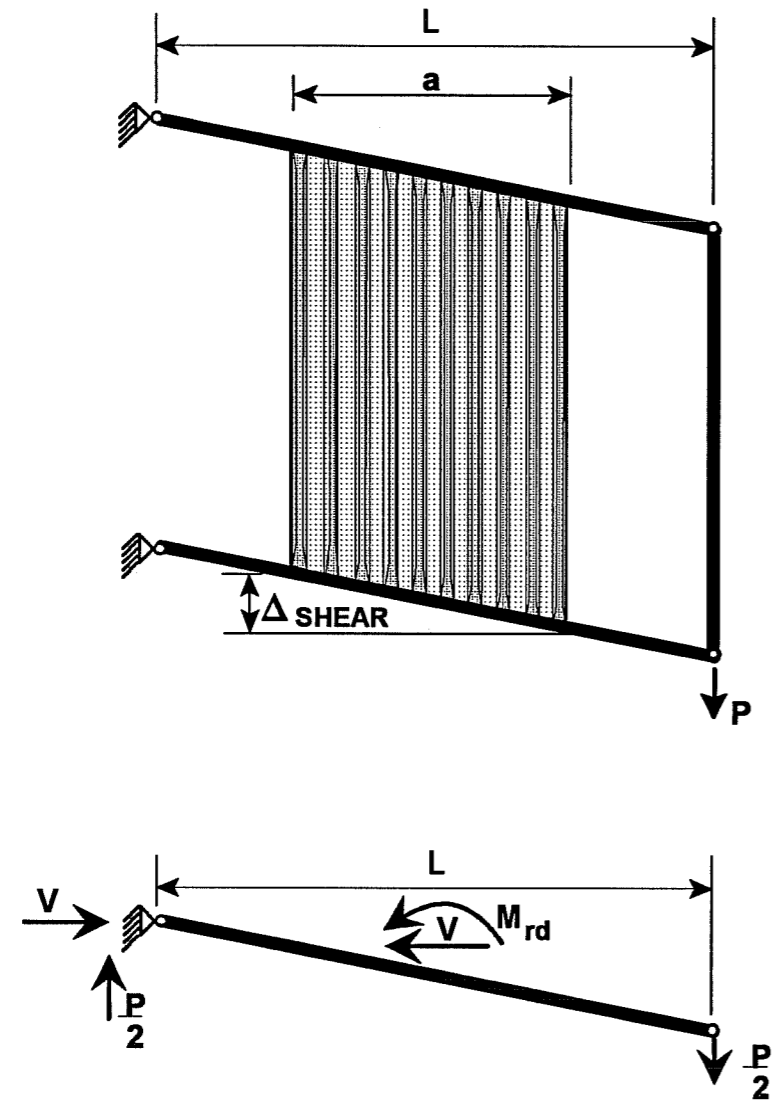
M_{rd} **Restraining Moment from Deck**

$$\frac{P}{2} \times L = M_{rd}$$

M^{*}_{rd} = **Restraining Moment from Deck per foot**

$$M^{*}_{rd} = \frac{\frac{P}{2} \times L}{a}$$

Figure 9.13 : Capacity of deck from experimental tests.

In order to compare the forces in the deck from the large deflection analyses, the forces in each deck panel will be represented by a couple which restrains the top flange from lateral movement as shown in Figure 9.14. The couples for each panel in Figure 9.14 are calculated as a restraining moment per foot. Figure 9.15 shows a plot of the restoring moment from the deck along the length of the girder for the case with a 1 degree initial twist and a deck shear rigidity of 660 k/rad. The brace forces along the girder length increased significantly with increasing load. This can be observed in Figure 9.15 by the larger increase in brace force when the load was increased from $0.6 * M_{cr}$ to $0.7 * M_{cr}$ when compared to the brace force increase between loads of $0.5 * M_{cr}$ and $0.6 * M_{cr}$.

In order to compare the brace forces for the four different large displacement analyses, the brace forces were averaged between stations at 5 feet and 15 feet along the girder length. Figure 9.16 shows a plot of the moment versus the average brace force for the four different cases. The moments have been normalized by M_g which is the capacity of the girder with no deck for bracing. For a given value of M/M_g and magnitude of imperfection, the brace forces for the cases with a deck shear rigidity of 660 k/rad were larger than the cases with a deck shear rigidity of 1320 k/rad. It is necessary, however, to consider that the girders with the larger deck shear rigidity would be designed for a larger load. Figure 9.17 shows a plot of the applied moment normalized by the bifurcation moment versus the average brace force. For a given imperfection magnitude and value of M/M_{cr} the brace forces for the decks with shear rigidities of 1320 k/rad are larger than for the decks with shear rigidities of 660 k/rad. An interesting comparison can be made if the average brace forces for each case are normalized by the initial imperfection. This has been done in Figure 9.18 which shows a plot of M/M_{cr} versus the normalized average brace force for the four different analyses. The curves for a given deck shear rigidity plot directly on top of one another. This indicates that the brace forces are linearly dependent on the initial imperfection.

Table 9.4 shows the average brace force per foot for the four analyses. The loads are given relative to the capacity of the girder with no deck for bracing and also the bifurcation load of the perfect girder.

Denotes coupling of translational degrees-of-freedom in x, y, and z-direction between deck and girder nodes
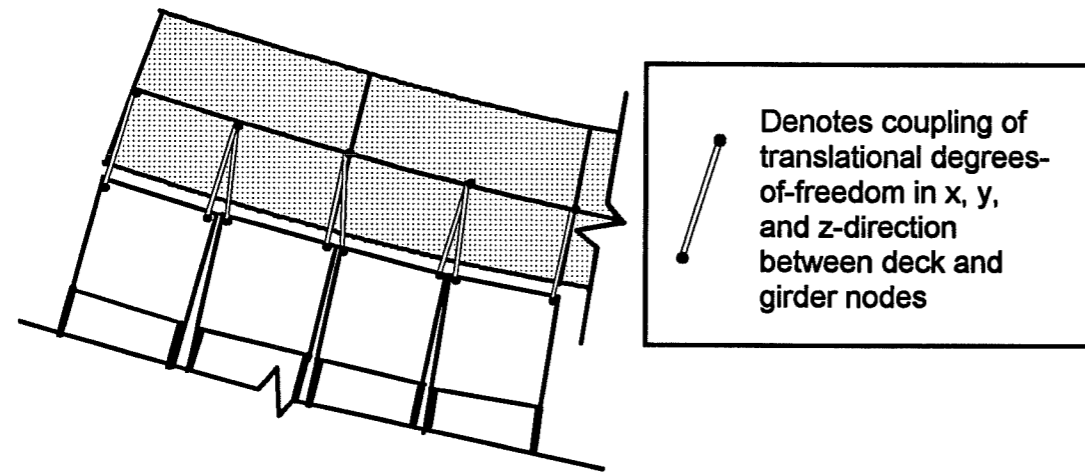
Restoring reactions from each panel

F_1 F_1 F_2 F_2 F_3 F_3 F_4 F_4

p_w

width of one panel
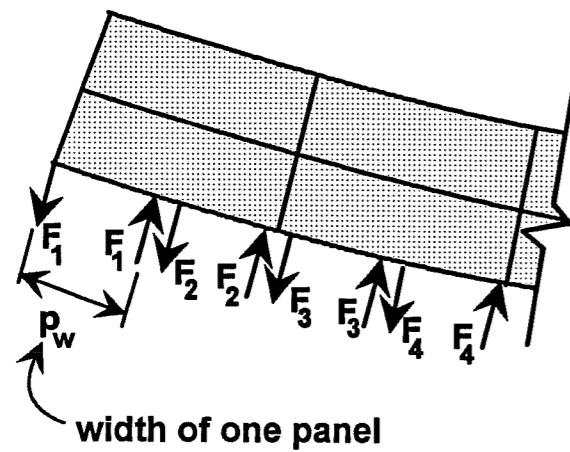
Restoring couple from "panel i" :

$$T_i = \frac{F_i \times p_w}{(p_w / 12 \text{ in/ft})} \quad \text{(k-in / ft)}$$

Figure 9.14 Brace forces in deck shown as a "restoring couple"
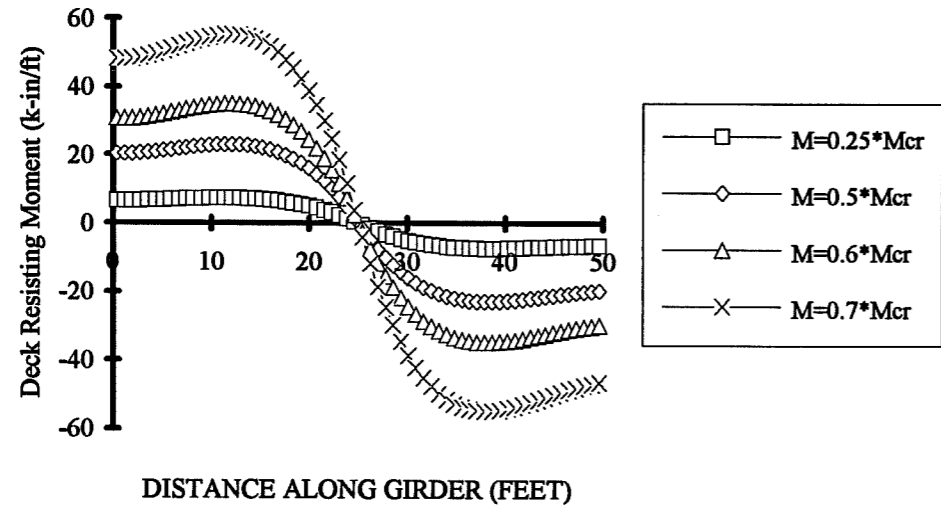
Figure 9.15 Force in deck along girder length with increasing load.
Section #1 with 50 foot span and top flange point load at midspan.
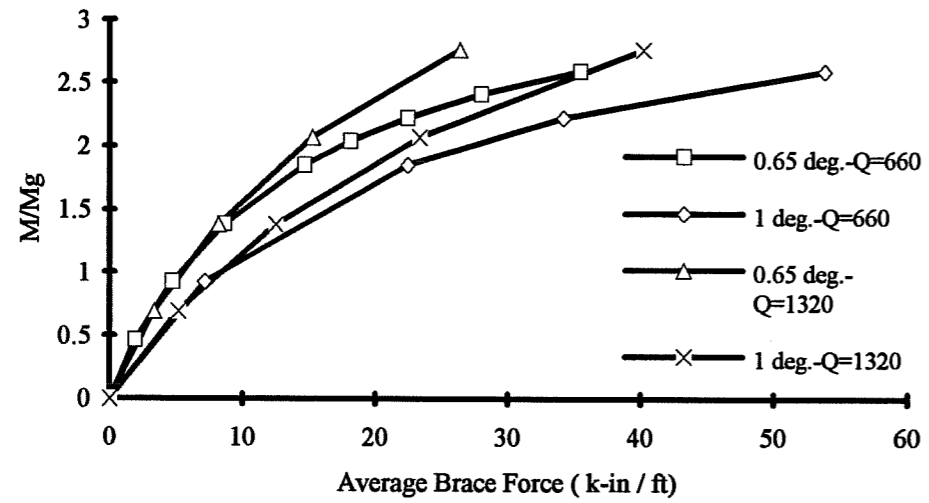
Figure 9.16 M/Mg versus average brace force. Section #1 with
50 foot span and top flange point load at midspan.
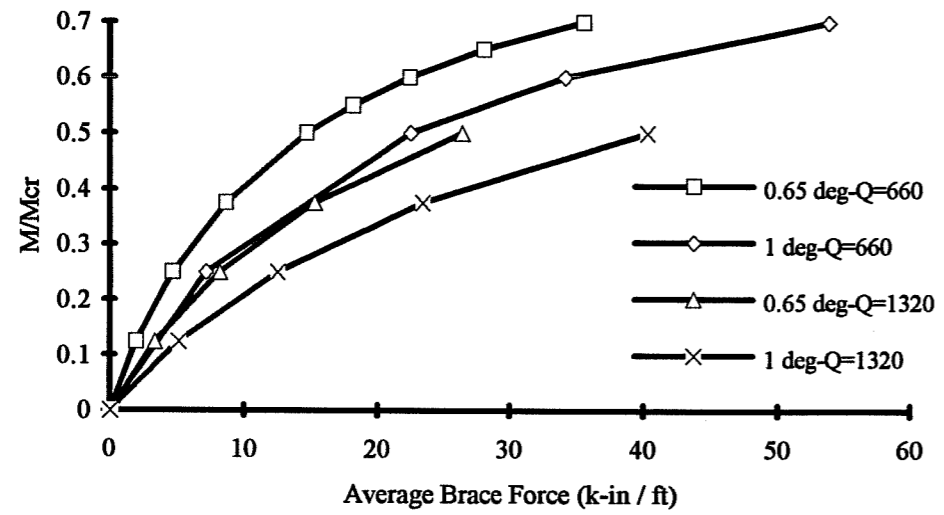
Figure 9.17 M/Mcr versus average brace force. Section #1 with 50 foot span and top flange point load at midspan.
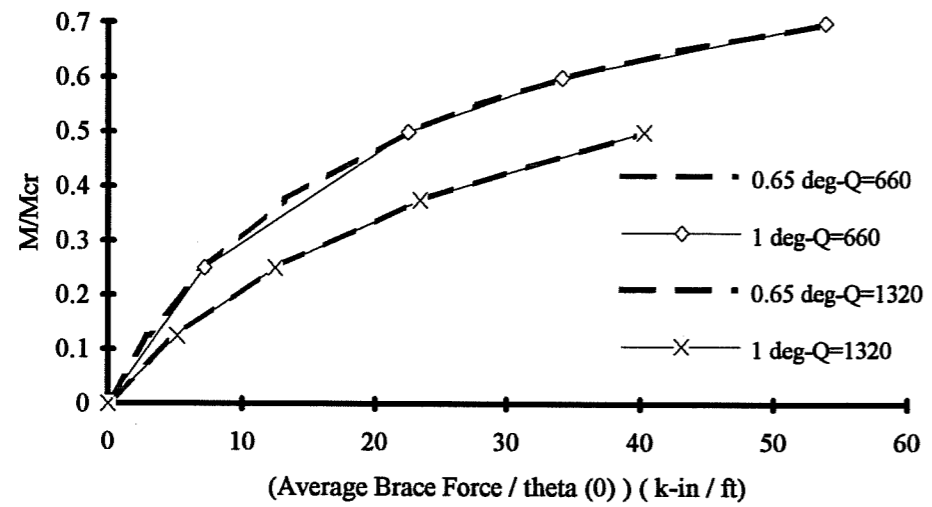
Figure 9.18 M/Mcr versus normalized average brace force. Section #1 with 50 foot span and top flange point load at midspan.

Table 9.4 Average Brace Forces				
Q (k/rad)	Theta(0) (degrees)	M/M_g	M/M_{cr}	Avg. Brace Force (k-in/ft)
660	0.654	2.594	0.7	35.46
660	1	2.594	0.7	53.75
1320	0.654	2.765	0.5	26.32
1320	1	2.765	0.5	40.22

The values in Table 9.4 range from 26.32 k-in/ft to 53.75 k-in/ft. Recalling from above, the capacities which were calculated from the experimental deck tests were 15.1 k-in/ft and 46.4 k-in/ft. It should be noted that these capacities neglect the bending stiffness of the deck which would slightly reduce the displacements and brace forces in the a girder system. The large displacement results which have been presented have clearly shown that imperfections may considerably reduce the effectiveness of the deck and must be considered before the effectiveness of the metal deck forms as a bracing element can be adequately assessed.

9.5 Summary

This chapter has presented design examples which indicate how to use the proposed design equations for the stiffness requirements of a shear diaphragm used for bracing of bridge girders. The design equations are relatively easy to use. The bridges which were considered have been existing bridge designs, and have ranged from a short span bridge (50 feet) to a continuous bridge with a relatively long center span (200 feet). In each of the bridges which were considered, cross-frames were eliminated from the original design by using the metal deck forms for bracing during the construction stage. Eliminating these cross-frames make the bridge easier to erect, and also eliminates fatigue prone details which occur at the cross-frame locations.

The large displacement results which were presented have demonstrated that strength requirements of the metal deck forms must be investigated in order to obtain adequate design guidelines. In addition, the imperfections may also have an effect on the stiffness requirements of the deck forms.

CHAPTER 10

Summary and Recommendations

The purpose of this research study was to develop a design approach to incorporate stay-in-place metal deck forms as bracing elements in bridge girders during the construction of the concrete deck. The project consisted of an experimental phase and a computational phase. The purpose of the experimental phase was to determine the shear strength and stiffness characteristics of the metal deck forms and corresponding connection. The results of the experimental portion of this study are contained in related theses by Currah [9] and Soderberg [21]. The purpose of the computational phase was to study the behavior of the girders braced by metal deck forms using the finite element method. The results of the computational study were the subject of this dissertation.

The computational study concentrated on bifurcation analyses in order to determine stiffness requirements for the metal deck forms to provide bracing to bridge girders. In the process of developing a design approach for bracing of bridge girders by metal deck forms, the following parameters were considered:

1) type of loading (constant moment, concentrated point load, or
   distributed load),

2) load height,

3) girder cross-section (single-symmetry versus double-symmetry),

4) presence of discrete bracing,

5) girder span,

6) shear rigidity of deck forms,

7) number of transverse web stiffeners,

8) web slenderness, and

8) in-plane boundary conditions of girders.

Finite element results which showed the effects of these parameters on the lateral-torsional buckling capacity of girders were presented in Chapters 4-8. In addition, closed formed solutions and approximate solutions were compared with the finite element results in order to develop a design approach for the stiffness requirements of metal deck forms used to brace bridge

girders. The use of the design equations were demonstrated in three design problems presented in Chapter 9.

10.1 Conclusions and Recommendations

Based on the results presented in Chapter 4 on the buckling capacity of girders braced by cross-frames at the ends (not relying on the deck for bracing), the following recommendations can be made:

1.) The effects of moment gradient were studied by comparing the finite element results with the modified Kirby-Nethercot formula. The modified Kirby-Nethercot formula agreed with the ANSYS results for doubly-symmetric sections with transverse loads applied at midheight. The modified Kirby-Nethercot equation also agreed with the ANSYS results when transverse loads were applied at midheight of singly-symmetric sections with ratios of I_{yc}/I_y greater than 0.1. For singly-symmetric girders with I_{yc}/I_y greater than 0.1 (but less than 0.5), loading applied below midheight (closer to tension flange) produced buckling loads which were larger than predicted by the modified Kirby-Nethercot formula.

2) Reasonable estimates of the buckling load for top flange loading were obtained by neglecting the warping term in the closed formed solutions. Although the accuracy of this approach did fluctuate slightly with respect to the finite element studies, it is the simplest approach to account for top flange loading.

3) For girders subjected to transverse loads applied at the top and bottom flange, the equations in the 3rd and 4th editions of the SSRC Guide [14, 13] provide a good estimate of the load height effects for doubly-symmetric sections. Although the equations are not intended for singly-symmetric sections, the equations in the 4th edition of the SSRC Guide provided good estimates of load height effects for singly-symmetric girders with I_{yc}/I_y greater than approximately 0.1. The equations were more accurate and in some cases conservative if the singly-symmetric section was treated like a doubly-symmetric section for calculating the warping coefficient (i.e. $C_w = I_y d^2/4$).

4) For beams with intermediate cross-frames and top flange loading, the buckling capacity can be calculated by neglecting effects of load height and moment gradient and using the formula for constant moment ($C_b = 1.0$).

For simply-supported girders braced by a shear diaphragm with constant moment loading, the following conclusions and recommendations can be made:

5) The lateral displacement and cross-sectional twist of the girders are a sine curve. The center of twist of the girders was uniform along the girder length, and was positioned below the girders with no deck for bracing. When the deck was introduced as a bracing element, the center of twist of the girder migrated upward with increasing shear rigidity and approached the bottom flange.

6) The energy-based solution shown in Equation 10.1 which was presented by Errera [12], agreed very well with the finite element results for doubly-symmetric girders with a shear diaphragm for bracing and constant moment loading. If I_y in Equation 10.1 is replaced with $2I_{yc}$ and the value for the variable "e" was taken as half the girder depth (same as for doubly-symmetric beams), the Errera solution also provided good agreement with the finite element results for singly-symmetric sections.

$$M_{cr} = \sqrt{\left(\frac{\pi^2 E I_y}{L_b^2} + Q\right)\left(\frac{\pi^2 E C_w}{L_b^2} + GJ + Qe^2\right)} + Qe \qquad (10.1)$$

7) Very accurate estimates of the buckling capacity of girders braced by a shear diaphragm with constant moment loading were obtained with the simple approximation shown in Equation 10.2 which was suggested by Errera [11] as well as Nethercot with Trahair [18].

$$M_{cr} = M_{AASHTO} + Qd \qquad (10.2)$$

For simply-supported girders braced by a shear diaphragm and a moment gradient caused by transverse loading applied at midheight, the following conclusions and recommendations can be made:

8) The lateral displacements and twist of girders with no shear diaphragm for bracing deviated slightly from a sine curve, however, a good approximation of the buckled shape could still be attained with a sine curve. When the deck was introduced as a bracing element, the buckled shape of the girders changed a great deal from a sine curve.

9) The center of twist varied along the length of the girder, and was the highest on the section at the supports. Moment gradients caused by a point load at midspan had a higher center of twist than the same girder subjected to a uniform distributed load. Increases in the girder length also caused higher locations of the center of twist.

10) The effectiveness of the deck as a bracing element is reduced when girders were subjected to moment gradients. In most of the cases which were considered, the Errera solution was unconservative with respect to the finite element results, especially when C_b factors were applied to the entire expression. Reasonable estimates of the buckling capacity were obtained, however, by using the approximation shown in Equation 10.3.

$$M_{cr} = C_b M_{AASHTO} + \frac{3}{4} Qd \qquad (10.3)$$

For simply-supported girders braced by a shear diaphragm with transverse loads applied at the top flange, the following conclusions and recommendations can be made:

11) The height of a point load at midspan, did not change the buckled shape of the top flange a significant amount, however, the center of twist was much higher on the section for top flange loading. Variable load height for uniform distributed loads changed the buckled shapes of both flanges. The center of twist for uniform distributed loads was highest on the section with top flange loading.

12) When compared to loading at midheight, the effectiveness of the deck was reduced further when the girders were subjected to top flange loading. The deck was slightly less effective as the span of the girders is increased. Reasonable estimates of the buckling capacity were obtained with the simple approximation shown in Equation 10.4.

$$M_{cr} = C_b^* M_{AASHTO} + \frac{3}{8} Qd \qquad (10.4)$$

For continuous girders braced by a shear diaphragm with transverse loads applied at the top flange, the following conclusions and recommendations can be made:

13) For relatively small values of the deck shear rigidity, the buckling mode is generally dominated by the lateral displacement of the top flange near midspan. For larger values of the deck shear rigidity, the buckling mode changes and the lateral displacements of the bottom flange control the buckling mode due to large compressive stresses near interior supports.

14) When the buckling mode is dominated by the top flange, increases in the deck shear rigidity cause corresponding increases in the buckling capacity of the girder. When the bottom flange controls the buckling capacity, changes in the deck shear rigidity do not significantly influence the buckling capacity.

15) When the support section controls the buckling mode, the girder behaves in a manner similar to girders with the top flange continuously restrained from laterally displacement along the span. Equation 10.5 is a reduced form of an equation presented by Yura [25] for the C_b factor for girders with the top flange continuously restrained from lateral displacement. The equation produced conservative estimates of the buckling capacity when compared to finite element results. In some instances, the reduced equation was overly-conservative, and a lower limit was established based on the C_b factor for the unbraced girder in the region around the fixed support.

$$C_b = 2.25 - \frac{1}{2}\left(\frac{M_1}{M_0}\right) + \frac{2\,M_{cl}}{\left(M_0 + M_1^*\right)} \tag{10.5}$$

By comparing the results for girders with fully-stiffened webs with those from girders with unstiffened webs and partially-stiffened webs, the following conclusions and recommendations can be made:

16) The lateral-torsional buckling capacity of girders with unstiffened webs and the partially-stiffened slender web were lower than the capacity for girders with fully-stiffened webs. The loss in capacity with the unstiffened webs and partially-stiffened webs was caused by two factors: cross sectional distortion, and web shear and bend buckling.

17) In order to account for the loss in capacity due to web buckling, the maximum increase in the lateral-torsional buckling capacity provided by the deck was limited by the bend buckling and/or shear buckling capacity of the girder webs.

18) Web distortions reduced the effectiveness of the deck to provide bracing to the girders. For buckling dominated by the top flange, the effect of these web distortions were accounted for in Equation 10.4 by reducing the contribution of the deck from $1/2Qd$ to $3/8Qd$ which is the value shown in the equation. In some instances with continuous girders braced by a shear diaphragm, web distortions reduced the buckling capacity, so that the C_b factors for the bottom flange of the unbraced girders (modified Kirby-Nethercot formula) overestimated the buckling capacity by up to 10 percent. As will be explained in point 19 below, however, this will typically not be a problem in bridge girders.

Based on the design examples which were considered, the following conclusions can be made:

19) Lateral-torsional buckling at the support section will generally not be critical during the construction stage. The critical stage for buckling of the support section occurs in the completed bridge with the design traffic load applied.

20) A number of cross-frames can be eliminated in many bridge designs by using the metal deck forms for bracing during the construction stage. Eliminating these cross-frames make the bridge easier to erect, and also reduces a number of fatigue prone details which occur at the cross-frame locations.

10.2 Additional Work

This dissertation has presented recommendations for the stiffness requirements of metal deck forms used as bracing elements for bridge girders during the construction of the concrete deck. The recommendations have been based on bifurcation analyses. In order for a bracing solution to be complete, however, the bracing must satisfy both strength and stiffness criteria.

The large displacement results which were presented in Chapter 9 demonstrated that strength requirements of the metal deck forms must be investigated in order to obtain adequate design guidelines. In addition, the imperfections may also have an effect on the stiffness requirements of the deck forms.

Additional work which is proposed would involve experimental testing of the support angle connection and computational studies concentrating on large displacement analyses.

REFERENCES

1.   American Association of State Highway and Transportation Officials (AASHTO), *Standard Specifications for Highway Bridges*, Fifteenth Edition, Washington, D.C., 1992.

2.   American Iron & Steel Institute (AISI), *Design tables for short span bridges*.

3.   American Institute of Steel Construction (AISC), *Manual of Steel Construction, Load and Resistance Factor Design*, First Edition, USA, 1986.

4.   Anderson, J. M., and Trahair, N. S., "Stability of Monosymmetric Beams and Cantilevers," *Journal of the Structural Division*, ASCE, Vol. 98, No. ST1, Proc. Paper 8648, January 1972, pp. 269-286.

5.   *ANSYS User's Manual*, Swanson Analysis Systems, Inc., 1992.

6.   *Bridges: A Preliminary Design Study for the Akers Mill Road over I-75, Marietta, GA*, AISC Marketing, Inc., Pittsburgh, PA., PDS 92/028, March 1992.

7.   *Bridge Welding Code*, ANSI / AASHTO / AWS D1.5-88.

8.   Clark, J. W., and Hill, H. N., "Lateral Buckling of Beams," *Journal of the Structural Division*, ASCE, Vol. 86, No. ST7, July 1960, pp.175-196.

9.   Currah, R. M., "Shear Strength and Shear Stiffness of Permanent Steel Bridge Deck Forms," Unpublished M.S. Thesis, The University of Texas at Austin, August 1993.

10.   Dux, P., and Kitipornchai, S., "Elastic Buckling Strength of Braced Beams," *Steel Construction*, Journal of the Australian Institute of Steel Construction, Vol. 20, No. 1, May 1986, pp. 2-20.

315

11. Errera, S., Apparao, T., "Design of I-Shaped Beams with Diaphragm Bracing," *Journal of the Structural Division,* ASCE, Vol. 102, No. ST4, Proc. Paper 12051, April 1976, pp. 769-781.

12. Errera, S., Pincus, G., and Fisher, G., "Columns and Beams Braced by Diaphragms," *Journal of the Structural Division,* ASCE, Vol. 93, No. ST1, Proc. Paper 5103, February 1967, pp. 295-318.

13. Galambos, T.V., Ed., *Guide to Stability Design Criteria for Metal Structures,* Fourth Edition, Structural Stability Research Council, John Wiley & Sons, Inc., New York, 1988.

14. Johnston, B., Ed., *Guide to Stability Design Criteria for Metal Structures,* Third Edition, Structural Stability Research Council, John Wiley & Sons, Inc., New York, 1976.

15. Kitipornchai, S., and Trahair, N., "Buckling Properties of Monosymmetric I-Beams," *Journal of the Structural Division,* ASCE, Vol. 106, No. ST5, May 1980, pp. 941-957.

16. Lawson, R., and Nethercot, D.,"Lateral Stability of I-beams restrained by Profile Sheeting," *Structural Engineer,* Vol. 63B, No. 1, March 1985, pp. 3-13.

17. Luttrell, Larry D., *Steel Deck Institute Design Manual,* Second Edition, Canton, Ohio, 1987.

18. Nethercot, D., and Trahair, N., "Design of Diaphragm-Braced I-Beams," *Journal of the Structural Division,* ASCE, Vol. 101, No. ST10, Proc. Paper 11615, October 1975, pp. 2045-2061.

19. Plaut, R., "Requirements for Lateral Bracing of Columns with Two Spans," *Journal of Structural Engineering,* ASCE, Vol. 119, No. 10, October 1993, pp. 2913-2931.

20. Plaut, R., "Requirements for Lateral Bracing of Columns with Two Spans," *Original Unpublished Manuscript.*

21.   Soderberg, E., "Strength and Stiffness of Stay-in-Place Metal Deck Form Systems," Unpublished M.S. Thesis, The University of Texas at Austin, to be submitted December 1994.

22.   Thompson, J., and Hunt, G., *A General Theory of Elastic Stability*, John Wiley & Sons, Inc., London, 1973.

23.   Timoshenko, S. and Gere, J., *Theory of Elastic Stability*, Second Edition, McGraw-Hill Book Co., N.Y., 1961.

24.   Winter, G., "Lateral Bracing of Columns and Beams," *Journal of the Structural Division*, ASCE, Vol. 84, No. ST2, Proc. Paper 1561, March 1958, pp. 1-22.

25.   Yura, J., *Class notes from Professor Yura's stability class*.

26.   Yura, J., "Fundamentals of Beam Bracing," *Is Your Structure Suitably Braced?*, SSRC 1993 Conference Proceedings, Milwaukee, WI, April 1993, p.1.

27.   Yura, J., Phillips, B., Raju, S., and Webb, S., "Bracing of Steel Beams in Bridges," Report No. 1239-F, *Center for Transportation Research*, The University at Texas, October 1992.

VITA

Todd Aaron Helwig was born in Rapid City, South Dakota, on March 2, 1965, to Ramona Manska Helwig and Lawrence Leonard Helwig. After graduation from Brookings High School in Brookings, South Dakota in 1983, he moved to Texas to attend the University of Texas at Austin. He received his Bachelor of Science degree in Civil Engineering in 1987, and his Master of Science degree in Engineering in August 1989. In September 1989 he entered the doctoral program in the Graduate School of Engineering at the University of Texas at Austin. In February of 1991 Todd married Karen Ryals. In April of 1994, he accepted a position as Assistant Professor at the University of Houston to begin in the Fall of 1994.

Permanent address: 319 Dogwood Avenue, Brookings, South Dakota 57006

This dissertation was typed by the author.